ΠΑΝΕΠΙΣΤΗΜΙΟ ΚΡΗΤΗΣ ΙΑΤΡΙΚΗ ΣΧΟΛΗ ΚΡΗΤΗΣ

ΔΙΔΑΚΤΟΡΙΚΗ ΔΙΑΤΡΙΒΗ

BIOCHEMICAL CHARACTERIZATION OF THE CXXC- AND PHD- FINGERS OF THE NOVEL ONCOGENE KDM2B

ΒΙΟΧΗΜΙΚΟΣ ΧΑΡΑΚΤΗΡΙΣΜΟΣ ΤΩΝ ΠΡΩΤΕΙΝΙΚΩΝ ΕΠΙΚΡΑΤΕΙΩΝ CXXC ΚΑΙ PHD ΤΟΥ ΟΓΚΟΓΟΝΙΔΙΟΥ KDM2B

ΕΛΕΥΘΕΡΙΟΣ ΔΕΙΚΤΑΚΗΣ

ΗΡΑΚΛΕΙΟ ΚΡΗΤΗΣ

ΜΑΙΟΣ 2020

FUNDING

This research was funded by the State Scholarship Foundation (IKY) Partnership Agreement Program “Development of Human Resources, Education and Lifelong Learning” (ΕΣΠΑ 2014-20) that was co-financed by the European Social Fund (ESF) and the Greek State, grant no. 2017-050-0504-10806.

ΕΠΙΒΛΕΠΩΝ

Χρήστος Τσατσάνης

Καθηγητής Κλινικής Χημείας, Ιατρική Σχολή, Πανεπιστήμιο Κρήτης

ΤΡΙΜΕΛΗΣ ΕΞΕΤΑΣΤΙΚΗ ΕΠΙΤΡΟΠΗ

Χρήστος Τσατσάνης

Καθηγητής Κλινικής Χημείας, Ιατρική Σχολή, Πανεπιστήμιο Κρήτης

Σωτήριος Καμπράνης

Αναπληρωτής Καθηγητής, Τομέας Βιοτεχνολογίας Φυτών, Πανεπιστήμιο Κοπεγχάγης

Δημήτριος Καρδάσης

Καθηγητής Βιοχημείας, Ιατρική Σχολή, Πανεπιστήμιο Κρήτης

ΕΥΧΑΡΙΣΤΙΕΣ

Θα ήθελα να ευχαριστήσω θερμά τα μέλη του διοικητικού συμβουλίου της Ιατρικής Σχολής του Πανεπιστημίου Κρήτης για την ευκαιρία που μου έδωσαν, να εκπονήσω και να ολοκληρώσω την Διδακτορική Διατριβή στην χώρα μου.

Θα ήθελα να εκφράσω την βαθύτατη ευγνωμοσύνη μου στους υπεύθυνους καθηγητές μου, Σωτήριο Καμπράνη και Χρήστο Τσατσάνη, για τις γνώσεις που μου μεταλαμπάδευσαν, για την υπομονή και επιμονή που έδειξαν όλον αυτόν τον καιρό στην εκπαίδευση μου και για την βοήθεια που παρείχαν και συνεχίζουν να παρέχουν στην πορεία της επιστημονικής σταδιοδρομίας μου.

Θα ήθελα να ευχαριστήσω τον πρώην καθηγητή μου, Κρίτωνα Καλαντίδη, και τα μέλη της ομάδας του για το ενδιαφέρον που έδειξαν για το επιστημονικό αυτό έργο και ιδιαίτερα τον διδάκτορα Ιωάννη Βλατάκη που ήταν εχέγγυος και βοηθητικός σε οτιδήποτε χρειάστηκα στα EMSA πειράματα.

Θα ήθελα να ευχαριστήσω τον καθηγητή Αναστάσιο Οικονόμου (IMBB-FORTH) για την ευγενή καλοσύνη να μου επιτρέψει να χρησιμοποιήσω το μηχάνημα του ITC, μα κυρίως θα ήθελα να εκφράσω την ευχαριστία μου στην διδάκτορα Μαρίνα Κουκάκη, η οποία ανέλαβε την εκπαίδευση μου και ήταν παρούσα σε κάθε πείραμα για να παρέχει τις γνώσεις της στην ανάλυση των αποτελεσμάτων.

Θα ήθελα να ευχαριστήσω τον καθηγητή Χρήστο Στουρνάρα (Ιατρική Σχολή Παν/μίου Κρήτης) και ειδικότερα την διδάκτορα Άννα Τσαπάρα, για την συμβολή της στην εκπαίδευση μου πάνω σε τεχνικές κυτταροκαλλιέργειας.

Θα ήθελα να ευχαριστήσω όλα τα μέλη από τα εργαστήρια στις πτέρυγες 2Β και 3Γ της Ιατρικής Σχολής του Παν/μίου Κρήτης για την βοήθεια τους και τις συμβουλές τους.

Θα ήθελα να ευχαριστήσω τους συναδέλφους μου: διδάκτορα Codruta Ignea, Αναστασία Αθανασάκογλου, Μαρία Δασκαλάκη, Γρήγορη Παντέλογλου και Νεφέλη Ζαχαροπούλου, όχι μόνο για την πνευματική συνεισφορά τους στο έργο αυτό, αλλά και την εμπιστοσύνη που μου έδειξαν στην διάρκεια αυτής της τετραετίας.

Δεν θα μπορούσα να παραλείψω ένα μεγάλο ευχαριστώ στους ανθρώπους, φίλους και έτερα μισά, που στάθηκαν κοντά μου όλα αυτά τα χρόνια, για την εξισορροπούσα δύναμη που προσέφεραν στην καθημερινότητα μου, και που δίχως αυτήν θα ήμουν αναπόφευκτα ελλιπής, ως άνθρωπος.

Το βασικότερο στοιχείο για το οποίο είμαι ευγνώμων και υπερήφανος είναι η οικογένειά μου. Ο Εμμανουήλ Δεικτάκης και η Νικολέττα Τσαμουρά ήταν, και είναι, αρωγοί σε κάθε κατόρθωμα μου. Δίχως την συμβολή τους και την αγάπη τους, σίγουρα δεν θα είχα φτάσει έως εδώ. Σας ευχαριστώ εκ καρδίας:.

Εν κατακλείδι, θα ήθελα να αφιερώσω αυτή τη Διδακτορική Διατριβή στον άνθρωπο που με μεγάλωσε και με δίδαξε πολλά και ας είχε τελειώσει μόνο την Γ’ Τάξη του Δημοτικού, την γιαγιά μου, Κωνσταντίνα Τσαμουρά.

SUMMARY

The fine line between physiological and pathological cell fate does not only depend on DNA sequence but also on a multifaceted matrix of regulatory elements derived from chemical modifications on the histone proteins or the DNA itself. Specific histone and DNA interacting factors that contain dedicated reader domains for specific modifications or combinations of them mediate the interpretation of this regulatory information. Deciphering what is written on chromatin with posttranslational modifications, elucidating their potential role in pathological cellular states, identifying the army of proteins that associate with them and understanding the way of function of those key player proteins, has become an exponentially growing field of research. Successful efforts on identifying readers and writers of the methyl mark on histone tails introduced an broaden spectrum of methyl transferases and demethylases that coordinate spatially and temporally, resulting in a dynamic epigenome that affects not only chromatin structure but physiological functions such as cellular development and proliferation while it is associated with several human diseases and cancer.

Up until now, more than 20 proteins have been found being able to remove methyl groups from lysine residues on histone tails and they are classified into two super families. The amine oxidase superfamily includes demethylases that require FAD as co-factor and the oxygenase superfamily consists of proteins of which the demethylase activity, derived from their Jumonji C (JmjC) domain, is dependent on α-ketoglutarate and Fe^{2+}. In human, the lysine specific demethylases are divided into seven families (KDM1-7), and most of them have been addressed as key epigenetic regulators. Some of them constitute vital components of more elaborate protein complexes (i.e. PRCs, NuRD, CoREST, MMLs) and participants in an abundance of physiological cellular processes (i.e transcription, DNA replication, DNA repair, etc.) in several signaling pathways (i.e Notch, TGF-β, FGF, NF-κB). Deregulation in the expression of these factors has been interconnected with numerous cases of cancer, leukemia and human tumorigenesis, suggesting a bivalent role as both oncogenic and tumor suppressor proteins.

One such case is the lysine-specific demethylase 2B (KDM2B), a major PRC1-associated factor that targets H3K36me2, H3K4me3 and H3K79me2/3. Upon PRC2 recruitment, KDM2B participates in the repression of the senescence-associated expression genes. KDM2B functions by coupling several chromatin modifications, including histone H3K36me2 demethylation, with histone H3K27 trimethylation and histone H2AK119 monoubiquitination. Numerous studies revealed that KDM2B has a central role in occurrences of colon, prostate and pancreatic cancer and leukemogenesis. In addition, KDM2B functions as a master regulator of a set of microRNAs that target several members of the Polycomb complexes PRC1 and PRC2 and its deregulation has important effects on PRC gene

expression in both normal and cancer cells. KDM2B has also been associated with inhibition of NF-κB/p65-dependent cellular apoptosis, by a mechanism where NF-κB upregulates KDM2B expression, resulting in the repression of c-FOS and the interception of apoptosis in human cancer cells. Moreover, KDM2B has been suggested to regulate genes of the glycolytic pathway and proteoglycan synthesis, as well as several other metabolic, antioxidant and pluripotency genes during morphogenesis and development.

The protein structure of the KDM2B includes at the N-terminal the JmjC domain that responsible for the histone demethylation reaction and at the C-terminal several leucine-rich regions (LRRs) and an F-box domain that participate in protein-protein interactions. In addition, KDM2B contains two Zn^{2+} finger motifs, CxxC and PHD (Plant homeodomain), located at the center of the amino acid sequence. There is strong structural interdependence between these domains that prevents either of the two from being produced independently in a stable form. The KDM2B CxxC finger has been implicated in the DNA binding and the recognition of non-methylated CpG DNA sequences, however the structural determinants responsible for this interaction remain unclear. As far as the KDM2B PHD finger is concerned, it is considered the facilitator of KDM2B interactions with chromatin, however there have been several conflicting arguments about the substrate specificity of this domain, and its precise role is still elusive. In the current thesis, we set out to elucidate the role of the two Zn^{2+} finger domains of KDM2B, CxxC and PHD, in order to improve our understanding, on a molecular level, of their involvement in the KDM2B function that would enable us to develop a high-throughput domain-specific inhibitor-screening assay for KDM2B.

Following this domain-wise approach, we cloned in a bacterial expression vector the CxxC-PHD coding sequence of the mouse KDM2B and the recombinant protein was submitted in a series of biochemical and biophysical assays. A series of side-directed mutageneses created several CxxC finger and PHD finger mutants that were used to identify the key residues involved in the interactions of these domains. Using electrophoresis mobility shift assays, we confirmed the Mg^{2+}- independent binding of mKDM2B to non-methylated CpG-containing DNA sequences and we identified residues R585, K608 and K616 as key players in this interaction. The mKDM2B mutants that contained point mutations of those residues showed up to 24-fold reduced DNA binding capacity. The identification of the structural elements in the CxxC finger of KDM2B that participate in the DNA binding mechanism enabled us to correlate its function with its biological role in replicative senescence bypass in MEFs. Furthermore, we examined the role of this domain in the process of cellular migration of prostate cancer cells, by employing *in vitro* wound healing assays. Our results showed that the overexpression of the mKDM2B that carried the K616A mutation failed to induce the

increased motility that was illustrated by the cells overexpressing the wild type KDM2B, suggesting that DNA recognition may be vital during metastasis and adhesion of cancer cells. With the view of our findings on the KDM2B CxxC finger, we aimed to develop a CxxC-targeting inhibitor screening by setting up a fluorescence-based assay that would provide a fast and easy way to assess the DNA recognition. The recombinant mKDM2B was fused with enhanced green fluorescent protein and a series of fluorescence resonance energy transfer experiments were designed. We managed to observe FRET between KDM2B-EGFP and DNA sequences that carried a Cy3 fluorophore, however, despite our best efforts, setting up a robust inhibitor-screening assay turned out to be unfeasible at that time due to several limitations set by the technical equipment.

As far as the KDM2B PHD finger is concerned, we employed the technology of MODified® Histone Peptide Array that enabled us to examine 384 unique histone modification combinations as possible interactors. We confirmed the previously reported interaction of the KDM2B PHD domain with H3K4me3 (K_D= 370 mM) and we revealed an unprecedented interaction with H4K20me3 (K_D= 3 mM) and a weaker interaction with H2B tail spanning from residues 1 to 19. The ability of KDM2B PHD finger to recognize a modification mark such as H3K4me3 that is associated with euchromatin, and H4K20me3 that is a hallmark of silencing in some cases and of cancer in others, supports vividly the notion that this demethylase has pleiotropic functions that depend on the temporal and spatial intracellular context. In addition, the relatively high K_D measured in the ITC experiments suggests that the overall binding of KDM2B with chromatin might be facilitated by additional interactions. Further investigation on the structural elements that participate in the histone recognition, illustrated that the phenylalanine residue (F654) that is placed in the expected active site of the PHD finger based on the *in silico* analysis, is not associated for this function, since the point-mutated protein successfully recognized H3K4me3 and H4K20me3, similarly to the wild type. Based on these results, we sought to investigated whether the substrate specificity of KDM2B PHD finger is similar to its sister protein, KDM2A. Comparative analysis of the MODified Histone Peptide Array results from both PHD fingers showed that KDM2A and KDM2B have different substrates, which is consistent with previous studies that have supported the idea of distinct and unrelated roles between these two demethylases.

As a conclusion, the characterization of the molecular interactions of the CxxC and PHD fingers of KDM2B that is presented in this thesis provides a more explicit idea of their role and contribution to the function of this significant epigenetic factor and creates contemporary paths for further research.

ΠΕΡΙΛΗΨΗ

Η λεπτή γραμμή μεταξύ φυσιολογικής και παθολογικής κατάστασης του κυττάρου δεν εξαρτάται μόνο από την αλληλουχία του DNA αλλά και από πολύπλοκους ρυθμιστικούς μηχανισμούς που προκύπτουν από χημικές τροποποιήσεις στις ιστόνες του DNA ή ακόμη και στο ίδιο. Παράγοντες αλληλεπίδρασης με το DNA ή/και τις ιστόνες, περιλαμβάνουν ειδικές πρωτεϊνικές επικράτειες που μεσολαβούν στην δημιουργία, αναγνώριση ή διαγραφή μιας ρυθμιστικής πληροφορίας. Η αποκρυπτογράφηση της πληροφορίας που βρίσκεται εγγεγραμμένη στην χρωματίνη, η διευκρίνηση του δυνητικού τους ρόλου των μετα-μεταφραστικών τροποποιήσεων σε καταστάσεις παθογένειας, η αναγνώριση των πρωτεϊνών που σχετίζονται με τις τροποποιήσεις αυτές καθώς και η κατανόηση του τρόπου λειτουργίας αυτών των πρωτεϊνών, αποτελούν πεδία έρευνας που συνεχώς εξελίσσονται. Επιτυχημένες προσπάθειες στην αναγνώριση επικρατειών που σχετίζονται με την μεθυλίωση και απομεθυλίωση των ιστονικών άκρων εισήγαγαν ένα ευρύ φάσμα μεθυλοτρανσερασών και απομεθυλασών που συντονίζονται χωρικά και χρονικά, οδηγώντας σε μια δυναμική κατάσταση του επιγενώματος, το οποίο επηρεάζει όχι μόνο τη δομή της χρωματίνης αλλά και τις φυσιολογικές λειτουργίες όπως την κυτταρική ανάπτυξη και τον κυτταρικό πολλαπλασιασμό, ενώ είναι επίσης συνδεδεμένο με αρκετές ανθρώπινες ασθένειες αλλά και με καρκίνο.

Έως τώρα, πάνω από 20 πρωτεΐνες εχουν ανακαλυφθεί να είναι υπεύθυνες για την αφαίρεση μεθυλομάδων από κατάλοιπα λυσίνης στα άκρα ιστονών και ταξινομούνται σε δύο υπεροικογένειες. Η οικογένεια της αμινοξειδάσης περιλαμβάνει απομεθυλάσες που απαιτούν FAD ως συμπαράγοντα και η οικογένεια των οξυγονασών που περιλαμβάνει πρωτεΐνες όπου η απομεθυλίωση, που εξαρτάται από α-κετογλουταρικό οξύ και δισθενή ιόντα σιδήρου (Fe^{2+}) και γίνεται από την Jumonji C επικράτεια. Στον ανθρώπινο οργανισμό, οι ειδικές για λυσίνης απομεθυλάσες χωρίζονται σε επτά οικογένειες (KMD1-7) και οι περισσότερες από αυτές παίζουν ρόλο κλειδί ως επιγενετικοί ρυθμιστές. Μερικές από αυτές απαρτίζουν στοιχεία περίπλοκων συμπλεγμάτων (π.χ. PRCs, NuRD, CoREST, MMLs) και συμμετέχουν στην πληθώρα φυσιολογικών κυτταρικών διαδικασιών (π.χ. μεταγραφή, αντιγραφή, επιδιόρθωση του DNA) μέσω διαφόρων μονοπατιών κυτταρικής σηματοδότησης (π.χ. Notch, TGF-β, FGF, NF-κB). Η απορύθμιση της έκφραση αυτών των πρωτεϊνών στον άνθρωπο είναι άμεσα συνδεδεμένη με μια πληθώρα περιπτώσεων κακοήθειας, λευχαιμιών, ανθρώπινης ογκογένεσης, αναδεικνύοντας ένα διττό ρόλο και ως ογκογονίδια και ως ογκοκατασταλτικά γονίδια.

Μια τέτοια περίπτωση είναι η ειδική για λυσίνης απομεθυλάση (KDM2B), η οποία σχετίζεται με το PRC1 σύμπλεγμα και στοχεύει τις τροποποιήσεις H3K36me2, H3K4me3 και H3K79me2/3. Η

KDM2B συμμετέχει στην καταστολή της έκφρασης γονιδίων που σχετίζονται με την κυτταρική γήρανση μέσω του PRC2 συμπλέγματος. Η απομεθυλάση αυτή συνδέει διάφορες τροποποιήσεις της χρωματίνης όπως την απομεθυλίωση της H3K36me2 με την τριμεθυλίωση της H3K27 και την ουβικουιτινιλίωση της H2AK119. Έρευνες έχουν δείξει ότι έχει κεντρικό ρόλο στην εμφάνιση καρκίνου στο παχύ έντερο, στον προστάτη και στο πάγκρεας, καθώς και σε διάφορες λευχαιμίες. Επιπλέον, η KDM2B λειτουργεί ως κεντρικός ρυθμιστής μιας ομάδας microRNAs τα οποία στοχεύουν μέλη των PRC1 και PRC2 συμπλόκων, έχοντας μεγάλη επίπτωση σε εκείνα τα γονίδια τόσο σε υγιή όσο και σε καρκινικά κύτταρα. Η KDM2B έχει συσχετιστεί με την αναστολή της NF-κB/p65-εξαρτώμενης κυτταρικής απόπτωσης μέσω ενός μηχανισμού όπου ο παράγοντας NF-κB προάγει την έκφραση της KDM2B, η οποία καταστέλλει τον παράγοντα c-FOS σε ανθρώπινα καρκινικά κύτταρα. Τέλος, η KDM2B έχει δειχθεί ότι ρυθμίζει γονίδια στο γλυκολυτικό μονοπάτι και στο μονοπάτι σύνθεσης πρωτεογλυκανών καθώς επίσης και μεταβολικά, αντιοξειδωτικά γονίδια και γονίδια που σχετίζονται με την πολυδύναμικότητα των κυττάρων κατά την μορφογένεση και την ανάπτυξη.

Η πρωτεϊνική δομή της KDM2B περιλαμβάνει στο αμινοτελικό άκρο την JmjC επικράτεια που είναι υπεύθυνη για την απομεθυλίωση και στο καρβοξυτελικό άκρο περιοχές πλούσιες σε λευκίνη και μια F-Box επικράτεια που συμμετέχουν στις αλληλεπιδράσεις της με άλλες πρωτεΐνες. Επιπλέον, η KDM2B διαθέτει δύο επικράτειες, τις CxxC και PHD, που προσδένουν δισθενή ιόντα ψευδαργύρου και οι οποίες βρίσκονται στο κέντρο της αμινοξικής αλληλουχίας. Έχει δειχθεί ότι υπάρχει ισχυρή δομική αλληλεξάρτηση μεταξύ αυτών των δύο επικρατειών η οποία αποτρέπει την απομόνωση έκαστης ανεξάρτητα σε σταθερή μορφή. Η CxxC επικράτεια έχει συσχετιστεί με την ικανότητα πρόσδεσης DNA και πιο συγκεκριμένα με την αναγνώριση μη μεθυλιωμένων αλληλουχιών που περιέχουν δινουκλεοτίδια κυτοσινης-γουανινης (CpG), ωστόσο, τα δομικά χαρακτηριστικά που είναι υπεύθυνα για αυτήν την αλληλεπίδραση παραμένουν αδιευκρίνιστα. Όσον αφορά, την PHD επικράτεια θεωρείται υπεύθυνη για τις αλληλεπιδράσεις της KDM2B με την χρωματίνη ωστόσο οι απόψεις διίστανται για το πια είναι η εξειδίκευσή της σε υποστρώματα και ποιος είναι ο ακριβής της ρόλος. Στην παρούσα διδακτορική διατριβή στοχεύσαμε να διαλευκάνουμε τον ρόλο αυτών των CxxC και PHD επικρατειών με στόχο να βελτιώσουμε την κατανόηση σε μοριακό επίπεδο της ανάμειξής τους στην λειτουργία της KDM2B το οποίο θα μας επέτρεπε να αναπτύξουμε ένα σύστημα εντοπισμού αναστολέων ειδικών για αυτές τις επικράτειες.

Για την μελέτη επικρατειών, κλωνοποιήσαμε σε βακτηριακούς φορείς έκφρασης την αλληλουχία που κωδικοποιούσε τις επικράτειες CxxC-PHD της KDM2B του ποντικού και η ανασυνδυασμένη πρωτεΐνη χρησιμοποιήθηκε σε μια σειρά από βιοχημικά και βιοφυσικά πειράματα. Μια σειρά από

μεταλλαξογενέσεις δημιούργησε μεταλλάγματα αυτών των επικρατειών τα οποία χρησιμοποιήθηκαν για την αναγνώριση των βασικών αμινοξέων που συμμετέχουν στις αλληλεπιδράσεις αυτών των επικρατειών. Επιβεβαιώσαμε την Mg^{2+}-ανεξάρτητη ικανότητα πρόσδεσης της KDM2B σε μη-μεθυλιωμένες DNA αλληλουχίες που περιείχαν CpG δινουκλεοτίδια και αναγνωρίσαμε τα κατάλοιπα R585, K608 και K616 ως βασικούς παίχτες αυτής της αλληλεπίδρασης. Οι πρωτεΐνες που περιείχαν μεταλλάξεις αυτών των αμινοξέων εμφάνιζαν μέχρι και 24 φορές μειωμένη ικανότητα πρόσδεσης DNA. Η αναγνώριση των δομικών στοιχείων της CxxC επικράτειας τα οποία συμμετέχουν στον μηχανισμό πρόσδεσης DNA, μας επέτρεψε να συσχετίσουμε την λειτουργία της με τον βιολογικό ρόλο στην διαδικασίας παράκαμψης της γήρανσης σε εμβρυικούς ινοβλάστες ποντικών. Επιπροσθέτως, εξετάσαμε τον ρόλο αυτής της επικράτειας αυτής στην διαδικασία της μετανάστευσης καρκινικών κυττάρων προστάτη. Τα αποτελέσματά μας έδειξαν ότι η υπερέκφραση της KDM2B η οποία έφερε την K616A μετάλλαξη απέτυχε να προκαλέσει την αυξημένη κινητικότητα που εμφάνιζαν τα κύτταρα που υπερέκφραζαν την αγρίου τύπου πρωτεΐνη υποδεικνύοντας πως η αναγνώριση του DNA να είναι σημαντική για την μετανάστευση και προσκόλληση καρκινικών κυττάρων. Με βάση αυτά τα δεδομένα σχεδιάσαμε ένα σύστημα εντοπισμού αναστολέων βασισμένο στο φθορισμό το οποίο θα μας παρείχε έναν γρήγορο και εύκολο τρόπο αξιολόγησης της αναγνώρισης DNA από την CxxC επικράτεια. Η ανασυνδυασμένη πρωτεΐνη συντήχθηκε με πράσινη φθορίζουσα πρωτεΐνη και σχεδιάστηκε μια σειρά από πειράματα στηριζόμενα στην τεχνική της μεταφοράς ενέργειας μέσω συντονισμού (FRET). Καταφέραμε να παρατηρήσουμε το φαινόμενο FRET κατά την πρόσδεση της ανασυνδυασμένη πρωτεΐνης με DNA αλλουλουχιες που έφεραν το κατάλληλο φθοροφόρο, ωστόσο παρόλες τις προσπάθειές μας, η δημιουργία ενός επιτυχούς συστήματος εντοπισμού αναστολέων αποδείχθηκε αδύνατη λόγω περιορισμών από τον τεχνικό εξοπλισμό.

Όσον αφορά την KDM2B PHD επικράτεια χρησιμοποιήσαμε την τεχνολογία MODified® Histone Peptide Array, η οποία μας επέτρεπε να εξετάσουμε 384 μοναδικούς συνδυασμούς από τροποποιήσεις ιστονών ως πιθανούς προσδέτες της. Επιβεβαιώσαμε την αλληλεπίδραση της PHD επικράτειας με την H3K4me3 τροποποίηση και αποκαλύψαμε μια πρωτοφανή αλληλεπίδραση με την H4K20me3 καθώς και μια πιο αδύναμη αλληλεπίδραση με την ουρά της H2B που περιλάμβανε τα αμινοξέα 1-19. Η ικανότητα της PHD επικράτειας να αναγνωρίζει μια τροποποίηση όπως τη H3K4me3, η οποία σχετίζεται με ευχρωματίνη και την H4K20me3, η οποία είναι σηματοδότης γονιδιακής σίγασης σε κάποιες περιπτώσεις και καρκίνου σε άλλες, στηρίζει επαρκώς την ιδέα ότι αυτή η απομεθυλάση έχει ποικιλότροπες λειτουργίες οι οποίες εξαρτώνται από το χωρικό και χρονικό ενδοκυτταρικό πλαίσιο. Ακόμα, η σχετικά υψηλή σταθερά διάσπασης που μετρήθηκε στα ITC

πειράματα υποδεικνύει ότι η συνολική πρόσδεση της KDM2B με την χρωματίνη διεκπεραιώνεται από περισσότερες αλληλεπιδράσεις. Επιπλέον, ερεύνα πάνω στα δομικά στοιχεία τα οποία συμμετέχουν πάνω στην αναγνώριση των ιστονών παρουσίασε πως το κατάλοιπο της φαινυλαλανίνης (F654), το οποίο βρίσκεται στο ενεργό κέντρο της PHD επικράτειας σύμφωνα με την *in silico* ανάλυση, δεν σχετίζεται με αυτήν την λειτουργία καθώς η πρωτεΐνη που έφερε μεταλλαγή στο συγκεκριμένο κατάλοιπο αναγνώρισε τις δύο προαναφερθείσες τροποποιήσεις παρόμοια με την αγρίου τύπου πρωτεΐνη. Τέλος, εξετάσαμε εάν η εξειδίκευση σε υποστρώματα που έχει KDM2B PHD επικράτεια είναι η ίδια με εκείνη της αδελφής της, της KDM2A. Συγκριτική ανάλυση των αποτελεσμάτων για τις δύο PHD επικράτειες έδειξε ότι αναγνωρίζουν διαφορετικά υποστρώματα και το οποίο συνάδει με προηγούμενες μελέτες που υποστηρίζουν ξεχωριστούς ρόλους για αυτές τις δύο απομεθυλάσες.

Εν κατακλείδι, ο χαρακτηρισμός των μοριακών αλληλεπιδράσεων των CxxC και PHD επικρατειών της KDM2B, ο οποίος παρατίθεται σε αυτήν την διδακτορική διατριβή παρέχει μια πιο ευκρινή εικόνα του ρόλου τους και της συνεισφοράς τους στην λειτουργία αυτού του σημαντικού επιγενετικοί παράγοντα και δημιουργεί νέα μονοπάτια για περαιτέρω έρευνα.

CONTENTS

Chapter 1

Introduction

1.1.Chromatin Structure

The DNA of an eukaryotic cell is orders of magnitude larger than its nucleus. However, its ability to condense enables it to fit easily inside it. This process derives from multiple sets of spatial and temporal packaging events that push chromatin into forming higher level structures. The process begins with DNA interacting with a set of proteins, histones. There are four core histones (H2A, H2B, H3, H4) which are recruited in pairs, forming an octamer. The amino acid sequences of the histones, including the N-terminal tails, are highly conserved from *S. cerevisiae* to human. The positively charged histones are attracting the negatively charged DNA, and this structure that contains a 146-base pair DNA fragment and one histone octamer, the nucleosome, is stabilized under the action of a histone protein, H1 (*Figure 1.1*). Series of nucleosomes are set in a helical layout that forms stacked layers. This structure is attributed to molecular interactions between the N-terminal tails of histones that extend away from the octamer cores as well as to H1. The folding of these nucleosomal fibers into loops further condenses the DNA. Finally, the loops packed to the maximum degree with the help of protein scaffolds, thus forming a structure known as chromosome (*Figure 1.2*) (Strayer, Biochemistry, Volume I, Chapter 31, 983-386; Lewis, Genes VII, 567-9).

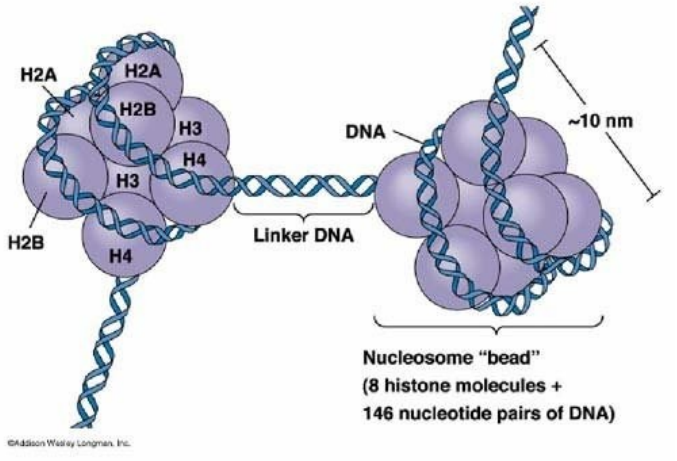

Figure 1.1. Schematic representation of the nucleosome structure. The two strands of DNA are wrapped around the histone octamer forming the basic unit of chromatin, the nucleosome. Adapted by Addison Wesley Longman (1999).

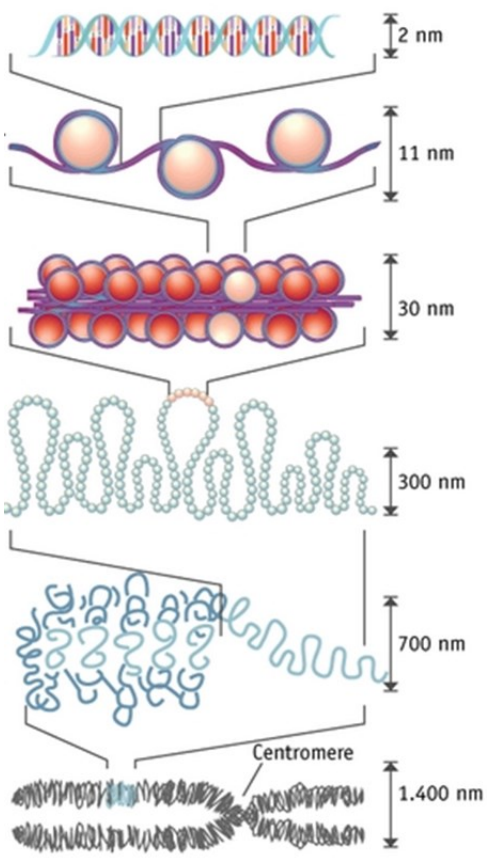

Figure 1.2. Schematic representation of the chromatin structure. Adapted by Felsenfeld & Groudine (2003).

The role of the packaging of the eukaryotic genome is directly related to the regulation of gene expression (Brink et al., 2006). The open state of chromatin, i.e. the regions where DNA is accessible to transcription factors and the RNA polymerase, describe the euchromatin while the regions of the genome that do not facilitate the onset of transcription describe heterochromatin (Kwon et al., 1994; Reyes et al.,

2002). The transition from one state to the other is the basic feature of the potential of gene expression in eukaryotic organisms, and is due to forces acting on the structure of the nucleosome (Horvath et al., 2001; Liu et al., 2003). Eukaryotic cells handle the expression of their genes with greater complexity than prokaryotic organisms. Cells in multicellular organisms must have full control of the start, end and duration of gene expression. This control is the result of the endogenous cellular state and its successful interactions with the environment. Gene regulation describes the collaboration between a particular part of the genome, the gene, the transcription factors or other regulatory factors that determine the fate of this gene. (Campbell, Biology, 2nd edition, p. 377-8). These players recognize specific patterns in both the sequence and structure of chromatin, and a great effort has been put to locate these regulatory element motifs, in order to elucidate gene regulation (Caselle et al., 2002).

1.2. Post –Translational Modifications (PTMs)

Over the last quarter century, studies focused on plant, mammalian and other eukaryotic cell gene regulation have proven its mere complexity. Covalent modifications on the N-terminal tails of histones, broadly known as post-translational modifications (PTMs), seem to play a crucial role in the process as well as in the chromatin structure (Strahl and Allis, 2000) and in a variety of other processes like DNA replication, and DNA damage (Murr, 2010). PTMs exist also on the histone cores, but we know little about the impact they have on gene expression (Zhang et al., 2010). Up until now, almost 15 different classes of modifications (such as methylation, acetylation, phosphorylation, ubiquitination, etc) have been documented (Zhao & Garcia, 2015) on specific histone residues, affecting dynamically the DNA interactions with histones as well as with other non histonic proteins (Kourazides, 2007) (*Figure 1.3*). For example, residues H3K4, H3K9, H3K27, H3K36, H3K79 and H4K20 can be mono-, di- and tri- methylated, with each methylation state representing a specific epigenetic mark with a specific biological meaning (Margueron et al., 2005). H3K4, H3K36,

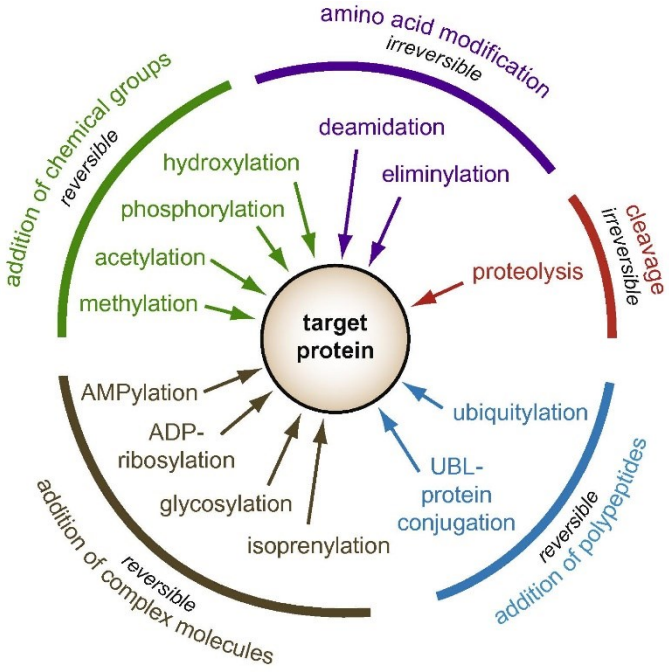

Figure 1.3. Post-translational modifications on proteins. Adapted by Ribet & Cossart (2010)

and H3K79 are markers of actively transcribed genes, whereas H3K9, H3K27 and H4K20 are frequently found in promoters of repressed genes (Bhaumik et al., 2007). Furthermore, the plethora of these PTMs and the cross-talk between them, can result in a combinatorial outcome, not fully understood even nowadays. Deciphering this "histone code" (Strahl & Allis, 2000; Fischle et al., 2005) that is written on chromatin with these PTMs, identifying the army of proteins that catalyze them (Grant, 2001), elucidating their potential role in pathological cellular states, like cancer (Feinberg, 2004) and understanding the way of function of those key player proteins that associate with them, using ChIP-seq analysis and other biochemical methods (Li & Li., 2012; Rothbart and Strahl, 2014), has become an exponentially growing field of research.

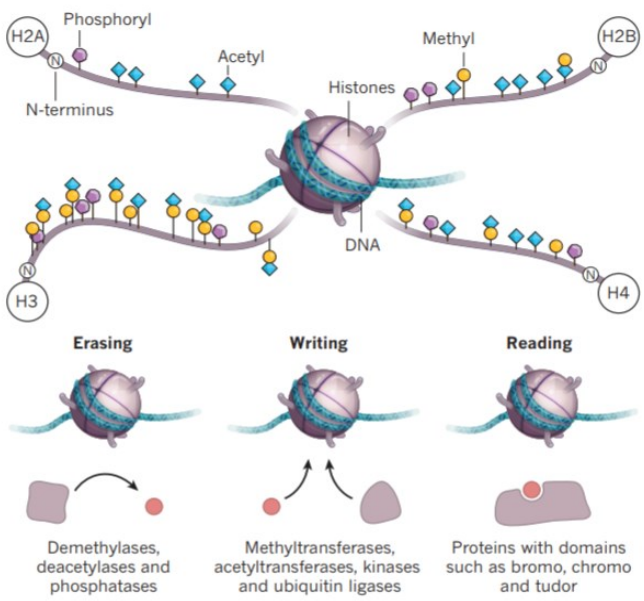

Figure 1.4. The molecular interactions of the 'histone code'. The PTMs on histone tails exist under a dynamic state as they are created by writers, removed by erasers and recognized by readers during gene regulation. Adapted by Helin & Dhanak (2013)

Based on their effect, three models have been proposed for the effect of PMTs on histones. The most important element of the histone code is the communication between the modifications. Histone modifications do not occur separately but in a combinatorial manner whereby any set of them near a regulatory region of a gene may have a different effect on the chromatin structure and thus on gene expression (Wang et al., 2008). Some modifications may promote the formation or removal of some others in the same (*cis* action) or different (*trans* action) histone (Murr, 2010). The proteins that interact with these PTMs are divided into three major categories: the "writers" who place the modifications, the "erasers" that remove them and the "readers" that recognize and regulate the gene expression (Berger, 2002; Taverna et al., 2007, Helin & Dhanak, 2013) (*Figure 1.4*). Some of these chromatin traits, like methyl marks on histone residues, specifically lysine and arginine, were considered irreversible epigenetic marks until histone demethylases emerged into the scenery. As a result, a more complex pathway of chromatin epigenetic regulation was suggested, thus reshaping the common belief of a predestined gene expression pattern derived from the histone methylation status (Bannister and Kouzarides, 2005; Agger et al. 2008). Successful efforts on identifying readers and writers of the methyl mark introduced an broaden spectrum of methyl transferases and demethylases that coordinate spatially and temporally, resulting in a dynamic

epigenome that affects not only chromatin structure but physiological cellular functions such as proliferation, aging and development (Lachner et al., 2003; Margueron et al., 2005; Dimitrova et al., 2015) and is also interconnected with several human diseases (Shi & Whetstine, 2007) and cancer (Lizcano & Garcia, 2012).

1.3. Lysine specific demethylases (KDMs)

Since the identification of the first protein with histonic demethylase activity, several studies have followed identifying and elucidating the function of these molecules in cellular processes. Up until now, more than 20 proteins have been found being able to remove methyl groups from lysine residues on histone tails and they are classified into two superfamilies based on the nature of their catalytic reaction. One superfamily is the amine oxidase superfamily, which includes demethylases that require FAD as co-factor, while the Jumonji C (JmjC)-containing superfamily (oxygenase superfamily) consists of proteins of which the demethylase activity is dependent on α-ketoglutarate and Fe^{2+} Lizcano & Garcia, 2012) (*Figure 1.5*).

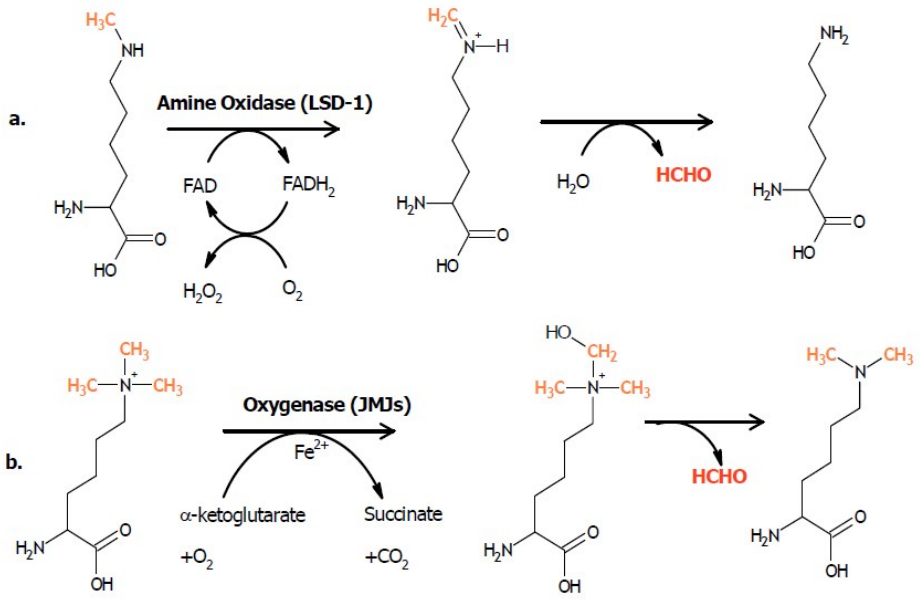

Figure 1.5. Mechanism of demethylation. (a) Proteins with FAD-dependent demethylase activity target mono- and dimethylated forms of modified residues. (b) Demethylases with oxygenase activity are able to act also on the quaternary form of a methylated amine. Adapted from Lizcano & Garcia (2012).

Most of these demethylases have been addressed as key epigenetic regulators during physiological cellular processes (Lan et al., 2008) but also as participants in numerous cases of cancer, leukemia and human tumorigenesis, resulting in constant efforts being made to elucidate their way of function in order to identify potential inhibitors of these proteins (Jambhekar et al., 2017; Janardhan et al.,

2018). Previous studies have examined the evolutionary relationship between JmjC domain-containing proteins as well as the interplay of enzymatic activities within this epigenetic modification system in human (Klose et al., 2006a; Tsukada & Zhang, 2006), while most recently significant progress has been made to unravel the role of the Jmj-containing proteins in maize (Qian et al., 2019). In human, the KDMs can be divided into seven families (KDM1-7), and all protein members have distinct roles (*Figure 1.6*).

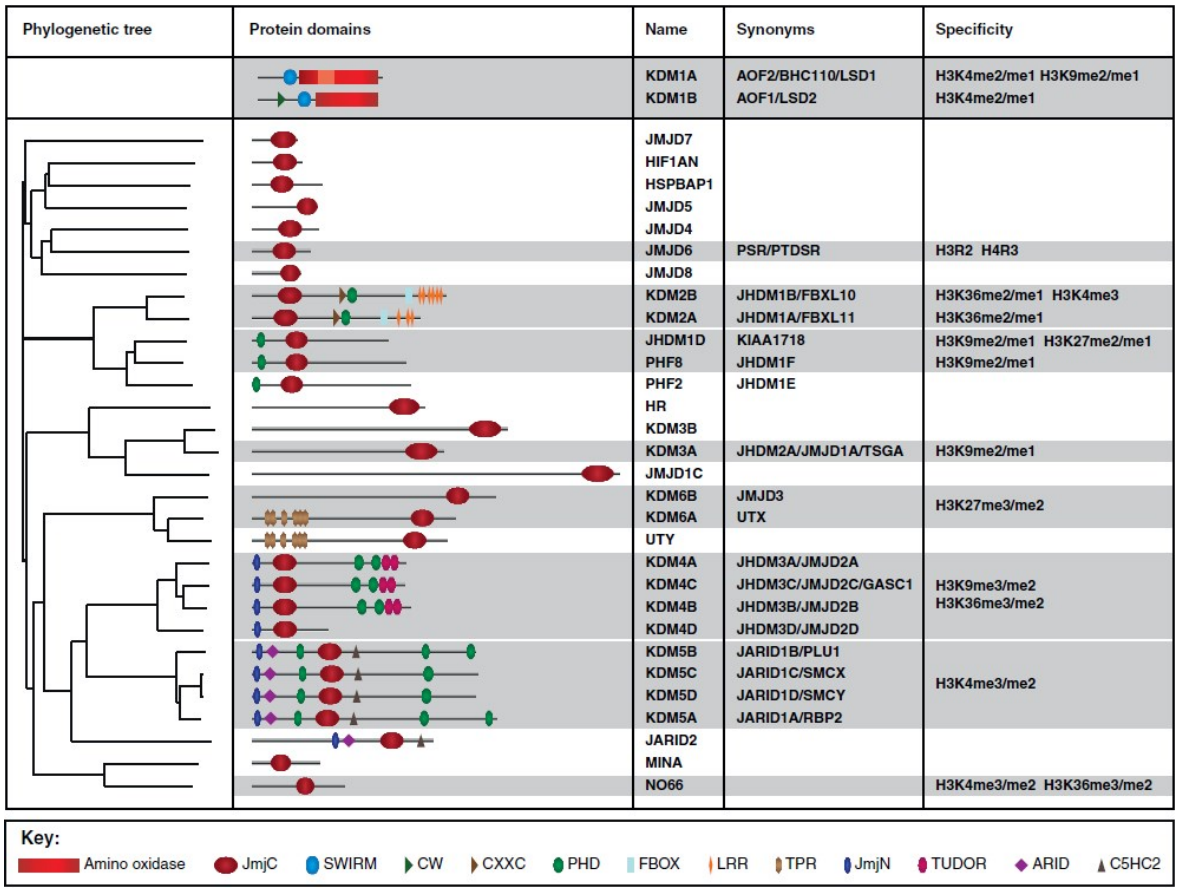

Figure 1.6. Classification of Lysine specific demethylases. The lysine specific demethylases are divided into seven families (KDM1-7) based on their phylogenetic origin. Adapted from Pedersen & Helin (2010)

1.3.1. The KDM1 family

KDM1A demethylates lysine 4 of histone H3 and acts as a component of the CoREST complex promoting histone acetylation (Shi et al., 2005; Yang et al., 2006). It plays an essential regulatory role during cellular differentiation and organ development (Choi et al., 2010; Sun et al., 2011) as well as associates with determination of ESCs cellular fate (Adamo et al., 2011). LSD1 in cooperation with HDAC1 promote repression inflammatory-associating genes (Janzer et al., 2012) while association with JMJD2C/KDM4C (Kahl et al., 2006) and JMJD2A/KDM4A (Kauffman et al., 2011)

implicates LSD1 in the development of prostate and bladder cancer, respectively. Furthermore, recent studies have shown high levels of LSD1 in several cases of cancer, such as neuroblastoma (Schulte et al., 2009), breast cancer (Lim et al., 2010), leukemia (Li et al., 2012), Ewing's sarcoma (Bennani-Baiti et al., 2012) and lung cancer (Lv et al., 2012). On the other hand, as part of the Mi-2/nucleosome remodeling and deacetylase (NuRD) complex, LSD1 has been shown to suppress metastatic potential of breast cancer cells in vivo (Wang et al., 2009), indicating a rather more complex function. Further research on the crystal structure of LSD1/KDM1A shed light on the steric requirements for substrate specificity of most Jumonji-containing histone demethylases (Anand & Marmorstein, 2007).

LSD2/KDM1B is another member of the FAD-dependent demethylases family, with H3K4me1 and H3K4me2 substrate specificity and is not associated with CoREST or NuRD complexes like its homolog, LSD1 (Karytinos et al., 2009; Fang et al., 2010). On the other hand, KDM1B has been shown to associate with NF-κB, regulating inflammatory genes (Van Essen et al., 2010). Furthermore, KDM1B is highly expressed in growing oocytes and facilitates the maternal genomic imprints, establishing H3K4me0-depedent DNA methylation during oogenesis (Ciccone et al., 2009). In addition, KDM1B has been associated with the indirect regulation of reprogramming genes like Nanog, Oct4 and Sox2, being an epigenetic key player in the induced pluripotent stem cells (iPSCs) generation process. (Lin et al., 2011).

1.3.2. The KDM2 family

The lysine specific demethylase 2A (KDM2A), and the mammalian paralog KDM2B, are evolutionarily conserved and ubiquitously expressed members of the JmjC-domain-containing histone demethylase family. KDM2A targets H3K4me3 (Gao et al., 2013) and H3K36me3 (Dhar et al., 2014; Tanaka et al., 2014) and regulates cell proliferation and arrest cell cycle progression at the G1/S-phase in human stem cells from apical papilla (SCAPs) through histone demethylation on ink4b and Kip1 genes that encode p15 and p27, respectively (Gao et al., 2013). KDM2A binds to numerous CpG-rich promoters via its CxxC-PHD domains recruiting more than 90 nuclear factors that are involved in replication, ribosome synthesis, and mitosis (Iuchi et al., 2019). A study by Zhou *et al.* (2012) showed that the KDM2A PHD finger does not play a direct or indirect role in the interaction with DNA since destabilization of the PHD finger by replacing one of the structural cysteine residues did not reduce the efficiency of DNA binding attributed to the KDM2A CxxC finger. KDM2A is highly active during mitosis when it participates in with the transcriptional repression of small non-coding RNAs that are present at the centromere of chromosomes, thus promoting the heretochromatin

state (Frescas et al., 2008). In addition, this demethylase interacts directly with the Heterochromatin Protein 1 (HP1) that occupies repressed genes and is able to anchor HP1 in H3K9me3- modified chromatin, thus maintain gene silencing (Borgel et al., 2017). Other non-histonic interactions, by targeting directly developmental proteins, such as Wtn during early embryogenesis in *Xenopus*, and demethylates lysine residues of NF-kB p65 subunit or β-catenin in mouse embryonic fibroblasts, suggesting a more elaborative role (Lu et al., 2015, Lu et al 2010). KDM2A has been associated with human breast cancer by regulating genes such as JAG1, HOTCH1 and HEY1 in the Notch signaling pathway in a JmjC-dependent manner (Chen et al., 2016). Full length KDM2A is able to reduce ribosomic RNA (rRNA) transcription in a JmjC and CxxC- dependent manner in triple-negative breast cancer cells (Okamoto et al., 2019) and in human breast adenocarninoma cells (Tanaka et al., 2014). However, it has been shown that the short form of KDM2A, that lacks the JmjC domain directly induces trnascription by binding to ribosomal RNA gene promoters and activate transcription (Okamoto et al., 2017) or indirectly by occupying H3K36me2-modified pericentromeric regions, averting full length KDM2A to remove the mark (Lađinović et al., 2017).

KDM2B (also known as Fblx10, Ndy1, and Jhdm1b) is a lysine-specific histone demethylase that targets H3K36me2 (He et al., 2008; Tzatsos et al., 2009), H3K4me3 (Tzatsos et al., 2009, Janzer et al., 2012) and H3K79me2/3 (Kang et al., 2018). KDM2B is a major PRC1-associated factor and a bona fide oncogene (Pfau et al., 2008; He et al., 2008; Tzatsos et al., 2009; He et al., 2011). The role and function of KDM2B is discussed extensively in paragraph 1.4.

1.3.3. The KDM3 family

JMJD1A/ KDM3A is a histone demethylase specific for H3K9me1 and H3K9me2 (Yamane et al., 2006). KDM3A is key epigenetic factor in germ cell lines, regulating expression of cAMP-response element modulator- associated genes, like Tnp1 and Prm1, which are involved in chromatin condensation (Okada et al., 2007; Liu et al., 2010). Furthermore, KDM3A has been associated with regulation of metabolic genes in muscle and adipose cells (Inagaki et al., 2009; Tateishi et al., 2009) and it also, similarly to KDM1A, regulates self-renewal in ESCs (Loh et al., 2007) and tumorigenic growth (Krieg et al., 2010). There are two KDM3A homologues, JMJD1B/ KDM3B and JMJD1C/ KDM3C, although there has been no evidence suggesting demethylase activity.

1.3.4. The KDM4 family

JMJD2A/KDM4A indicates demethylase activity on H3K9me3/me2 and H3K36me3/me2 (Klose et al., 2006b) and also on H1.4K26me3/me2 (Trojer et al., 2009). KDM4A is a key epigenetic regulator of proliferation genes and interacts with chromatin-modifying and cell cycle regulator proteins (Gray et al., 2005).Furthermore, KDM4A is associated with skeletal muscle cell differentiation (Verrier et al., 2007), self-renewal of ESCs (Loh et al., 2007), and DNA damage repair (Mallete et al., 2012). Moreover, high expression levels of KDM4A have been found is several cancer cases, such as prostate cancer (Chen et al., 2010), breast cancer (Li et al., 2011), colon cancer (Kim et al., 2012), and bladder cancer (Kauffman et al., 2011), suggesting a vital role in tumorigenesis.

Very few is known about the function of JMJD2B/KDM4B. It has been identified as possible oncogene since amplification of KDM4B and JMJD2C/KDM4C genes has been detected via genomic analysis in several medulloblastoma cases (Ehrbrecht et al., 2006) and also ectopic expression of KDM4B and KDM4C decreases H3K9me3/me2 levels, delocalizes HP1 and reduces heterochromatin in vivo (Cloos et al., 2006).

The JMJD2C/KDM4C has showed oxygenase activity with the capacity to demethylate H3K9me3/me2 marks (Cloos et al., 2006). KDM4C has also been involved in the regulation of self-renewal process and the cellular fate of undifferentiated ESCs (Loh et al. 2007) and the regulation of adipogenesis (Lizcano et al., 2011). Furthermore, studies have shown that hypoxia-inducible factor (HIF)-1α regulates the expression levels of KDM4C, along with other lysine demethylases, as a response to a hypoxic signal (Pollard et al., 2008). Similarly, to KDM4B, genetic analysis in several different cancer cases, such as sarcomatoid carcinomas (Italiano et al., 2006) and Mucosa-associated lymphoid tissue (MALT) lymphomas (Vinatzer et al., 2008), mediastinal B-cell lymphomas (PMBL) and Hodgkin lymphomas (HL) (Rui et al., 2010) have been associated with the amplification of the KDM4C gene, suggesting a vital oncogenic role. This function as oncogene has also been supported by the elevated expression levels of KDM4C in cases of desmoplastic medulloblastoma (Ehrbrecht et al., 2006), breast carcinomas (Liu et al., 2009; Wu et al., 2012) and glioblastoma (Haque et al., 2011).

JMDJ2D/KDM4D, like the other members of that family, demethylates via the JmjC domain, specifically the H3K9me3 and H3K9me2 repressive marks (Chen et al., 2006). By associating with Cdc45, proliferating cell nuclear antigen (PCNA) and DNA polymerase δ during S phase, a KDM4D-dependent DNA replication mechanism has been proposed, where demethylation of H3K9me3 mark resulted in the recruitment of the pre inition complex at transcription starting sites (Wu et al. 2017). Furthermore, it has been shown that KDM4D carries two distinct regions with a RNA binding

capacity. Interestingly, one of the two regions is located in the JmjC domain, revealing an unprecedented function for this domain (Zoabi et al., 2014).

1.3.5. The KDM5 family

JARID1A/KDM5A demethylates specifically H3K4me2 and H3K4me3 marks (Christensen et al. 2007) and as part of the Notch–RBP-J repressor complex, KDM5A has shown a vital regulatory key in Notch-associated cellular growth (Liefke et al., 2010). KDM5A is regulated by miR-132, during light response and participates in the fine-tuning of the mammalian and Drosophila circadian clock in a demethylase-independent manner (Alvarez-Saaverda et al., 2011; DiTacchio et al., 2011). KDM5A, as well as KDM5B, has indicated a tumor suppressing role, by promoting the demethylation- dependent silencing of genes regulated by retinoblastoma (Rb) in senescent cells (Chicas et al., 2012). On the contrary, there is evidence of KDM5A overexpression in gastric cancer (Zeng, J. et al., 2010) and gene amplification in acute leukemia cases (Van Zutven et al., 2006), suggesting a possible oncogenic role for KDM5A.

The JmjC domain of JARID1B/KDM5B manifests the same substrate specificity as KDM5A, removing the di- and trimethyl mark of lysine 4 on histone H3 (Yamane et al., 2007). KDM5B has been found to interact with several Polycomb proteins, thus participating in gene silencing (Lee et al., 2007b). KDM5B plays an essential regulatory role, through H3K4 demethylation, in cell development and proliferation (Dey et al., 2008) and also is regulated by miR-134 during ESCs differentiation (Tarantino et al., 2010) and neural lineage differentiation (Schmitz et al., 2011). Studies have confirmed high expression levels and a significant regulatory role of KDM5B in breast cancer cells, with the protein localized in discrete foci inside the nucleus, through its DNA-binding domain and PHD/LAP fingers (Lu et al., 1999; Yamane et al., 2007; Barrett et al. 2007), as well as in testicular cancer cells (Liggins et al., 2010) and prostate cancer cells (Xiang et al., 2007b). On the other hand, KDM5B is has been shown to participate in TGF-β signaling, via interaction with TIEG1/KLF10, which suggests a possible role in suppressing tumorigenesis (Kim et al., 2010). Furthermore, KDM5B regulates proliferation and apoptosis of acute promyelocytic leukemic (HL-60) cells by promoting the p27 expression and suppressing c-myc expression, via its demethylase activity (Wong et al., 2012).

JARID1C/KDM5C recognizes the H3K9me3 mark via its PHD finger, and catalyzes H3K4 demethylation during transcriptional repression (Iwase et al., 2007). It was initially identified as partner of the REST complex, promoting gene repression and resulting to the X-linked mental

retardation (Jensen et al., 2005; Tahiliani et al., 2007; Abidi et al., 2008), and later on it implicated to brain function-associated gene regulation and cognitive development (Adegbola et al., 2008; Jensen et al. 2010). The H3K4me3 demethylase activity of KDM5C has been shown to play a vital role in VHL-suppressed clear cell renal cell carcinoma (CCRCC), in which KDM5C acts as tumor suppressor gene, and alterations in expression or mutation can lead to tumorigenesis (Niu et al., 2012). As an oncogene, KDM5C has also been implicated in cervical cancer, as target of the human papillomavirus (Smith et al., 2010).

1.3.6. The KDM6 family

UTX/KDM6A catalyzes in a highly specific manner (Hong et al., 2007; Sengoku & Yokoyama, 2011) the demethylation of mono- and di-methylated forms of lysine 27 in histone H3 and is also part of the mixed lineage leukemia complexes MLL3 and MLL4, promoting gene activation via H2A ubiquitination (Lee et al., 2007a). It has been associated with regulation of tissue-specific chromatin changes that result in specific gene expression and cellular differentiation, such as myogenesis (Seenundun et al., 2010) brain (Xu et al., 2011) and cardiac development (Lee et al., 2012), spermatozoa maturation (Yap et al., 2011) and hematopoiesis (Thieme et al., 2013). Disruption of the physiological function of KDM6A in these processes, in cases where Rb was included, resulted in tumorigenesis, indicating an essential tumor suppression role for this enzyme. On the other hand, high expression levels of KDM6A have been documented in several tumors and malignancies, such as renal cell (Dalgliesh et al., 2010) and bladder carcinomas (Gui et al., 2011), multiple myeloma (Van Haaften et al., 2009; McDevitt et al., 2012), acute lymphoblastic (Mar et al, 2012) and chronic myelomonocytic leukemias (Muramatsu et al. 2012), suggesting a dual role as TGS and as oncogene.

JMJD3/KDM6B, like its sister demethylase KDM6A, illustrates a narrow substrate specificity for the trimethylated form of lysine 27 on histone H3 (Xiang et al., 2007a; Hong et al., 2007), and has been shown to be significantly upregulated in prostate cancer cells, accompanied with a genome-wide depletion of H3K27me3 mark (Xiang et al., 2007b). Participating as a component in the MLL complexes, it antagonizes the activity of the repressive Polycomb proteins (Lee et al., 2007a; Dahle et al., 2010), thus suggesting an epigenetic role in cellular differentiation. Studies have shown that KDM6B regulates the bone marrow cells differentiation to M2 macrophages via Irf4 in a JmjC-dependent manner (Satoh et al., 2010), or to osteoclasts through NF-κB (Yasui et al.,2011). Furthermore, KDM6B has been associated indirectly with regulation of endothelial lineage committed genes, since silencing of KDM6B resulted in apoptotic and senescent proangiogenic cells

and reduction of the expression levels of endothelial nitric oxide synthase (eNOS),which facilitates endothelial commitment (Ohtani et al., 2011). In addition, KDM6B-derived faulty enrichment of H3K27me3 mark at the promoter of hematopoietic progenitor kinase 1 (HPK1) resulted in T cell overactivation and B cell overstimulation in CD4+ cells of systemic lupus erythematosus. Moreover, elevated expression levels of KDM6B have been found in colon cancer cells (Periera et al., 2011), and Hodgkin's lymphoma (Anderton et al., 2011). As far as its tumor suppressing role, studies have shown that KDM6B in mouse embryonic fibroblasts (MEFs) can be induced by RAS-RAF signaling pathway and demethylates ink4a-Arf promoter, causing p16-p19 dependent arrest and thus inducing cellular senescence (Agger et al., 2009; Barradas et al., 2009; Martinelli et al., 2011).

1.3.7. The KDM7 family

JHDM1D/ KDM7A catalyzes the demethylation of both H3K9me2/me1 and H3K27me2/ me1 marks (Tsukada et al., 2010), acting as transcriptional activator, since these modifications are correlated with silenced genes (Bannister et al., 2002). KDM7A has been associated with brain development by regulating the follistatin – TGF-β axis (Tsukada et al., 2010) and with regulation of neural differentiation through activation of FGF-4 (Huang et al., 2010) as well as with regulation of angiogenesis acting as suppressor of tumor development and progression under starvation conditions (Osawa et al., 2011).

PHF8/KDM7B also possesses H3K9me2/me1 demethylase activity and it was initially identified as key player in the development of X-linked mental retardation and cleft lip/cleft palate formation (Laumonnier et al., 2005; Abidi, et al., 2007). KDM7B and KDM7A and KDM7C (the last member of this family) harbor a similar PHD finger, which recognizes and binds to H3K4me3, resulting in an antagonistic status between these two demethylases in cases of combinatorial readout of multiple cis-modifications (Horton et al., 2010; Shi et al., 2014). In addition, KDM7B has been implicated in hypoxia- induced prostate cancer, where high expression levels of KDM7B upregulate HIF1a and HIF2a, resulting in an AR-dependent prostate cancer progression. Furthermore, KDM7B has been associated also with breast cancer, by regulating deubiquitinase USP7, which under a positive feedback loop upregulated KDM7B and cyclin A2, resulting in cellular proliferation (Wang et al., 2016). KDM7B also has been found to interact with acetyltransferase TIP60 forming a chromatin modification complex, that activates the expression of Arc, thus regulating neuronal-specific genes (Oey et al., 2015).

PHF2/KDM7C was identified as tumor suppressor gene in studies associating with chromosomal alterations during head and neck squamous cell carcinoma (HNSCC) development (Ghosh et al., 2012) as well as in colon and stomach cancers in a p53/p21- dependent manner (Lee et al., 2015). KDM7C has been found to demethylate specifically H3K9me2 in promoters of rDNA, indicating vital regulatory role (Wen et al., 2010). Studies have supported the multiple interactions of KDM7C with other regulatory elements, such as CCATT/enhancer binding proteins α and δ (C/EBPα and C/EBPδ), suggesting a direct role in adipogenesis (Okuno et al., 2013; Lee et al., 2014) and in CCRCC development (Lee et al., 2017; Park et al., 2017). In addition, strong interplay between KDM7C and transcription factor Arid5b has been shown participate in the regulation of many Sox9 target genes, during skeletal development (Hata et al., 2013).

1.4. A deeper look into lysine specific demethylase 2B

1.4.1. KDM2B is a novel oncogene

Following its identification as an oncogene that is activated by provirus insertion in Moloney Murine Leukemia Virus (MoMuLV)-induced rodent lymphomas, it was demonstrated that KDM2B promotes the immortalization of mouse embryo fibroblasts (MEFs) by allowing them to bypass replicative senescence (Pfau et al., 2008). This is the result of the binding of KDM2B to the Ink4a-Arf-Ink4b locus, which, combined with PRC2 recruitment, represses the senescence-associated induction of the p15Ink4b (He et al., 2008), p16Ink4a and p19Arf proteins (Tzatsos et al., 2009). Subsequent studies revealed that KDM2B has a central role in epigenetic regulation and cancer. In leukemic stem cells, modulation of the levels of p15Ink4b by KDM2B regulates cell proliferation and self-renewal (He et al., 2011). Furthermore, KDM2B has been linked to acute myeloid leukemia (AML) as its knock-down impairs MLL-AF9-induced leukemogenesis and affects primary patient-derived acute myeloid leukemia cell growth in mice (Van den Boom et al., 2016).

KDM2B functions by coupling several chromatin modifications, including histone H3K36me2 demethylation, with histone H3K27 trimethylation and histone H2AK119 monoubiquitination. H3K27 trimethylation is due to the KDM2B-dependent upregulation of EZH2, along with the KDM2B-dependent binding of EZH2 to the promoters of a subset of target genes which are regulated in concert by EZH2 and KDM2B (Tzatsos et al., 2009; Kottakis et al., 2011). The binding of EZH2 to the promoters of these genes depends on the demethylase activity of KDM2B and the concerted binding of the two is required for transcriptional repression (Kottakis et al., 2011). Following DNA binding, the variant PRC1 complexes monoubiquitinate histone H2A at K119. This

monoubiquitination event is the signal for the recruitment of PRC2 and histone H3K27 trimethylation via EZH2, the catalytic component of PRC2 (Blackledge et al., 2014). Through this mechanism, KDM2B is involved in many tumors and human carcinomas (Kottakis et al., 2011; Zacharopoulou et al., 2018a; Zacharopoulou et al., 2018b).

In bladder cancer, KDM2B is induced by FGF2 and promotes in concert with EZH2, the establishment of EMT, cell migration, invasiveness and angiogenesis. In basal-like breast cancer, it promotes cancer stem cell self-renewal by upregulating multiple components of the polycomb complexes via direct repression of the microRNAs that regulate them (Kottakis et al., 2011). The involvement of KDM2B in cancer was further substantiated by the development of tumors in mouse xenograft models when KDM2B was overexpressed in human pancreatic ductal adenocarcinoma cells in combination with a mutant KRAS gene (Tzatsos et al., 2013). In these cells, KDM2B promotes tumor progression by repressing developmental genes that are under the control of Polycomb complexes and by activating, in co-operation with c-MYC and KDM5A, genes that regulate metabolism. In addition, in synovial sarcomas, SS18-SS1/2 chimeric proteins encoded by hybrid genes generated via chromosomal translocation interact with KDM2B-targeted PRC1.1 complexes to activate developmental genes normally repressed by PRC1.1, a process giving rise to irreversible mesenchymal differentiation (Banito et al., 2018). Furthermore, expression of KDM2B from a Sca1 promoter-driven transgene in mice and ectopic expression of KDM2B in murine hematopoietic stem and progenitor cells result in the development of both lymphoid and myeloid malignancies (He et al, 2011; Ueda et al, 2015).KDM2B has also been associated with inhibition of NF-κB/p65-dependent cellular apoptosis, by a mechanism where NF-κB upregulates KDM2B expression, resulting in the repression of c-FOS and the interception of apoptosis in human cancer cells (Ge et al., 2011). In addition, KDM2B has been suggested to positively regulate genes of the glycolytic pathway (Yu et al., 2015) and proteoglycan synthesis (Wang et al., 2015), as well as several other metabolic (Janzer et al., 2013) and antioxidant genes (Polytarchou et al., 2008). In addition, KDM2B functions as a master regulator of a set of microRNAs that target several members of the Polycomb complexes PRC1 and PRC2 and its deregulation has important effects on PRC gene expression in both normal and cancer cells (Tzatsos et al., 2011; Kottakis et al., 2014).

Besides its involvement in replicative senescence and leukemogenesis, KDM2B also plays a significant role in morphogenesis and development via the regulation of pluripotency genes like Oct4 and Nanog (Lu et al., 2015; Zhou et al., 2017; Li et al., 2017), and Col1, Col2 and Sox9 (Wang et al., 2011). Reciprocally, it has been shown that Oct4 and Sox2 regulate KDM2B/PRC1.1 action in a positive feedback loop that involves repression of lineage-specific genes, thus contributing in the

maintenance of pluripotency of mouse ESCs (He et al., 2013). Moreover, both the JmjC and CxxC domains of KDM2B are required for the activation of early responsive genes in reprogramming of induced pluripotency stem cells (iPSCs) (Wang et al., 2011; Liang et al., 2012).

1.4.2. KDM2B as tumor suppressor

Even though KDM2B exhibits a clear oncogenic behavior, it was also reported as a tumor suppressor gene in retroviral insertion mutagenesis studies in Blm-deficient mice (Suzuki et al., 2006), while its homologue in C. elegans was identified as a gatekeeper against genome-wide RNAi mutagenesis (Pothof et al., 2003). In HeLa cells, KDM2B associates with ribosomal DNA and its downregulation promotes cell proliferation (Frescas et al, 2007). In these cells, the KDM2B was localized in nucleoli and its overexpression resulted in repression of ribosomal gene expression and inhibition of cell proliferation. Furthermore, although KDM2B maintains lymphoid leukemias, it was found to restrain RAS-driven myeloid transformation (Andricovich et al., 2016). These observations suggest that there might be opposing functions of KDM2B, and these functions may be cell type or context dependent. Indeed, recent evidence suggests that there are distinct KDM2B complexes. Although KDM2B cooperates with PcG and TrxG complexes to regulate cell fate decisions in human leukemias or in PANC1 cells (Tzatsos et al., 2013, Andricovich et al., 2016), it also cooperates with c-MYC and the histone demethylase KDM5A in the transcriptional activation of mediators of protein synthesis and mitochondrial function (Tzatsos et al., 2013).In leukemic stem cells, besides a set of genes that is targeted by PRC1 and PRC2, ChIP-seq studies show that KDM2B also binds a distinct set of genes that are devoid of H3K27me3, suggesting that it plays a gene-regulatory role that is independent of PRC2 (Banito et al., 2018). Furthermore, recent findings revealed an unprecedented function of KDM2B in the demethylation of H3K79 and the transcriptional repression of HOXA7 and MEIS1 (Kang et al., 2018). Overall, these observations indicate that there are important additional cellular functions of KDM2B that remain to be explored.

1.4.3. The protein structure of KDM2B

The KDM2B protein contains several functional domains. The N-terminal JmjC domain is responsible for the histone demethylation reaction (Tzatsos et al., 2009). At the C-terminal part of the protein, a leucine-rich region (LRR) and an F-box domain participate in protein-protein interactions and are involved in ubiquitination (Kipreos and Pagano, 2000). This region is essential for the ability of KDM2B to tether a ubiquitin chain to H2AK119 leading to gene repression (Sanchez et al., 2007,

Tzatsos et al., 2009, Farcas et al., 2012; Wu et al., 2013; He et al., 2013, Wong et al., 2016). In addition, KDM2B contains two zinc-finger motifs, CxxC and PHD (Plant homeodomain), located at the center of the amino acid sequence (*Figure 1.7*). The structure of this central region has been elucidated by X-ray crystallography (Xu et al., 2018).

Figure 1.7. The structure of KDM2B protein. The full-length protein of KDM2B consists of a JmjC domain, a CxxC and a PHD finger, an Fbox domain and six leucine-rich regions (LRRs).

1.4.4. The two Zn^{2+} fingers of KDM2B

A zinc-finger is a small protein structural motif which is characterized by the coordination of one or more zinc ions in order to stabilize the fold (Klug et al., 1987). Zinc finger-containing proteins, like KDM2B, participate in many cellular processes like gene transcription, protein translation, chromatin remodeling, protein folding, cytoskeleton organization, mRNA trafficking, and zinc sensing (Laity et al., 2001). Their binding properties depend on the amino acid sequence of the finger. The KDM2B CxxC domain has similar structure to that of the CxxC fingers of MLL and CFP1 proteins, consisting of two cysteine-rich clusters that chelate two Zn2+ ions and stabilize the domain (Long et al., 2013). This domain has been implicated in DNA binding and the recognition of non-methylated CpG DNA sequences (Koyama-nasu et al., 2007; Farcas et al., 2012). It has been shown to be essential for the recruitment of KDM2B and the tethering of PRC1 to the c-jun promoter (Koyama-nasu et al., 2007) and for protecting CG- islands from hypermethylation (Boulard et al., 2015). KDM2B regulates the transcription of mir-101, which controls the expression of EZH2, in a CxxC and JmjC-dependent manner (Pfau et al., 2008; Tzatsos et al., 2009; Kottakis et al., 2011). These results highlight the importance of a functional CxxC domain, but do not correlate these phenotypes with the DNA-binding function of the protein as they were performed with CxxC finger deletion or structure destabilizing mutants. Considering that the loss of 60-80 amino acids from the central part of the protein or the destabilization of Zn coordination could

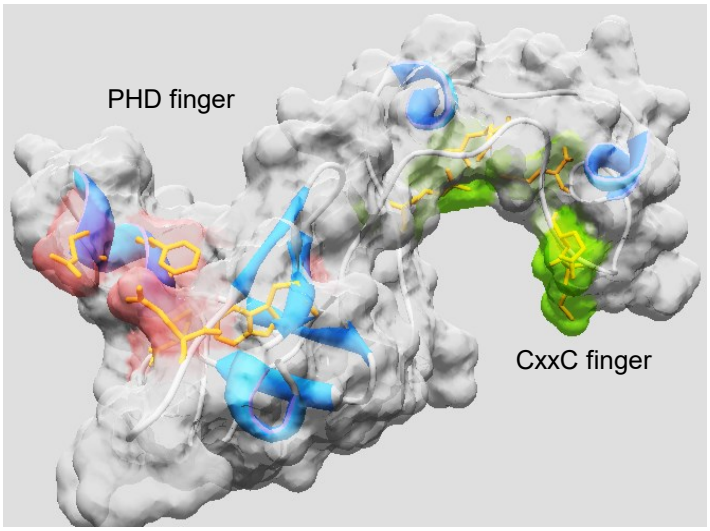

Figure 1.8. Structure of the two Zn^{2+} fingers of KDM2B. The KDM2B CxxC (DNA binding domain) and the PHD (histone binding domain) fingers are depicted with green and red, respectively. The predicted residues participating in KDM2B molecular interaction are represented with yellow sticks.

have a strong impact on the proper structure of the enzyme, these experiments do not discern the involvement of the CxxC domain from that of other structural components of the protein.

The second Zn^{2+} finger of KDM2B is the PHD domain that consists of 70 amino acids and forms a two-strand antiparallel β-sheet and a C- terminal α-helix stabilized also by two zinc ions. There is strong structural interdependence between these domains that prevents either of the two from being produced independently in a stable form (Xu et al., 2018) (*Figure 1.8*). There have been over 170 PHD fingers in the human genome identified as epigenetic reader domains (Liu et al., 2012). In general, PHD fingers recognize specific peptides and their most commonly reported targets are histone H3 tail sequences (Sanchez & Zhou, 2011) carrying different posttranslational modifications such as H3K4me3 (Li et al., 2006; Peña et al., 2006, Wysocka et al., 2006; Iwase et al., 2007), H3K9me3 (Iwase et al., 2011) H3K14Ac (Zeng, L. et al., 2010), or H3 tails with no modifications (Lan et al., 2007). Other PHD domains are able to bind PTMs such as acetylation on H4 (Li & Li, 2012) while some non-histonic interactions have also been documented (Fiedler et al., 2008; Wang et al., 2010). PHDs that recognize methylation on a lysine residue usually bind their ligands through an aromatic cage, where the presence of a negatively charged residue in the cage can alter their binding selectivity (Taverna et al., 2007; Kampranis and Tsichlis, 2009, Sanchez and Zhou, 2011). Interestingly, a recent study by Bortoluzzi *et al.* (2017) revealed that beside the structure of PHD finger, the secondary conformations within the H3 histone tail also play an important role in the molecular recognition. As far as the KDM2B PHD finger is concerned, it has been proposed to recognize the transcriptional activation marks H3K4me3 and H3K36me2 (Janzer et al., 2012), however the details of this interaction and its functional significance remain unclear.

1.5. Aim of Research

It is understood that the role of KDM2B as epigenetic key regulator in cell physiology and disease has been the focus of numerous studies to this date. Examination of this protein domain-wise shed light on a plethora of interactions that KDM2B participates during both physiological and pathogenic cellular state. In the current thesis we set out to elucidate the function of the Zn^{2+} finger domains of KDM2B, CxxC and PHD, in order to improve our understanding on a molecular level of their involvement in the KDM2B function. In the present study, we aimed to characterize the interaction of the CxxC and PHD fingers of KDM2B with ligands using a combination of biochemical and biophysical studies. The optimum goal was to acquire new structural insights into the molecular

interactions of those domains that could serve as a stepping stone for developing domain-specific inhibitors for KDM2B.

In order to examine the interaction of KDM2B CxxC finger with DNA ligands we employed electrophoresis mobility shift assay (EMSA). EMSA is a standard technique used to detect qualitatively and/or quantitatively (i.e. determination of stoichiometry, kinetics, and binding affinity) protein-nucleic acid interactions (Hellman & Fried, 2007). Upon successful completion of these sets of experiments that sought the structural determinants of the CxxC-DNA recognition, the second step in the CxxC finger characterization included setting up a high-throughput inhibitor screening assay based on Fluorescence Resonance Energy Transfer (FRET). FRET is sensitive technique for investigating a variety of molecular interactions (dos Remedios et al., 1987) and FRET- based assays have already been exploited *in vivo* (Sekar and Periasamy, 2003) and *in vitro* (Boichenko et al., 2016). We aimed to create a prototype, economically feasible and robust technique that would be used for identifying molecular compounds able to act as domain-specific inhibitors of KDM2B.

The final step of the research on the CxxC finger included the correlation between its DNA binding capacity and its role in KDM2B function. Previous studies have correlated KDM2B with cellular motility, migration and cytoskeleton organization (Kottakis et al., 2011; Zacharopoulou et al., 2018b). Thus, we investigated whether the CxxC finger is participating in these processes by employing *in vitro* would healing assays. The wound healing assay is an easy, robust and highly reproducible technique that is used to study the movement of different cell population and measure their migration potential under a wide range of conditions (Jonkman et al., 2014).

As far as the KDM2B PHD finger is concerned, there have been several conflicting arguments about the substrate specificity of this domain. In order to elaborate further on the binding capacity of the KDM2B PHD finger we employed the technology of MODified Histone Peptide Array (Active Motif®, US) that enabled us to examine 384 unique histone modification combinations as possible interactors. Following the identification of possible PHD binders, the next step was to measure qualitatively their kinetics using Isothermal Titration Calorimetry (ITC). ITC is a powerful tool for studying the thermodynamics of macromolecular interactions (Malecek et al., 2012) and is broadly applicable for the study of biological systems (Velazquez-Campoy et al., 2005). A basic advantage of ITC is that all reactions take place in an aqueous buffer obviating the need for chemical preparations or modifications and mobilization on a surface. In addition, based on the equilibrium point, the stoichiometry of the reaction can be easily calculated, while the identification of synergy in systems that include multiple interactions, defined ITC as the best technique for analyzing

interactions such as the formation of multi-protein complexes (Rickert et al., 2004) or the binding of more than one ligands (Dam et al., 2000).

Previous studies have shown that KDM2B and KDM2A, as well as their alterative isoforms that lack the JmjC domain, have distinct roles in cellular physiology (Vacík et al., 2019). Despite the fact that these two proteins share more than 93% similarity in amino acid sequence, there has been no substantial data explaining the reason behind their participation in different processes. By employing MODified Histone Peptide Array (Active motif ®,US) and comparative analysis we sought to identify the PHD binders of KDM2A and we investigated whether the substrate specificity of KDM2B PHD finger is similar to its sister protein. We believed that the results from this analysis would shed light into the interesting role of the PHD finger of those histone demethylases and create a new path for further research.

Chapter 2

Materials & Methods

2.1. *E. coli* strains.

Strain	*Mach1*	*BL21 Codon Plus*
Genotype	W ΔrecA1398 endA1 fhuA Φ80Δ(lac)M15 Δ(lac)X74 hsdR($r_K^-m_K^+$)	B F– ompT hsdS(r_B–m_B–) dcm+ Tetr gal endA Hte [argU ileY leuW] CamR
Manufacturer	Invitrogen	Agilent
Usage	Cloning	Heterologous protein production
Characteristics	T1/T5/Φ80 phage resistant Fast growth	Codon optimized for plant proteins Chloraphenicol resistance

2.2. Preparation of bacterial growth media. For preparation of liquid LB medium 0.5% w/v NaCl, 1% w/v bacto-tryptone and 0.5% w/v yeast extract were dissolved in ddH_2O and autoclaved at 121°C for 30 min. For LB-agar medium, 2% w/v agar was supplemented in the previous mix, before autoclave at 121°C for 30 min. For Terrific Broth (TB) medium preparation 12 g bacto-tryptone, 24 g yeast extract and 4 mL glycerol were dissolved in 900 mL ddH_2O and autoclaved at 121°C for 30 min. For pH adjustment at 7.5, 100 mL of autoclaved phosphate buffer (0.17 M KH_2PO_4, 0.72 M K_2HPO_4) were added in the medium.

2.3. Preparation of *E. coli* competent cells. 1 mL of overnight bacterial culture was used to inoculate 400 mL antibiotic-free LB medium. When cell culture reached OD_{600}= 0.2, the cells were transferred in 50 mL falcons for 10 min incubation on ice. Centrifugation at 5,000 rpm for 10 min at 4ºC was followed by resuspension in 50 mL cold Buffer-X (50 mM $CaCl_2$, 5% v/v glycerol, 10 mM MOPS (pH 6.6)). After 20 min on ice, the cells were again centrifuged and resuspended in 3 mL Buffer X. Finally, 50 μL aliquots were prepared in 1.5 mL Eppendorf tubes, fast-frozen in liquid nitrogen and stored at -80°C.

2.4. Bacterial transformation. 1 ng of plasmid DNA was mixed with 50 μL of bacterial competent cells and incubated for 30 min on ice. 45 s of heat shock at 42°C were followed by supplementation of 200 μL antibiotic-free LB medium and 1 h incubation at 37°C, shaking, for cell recovery. Plating of 100 μL of the transformed cells on Petri dishes that contained LB-agar with the proper antibiotics was followed by overnight incubation at 37°C.

2.5. Mini preparation of plasmid DNA. 4 mL of a bacterial overnight culture were centrifuged at 13,000 rpm for 5 min. After discarding the supernant, addition of 250 μL Resuspension Buffer P1 (50 mM glucose, 25 mM Tris-HCl (pH 8.0), 10 mM EDTA, 100 μg/mL RNase A) was followed by a short vortex stirring until the pellet was fully diluted. 250 μL Lysis Buffer P2 (0.2 N NaOH, 1%

SDS) were added and after 5 min incubation at room temperature, 350 μL Neutralization Buffer N3 (3 M guanidine-HCl (pH 4.8)) were added. After centrifugation at 13,000 rpm for 5 min the supernant was placed in a Qiagen® miniprep column, attached on the QIAvac Vacuum Manifolds® dock, which was connected to a vacuum pump. Subsequently, 500 μL Wash Buffer PE (10 mM Tris-HCl (pH 7.0), 50 mM ethanol) were used, followed by750 μL Purification Buffer PB (1.6 M guanidine-HCl (pH 4.8), 40% 2-propanol) had been added sequentially. Finally, the column was detached from the dock and placed in a 1.5 mL Eppendorf tube. 50 μL Elution Buffer EB (10 mM Tris-HCl (pH 8.5)) were used to obtain 60-70 ng of plasmid DNA, which was stored at -20°C.

2.6. DNA enzymatic digestion and fragment ligation. In a plasmid vector the gene of interest was inserted in frame in the cloning site in order to be expressed. For our experiments, the *in silico* cloning was designed in Vector NTI v11.5 (Invitrogen). The *in vitro* part of the enzymatic digestion was carried out according to each enzyme specifications (5-10 ng of plasmid DNA, enzyme buffer and restriction enzyme). All enzymes used are shown in Appendix 1: Table 2. The efficiency of the enzymatic digestion was confirmed via agarose gel electrophoresis. For the ligation of the DNA fragments the T4 DNA Ligation (New England Biolabs) protocol was followed. All the designed constructs are shown in Appendix 2.

2.7. Agarose gel electrophoresis. In order to prepare a 0.8% agarose gel, 0.8 g agarose were diluted in 100 mL 1X TAE (0,48 % w/v Tris base, 0,12 % v/v glacial acetic acid, 2 mM EDTA (pH 8.0)). After short boiling and replacement of the evaporized TAE buffer, 3% v/v GelRed® was added. The solution was left to solidify in the caster for 15 min with the proper combs. The gel was placed in the electrophoresis tank filled with 1x TAE, the DNA samples were mixed with 6x loading buffer (0.6 M Tris-HCl (pH 7.5), 6 mM EDTA, 30% w/v glycerol, grains of bromophenol blue) and loaded in the wells. The electrophoresis run at 150V for at least 25 min for sufficient band separation. The electrophoresis was viewed over a UV light box.

2.8. DNA agarose gel extraction. In order to isolate the desired DNA fragment (vector or insert) from the agarose gel, the gel piece that contained it was cut, placed in an Eppendorf tube and incubated with 400 μL QG buffer (guanidine thiocyanate) at 55°C for 5 min. Then it was transfer in a Qiagen® miniprep column, attached on the QIAvac vacuum manifold dock and the steps as described in mini preparation of plasmid DNA were followed.

2.9. Polymerase Chain Reaction (PCR). PCR was used to amplify a specific DNA sequence. For the reaction a template DNA sequence, DNA primers that provide a free 3' end for the polymerase to produce the newly synthesized strand, and dNTPs are needed. The reaction includes three basic steps:

denaturation of the double strand DNA, primer annealing and extension (Polymerization). The PCR product can be stored at 4°C until confirmation via agarose gel electrophoresis and insertion to the plasmid vector. In the basic (pCRII-TOPO TA) cloning technique, the mutagenesis and the USER cloning, MyTaq® Polymerase, Phusion®– High Fidelity Polymerase and Kapa® HiFi Uracil+ HotStart Polymerase were used, respectively.

2.10. MyTaq® A- overhangs Reaction. This reaction exploits the capacity of My Taq® polymerase to add 3' adenine overhangs to create sticky ends for the pCRII-TOPO TA cloning technique. The reaction requires 6.5 μL reaction buffer MyTaq®, 1 μL dNTPs, 2 μL PCR product or linear DNA, and 0.5 μL MyTaq® polymerase mixed together and incubated for 20 min at 72°C. The products of the reaction can be used in pCRII-TOPO TA cloning or stored at -20°C until use.

2.11. pCRII-TOPO (A-overhangs) Cloning. This technique is highly efficient in cloning Taq-derived PCR products in a high-copy pCRII-TOPO bacterial vector. The TOPO vector, upon linearization provide 3' thymidine sticky ends that hybridize with the adenine tails of the insert. The reaction requires 3 μL PCR product with A-overhangs, 1 μL salt solution (1.2 M NaCl, 0.06 M $MgCl_2$), 1 μL ddH_2O and 1μL of the pCRII-TOPO (TA) vector incubated for 20 min at room temperature. The product of this reaction was used to transform *E. coli Mach1* competent cells.

2.12. Cloning CxxC and PHD domains of mKDM2B in bacterial expression vector. The coding sequences of the region sanning the CxxC and PHD domains of mKDM2B, were cloned in a pET102 vector with a V5 epitope, using the TOPO TA Cloning® Protocol. The recombinant protein, $mKDM2B_{577-707}$, was thioredoxin- fused at the N- terminus and carried a 6x His- tag at the C-terminus. Transformed Mach1 $T1^R$ *E. coli* cells with the pET102/ D-$mKDM2B_{577-707}$ construct (6.7 kb) were grown on LB agar plates supplemented with 100 μg/ mL of ampicillin overnight at 37ºC. Single colonies were picked to inoculate 6 mL of LB medium with ampicillin and incubated overnight at 37ºC. The plasmid DNA was isolated as described above, with QIAprep Spin Miniprep Kit. The $mKDM2B_{577-707}$ cloning was confirmed via enzymatic digestion and agarose gel electrophoresis.

2.13. Site-directed mutagenesis of CxxC and PHD. In order to generate $mKDM2B_{577-707}$ mutants, I followed the protocol described in (Ignea *et al*., 2014). The mutations were introduced into pET102/D–$mKDM2B_{577-707}$ by polymerase chain reaction (PCR) amplification of the original construct using Phusion® HF DNA Polymerase with a specific forward primer for each mutation as shown in Appendix 1: Table 6. The single point mutations (R585A, K608A, K616A and F654A) and the double point mutation (R585A/ K616A) of the pET102/ D-$mKDM2B_{577-707}$ construct were

confirmed via Sanger sequencing (CEMIA, Greece). Replication and isolation of the mutant mKDM2B$_{577-707}$ constructs was performed as described above.

2.14. mKDM2A USER cloning. One of our goals was to examine whether the PHD fingers of mKDM2B and mKDM2A illustrate the same histone binding specificity. To this end, the CxxC and PHD fingers of mKDM2A were cloned in pET102/ USER vector. A chemically synthesized nucleotide sequence, encoding mKDM2A$_{560-690}$, was PCR amplified, using specific USER primers (shown in Appendix 1: Table 6) and the recombinant protein was fused with theoredoxin and 6xHis tag at N- and C- terminus, respectively. The USER cloning protocol was carried out as described in (Genee *et al*., 2014), and the USER primers were designed with the online software by DTU Bioinformatics (AMUSER 1.0) (http://www.cbs.dtu.dk/services/AMUSER/).

2.15. Sub-cloning of Enhanced Green Fluorescent Protein (EGFP). In order to develop a fast and easy high- throughput screening assay for detecting KDM2B inhibitors, the coding sequence of the enhanced green fluorescent protein was cloned from the pEGFP – C1 vector to pET102/ D-mKDM2B$_{577-707}$ and also in the pET102/ D-mKDM2B$_{577-707}$(K616A) via basic enzymatic digestion/ fragment ligation cloning technique.

2.16. pET102/ D- mH4- mRFP cloning. One of our side goals was to exploit the Fluoresence Resonance Energy Transfer (FRET) technique, to examine the interaction of the PHD domain with parts of the mouse H4 histone protein. Previous results indicated a binding affinity towards the unmodified 11-30 residues of the N-terminus tail of mH4. On that note, the coding sequences of the residues 1-18, 17-34, 33-50 and 49-69 were cloned in the bacterial expression vector pET102/D. In addition, the coding sequence of the monomeric Red Fluorescent Protein (mRFP) was also cloned next to the mH4 sequence, creating a recombinant protein fused with Theoredoxin and 6xHis tag at the N- and C- terminus, respectively. The aminoacid sequence of the TRX-mH4-mRFP recombinant proteins are shown in Appendix 3.

2.17. Heterologous expression and purification of the recombinant proteins. BL21 CodonPlus *E. coli* cells were transformed for the heterologous expression of the recombinant proteins. The successfully transformed cells were cultivated in Luria- Bertani (LB) medium or Terrific Broth (TB) medium in the presence of ampicillin, kanamycin and chloramphenicol in concentration of 50, 50 and 12 μg/ mL, respectively. The cells were incubated for 3 h at 37°C before adding 0.5 mM of IPTG, followed by incubation for another 24 h at 17°C before cell harvest. Osmotic disruption of cells in Lysis buffer (0.06 M Tris- HCl (pH 8.0), 0.3 M NaCl, 0.01 M imidazole, 0.1 mM PMSF, 0.5 % w/v lysozyme) was followed by 10 min sonication at max power, to obtain soluble recombinant proteins

from the lysate. A 15% denaturating polyacrylamide gel electrophoresis (SDS-PAGE) was used to quantify the efficiency of the protein expression before further purification. The recombinant proteins were isolated via His-tag affinity chromatography protocol using Ni-NTA agarose resin.

2.18. Sodium Dodecyl Sulfate-Polyacrylamide Gel Electrophoresis (SDS-PAGE). Denaturating polyacrylamide gel electrophoresis is a broadly used technique to quantitatively and qualitatively evaluate a protein sample. By creating an electic circuit, the negatively charged proteins, based on their molecular weight, migrate throughout the gel. In our experiment, this technique was used to confim the production and purification efficiency of heterologous expressed proteins. The BioRad® gel caster was assembled according to the manufacturers' guidelines. The resolving gel covered 2/3 of the space between the two glass sheats and after 20 min of polymerization, the stacking gel was added, covering the remaining 1/3 and a 10-slot Teflon comb created the wells. After stacking gel polymerization, the gel was placed in the anode/cathode apparatus inside an electrophoresis tank. All gels run in 1x Running Buffer (1.44% w/v glycine, 0.3% w/v Tris base, 0.1% w/v SDS) at 200 V/ 40 mA. The protein samples were mixed properly with 4x Sample Application Buffer (250 mM Tris-HCl (pH 6.8), 20% v/v glycerol, 4 % w/v SDS, 1.43 M β-mercaptoethanol, grains of bromophenol blue), heated (95°C for 5 min) spinned down and loaded in the wells. After 45 min of running, the gel was carefully removed from the glass sheats and placed in Coomassie Blue Staining Buffer (50% v/v methanol, 10% v/v glacial acetic acid, 0.2% w/v coomassie dye) for an hour followed by an overnight destaining in ddH_2O.The following table describes the mastermix composition of 12% and 15% acrylamide resolving gels and stacking gel.

Recipe for 2 Gels	12%	15%	Stacking
ddH_2O	3 mL	2.5 mL	3.7 mL
1M Tris (pH 8.8)	3.75 mL	3.75 mL	-
1M Tris (pH 6.8)	-	-	620 μL
Acrylamide: Bisacrylamide 37.5:1	3 mL	3.5 mL	500 μL
10% w/v SDS	100 μL	100 μL	50 μL
10% w/v Ammonium persulfate (APS)	100 μL	100 μL	50 μL
Ready-to-useTEMED	10 μL	10 μL	5 μL

2.19. Ni-NTA affinity chromatography. Imidazole interacts with the histidine residues of the 6xHis tag via Ni^{2+} ions. In Lysis and Wash buffer the imidazole concentration was low (10 mM and 20 mM, respectively) to avoid non specific interactions and to improve the purity of the target protein sample. The protein lysate was mixed with 0.5 mL Qiagen® Ni-NTA agarose resin and incubated for 1 h at

4˚C with mild shaking. Then, the lysate was centrifuged at 1500 rpm for 4 min and the resin pellet was washed 3x times with 2 mL Wash buffer to remove any non specific binders, before protein elution step. In the elution step, the Elution buffer used, contained 250 mM imidazole which acts as antagonist to the 6xHis tag leading to the protein release from the resin, and accumulation in the supernant. In order to minimize imidazole concentration in the final protein solutions, wild type and mutant mKDM2B$_{577-707}$, mH4-mRFP and mKDM2A$_{560-690}$ recombinant proteins were dialyzed through SnakeSkin® Dialysis tubing and stored in Reaction Buffer (0.06 M Tris-HCl (pH 8.0), 0.3 M NaCl,1 mM $ZnCl_2$, 1 mM β- mercaptoethanol, 10% glycerol). The final concentrations of the protein solutions, measured in Nanodrop™ Spectrophotometer (ThermoFisher), ranged from 25 to 30 μM and showed more than 90% purity with Coomassie staining of the 15% SDS PAGE.

2.20. Protein dialysis. A SnakeSkin® tubing membrane with a cut-off at 7,000 Da was used. The membrane was equilibrated for 15 min in the Reaction buffer before use. The dialysis bag was submerged in Reaction buffer, which after 3, 6 and 9 hours was renewed. Mild strirring at 4°C throughout the process enhanced the quality of the dialysis and prevented in most cases the formation of protein aggregates. In cases where the protein concentration was low, Amicon Ultra® spin columns were used (centrifugation at 13,000 rpm for 30 min at 4°C) to increase it.

2.21. Ni-NTA agarose resin recycle. In order to reuse the agarose resin for protein purification, the NTA requires reactivation. To do so, all used resin was gathered in a 50 mL falcon and centrifuged at 1,000 rpm for 2 min at room temperature. After removing the supernant, the resin was washed and dried two times with 2 volumes of ddH_2O. Mixing the resin with one volume of 50 mM NaOH, was followed by centrifugation at 1,000 rpm for 2 min. After removal of the supernant the resin was washed and dried 3 times with 2 volumes of ddH_2O. One volume of 0.6 M guanidine-HCl was mixed and removed after another centrifugation. After washing the resin like before, one volume of 0.2 M $NiCl_2$ was used to activate NTA and then removed. The activated resin was finaly washed and dried two times with 2 volumes of ddH_2O before resuspending it in one volume of 30% ethanol. The recycled resin can be stored in 4°C until use.

2.22. [γ- ^{32}P] ATP labeling of DNA substrate. One of our basic goals in this thesis was to study the DNA binding capacity of mKDM2B CxxC domain. To do so, Electrophoresis Mobility Shift Assay (EMSA) was suited for our purposes. The initial step was to prepare ssDNA substrates for radiolabeling. Oligonucleotides CpG2D, CpG6D, GpC6D and ORI2.5D (sequences showed in Appendix 1: Table 6) were chemically synthesized and purified by Invitrogen, UK. 50 pmol of each strand were used for the 5' prime radio phosphorylation following the T4 PNK protocol (New

England Biolabs). This protocol was used to label the 5' end of a single strand DNA with γ- ^{32}P. The protocol was provided with the T4 phosphokinase, which catalyzes the reaction. 50 pmol of ssDNA are mixed with 3 μL of γ-ATP, 5 μL enzyme buffer and 2 μL T4 PNK enzyme in 50 μL total volume. After 1h incubation at 37°C, the ssDNA sample was passed 2 times through a Sepharose-25 column and via centrifugation at 2.7 rpm for 2 min all the small unincorporated γ-ATP molecules are discarded. The radiolabeled ssDNA was loaded in a well of a 7 M Urea-15% Polyacrylamide gel for denaturation.The electrophoresis run in 1X TBE at 500V/ 40 mA for 90 min.The desired bands were visualized by autoradiography and gel extraction was performed overnight using Gel Extraction Buffer (390 mM CH_3COONa, 1 mM EDTA (pH 8.0), 20% v/v phenol).The phenol/ $CHCl_3$ DNA purification protocol was used to obtain the radiolabeled ssDNA.

2.23. Phenol/ $CHCl_3$ DNA purification protocol. The radiolabeled ssDNA extracted from the polyacrylamide gel was transferred to a new Eppendorf tube and mixed with 500 μL phenol. Centrifugation for 2 min at 13,000 rpm was followed by tranferring the supernant into a new Eppendorf tube. Addition of 500 μL $CHCl_3$ and repetition of the centrifugation took place. The upper phase was extracted, mixed with 1 mL 100% Ethanol and incubated for 15 min at -80°C. Centrifugation at 13,000 rpm for 45 min at 4°C created a radioactive pellet at the bottom of the tube. Resuspension of pellet in 30 μL ddH_2O can obtain up 30 pmols of radiolabeled ssDNA, which can be stored in -20°C for up to 2 weeks.

2.24. Electrophoresis Mobility Shift Assay (EMSA). The radioactive synthetic double oligonucleotides CpG2, ORI2.5, CpG6 and GpC6 were produced by annealing of the ssDNA strands (^{32}P- CpG2D, ^{32}P-ORI2.5D, ^{32}P-CpG6D and ^{32}P-GpC6D) with their complementary strands. To do so, the two strands were boiled for 5 min and then cooled down slowly until room temperature. In the EMSA experiments, wild type mKDM2B$_{577-707}$, its mutants and mKDM2B$_{577-707}$-EGFP were incubated with the radiolabelled CpG2, ORI2.5, CpG6 and GpC6 in Reaction buffer supplemented with 10 μg/ mL BSA for blocking, in total volume of 10 μL for 30 min at 37 ºC. The samples were mixed with 10 μL of 2x loading dye (5 mM Tris-HCl pH 8.0, 5% Glycerol, 1% w/v bromophenol blue, 1% w/v xylene cynool) and loaded in a native 8% polyacrylamide gel in 0.5x TBE run at 100V for 70 min. Afterwards, the gel was detached carefully from the glass plates, sealed in plastic membrane to prevent radioactive contamination and placed in a cassette with developing film. The bands were visualized by autoradiography.

2.25. Fluorescence– based DNA binding assay. A set of fluorescence- based experiments was conducted in order to detect the CxxC domain – DNA interaction. The first parameter was to choose

a fluorophore with the proper absorption/ emission wavelengths like FAM (Abmax: 490 nm/ Emmax: 520 nm) to conjugate with CpG2D. Other parameters like, adding protein blockers to avert non specific binding of FAM- CpG2 on the surface, optimizing the elution buffer and minimizing background noise, were also tested. 0.1 μM of mKDM2B$_{577-707}$ was used to sufficiently cover the well surface, followed by 0.25 μM of FAM-CpG2. A step of washing with Reaction buffer was required to remove unbound DNA before elution. The eluted DNA was transferred in black microplates for the fluorescence measurement in Victor X5® Light Plate Reader with Excitation Filter at 485 nm/ Emission Filter at 535 nm.

2.26. Fluorescence Resonance Energy Transfer (FRET) and Time-Related Fluorescence Attenuation (TRFA) DNA Binding Assay. The second set of experiments on DNA binding assay was based on FRET. The mKDM2B$_{577-707}$- EGFP (donor) recombinant protein (Ab$_{max}$: 495 nm/ Emmax: 520 nm) was tested with two acceptor fluorophores: TET (Ab$_{max}$: 520 nm/ Em$_{max}$: 540 nm) and Cy3 (Ab$_{max}$: 550 nm/ Em$_{max}$: 570 nm). There are two binding sites of CxxC domain on the CpG2 sequence, so both DNA strands had to carry the fluorophore on the 5'end to ensure the shortest distance between acceptor and EGFP. In addition, a shorter version of CpG2 was also tested, CpG2short (sequence shown in Appendix 1: Table 6), conjugated with Cy3. We tested the FRET-based DNA binding assay in the FluoroMax® 2 Spectrofluorometer (SPEX) that allowed only one reaction per time to take place. The optimal concentration ration [EGFP]/ [Cy3] was 1:7.5, to avoid photobleaching. The photospectrometer scanned from 400 nm to 700 nm after a single energy hit. Background fluorescence was calculated and extracted from signal fluorescence. The data were analyzed with JY Viewer (Horiba®) and Excel (Microsoft®). In the microplate FRET-based experiments, the fluorescence of subsequently increaded concentrations of Cy3- CpG2 tested on 5 nM, 20 nM and 200 nM of well surface absorbed mKDM2B$_{577-707}$- EGFP was measured at 535 nm in Victor X5® Light Plate Reader. Signal-to-noise ratio was calculated with Excel (Microsoft®). In TRFA, 0.5 uM mKDM2B$_{577-707}$- EGFP and 0.5 uM mKDM2B$_{577-707}$(K616A)- EGFP with 2 uM Cy3-CpG2 for 5 min inside the plate reader before apply a single energy hit for 1 s, upon which the fluorescence attenuation was measured for 40 us. As control we examined the fluorescence attenuation of 2 uM Cy3-CpG2 alone. Analysis was done using Excel (Microsoft®).

2.27. Modified Histone Peptide Arrays. Focusing on elucidating the mKDM2B PHD domain function, we tried to detect possible interactors by using a commercial histone peptide array (MODified® Histone Array). The slide was blocked for 1 h at room temperature with TBS containing 1% Triton X-100 (TBS-T) and 5% w/v non-fat powder milk. Following 3 washes of TBS-T, the microscope slide containing the array was incubated with 1 μg/mL recombinant mKDM2B$_{577-707}$

protein for 1 h at 4°C. Following 3 washes with TBS-T, the slide was incubated for 1 h at room temperature with anti-V5-HRP antibody and developed using the Thermo Scientific Pierce ECL Western Blotting kit. List of peptide position and modifications on the slide is shown in Appendix 4.

2.28. Isothermal Titration Calorimetry (ITC). All calorimetric experiments were performed on a MicroCal VP-ITC Microcalorimeter (GE Healthcare) at 16ºC in Reaction buffer. The custom chemically synthesized and lyophilized 11-mer and 19-mer oligopeptides (Caslo, Denmark), shown in Appendix 1: Table 3, were dissolved in an appropriate volume of Reaction Buffer to obtain the desired concentration. Titration of different peptide solutions (2-3 mM) was performed by applying 19 microinjections of 15 μL each, into protein solutions (30- 45 μM) loaded in the cell. The data were acquired using the MicroCal™ software, analyzed and fitted, using a single-binding site model, on Origin (OriginLab).

2.29. Virus Production in HEK293T cells. One of the goals of this thesis was to elucidate the biological role of KDM2B and the importance of the CxxC domain in the migration of cancer cells. To do so, we created a retrovirus pBABE-mKDM2B(K616A) mutant and transfected human prostate cancer cells (DU145), to examine their metastatic potential. The single mutant pBABE-mKDM2B(K616A) plasmid was created via USER mutagenesis protocol (Genee *et al*., 2014) and by using the pBABE-mKDM2B construct as template. Replication and isolation of the plasmid DNA was performed as described above. Human Embryonic Kidney cells (HEK293T) were used to produce the retrovirus. 10^6 HEK293T cells were plated in 100 mm dishes with 10mL DMEM medium (high glucose, 10% v/v Fetal Bovine Serum, 1% v/v Penicillin/ Streptomycin) and after 24 h, the medium was replaced with DMEM without antibiotics before transfection with the 3 ug of pBABE-mKDM2B(K616A) plasmid DNA, 1 ug pE- ampho vector (Takara) and 15 μL ready-to-use Attractene Reagent (Qiagen). The pE- ampho vector (amphopac), kindly provided by Dr Tsapara, contains the envelop protein genes of the retrovirus and Attractene is a nonliposomal lipid that enables transfection of all adherent cells. To increase transfection efficiency, attractene, amphopac and plasmid DNA are incubated for 15 min in room temperature before use. After 24 h, the medium was replaced with full DMEM with 1% v/v Pen/Strep and 24 h later the virus, secreted into the medium, was collected, filtered through 0.45 μm filter and stored in -80 ºC until use.

2.30. Freezing, defreezing and trypsin treatment of DU145 prostate cancer cells. DU145 human prostate cancer cells have a moderate metastatic potential, but sufficient for our research purposes. The cell stock provided, already had been through 15 passages and was kept in -80 ºC for two years. The growth medium used in our experiments was RPMI+/+ (supplemented with 10% v/v Fetal

Bovine Serum and 1% v/v Pen/Strep). Our first step before the retroviral transfection was defreezing the cell stock. The defrozen cells were spinned down at 900 rpm for 5 min and the freezing buffer (70% RPMI+/+, 20% FBS and 10% DMSO) was removed. The cells were resuspended in 2 mL RPMI+/+ and transferred in a 75 mL Corning® cell culture flask. The cells were cultivated until they reached 80-90% confluency (8-10 days) followed by trypsin treatment. 3 mL of ready-to-use trypsin were used to cut the focal adhesions that are anchoring the cells to the culture flask and the cells were transferred in a 15 ml falcon tube with 3 ml RPMI +/+. Using a hemocytometer plate under an electric microscope the cell density was calculated. Upon proper dilution, 10^5 cells were placed in a 6-well plate and incubated for 24 h before viral transfection. The rest of the cells were transferred into a 75 mL Corning® cell culture flask, for further growth. When they reached 90% confluency, they were treated with trypsin (after two washes with PBS), transferred into a 15 mL falcon and centrifuged at 900 rpm for 5 min. The supernant was discarded and the pellet was resuspended in 3 ml freezing buffer. Three aliquots of 1 mL each were prepared and stored at -80˚C for future use.

2.31. DU145 transfection and growth. Before the viral transfection of the DU145 cells that were cultivated in the 6- well plate, 2 mL of the pBABE-mKDM2B(K616A) virus were incubated with 36 ng Polybrene reagent for 15 min at room temperature to enhance the efficiency of the process. In parallel the cells were washed 2 times with PBS before adding the virus. During the 24 h of the retroviral transfection no medium was supplemented to the cells, in order to create a proportionate starvation status and maximize the DNA transfer capacity inside the cells, after which the cells where cultivated for another 24 h in RPMI+/+ medium for recovery. In order to select the transfected cells, 2 ug Puromycin were added in RPMI+/+. One well that contained no transfected DU145 cells was used as positive control, to examine the efficiency of puromycin. The successfully transfected cells were grown in RPMI+/+/+ until they formed visible colonies.

2.32. Pick single DU145 colonies and cell lysis. In order to examine the effect of the mutant CxxC domain on cellular migration, our initial step was to select the cell colonies that overexpressed the mutant mKDM2B. To do so, the transfected cells that formed small colonies were washed 2 times with PBS and treated with ready-to-use trypsin. Pipeting 20 μL of trypsin on top of each colony separately led to collecting the cells, which then were transferred into a 24-well cell culture plates with 1mL RPMI+/+/+ each, for further growth. After 10-14 days the cells were >85 % confluent, and treated with trypsin. 1/3 of the cells was transferred to 60 mm cell culture plate for further growth, destined to verify the protein expression via Western blot, and 2/3 of the cells we transferred to a 25 mL culture flask for further growth destined to be stored at -80˚C.When the cells, grown in the 60

mm plate, reached 90% confluency they were collected in 0.5 mL cell lysis buffer by using a scraper, sonicated for 45 s and stored at -80˚C until use.

2.33. Western blot. In a Western blot, proteins that are separated on polyacrylamide gels on the basis of size, are transferred to a membrane and then specifically detected in the immunoassay step using specific antibodies to the protein. The technique involves transferring of electrophoretically separated components from a gel to a solid support, such as a nitrocellulose, and probing with reagents that are specific for particular sequences of amino acids. The probes are usually antibodies that bind to antigenic epitopes displayed by the target protein attached on the solid support. Western blotting is extremely useful for the identification and quantitation of specific proteins in a complex mixture of proteins. A 1-5 ng of an average sized protein can be detected by western blotting. The gel cassette was opened and lifted gently and the gel was cut, stacking gel was thrown away, resolving gel was immersed in transfer buffer for 15 min, thus allowing it to equilibrate. A piece of the nitrocellulose membrane was cut to the dimension of the gel. One corner of the membrane was notched for later correspondence with the corner of the gel. Several Whatman® filter papers, the PVDF membrane and the gel were assembled in the cassette in the following order starting from the black part: foam pad, paper, gel, membrane, paper, foam pad. Care should be taken to exclude bubbles between gel and nitrocellulose membrane, and between nitrocellulose and paper. The cassette was closed and placed in the tank blotting apparatus so that the side of the cassette holder with the gel was facing the cathode. Transfer buffer (15.2 % w/v Tris-HCl (pH 8.0), 72 % w/v glycine. 20% v/v methanol) was then added to the blotting apparatus until the cassette was totally covered. The tank was then connected to the power output and the system was turned on for 1 hour and a half at 400 mA. The tank was soaked in ice to prevent overheating of the buffer during the transfer process. After removing the foam pad and filter papers, the membrane was blocked in TBS-T with 5% w/v milk powder to allow the saturation of all non-specific protein binding sites on the blots, for 1 hour and then washed three times for 5 min each in 1X TBS-T (10 mM Tris-HCl, (pH 7.5), 150 mM NaCl, 0.1% v/v Tween 20). The membrane was then transferred to a plastic bag containing the primary antibodies (1:1,000 for anti-JHDM1B, 1:30 for anti-tubulin) in TBS-T, and it was incubated slowly shaking overnight at 4˚C. The membrane was washed 3 times for 5 min each in 1X TBS-T. The membrane was transferred to a new plastic bag, and the HRP-labelled secondary antibodies (1:10,000 each) in TBS-T+ 5% milk were added and incubated with the membrane for 2 h at room temperature. The membrane was washed again 4 times for 5 min each with 1X TBS-T. 1 mL of ECL detection buffer was prepared and the membrane was incubated for 5 min. The membrane was transferred in a clean container until the development of the

bands. The size of protein of interest was identified by comparison with the molecular markers, and the efficiency of overexpression was quantified by comparing tubulin expression.

2.34. *In vitro* Wound Healing Assay. In order to evaluate the role of KDM2B CxxC finger in the process of cellular motility we employed *in vitro* would healing assays. Approximately 10^5 DU145 prostate cancer cells, which expressed empty vector pBABE, pBABE-mKDM2B and pBABE-mKDM2B(K616A) were plated onto 12-well dishes in RPMI+/+/+ medium and incubated until cultures reached 90% confluency. Two sets of experiments were designed˙ one included serum-starved (RPMI+/+/+/–FBS) cultures for 24 h before wounding and and one without starvation. A sterile pipette tip was used to produce a wound on the cell monolayers in the middle of the well at time point zero and the medium of all cultures was exchanged to full RPMI medium. The wounded areas in each well were marked and photographed in specific time points (0, 6, 12 & 24 hours) using an inverted microscope (Appendix 1 Table 5) with a 10× objective lens. Image J Analysis Software was used to measure the wound width and Microsoft Excel was used for the statistical analysis. The wound width was expressed as percentage of the initial wound width (100%).

Chapter 3

Results

3.1. Biochemical characterization of mKDM2B CxxC finger

3.1.1 Heterologous production of recombinant protein mKDM2B$_{577-707}$.

The CxxC domain of KDM2B binds non-methylated CpG DNA sequences (Koyama-Nasu et al., 2007; Blackledge et al., 2010; Farcas et al., 2012, Xu et al., 2018a). As DNA recognition can act as a sampling mechanism of KDM2B target genes (Long et al., 2013), elucidating the structural determinants of this interaction would enable targeted studies on understanding its role in KDM2B-associated gene regulation. In order to examine the biochemical properties of the CxxC and the PHD fingers, primers were designed in order to clone their coding sequences into the bacterial expression vector pET102/D. The pET102/ D-mKDM2B$_{577-707}$ construct (shown in Appendix 2) used to transform BL21 Codon+ *E. coli* cells for heterologous protein production. The recombinant protein mKDM2B$_{577-707}$ (shown in Appendix 3), consisted of 300 residues, was thioredoxin- fused at the N-terminus to increase the solubility of the protein and had a 6x His- tag at the C- terminus to facilitate quick protein purification through affinity chromatography. During protein production trials the cells were grown at 37°C, 25°C *(Figure 3.1)* and 17°C, concluding to optimal conditions for soluble proteins were to incubate the cells at 17°C for 16 h before adding the inducer and then incubate at 17°C for another 24h. SDS-PAGE was used to quantify the efficiency of the protein production before conducting protein purification through affinity chromatography. The 6xHis-tag at the N- terminus of the mKDM2B$_{577-707}$ enabled isolating the recombinant protein on nickel- NTA agarose resin and eluting it via imidazole, which acts as a competitor. As shown in *Figure 3.2*, increasing the salt concentration of the Lysis, Wash and Elution buffers in the affinity chromatography resulted in improved protein solubility and higher yields. To establish optimal assay conditions, a range of parameters was evaluated, including the effect of different

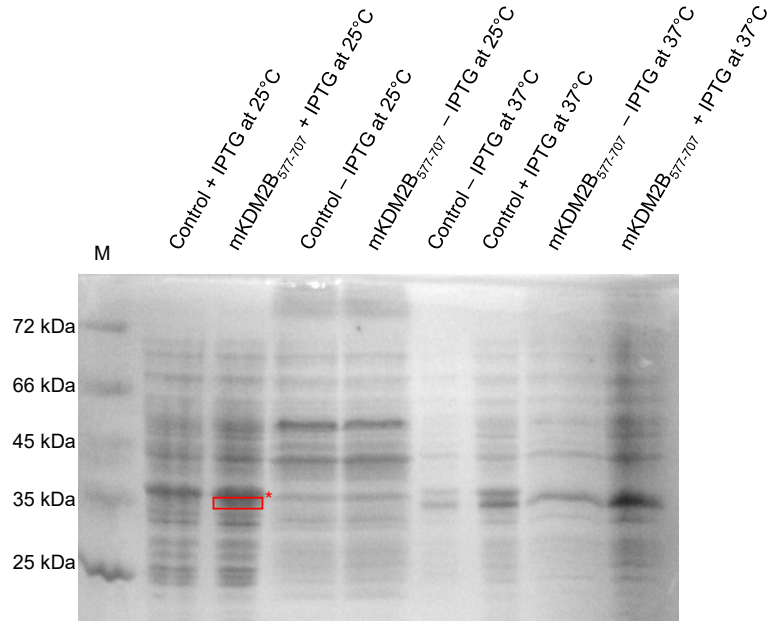

Figure 3.1. Recombinant protein mKDM2B$_{577-707}$ production trials. Cell growth temperatures 37°C and 25°C were tested for protein production optimization. At 37°C no band was detected and at 25°C the presence of the desired band (shown in red) indicated higher production efficiency at lower temperatures. Cells transformed with empty vector were used as negative control.

buffers (Tris and Phosphate), pH, salt concentrations and presence of reducing agents like DTT and β- mercaptoethanol on the protein stability and activity. In the optimal conditions, applied in Reaction buffer (described in Chapter 2) the protein maintained its activity for up to 3 weeks at 4°C.

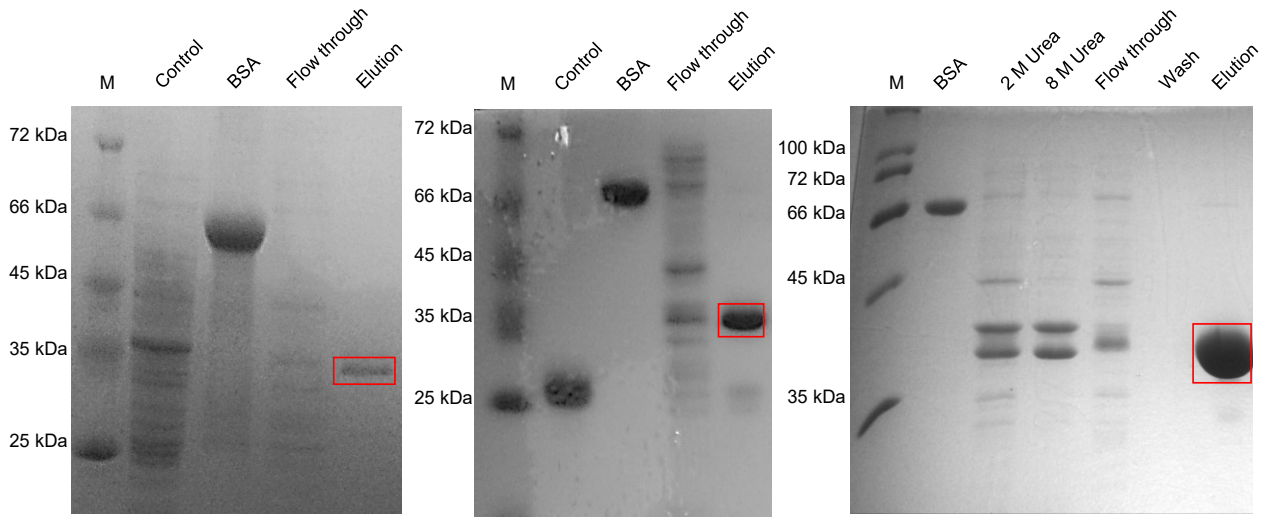

Figure 3.2. Increased buffer salt concentration affects mKDM2B$_{577-707}$ solubility. With 0.3 M NaCl concentration (right), the buffer maintains mKDM2B$_{577-707}$ protein soluble more efficiently compared to 0.1 M NaCl (left) and 0.2 M NaCl (center) thus resulting in higher eluted protein. Furthermore, 2 M and 8 M urea, used to denaturate possible protein aggregates formed in inclusion bodies, showed that more than 80% of the produced protein was in soluble state. Cells transformed with empty vector were used as negative control.

3.1.2. mKDM2B CxxC finger binds non methylated CpG sequences.

Based on previous results published by Koyama-Nasu and colleagues (Koyama-Nasu et al., 2007) on the DNA binding capacity of the CxxC domain of KDM2B, we focused on the interaction of the recombinant mKDM2B$_{577-707}$ with several synthetic double stranded oligonucleotides. We successfully radiolabeled three different CpG- containing oligonucleotide sequences, ^{32}P-CpG6, ^{32}P-CpG2 and ^{32}P-ORI2.5, as well as one GpC- containing oligonucleotide as negative control (shown in Appendix 1: Table 6) to be used in Electrophoresis Mobility Swift Assays. Our first aim was to confirm the results of Koyama-Nasu and also to examine several other binding parameters, including sequence specificity and Mg^{2+} dependence. In EMSA, the binding of mKDM2B$_{577-707}$ on the DNA substrate resulted in retardation of the migration of the radiolabeled substrate. As shown in *Figure 3.3*, KDM2B bound only CpG- containing sequence as substrate, thus verifying the previous reported data. Furthermore the reaction of ^{32}P-CpG6 with 2 μM mKDM2B$_{577-707}$ illustrated two distinct shifted bands (shown with black arrows), and also the presence of CpG6 competitor resulted in smear. Since the sequence of CpG6 contains 6 CG dinucleotides, each DNA molecule can bind up to 6 proteins. DNA strands that carry less than six proteins run lower than those fully occupied, leading to separate

bands. These results would also suggest a possible substrate specificity of the finger. To examine this possibility, mKDM2B$_{577-707}$ was tested with ^{32}P-CpG2 and ^{32}P-ORI2.5 oligonucleotides, which differ not only in length but also on the position of their CG dinucleotides. Our goal was to investigate whether multiple recognition events were taking place in each CpG. The super shift of ^{32}P-CpG2 incubated with 3 μM protein is explained by both CG dinucleotides being occupied by mKDM2B$_{577-707}$, instead of the simple shift with 0.5 μM protein, which probable leaves one of the two CpG available. In addition, ORI2.5 failed to have a proper shift upon incubation with 3 μM protein, indicating that the surrounding sequences of the CpG affects the recognition event *(Figure 3.4)*. These findings suggest that there is likely a correlation between DNA sequence and binding efficiency of mKDM2B$_{577-707}$ CxxC finger.

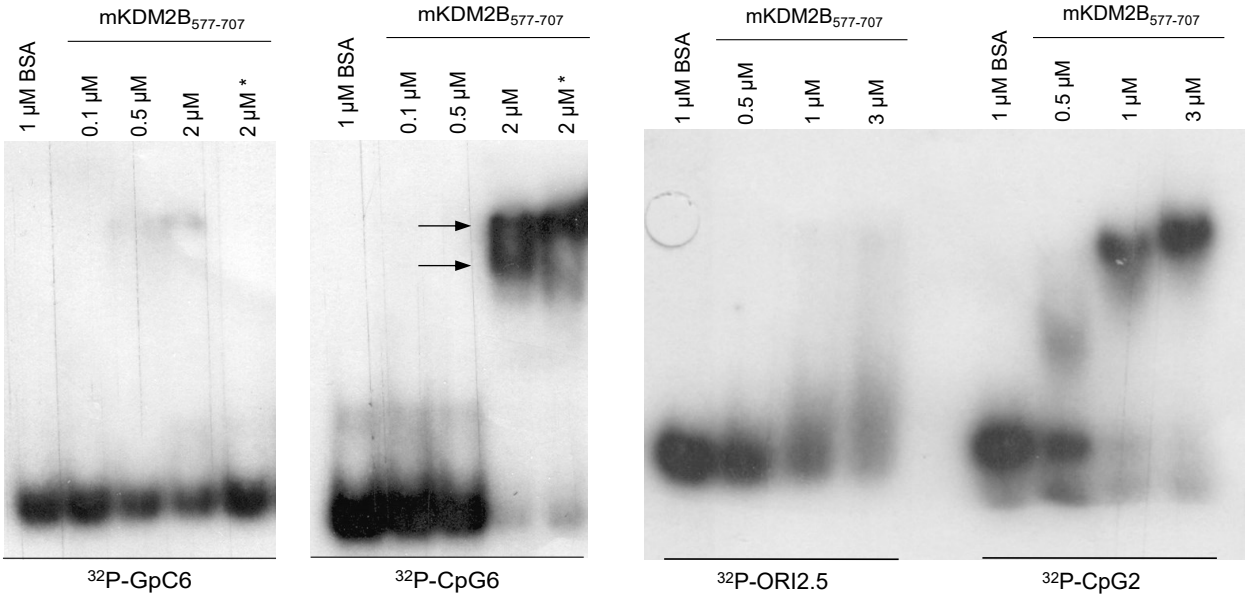

Figure 3.3. mKDM2B$_{577-707}$ binds non-methylated CpG sequences via the CxxC domain. 2 μM of mKDM2B$_{577-707}$ are sufficient for a total DNA migration retardation. mKDM2B$_{577-707}$ show no binding capacity for GC dinucleotides, indicating a significant sequence specificity. BSA was used as control and as blocker in all mKDM2B$_{577-707}$ reactions. (*) 5-fold increased concentration of non-radioactive CpG6 acts as competitor to ^{32}P-CpG6, resulting to a short smear, created from unoccupied CGs.

Figure 3.4. DNA Sequence- specific recognition of mKDM2B$_{577-707}$. The DNA sequence near the CG dinucleotide plays a role in the recognition event. As ^{32}P-ORI2.5 illustrates a smear rather than a band shift at high protein concentrations, suggests that one mKDM2B$_{577-707}$ molecule is not sufficient for DNA migration blockage. The existence of two different band shifts in ^{32}P-CpG reactions, indicate two different conformations, one with single binding event and one with both CG occupied.

3.1.3. mKDM2B CxxC finger binds DNA in a Mg^{2+}-independent manner.

Previous studies have shown that DNA recognition is significantly altered by the presence of metal ions, such as Mg^{2+}, which may affect protein stability and substrate specificity (Moll et al., 2002). In

order to investigate whether mKDM2B CxxC DNA binding is affected by Mg^{2+}, 5 μM $MgCl_2$ were supplemented in the reaction with ^{32}P-CpG2. Since CxxC finger is a Zn-finger domain, the Reaction buffer already contained 1 μM $ZnCl_2$ for protein stability. As seen in *Figure 3.5*, there was no significant change in the binding capacity of $mKDM2B_{577-707}$ to the oligonucleotide at the presence of Mg^{2+}, verifying that this is a specific recognition event. Moreover, chelation of the Zn^{2+} ions with EDTA, result in total loss of DNA binding capacity *(Figure 3.5)*.

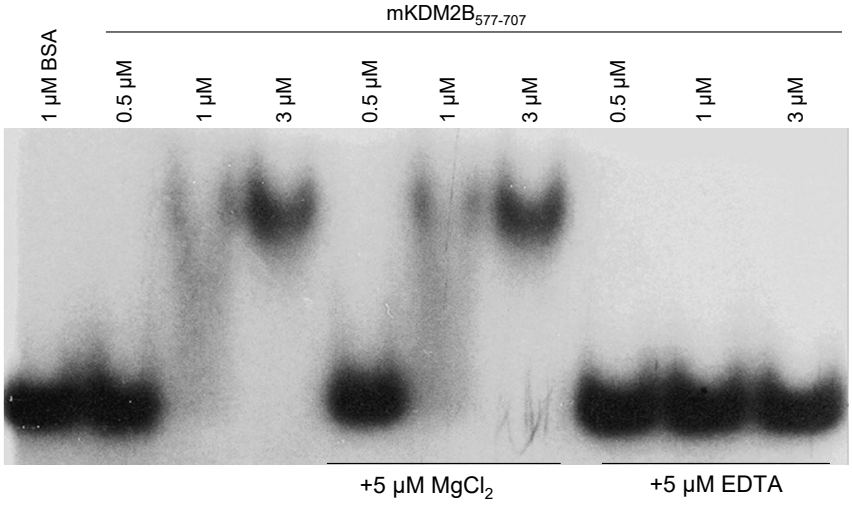

Figure 3.5. $mKDM2B_{577-707}$ binds non-methylated CpG sequences in a Mg^{2+}- independent manner. The $mKDM2B_{577-707}$ recombinant protein binds to synthetic double stranded ^{32}P- labeled 26-mer nucleotide (CpG2) that contains two CpG sequences. $MgCl_2$ has no effect on the binding and EDTA diminishes the binding due to Zn^{2+} chelation. BSA sample is used as negative control.

3.1.4. Several mKDM2B CxxC finger mutant variant show reduced DNA binding capacity.

When these studies were initiated, the structure of the KDM2B CxxC and PHD domains (RCSB PDB entry No 4O64) was not yet available. Therefore, in order to examine recognition elements of the domain we constructed a model of the CxxC-DNA interaction based on the structure of the MLL1-CxxC-DNA complex (Cierpicki et al., 2010). Using the online tool SWISS-MODEL, we identified candidate residues for DNA interaction, including R585, K608 and K616. To confirm whether these amino acids interact with DNA, we constructed three single mutant variants $mKDM2B_{577-707}$ (R585A), $KDM2B_{577-707}$ (K608A), $KDM2B_{577-707}$ (K616A) and a double mutant variant $mKDM2B_{577-707}$ (R585A/K616A). All plasmid constructs (Appendix 2) were produced with the megaprimer protocol and were confirmed with DNA sequencing as shown in *Figure 3.6*. All recombinant mKDM2B mutant proteins were fused with TRX and carried a 6xHis tag. The steps followed for protein purification were the same as described for the wild type protein, and the resulting proteins are shown in *Figure 3.7*.

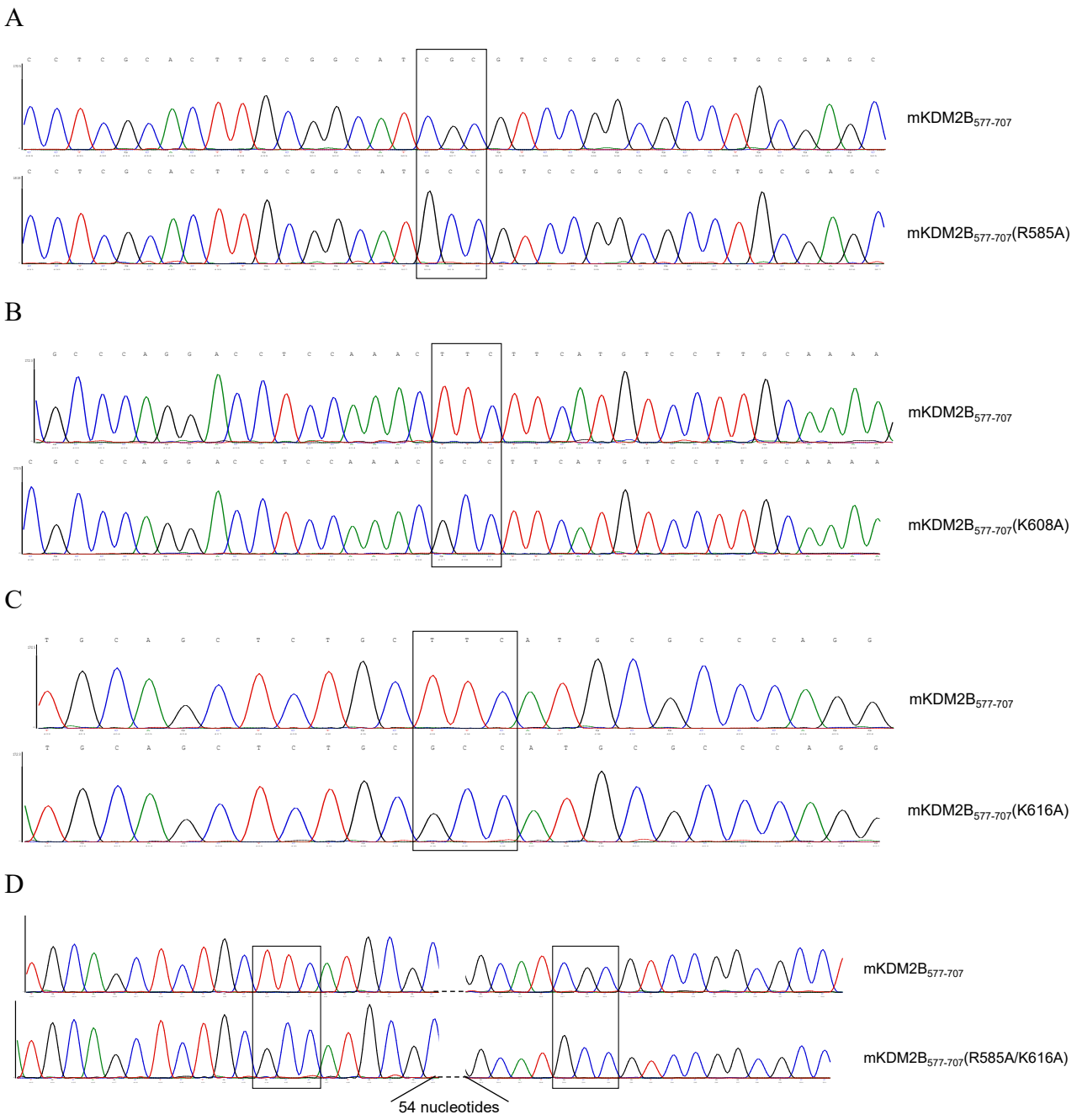

Figure 3.6. Chromatograms of the mKDM2B$_{577-707}$ mutant construct sequencing. The T7 reverse primer was used for all sequence readings. Adenine (green), thymine (red), guanine (black) and cytosine (blue) are depicted with single peaks on each chromatogram. The introduced single mutation (A) 5'CGC 3'[Arg]→ 5'CCG 3'[Ala], (B) 5'CTT 3'[Lys]→ 5'CCG 3'[Ala] (C) 5'CTT 3'[Lys]→ 5'CGC 3'[Ala] and the two mutations (D) 5'CGC 3'[Arg]→ 5'CCG 3'[Ala] & 5'CTT 3'[Lys]→ 5'CGC 3'[Ala] are shown with black box.

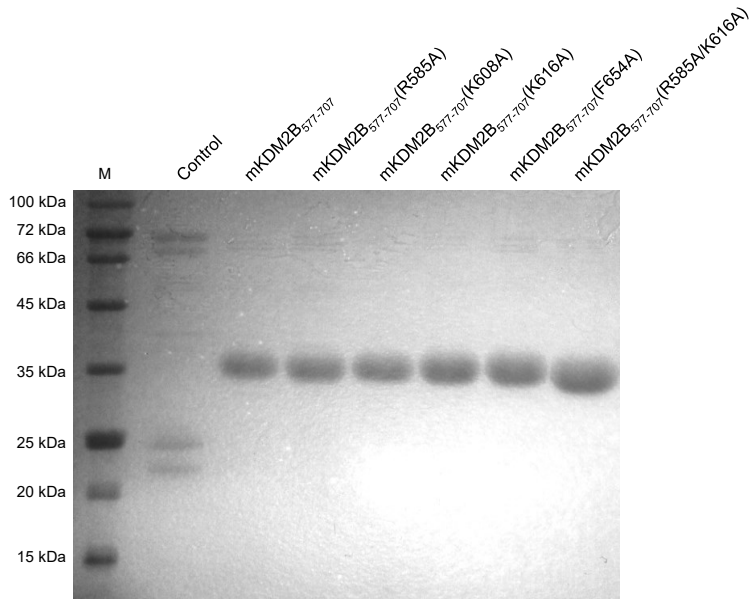

Figure 3.7. Heterologous production of mKDM2B$_{577-707}$ recombinant mutant proteins. 12% SDS-PAGE illustrates more than 95% purity of protein sample in all mKDM2B$_{577-707}$ mutants (34 kDa). mKDM2B$_{577-707}$(F654) is a PHD finger mutant, that was used in later studies (see 3.2.5.) The protein elution of pET102 empty vector- transformed cells was used as control.

To further evaluate the role of these residues as potential DNA recognition elements, their binding capacity to ^{32}P-CpG2 substrate was compared with the binding capacity of the wild type. Our results showed that all three single mutant variants failed to create a band shift in EMSA at the concentrations previously used with wild type mKDM2B, suggesting a significantly reduced binding affinity *(Figure 3.8)*. Both R585A and K616A mutations illustrated a strong effect on DNA binding, while the K608A mutation showed a weaker effect. To detect weaker interactions, we incubated ^{32}P-CpG2 with up to 16-fold higher protein concentration, and in addition we tested the double mutant mKDM2B$_{577-707}$ (R585A/K616A), as shown in *Figure 3.9*. The double mutant exhibited the weakest binding, where >24-fold higher protein concentration failed to promote a band shift. These results confirmed our hypothesis that residues R585, K608 and K616 are responsible for the DNA binding capacity of KDM2B CxxC finger, participate in DNA recognition and specificity. These data could serve as a starting point for developing KDM2B/ CxxC-targeted inhibitors.

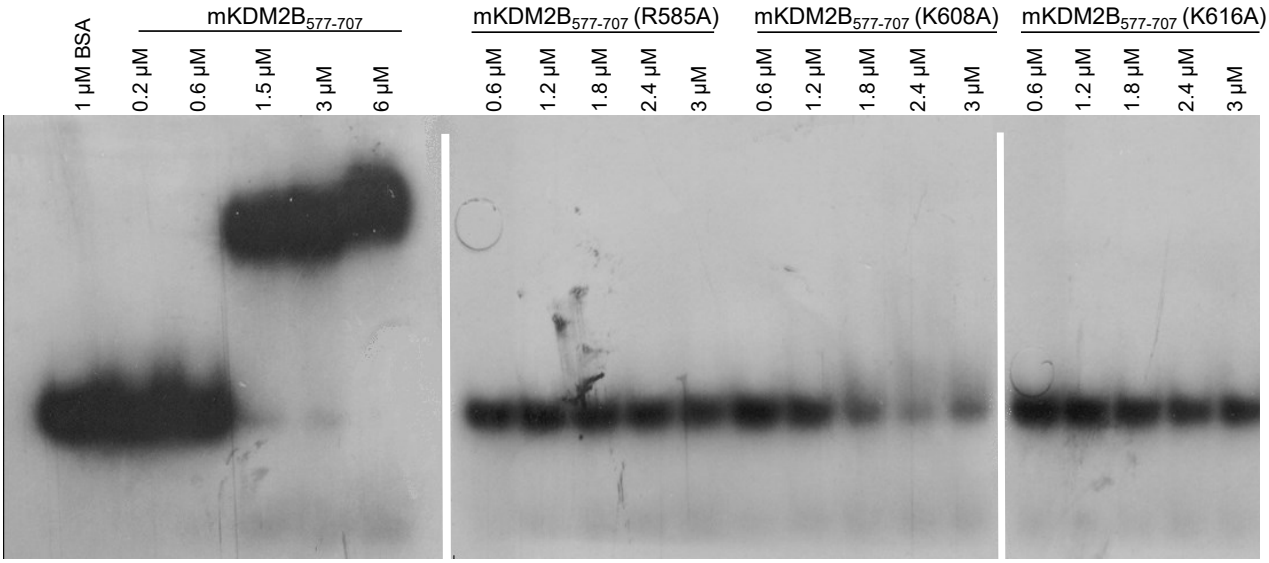

Figure 3.8. mKDM2B$_{577-707}$ mutants exhibit reduced DNA binding affinity. 10 nM radiolabelled dsDNA (^{32}P-CpG2) were incubated with mKDM2B$_{577-707}$ and mutants for 30 minutes at 37°C. Formation of the protein-DNA complex results in a band shift. Lack of a band shift in the mKDM2B$_{577-707}$ mutants reactions confirms the involvement of the specific residues in the interaction with DNA.

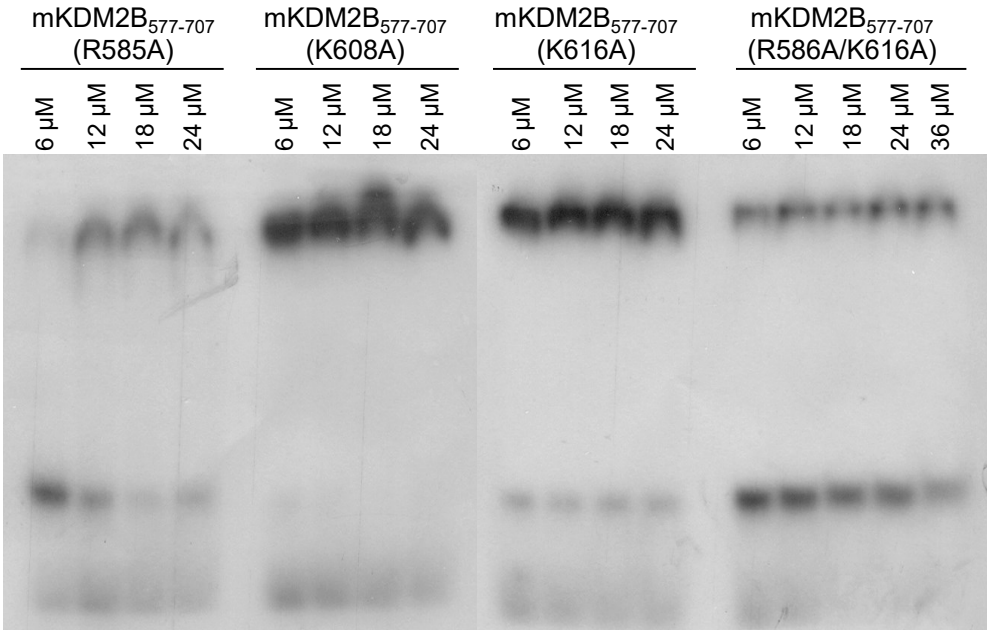

Figure 3.9. Analysis of mKDM2B$_{577-707}$ mutants reduced binding capacity. The single point mutations in the CxxC finger affected DNA recognition. Both mKDM2B$_{577-707}$(K608A) and mKDM2B$_{577-707}$ (K616A) indicated 4-fold reduced binding affinity to the DNA substrate, while mKDM2B$_{577-707}$ (R585A) showed more than 12-fold decrease. The CxxC double mutant mKDM2B$_{577-707}$ (R585A/ K616A) indicated the weakest DNA binding, with >24-fold reduced capacity. For these experiment 10 μM of ^{32}P-CpG2 were used in each reaction.

3.1.5. Setting up a fluorescence-based assay for detecting mKDM2B CxxC– DNA binding.

To establish a KDM2B/CxxC– targeted inhibitor screening, we designed a simple "on/off" assay based on fluorescence. It was agreed that a microplate platform, would provide an excellent scaffold for constructing our assays. In the wells of a microplate, the recombinant mKDM2B$_{577-707}$ was physically absorbed creating a docking surface for fluorescent DNA. In the presence of inhibitors, no DNA would bind, resulting in lack of fluorescence signal *(Figure 3.10)*. Before screening compounds as inhibition candidates, it was essential to examine the CxxC- DNA interaction at first. To do so, a set of preliminary experiments were conducted in order to evaluate this setup and optimize all the participating factors to reduce background noise *(Figure 3.11)*. It was decided, that lysozyme and EDTA will be used as surface blocker and DNA elution buffer respectively, as they indicated low intrinsic fluorescence. The next step was to evaluate the robustness of the protein-DNA interaction after consecutive washes.

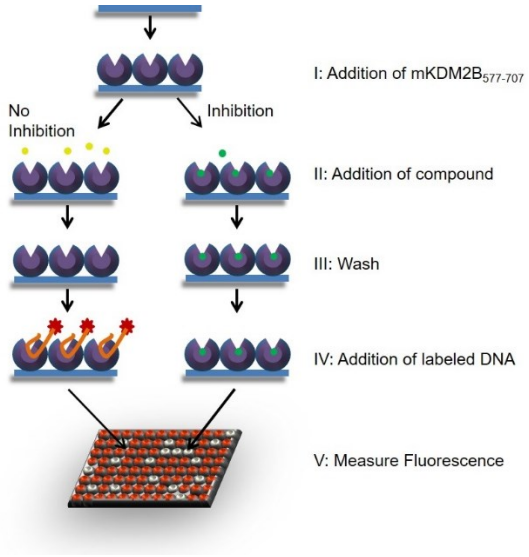

Figure 3.10. Model design of a high throughput CxxC inhibitor screening. In each well mKDM2B$_{577-707}$ (purple spheres) is absorbed on the surface and the inhibitor of CxxC domain (green dots) remains bound onto it, thus no DNA is recognized, resulting in no fluorescence

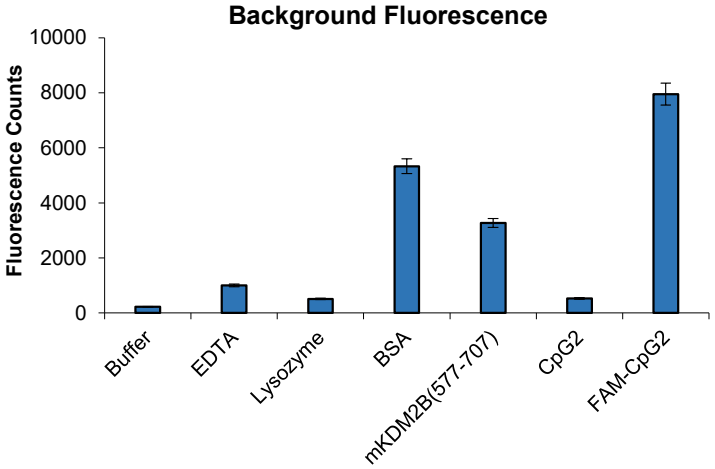

Figure 3.11. Measurement of background fluorescence of compounds and buffers. Lysozyme and BSA were tested for surface blockers. EDTA was tested for elution buffer. The concentration of FAM-CpG2 was 0.25 μM

Unfortunately, after the second wash almost all fluorescent signal was lost, indicating a fast –off reaction with mKDM2B$_{577-707}$ or non-specific binding on the well surfaces or with lysozyme *(Figure 3.12)*. In order to examine if this is the case we measured the fluorescence of 0.1 μM FAM-CpG2 after EDTA (2nd Step FAM-CpG2) and at the presence of an unlabeled DNA competitor *(Figure*

3.13). Based on the same levels of fluorescence detected in the 2nd step and the unsuccessful competition with unlabeled DNA, we concluded that FAM- CpG2 was binding non- specifically on the surface of the wells.

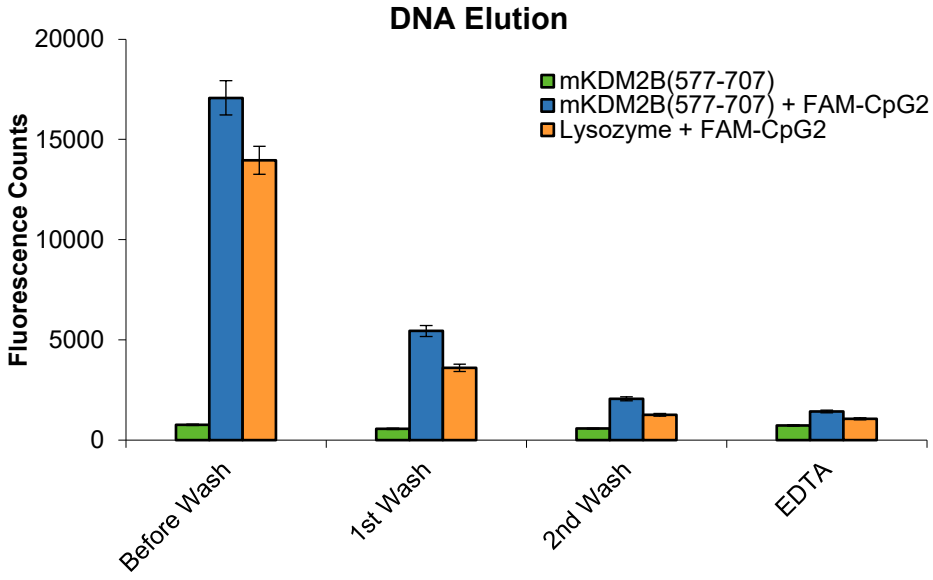

Figure 3.12. Depletion of FAM-CpG2 fluorescence after consecutive washes. The decrease of fluorescence after two washes indicate a fast- off binding reaction between $mKDM2B_{577-707}$ and DNA or a non- specific binding of the DNA on the surface or the protein blocker.

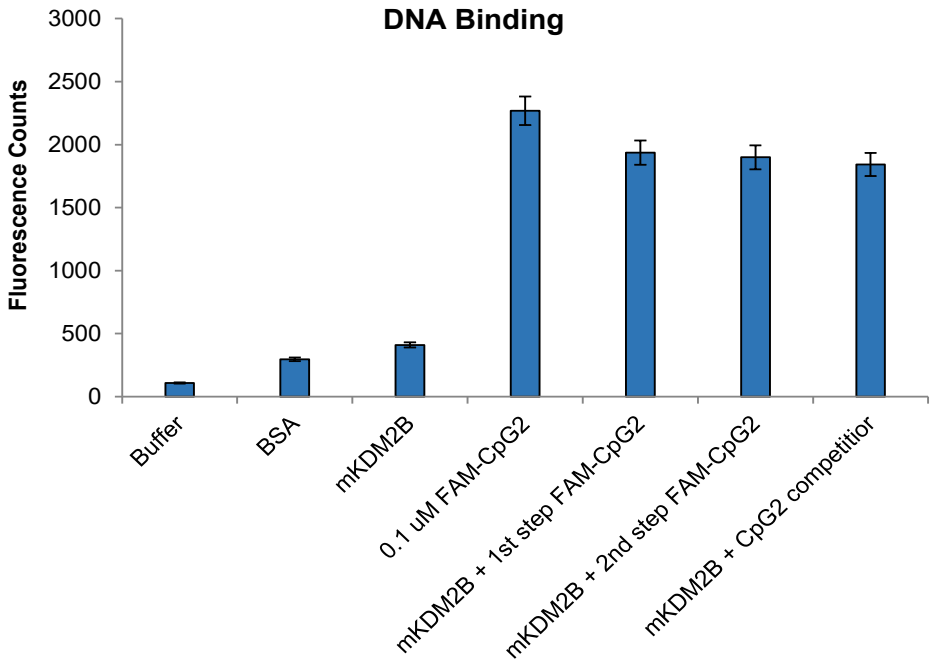

Figure 3.13. Fluorescence DNA binding assay. The 2nd step (addition of 0.1 μM FAM-CpG2 after EDTA) and 0.1 μM FAM-CpG2 at the presence of CpG2 competitor show the same fluorescence as the 1st step confirming the non- specific binding of FAM-CpG2 on the well surface. Buffer, BSA and mKDM2B were measured for background noise.

3.1.6. mKDM2B$_{577-707}$-EGFP binds Cy3-CpG2 resulting in FRET.

To establish an alternative DNA binding assay, we turned to Fluorescence Resonance Energy Transfer. In a FRET event there is a donor and an acceptor fluorophore and energy transfer can take place between them if they lay within a certain distance from each other (<40- 80Å, depending on the pair of fluorophores). In our case, the donor fluorophore, EGFP, was fused at the C- terminus of mKDM2B$_{577-707}$ and mKDM2B$_{577-707}$ (K616A) before the 6xHis tag *(Figure 3.14;* Appendix 2). TET and Cy3 were considered suitable acceptor candidates due to sufficient separation in excitation spectra for selective stimulation of the donor EGFP (Cy3), and sufficient overlap between the emission spectrum of the donor and the excitation spectrum of the acceptor (TET). Before starting to setup the screening platform, we examined whether fusion with EGFP caused steric hindrance on the interaction between the CxxC finger and DNA. Our data showed that mKDM2B$_{577-707}$-EGFP bound ^{32}P-CpG2 as efficiently as mKDM2B$_{577-707}$ without EGFP, resulting in band shift in EMSA *(Figure 3.15)*. Thus we continued with the setting up of a FRET-based DNA binding assay. The setup of the preliminary experiments included FRET detection in a high resolution spectrofluorometer. By using a cuvette in which mKDM2B$_{577-707}$-EGFP interacted Cy3-CpG2, we examined whether the energy transfer from EGFP to Cy3 could be measured. The recombinant mKDM2B$_{577-707}$ (K616A)-EGFP

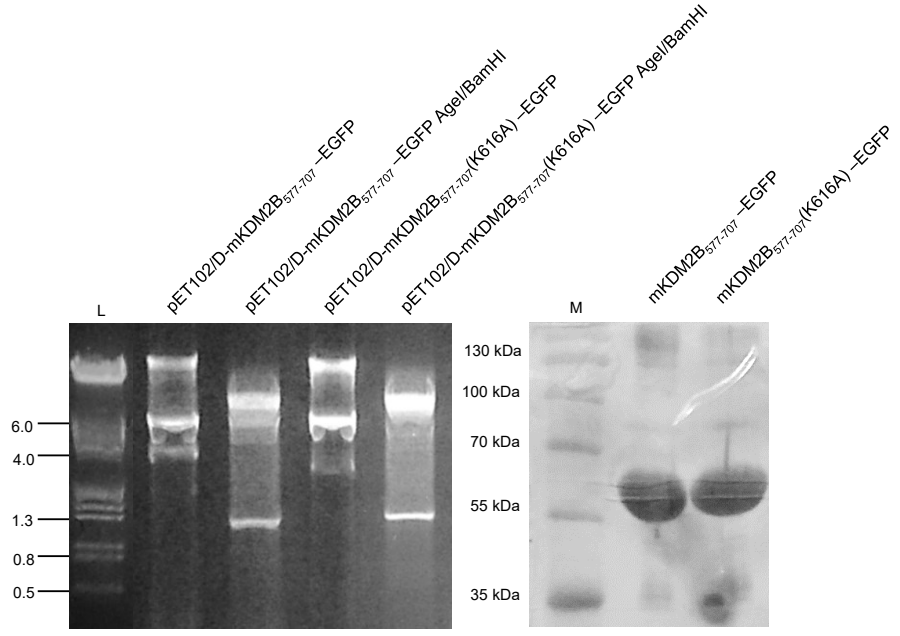

Figure 3.14. Cloning of EGFP coding sequence to pET102/D- mKDM2B$_{577-707}$ and mKDM2B$_{577-707}$(K616A). (Left) Enzymatic digestion with AgeI/ BamHI confirms the in frame insertion of EGFP coding sequence into pET102/D-mKDM2B$_{577-707}$ and mKDM2B$_{577-707}$(K616A). (Right) 12% SDS- PAGE shows more than 95% purity of mKDM2B$_{577-707}$-EGFP (59 kDa) and mKDM2B$_{577-707}$(K616A)-EGFP (59 kDa) recombinant protein samples.

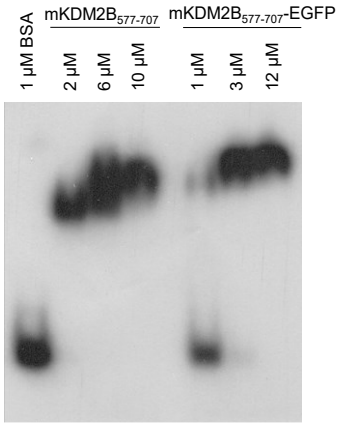

Figure 3.15. mKDM2B$_{577-707}$-EGFP binds CpG2. The band shift of ^{32}P-CpG2 upon incubation with 3 μM of mKDM2B$_{577-707}$-EGFP shows EGFP did not affect the DNA binding capacity of the CxxC finger.

was used as negative control. As shown in *Figure 3.16*, a fluorescence peak at 600 nm for mKDM2B$_{577-707}$, but not for the mKDM2B$_{577-707}$ (K616A) mutant, suggests energy transfer from EGFP to Cy3, due to CxxC-CpG2 binding. This data suggested that detecting CxxC-DNA interaction by FRET was feasible, however the spectrofluorometer used did not allow for a high throughput setup. In order to achieve this, we attempted to transfer the developed assay to a microplate format.

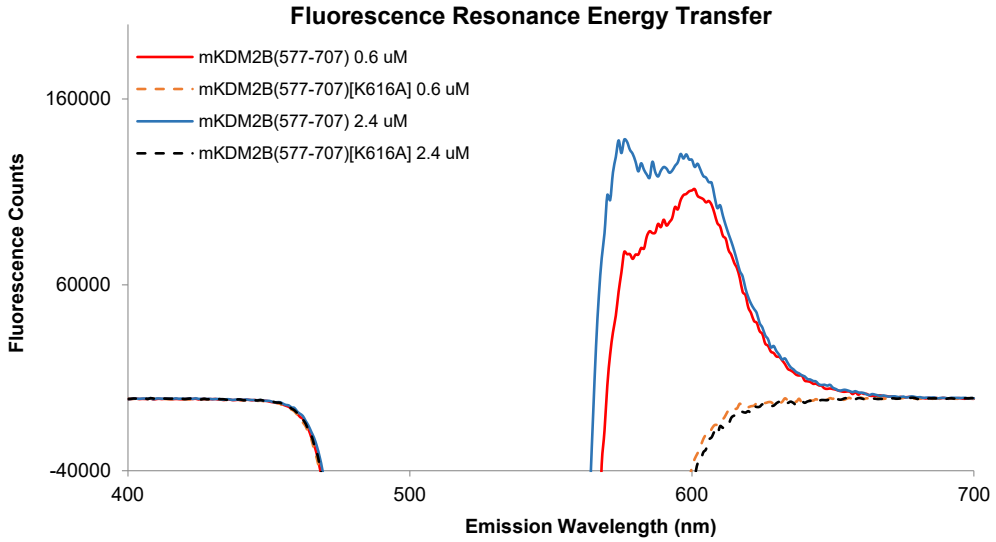

Figure 3.16. FRET-based DNA binding assay. Both 0.6 µM and 2.4 µM of mKDM2B$_{577-707}$ -EGFP demonstrate fluorescence at 580-600 nm, indicating the energy transfer to Cy3. mKDM2B$_{577-707}$ (K616A)-EGFP fail to bind DNA, thus no signal is detected at that wavelength. The graph depicts the total fluorescence of the EGFP- Cy3 complex, after extracting initial EGFP fluorescence.

In order to optimize the parameters of the new set of experiment in the microplate, we tested the fluorescent capacity of three different partners of mKDM2B$_{577-707}$- EGFP to examine which shows the best the signal-to-noise ratio. Signal is considered the fluorescence derived from the coupling of donor and acceptor fluorophore upon binding and noise is the fluorescence produced only from the acceptor fluorophore. To calculate the signal-to-noise ratio, the fluorescence spectrum of the three acceptor candidates (Cy3-CpG2, Cy3-CpGshort and TET-CpG2) was recorded, before and after addition of mKDM2B$_{577-707}$- EGFP in the reaction. Our analysis showed Cy3-CpG2 exhibited better overall signal-to-noise ratio compared to the other candidates *(Table 3.1)*, indicating mKDM2B$_{577-707}$- EGFP and Cy3-CpG2 as the most promising pair for FRET.

Table 3.1. FRET signal-to-noise ratio in the spectrofluorometer. TET – CpG2 and Cy3- CpG2 differ on the fluorophore. Cy3-CpG2 and Cy3- CpG2short differ on the length of oligonucleotide. mKDM2B$_{577-707}$-EGFP and DNA concentrations in each experiment were 80 nM and 30 nM, respectively

		Excitation (485 nm)		
		TET- CpG2	Cy3- CpG2	Cy3-CpG2short
Emission (nm)	530	1,4	1,59	1,02
	540	1,4	1,69	1,06
	550	1,4	1,76	1,24
	560	1,4	1,98	1,7
	570	1,4	2,17	2,13
	580	1,4	2,37	2,26
	590	1,3	2,51	2,33

3.1.7. Establishing a microplate- based FRET assay for detecting mKDM2B CxxC – DNA binding. To set up a microplate-based high throughput inhibitor screening assay, we designed the following procedure. As shown in *Figure 3.17* the recombinant mKDM2B$_{577-707}$-EGFP would physically absorbed on the wells surface, creating a docking matrix for fluorescent DNA. Evaluation of bound DNA would be established by measuring the fluorescence of the acceptor fluorophore (Cy3), which was chemically conjugated at the 5' of the DNA strands. In the presence of inhibitors, DNA binding to the CxxC finger would be reduced, resulting in lack of energy transfer to Cy3 and reduced fluorescence signal.

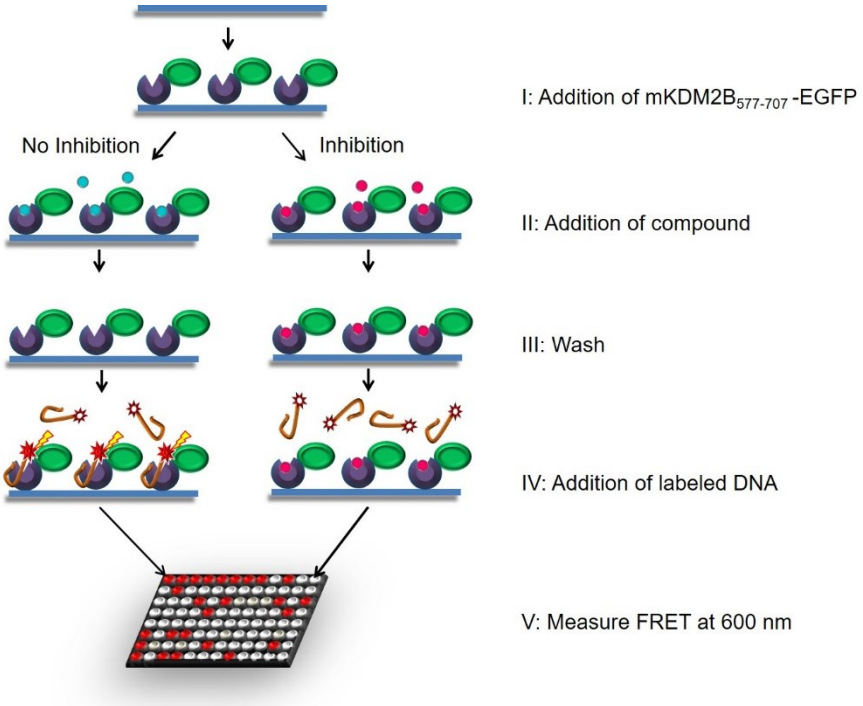

Figure 3.17. Microplate- based FRET inhibitor screening assay. Recombinant mKDM2B$_{577-707}$- EGFP is physically absorbed on the well surface and upon DNA binding, energy is transferred from EGFP to Cy3, resulting in fluorescent signal. CxxC-DNA inhibition due to compound (pink dots) leads to loss of fluorescence signal.

The available emission filters in the plate reader were set at 535 nm, which EGFP still emits fluorescence. In order to avoid photobleaching of EGFP and to minimize the detected background noise, several protein concentrations were evaluated by DNA titration. However, the analysis of the mKDM2B$_{577-707}$- EGFP interaction with Cy3-CpG2 illustrated significantly low signal-to-noise ratio even for DNA concentrations below 1 μM *(Figure 3.18)*. These data suggested that the wide band pass of the plate reader filter could not block EGFP- derived fluorescence, thus increasing the background, making this assay difficult to implement.

Because of the difficulties in detection FRET directly, we decided to develop an alternative method based on the detection of Time- Related Fluorescence Attenuation (TRFA). The principle of this method dictates that the fluorescence of the EGFP-Cy3 complex is quenched faster compared to the fluorescence of the EGFP alone, due to the energy transfer during DNA binding. To evaluate the binding interaction by TRFA, we used mKDM2B$_{577-707}$- EGFP and mKDM2B$_{577-707}$(K616A)-EGFP as negative control with Cy3-CpG2. As shown in *Figure 3.19,* no difference was observed between quenching time for both reactions. Furthermore, Cy3-CpG2 showed substantially high fluorescence and fast quenching time in the absence of both proteins in the well. Altogether, these results suggested that Cy3-derived fluorescence possibly masked the fluorescence from EGFP, and the signal detected was not attributed to the EGFP-Cy3 coupling but rather to Cy3 alone. These results suggested that the further development of this assay was hampered by the technical specifications of the microplate reader used. To establish a reliable assay, it is necessary to employ a monochromator, which would allow a narrow range of wavelengths to be detected, resulting in a tailor-made FRET detection method.

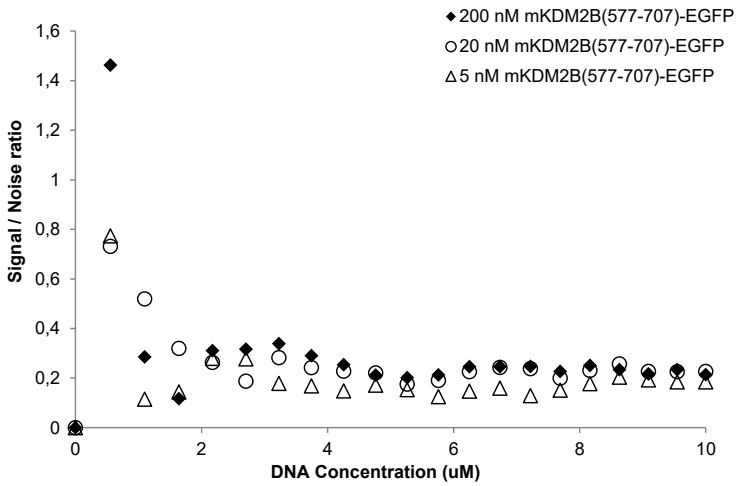

Figure 3.18. FRET Signal-to-noise ratio in Victor X5. Signal (mKDM2B$_{577-707}$ + Cy3-CpG2) to noise (Cy3-CpG2) ratio describes the efficiency of the FRET event. DNA titration with three different protein concentrations (200, 20 and 5 nM) show a signal to noise ratio of 0.2 after 1 μM of DNA, making it inappropriate for FRET detection.

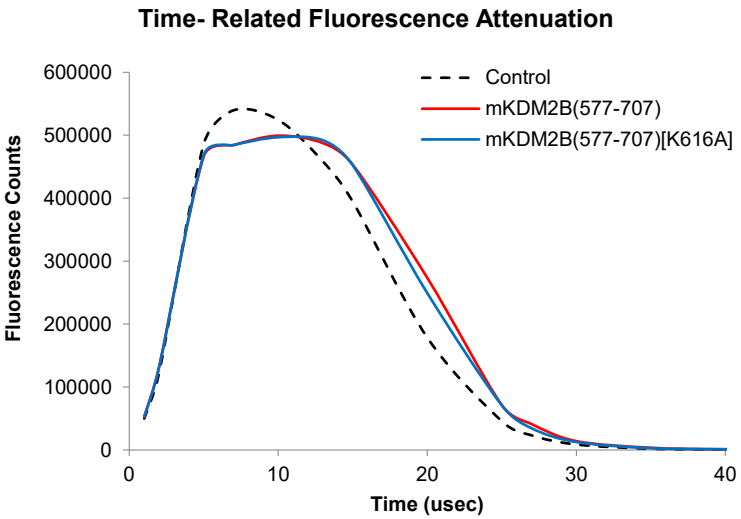

Figure 3.19. TRFA DNA binding assay. Upon DNA binding, FRET can be observed indirectly through faster quenching of fluorescence. Both wild type and mutant proteins (0.5 μM) showed same quenching time at the presence of 2 μM Cy3-CpG2. A sample containing only Cy3-CpG2 was used as control..

3.2. Biochemical characterization of mKDM2B PHD finger

3.2.1. The PHD finger of mKDM2B recognizes specific histone peptides.

To understand the function of the PHD-finger domain of KDM2B we set out to examine its potential involvement in histone recognition. To this end, we established a screening assay to detect the interaction of recombinant protein with a panel of 379 histone peptides that contain different combinations of covalent modifications (Appendix 4) spotted on a commercially available MODified™ Histone Peptide Array (Active Motif, USA). The recombinant protein mKDM2B$_{577-707}$, which contained the CxxC and PHD fingers, was fused to a V5 epitope. We incubated the recombinant protein with the array and evaluated its binding to specific peptides by detection with the anti-V5 antibody.

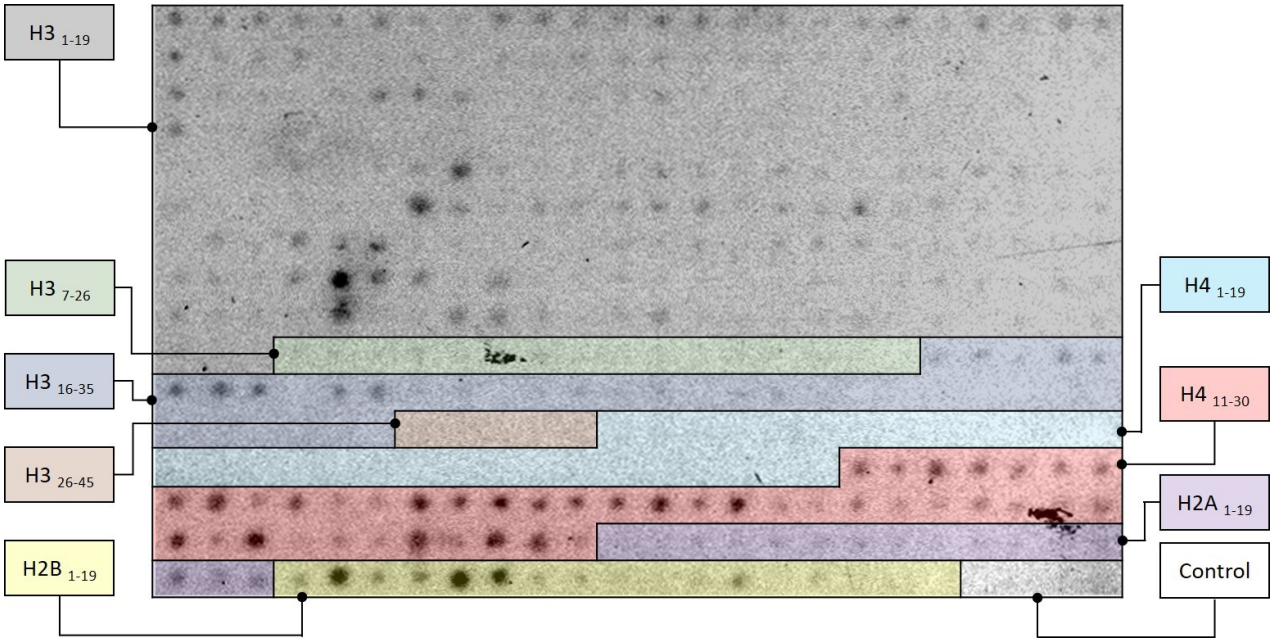

Figure 3.20. Histone peptide array analysis of mKDM2B$_{577-707}$. Recombinant mKDM2B$_{577-707}$ was incubated with MODified™ Histone Peptide Arrays and the interaction of the protein with histone peptides was analyzed by immunodetection. Here, only one of the two panel of the replicate array is shown for clarity and the areas of the array that correspond to the different peptide groups are shown in different colors to facilitate analysis by the reader. A more detailed diagram of the different spots and the corresponding modification is provided in Appendix 4. This analysis revealed strong interaction between mKDM2B$_{577-707}$ and H4$_{11-30}$ (red area). No binding was observed between PHD and H4$_{1-19}$ (blue area) indicating that the recognition depends on a critical residue that is present in the region 20-30 of histone H4. Significant interaction with H2B$_{1-19}$ (yellow area) can also be seen.

As shown in *Figure 3.20*, mKDM2B$_{577-707}$ showed strong interaction with different modified peptides in the region spanning amino acids 11-30 of histone H4. Since mKDM2B$_{577-707}$ displayed very little binding with all the different modified peptides covering the region 1-19 of H4, we concluded that

residues playing an essential role in this interaction are located downstream of amino acid 19 of H4. In agreement, correlation of the modifications present in each peptide *(Figure 3.21)* with the intensity of the binding signal highlighted the involvement of methylation of lysine 20 of histone H4 in the observed interaction. The peptide array analysis also revealed significant binding of mKDM2B$_{577-707}$ to different modified peptides in the region 1-19 of histone H2B. Weaker interactions could be observed with H3$_{21-36}$ peptides containing different methyl or acetyl marks at K27 and H3$_{1-19}$ peptides containing K4 trimethyl marks. No interaction was observed with any modified H2A$_{1-19}$ peptide. Although previous reports had implicated the binding of H3K4me3 by the PHD domain in a mechanism of cis H3K4me3 demethylation by KDM2B (Janzer et al., 2012), the present results suggest that the PHD domain of KDM2B preferentially recognizes other histone modifications.

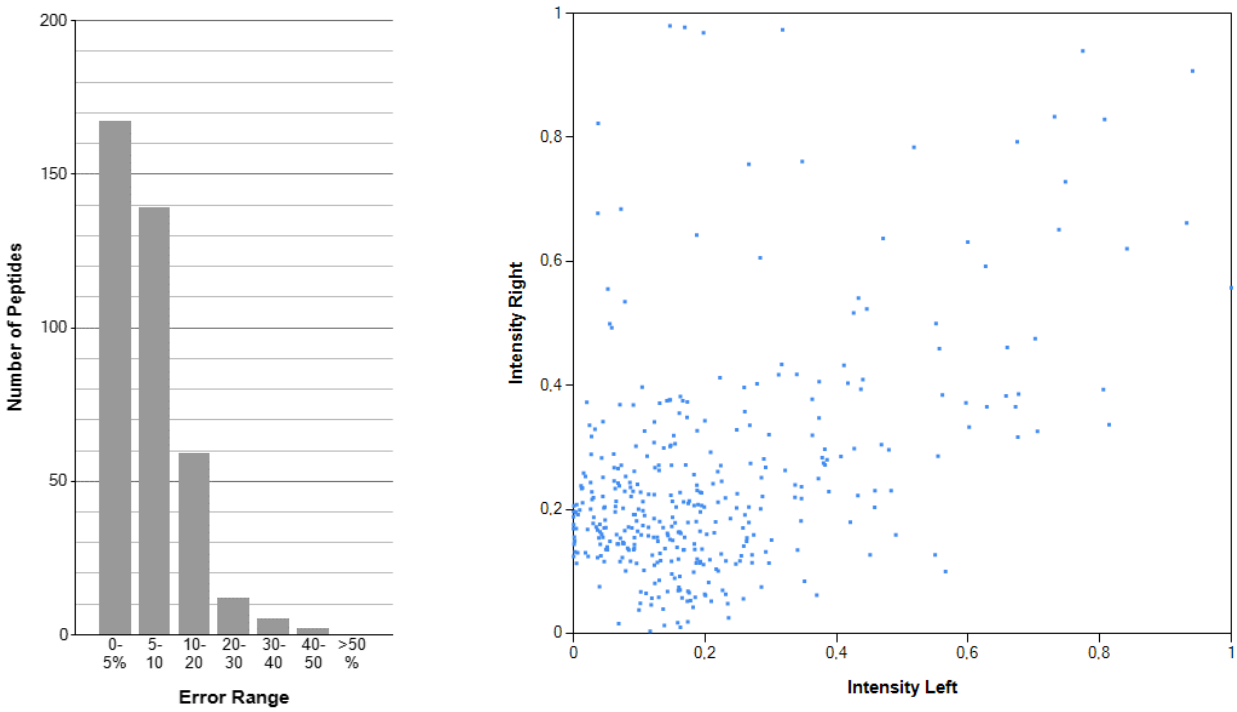

Figure 3.21. Reproducibility of the histone peptide array analysis of mKDM2B$_{577-707}$. (Left) The distribution graph presents the errors of the intensities between the right and the left grid. Most of the peptides contain 0-10% error range indicating minor discrepancies between the two grids. (Right) Comparative analysis of the measured intensities. Perfect duplicates follow the straight line between points (0,0) and (1,1). Most peptides illustrate intensities below 0.5 indicating mKDM2B PHD substrate specificity.

3.2.2. mKDM2B$_{577-707}$ does not recognize H4 N-terminal tail.

Taking a step further into investigating mKDM2B$_{577-707}$ H4 binding specificity, we tried to exploit the FRET technique that we had successfully developed for the CxxC domain, to examine the interaction of the PHD domain with parts of the histone H4. To evaluate whether establishing a FRET-based assay was possible, monomeric Red Fluorescent Protein (mRFP) was considered an appropriate partner for EGFP. To this end, the coding sequences of the residues 1-18, 17-34, 33-50 and 49-69 of H4 were cloned in the bacterial expression vector pET102/D, as shown in *Figure 3.22*, and the coding sequence of the monomeric Red Fluorescent Protein (mRFP) was also cloned next to the H4 sequences (Appendix 3). All four H4-mRFP recombinant proteins were heterologous produced and isolated via affinity chromatography *(Figure 3.22)*. In order to qualitatively examine whether the PHD domain of mKDM2B recognizes H4, we set up a FRET-based assay in the previously used spectrofluorometer. In this set of experiments, only PHD-H4 binding would result in mRFP fluorescence emission at 585-610 nm, similarly to Cy3, thus the mKDM2B$_{577-707}$-EGFP and Cy3-CpG2 reaction was used as positive control.

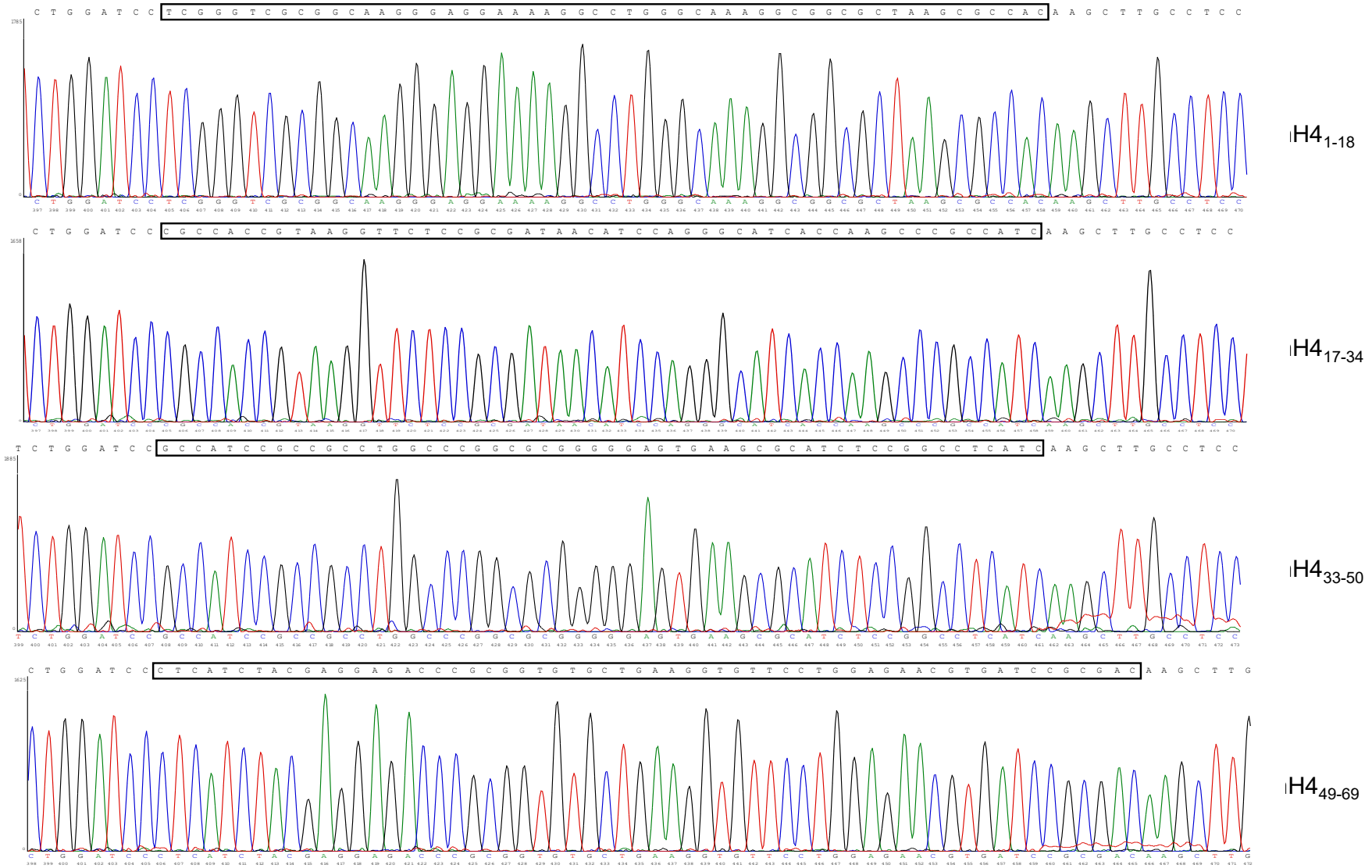

Figure 3.22. Chromatograms of the H4 construct sequence readings. T7 forward primer was used for all sequencing readings. Adenine (green), thymine (red), guanine (black) and cytosine (blue) are depicted with single peaks on each chromatogram. The 5'-3'nucleotide sequence of each H4 part is illustrated in black box.

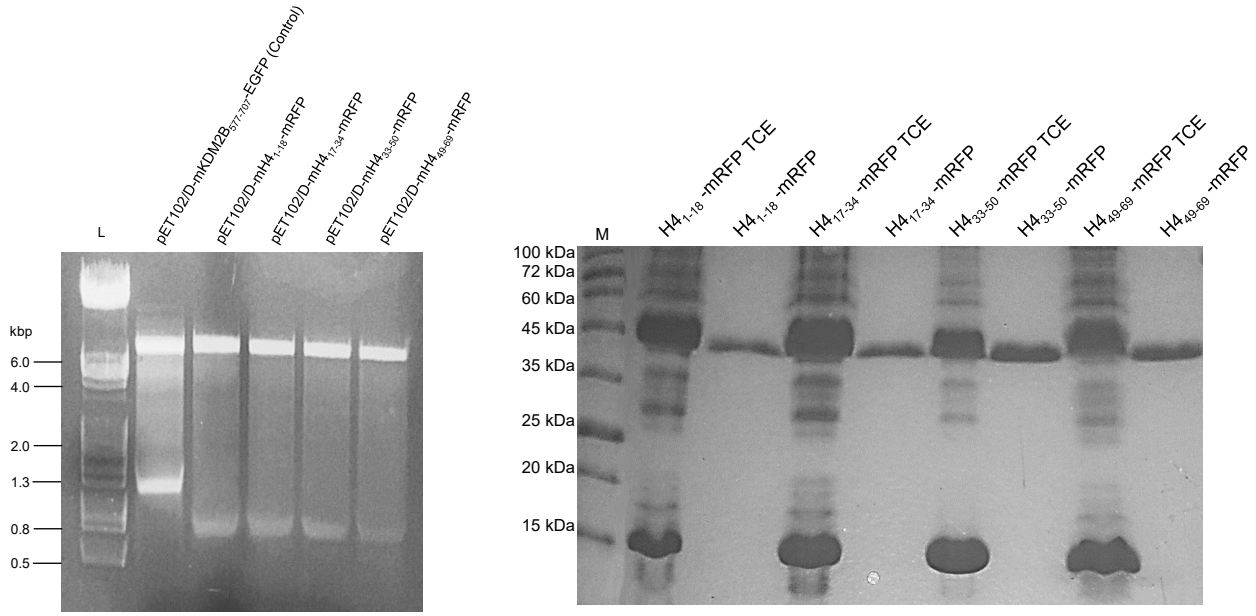

Figure 3.23. H4-mRFP recombinant proteins. (a) Construct verification via agarose gel electrophoresis. The pET102/D-mH4 constructs were doubly digested with restriction enzymes BamHI & AgeI to confirm the insertion of the mH4(aa)-mRFP sequences (Appendix 3). pET102/D-mKDM2B-EGFP was used as control. **(b) Heterologous production and isolation of H4-mRFP recombinant proteins.** 12% SDS- PAGE shows more than 95% purity of H4-mRFP (41 kDa) recombinant protein samples. Total Cell Extract (TCE) contained all proteins extracted from the disrupted BL21 cells.

However, we were unable to observe any peak of fluorescence in the region 585- 610 nm, indicating lack of FRET *(Figure 3.24)*. At this point, three possible explanations for this outcome were considered. First, the binding might not have occurred, due to steric hindrance between mKDM2B$_{577-707}$ -EGFP and H4-mRFP. Secondly, the PHD finger might not had recognized any part of the H4 due to misfolding of the histone part. Thirdly, by comparing these data with our previous results that showed interaction between the PHD domain and the 11-30 residues of H4, these findings suggested that the binding probably requires residues from both 1-18 and 17-33 oligopeptide sequences that may also carry specific post-translational modifications, such as methylation.

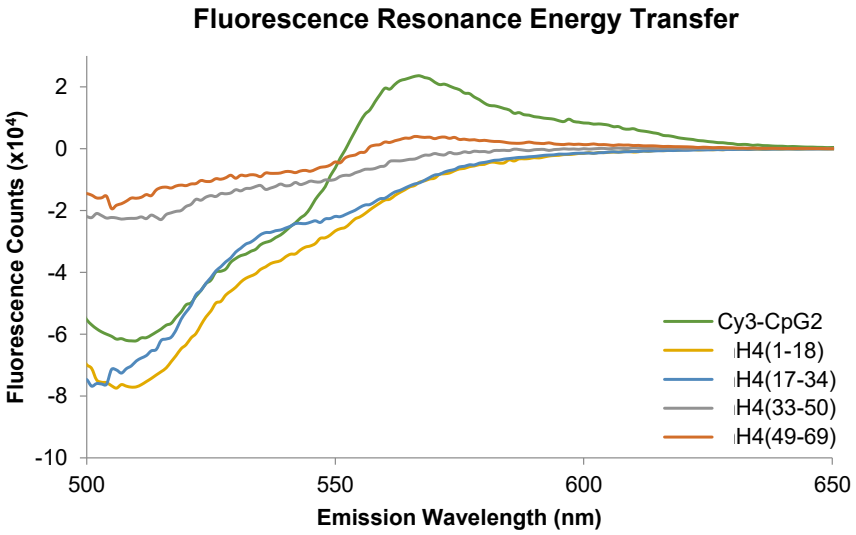

Figure 3.24. FRET-based Histone binding assay. All H4-mRFP recombinant proteins failed to bind to mKDM2B PHD, thus no signal is detected at 600 nm. The graph depicts the total fluorescence of the EGFP-mRFP complex, after extracting the buffer and initial EGFP fluorescence. Cy3-CpG2 was used as positive control.

3.2.3. mKDM2B$_{577-707}$ recognizes H4K20me3. To examine if this is the case and to expand further our initial results from MHPA, we focused on the observed interactions with histone H4, histone H3 and histone H2B, by studying the binding of mKDM2B$_{577-707}$ to a series of 11-mer and 19-mer synthetic oligopeptides (Appendix 1: Table 3) using isothermal titration calorimetry (ITC). Our first results revealed that mKDM2B PHD finger exhibits selective binding to an H4 oligopeptide spanning amino acids 16-25 and carrying a trimethyl group on lysine 20. Furthermore, there was a markedly weaker binding to similar oligopeptides carrying mono- or di- methylation marks on lysine 20 or to oligopeptides without any modification or any part of the recombinant H4 *(Figure 3.25)*, suggesting that the PHD of mKDM2B interacts specifically with H4K20me3. Moreover, we observed a significantly weaker interaction (8-fold) with a histone H3$_{1-11}$ oligopeptide carrying a trimethylation mark on lysine 4 (K_D= 370 mM), confirming the Modified Histone Peptide Array results. As shown in *Figure 3.26,* the rest of H3 peptides, carrying methylation marks on H3K27 or H3K36 showed very weak interaction that was independent of the presence of a methylated amino acid. Finally, titration of synthetic peptides with the sequence of the first 19 residues of H2B, depicted a weak interaction between mKDM2B and H2BK15ac, which was specific to the presence of the acetylation *(Figure 3.27)*, suggesting that may be more than one histone substrates of KDM2B.

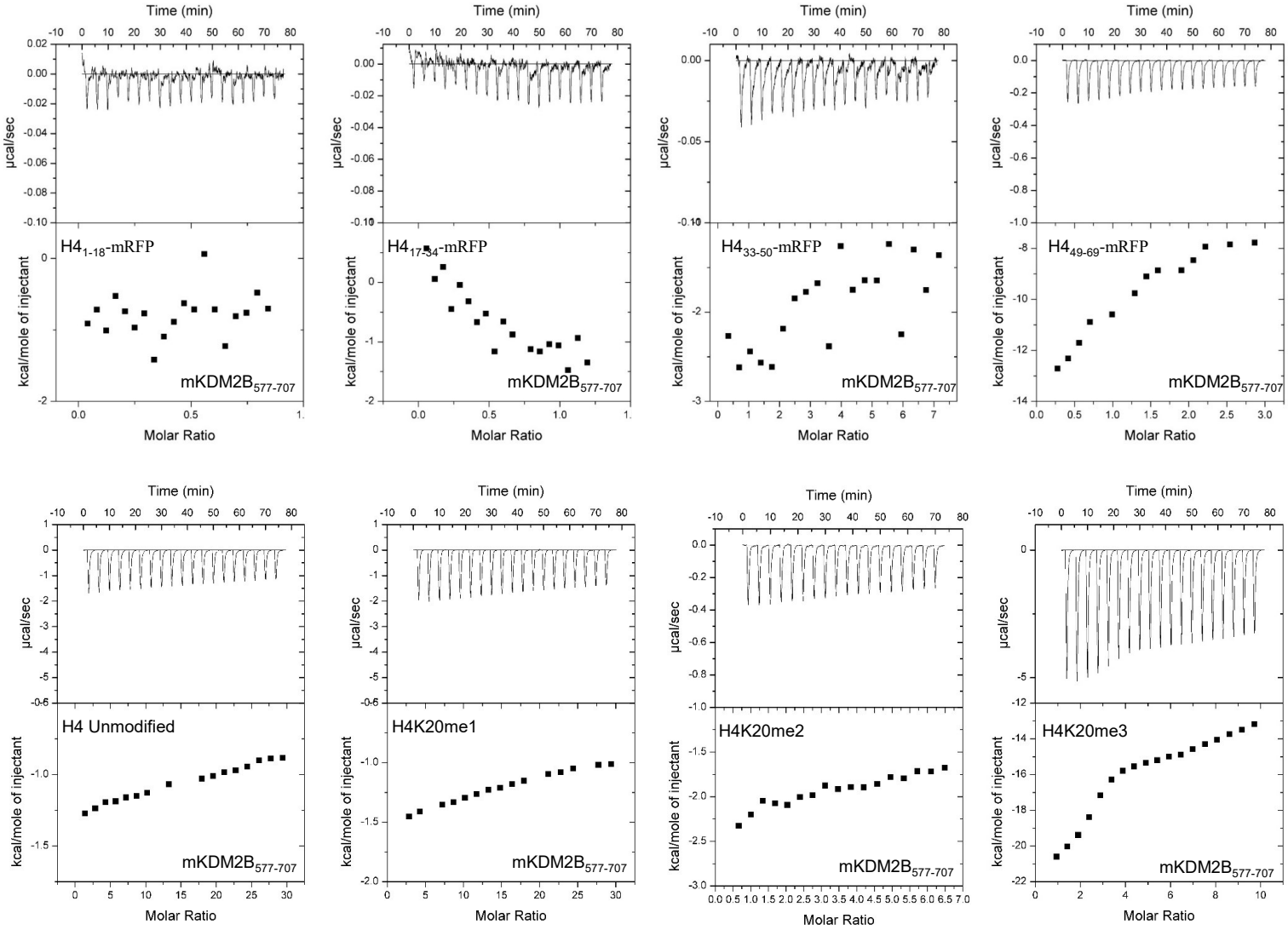

Figure 3.25. mKDM2B recognizes specifically H4K20me3. ITC binding curves of mKDM2B$_{577-707}$ with recombinant H4 proteins and H4 synthetic oligopeptides show substrate specificity. The integrated ΔH (kcal/mol) values are plotted versus the peptide/protein molar ratio and shown in the lower panel. Titration of the H4$_{49-69}$ with the recombinant protein mKDM2B$_{577-707}$ indicates a much weaker binding (K_d> 1 M) compared to H4K20me3 (K_d= 3 mM). The titrating peptide is shown in every graph.

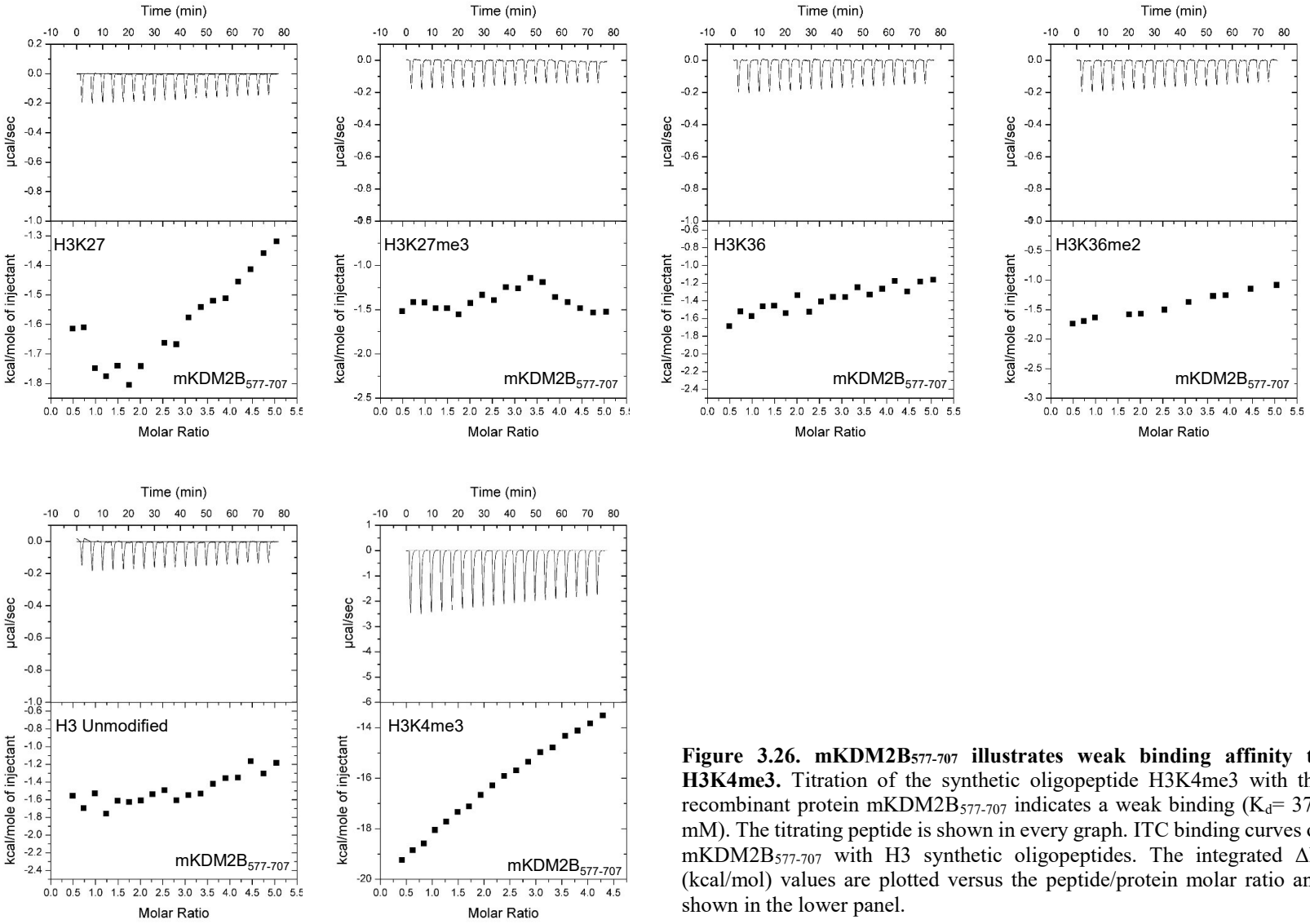

Figure 3.26. mKDM2B$_{577-707}$ illustrates weak binding affinity to H3K4me3. Titration of the synthetic oligopeptide H3K4me3 with the recombinant protein mKDM2B$_{577-707}$ indicates a weak binding (K_d= 370 mM). The titrating peptide is shown in every graph. ITC binding curves of mKDM2B$_{577-707}$ with H3 synthetic oligopeptides. The integrated ΔH (kcal/mol) values are plotted versus the peptide/protein molar ratio and shown in the lower panel.

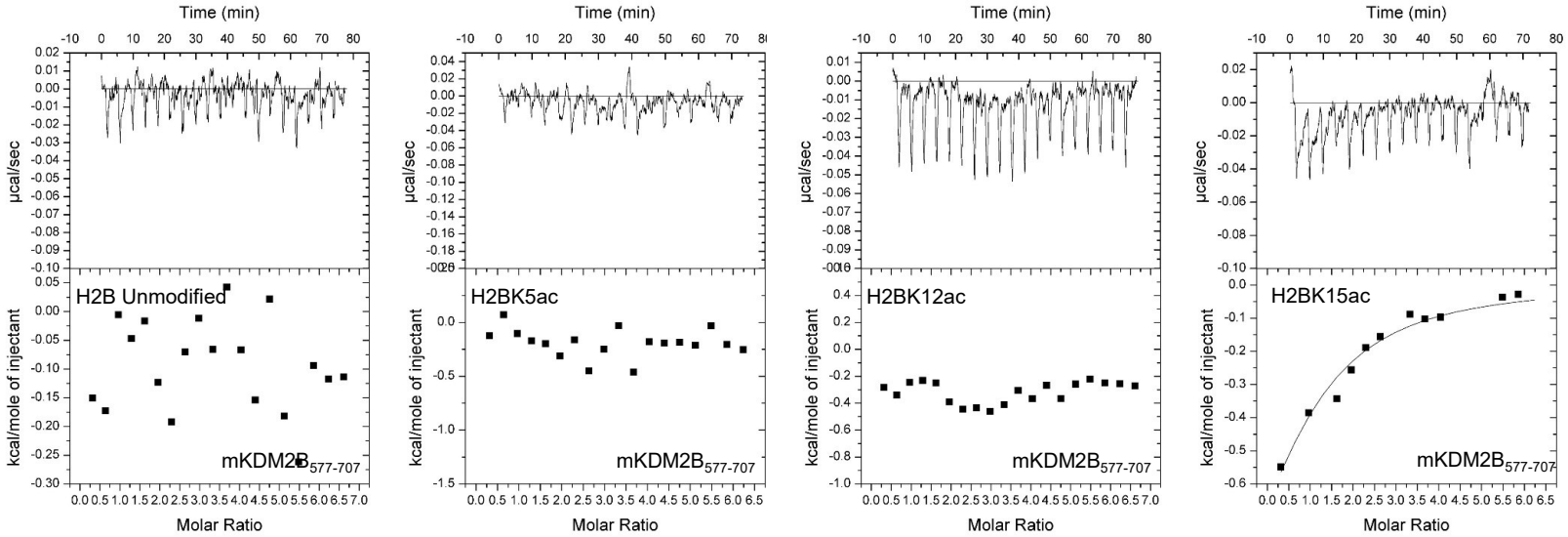

Figure 3.27. mKDM2B shows also weak interaction with histone H2BK15ac. ITC binding curves of $mKDM2B_{577-707}$ with H2B synthetic oligopeptides. The integrated ΔH (kcal/mol) values are plotted versus the peptide/protein molar ratio and shown in the lower panel. Titration of the synthetic oligopeptide H2BK15ac with the recombinant protein $mKDM2B_{577-707}$ indicates a very weak binding (K_d> 1 M). The titrating peptide is shown in every graph.

3.2.4. Residue F654 of mKDM2B PHD finger in not associated with histone binding capacity.

To further elucidate the mechanism behind histone binding, we sought out to examine the structure of the mKDM2B PHD finger. Previous studies showed that many histone binding domains recognize the trimethyl mark on lysine via a cage formed by aromatic residues (Taverna et al., 2007, Sanchez and Zhou, 2011, Musselman and Kutateladze, 2011). We examined the available structural information for the PHD of mKDM2B but were unable to identify a typical aromatic cage on the structure. However, we selected the closest possible structural element that could contribute to this interaction, consisting of residues F654, P670 and W690 for further analysis. To examine the possible involvement of this arrangement in ligand recognition, we selected F654 for mutagenesis (the other two residues appeared to play a structural role and were not selected). We constructed variant mKDM2B$_{577\text{-}707}$ (F654A) *(Figure 3.28)* and analyzed the interaction of the recombinant protein with the H4K20me3 and H3K4me3 oligopeptides. There was a small decrease in the binding affinity of the mutant for H4K20me3 but no difference in the binding affinity for H3K4me3 *(Figure 3.29)*, suggesting that it is unlikely that this phenylalanine residue plays a critical role in the recognition event. A summary of all ITC experiments is shown in *Table 3.2*.

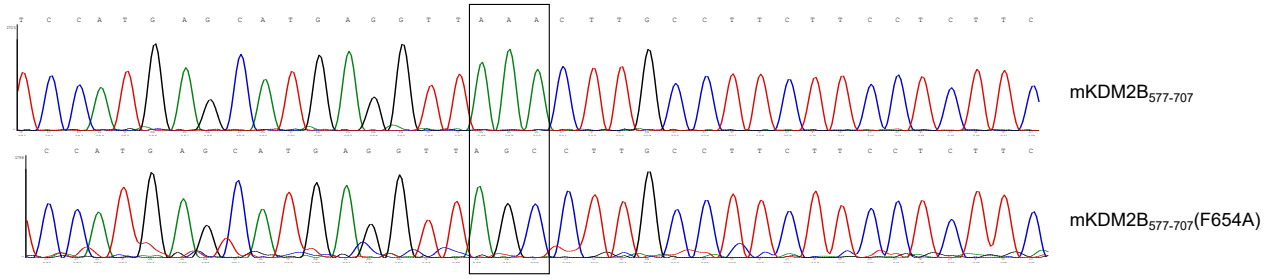

Figure 3.28. Chromatogram of the mKDM2B$_{577\text{-}707}$ PHD mutant construct sequencing. The T7 reverse primer was used for sequence reading. Adenine (green), thymine (red), guanine (black) and cytosine (blue) are depicted with single peaks on each chromatogram. The introduced single mutation (A) 5'AAA 3'[Phe] → 5'CGA 3'[Ala] is shown in a black box.

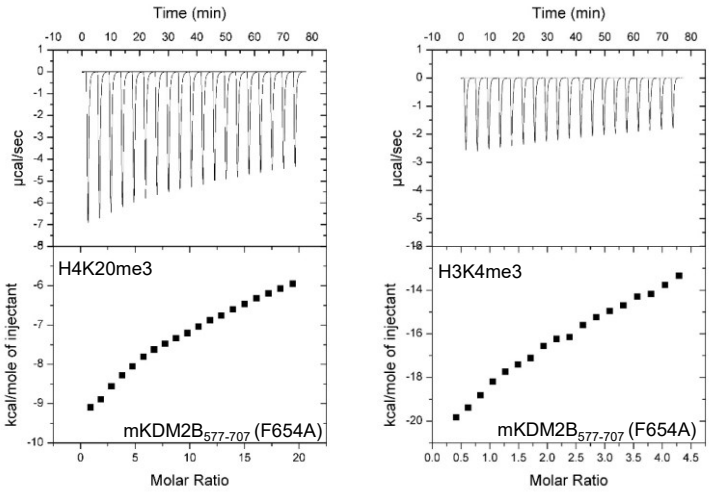

Figure 3.29. F654A mutation does not affect mKDM2B PHD binding affinity. ITC binding curves of mKDM2B$_{577-707}$(F654A), with H4K20me3 and H3K4me3 synthetic oligopeptides. The integrated ΔH (kcal/mol) values are plotted versus the peptide/protein molar ratio and shown in the lower panel. Titration of H4K20me3 and K3K4me3 with the PHD mutant (K_D= 6mM and K_D= 401 mM, respectively. The titrating peptide is shown in every graph.

Protein	Peptide	K_D (mM)
mKDM2B$_{577-707}$	H4K20me3	3 ± 1.1
mKDM2B$_{577-707}$	H3K4me3	374 ± 90
mKDM2B$_{577-707}$	H4$_{16-25}$ Unmodified	>1000
mKDM2B$_{577-707}$	H4K20me1	>1000
mKDM2B$_{577-707}$	mH4$_{49-69}$ -mRFP	>1000
mKDM2B$_{577-707}$	H2BK15ac	>10000
mKDM2B$_{577-707}$	H4K20me2	>10000
mKDM2B$_{577-707}$	H3$_{1-11}$ Unmodified	ND
mKDM2B$_{577-707}$	H3K27	ND
mKDM2B$_{577-707}$	H3K27me3	ND
mKDM2B$_{577-707}$	H3K36	ND
mKDM2B$_{577-707}$	H3K36me2	ND
mKDM2B$_{577-707}$	H4$_{1-11}$ Unmodified	ND
mKDM2B$_{577-707}$	H2B$_{(1-19)}$ Unmodified	ND
mKDM2B$_{577-707}$	H2BK5ac	ND
mKDM2B$_{577-707}$	H2BK12ac	ND
mKDM2B$_{577-707}$	mH4$_{1-18}$ -mRFP	ND
mKDM2B$_{577-707}$	mH4$_{17-34}$ -mRFP	ND
mKDM2B$_{577-707}$	mH4$_{33-50}$ -mRFP	ND
mKDM2B$_{577-707}$ (F654A)	H4K20me3	6 ± 0.8
mKDM2B$_{577-707}$ (F654A)	H3K4me3	401 ± 85

Table 3.2. Summary of the ITC-derived dissociation constant (K_D) describing the interaction of mKDM2B and mKDM2B(F654A) with different histone oligopeptides. Error values for the dissociation constant (K_D) correspond to the standard error of the nonlinear least-squares curve fit of the experimental data calculated using the program Origin 6.0 (OriginLab Corporation, USA). Abbreviations ND: Not detected

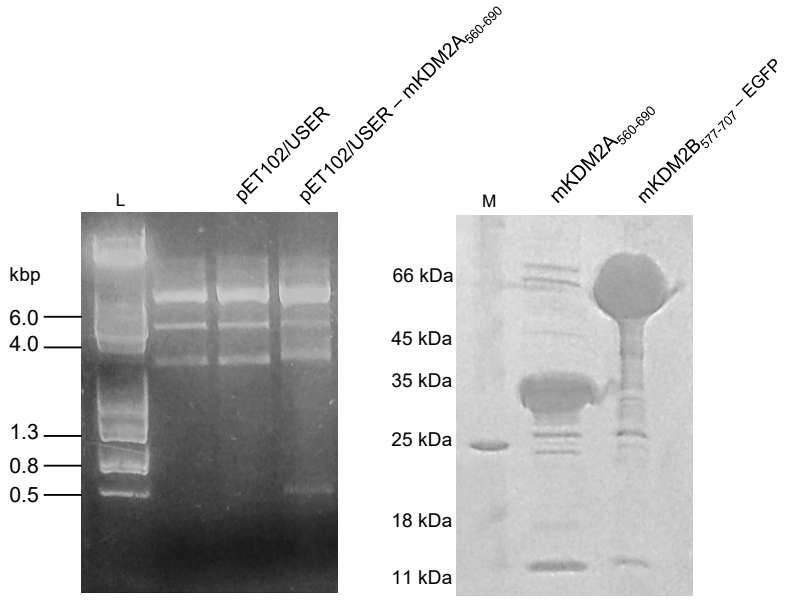

Figure 3.30. mKDM2A$_{560-690}$ recombinant protein. (a) Construct verification via agarose gel electrophoresis. The pET102/USER – mKDM2A$_{560-690}$ construct were doubly digested with restriction enzymes HindIII & AgeI to confirm the insertion of the sequence (Appendix 3). pET102/USER was used as control. **(b) Heterologous production of recombinant mKDM2A$_{560-690}$.** 12% SDS- PAGE shows total cell extract containing all proteins extracted from the disrupted BL21 cells. mKDM2A$_{560-690}$ (29 kDa) is produced in 50% lower yields compared to mKDM2B$_{577-707}$-EGFP.

3.2.5. mKDM2A does not bind H4K20me3.

The KDM2 family contains two members, KDM2A and KDM2B. To examine further the H4K20me3 recognition by mKDM2B PHD finger, we considered to test the binding capacity of its homolog protein, mKDM2A. Apart from its H3K36me2/me demethylase activity, KDM2A has been shown to interact with the heterochromatin protein, HP1 (Frescas et al., 2008) and histones at ribosomal DNA (rDNA) promoters (Frescas et al., 2007), but there has been no evidence of interaction with histone H4. Testing mKDM2B PHD finger substrates with mKDM2A PHD finger would shed light in possible new functions of these two sister proteins. The mKDM2A sequence, corresponding to the CxxC and PHD fingers was inserted in a pET102/USER vector, creating the pET102/USER-mKDM2A$_{560-690}$ construct (Appendix 2).

The mKDM2A$_{560-690}$ recombinant protein (sequence shown in Appendix 3) was purified via Ni-NTA affinity chromatography *(Figure 3.30)*, dialyzed in Reaction buffer, and used for H2BK15ac, H3K4me3 and H4K20me3 binding assay. Our results showed that mKDM2A$_{560-690}$ failed to recognize any of the KDM2B histone substrates, suggesting distinct functions between these two PHD fingers *(Figure 3.31)*.

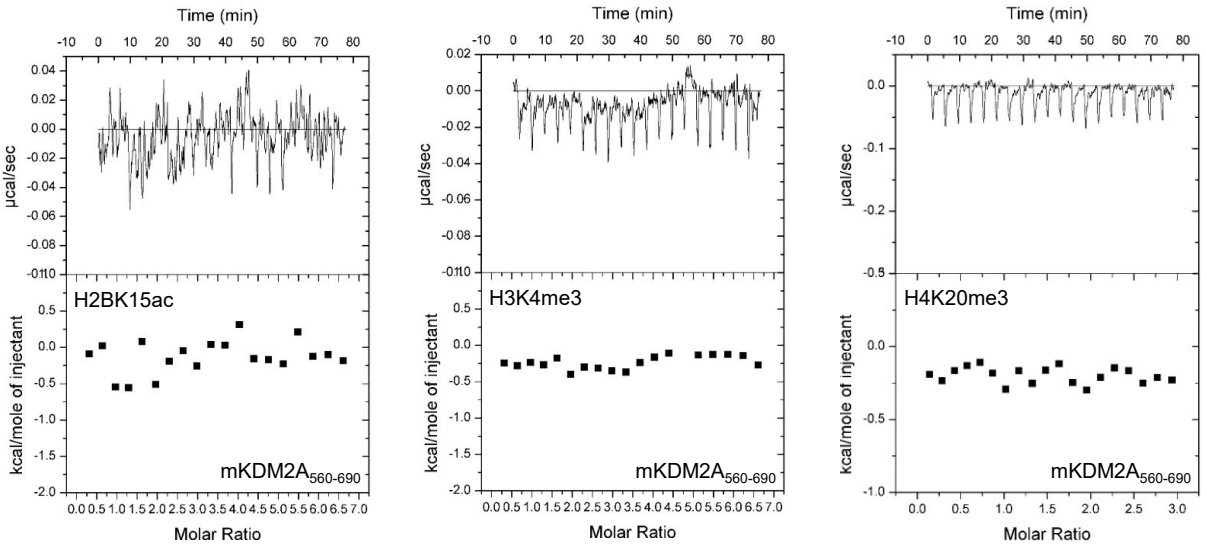

Figure 3.31. PHD fingers of mKDM2B and mKDM2A bind different substrates. ITC binding curves of $mKDM2A_{560-690}$ with H2BK15Ac, H3K4me3 and H4K20me3 synthetic oligopeptides show no binding, indicating distinct functions. The integrated ΔH (kcal/mol) values are plotted versus the peptide/protein molar ratio and shown in the lower panel.

3.2.6. The PHD fingers of mKDM2A and mKDM2B have different substrates.

In order to elaborate on the results that suggested that the PHD fingers of mKDM2A and mKDM2B have different substrates we employed MODified® histone peptide array for $mKDM2A_{560-690}$ and compared the mKDM2A binders with those of mKDM2B. Our findings verified that the PHD domains of the sister proteins recognize different post-translational modifications at different parts of the H4 histone (*Figure 3.32*) supporting further the notion that the KDM2 proteins may play different roles in the histone demethylation mechanism.

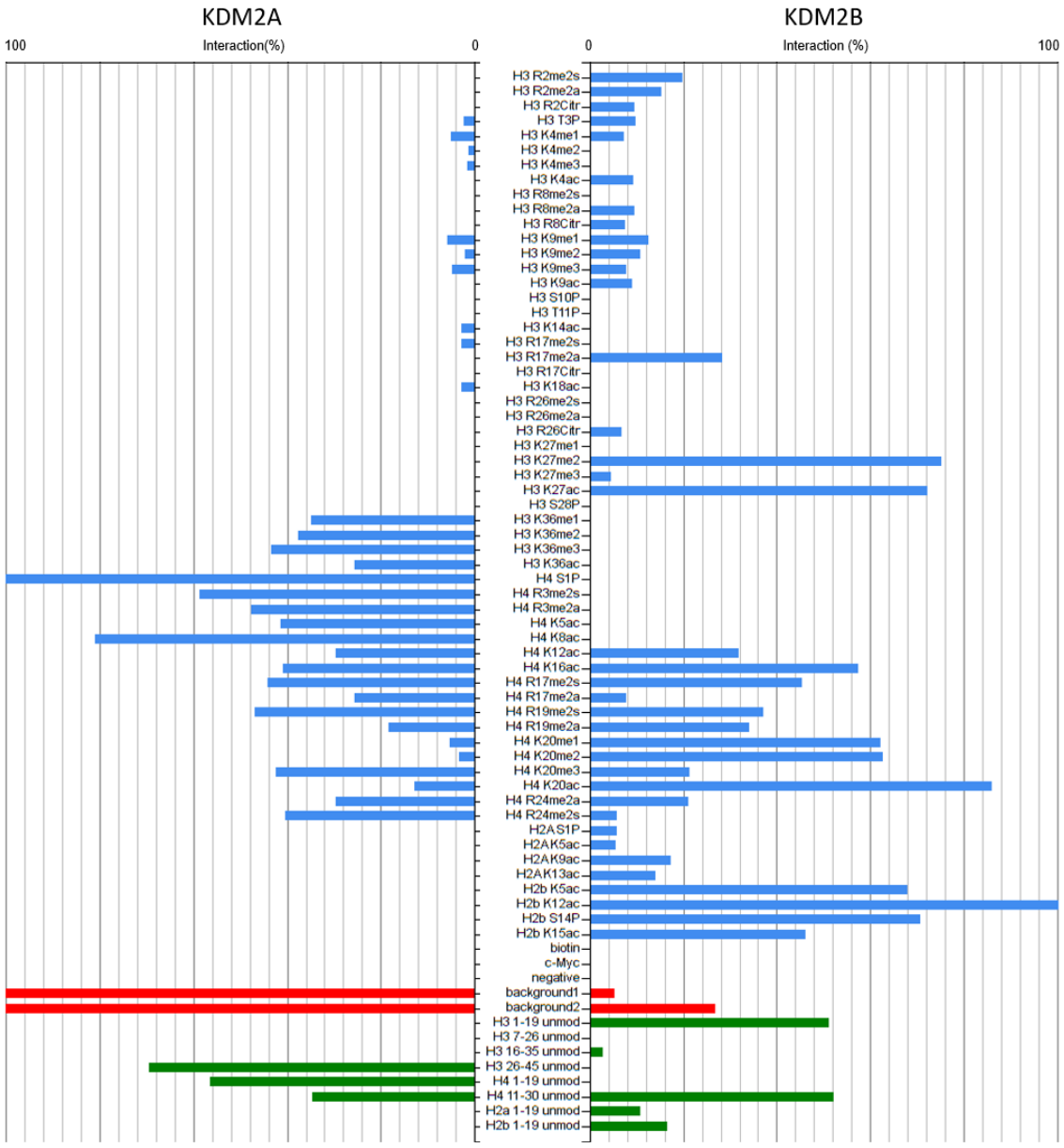

Figure 3.32. Comparative analysis of mKDM2A and mKDM2B PHD substrates based on MHPA results. The analysis revealed strong interaction between mKDM2A$_{560-690}$ and H4$_{1-19}$. Weaker binding was observed between PHD and H4$_{11-30}$ sequences, which was mKDM2B main target, while H3$_{26-45}$ sequences indicated interaction with mKDM2A$_{560-690}$, that were absent with mKDM2B. The percentage of interaction with each modification was normalized based on the interaction that showed the strongest binding for each protein. The background (1 & 2) sequences include random residue modifications on random aminoacid sequences (Appendix 4).

3.3. Biological role of mKDM2B CxxC finger

3.3.1. KDM2B DNA binding capacity is associated with cellular motility.

Previous studies have shown that KDM2B is implicated in the FGF-2 pathway, participating in cell proliferation, tumor metastasis and angiogenesis (Kottakis et al., 2011) and overexpression of KDM2B in DU145 cells can affect cytoskeletal organization-associated genes leading to a significant increase in their migration potential (Zacharopoulou et al., 2018). The molecular mechanism behind

this KDM2B function still remains elusive, thus our focus was placed on investigating whether KDM2B CxxC finger and its DNA binding capacity could be implicated in that matter. By using electrophoresis mobility shift assays, we have showed that residues R585, K608 and K616 of the CxxC finger play a key role in the binding of non-methylated CpG-containing DNA and substitution of K616 revealed that this residue plays the most prominent role. Our goal was to create stable DU145 cells lines, that overexpressed mKDM2B(K616A) and mKDM2B (as control) and compare cellular motility, via an *in vitro* wound healing assay. Mutating the pBABE-mKDM2B construct via USER mutagenesis led to pBABE-mKDM2B(K616A) *(Figure 3.33)*, which was produced in human embryonic kidney cells (HEK293T) and used to infect prostate cancer cells (DU145). The successfully transfected DU145 cells were cultivated and colony selection and western blot analysis with anti-KDM2B antibody verified the overexpression of the proteins *(Figure 3.34)*. In order to examine the motility of the transfected DU145 cells, two set of experiments were designed, one that included cell cultures undergoing a 24 h serum-starvation period prior to wounding to boost their migration potential and one without a starvation period. Representing micrographs of the *in vitro* would healing assay are shown in *Figure 3.35.*

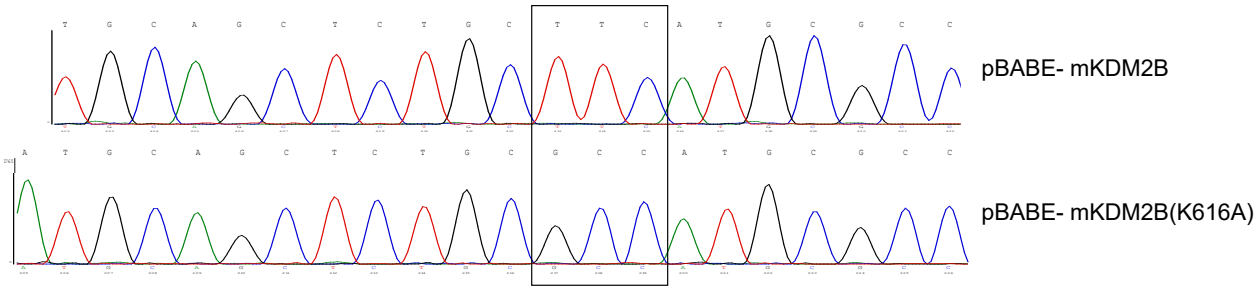

Figure 3.33. Comparing chromatograms of the pBABE-mKDM2B and pBABE-mKDM2B(K616A) sequencing readings. M13 reverse primer was used for sequencing reading. Adenine (green), thymine (red), guanine (black) and cytosine (blue) are depicted with single peaks on each chromatogram. The introduced mutation 5'CTT 3'[Lys]→ 5'CCG 3'[Ala] is shown in the black box.

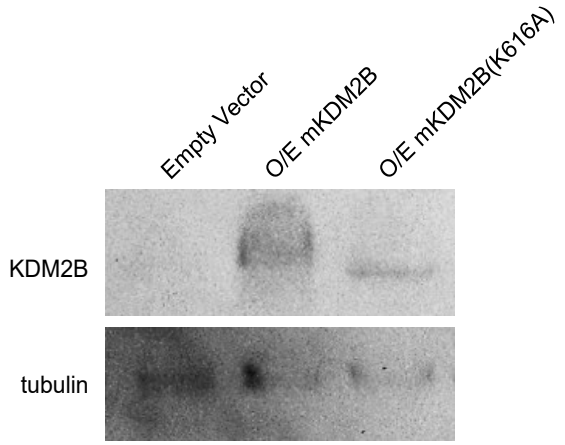

Figure 3.34. Prostate cancer cells (DU145) overexpressing wild type mKDM2B and CxxC mutant mKDM2B(K616A). Western blot analysis shows the overexpression of the mKDM2B and mKDM2B(K616A) proteins, using tubulin as reference.

The results from the *in vitro* would healing assays, showed that the migration potential of the starvation-free DU145 cells that overexpressed either the wild type or the mutant mKDM2B is not significantly changed compared to the normal DU145 cells *(Figure 3.36 upper panel)*. In addition, serum-starved cells that overexpressed the wild type mKDM2B illustrated enhanced motility compared to the normal DU145 cells, as the wounds were closing faster with would closure occurring in less than 24 hours. These results lay in accordance with previous reported data by Zacharopoulou *et al*., 2018b, and verify that a starvation period is a prerequisite for the wound healing assay with this cancer cell line. Moreover, our findings revealed that cells that overexpressed the CxxC mutant mKDM2B(K616A), showed reduced migration rate, almost similar to the normal DU145 cells, with would closure occurring later than 24 hours *(Figure 3.36 lower panel)*, suggesting that the DNA binding capacity of mKDM2B, could play an important role in the cellular migration and adhesion processes.

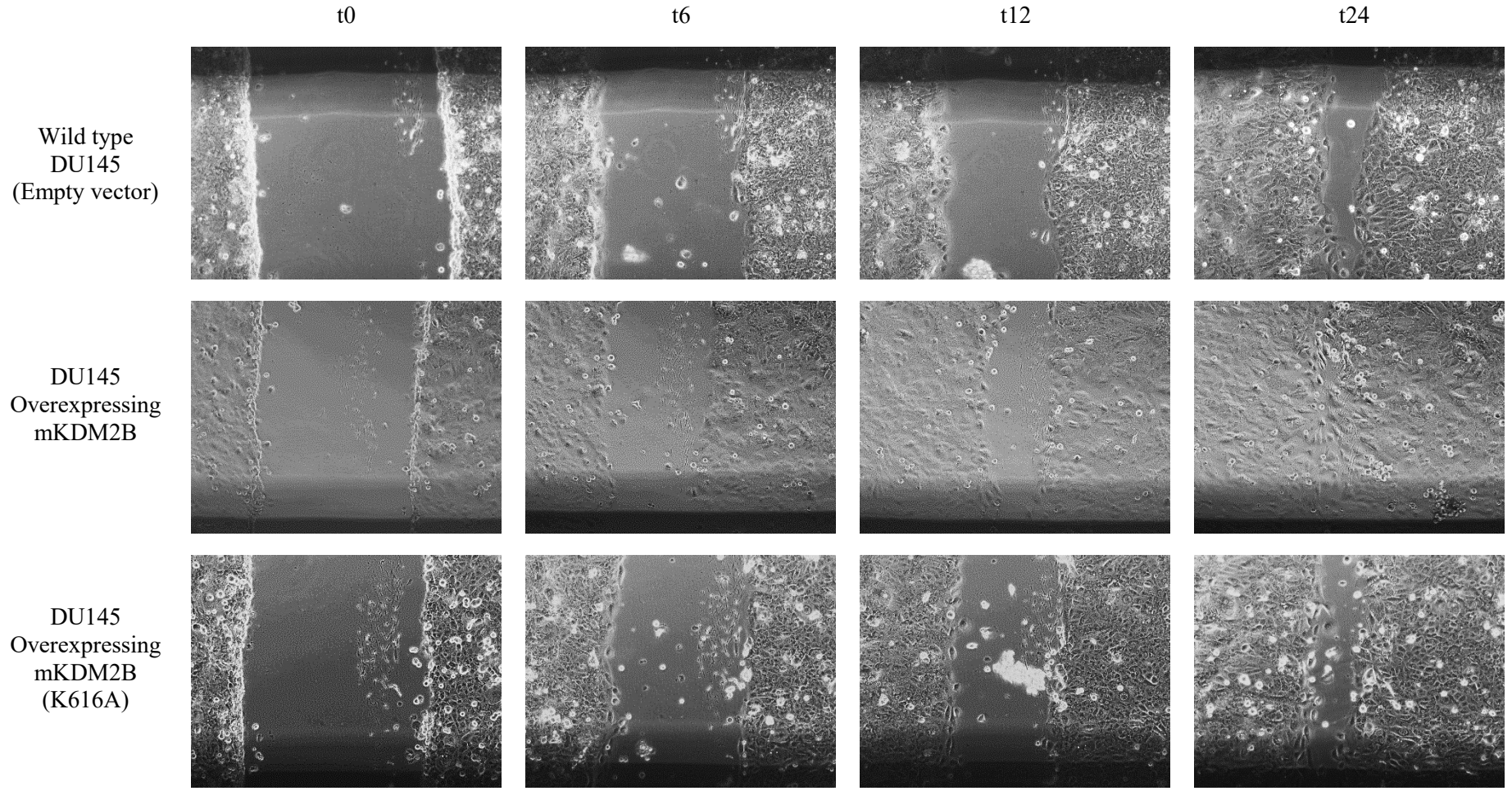

Figure 3.35. *In vitro* would healing assay. A scratch was made in each confluent monolayer culture of DU145 cells. Wound closure was monitored by microscope at 0, 6, 12 and 24 hours post wounding. Cells overexpressing KDM2B showed enhanced migration potential, compared to wild type DU-145 cells and the cells that expressed the CxxC mutant. Representative micrographs from n = 2 independent wound healing experiments with 24 h serum starvation before wounding.

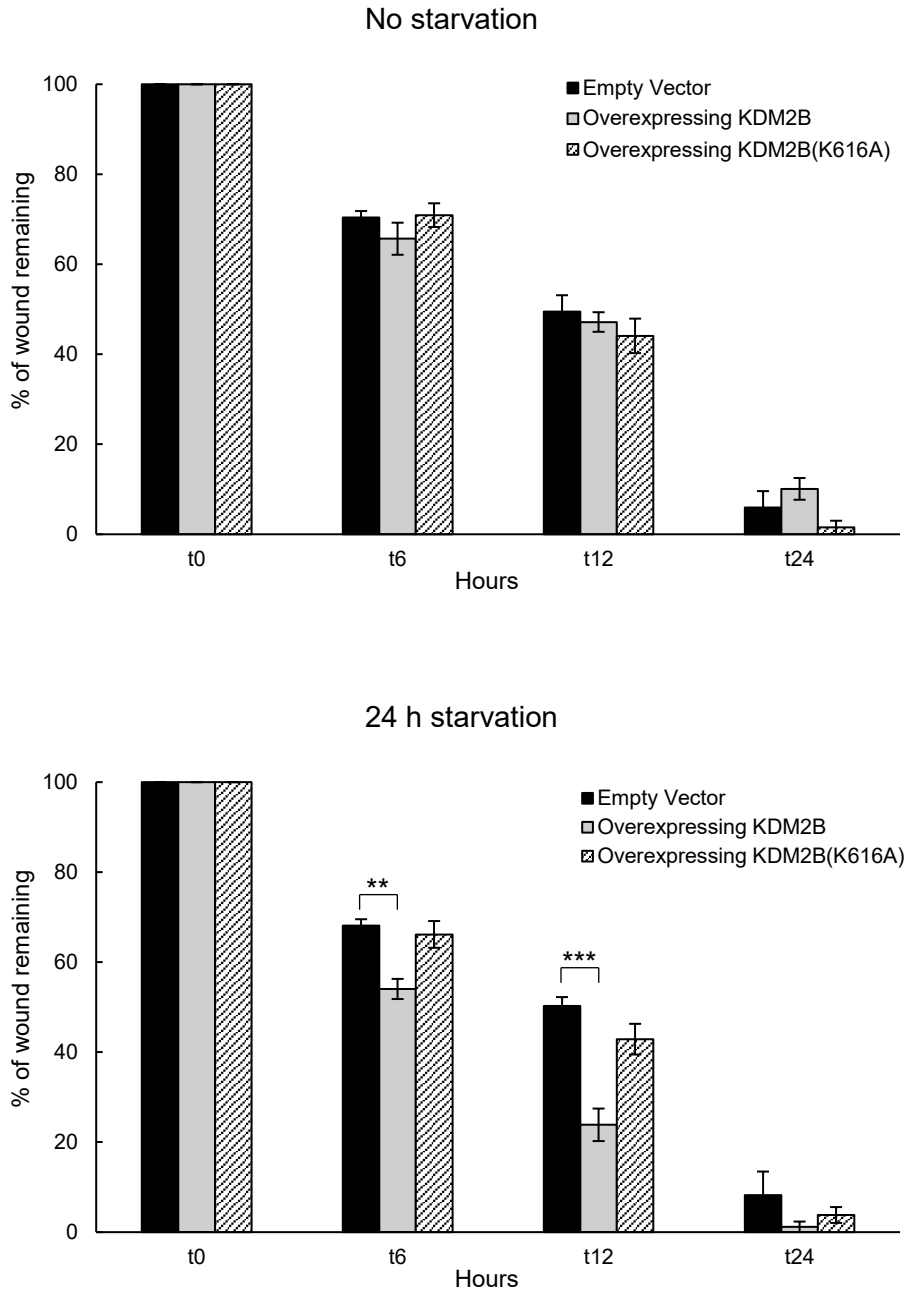

Figure 3.36. CxxC finger of KDM2B is associated with cellular motility. Upon 24h starvation prior to wounding DU145 cells that overexpressed the CxxC mutant mKDM2B indicated reduced migration potential compared to the cells expressing the wild type mKDM2B. Remaining wound area, at the indicated time points, was expressed as a percentage of the initial wound area from two independent experiments; *($p < 0.05$), ** ($p < 0.01$), ***($p < 0.001$) indicate statistical significance.

Chapter 4

Discussion

4.1. Biochemical characterization of mKDM2B CxxC finger

This PhD thesis aims to understand the function of the CXXC- and PHD- domains of KDM2B and their involvement in human disease. In order to elucidate the role of these domains, the recombinant mKDM2B$_{577-707}$ was initially analyzed using EMSA with several radiolabeled DNA substrates to study the interaction between the CxxC finger and DNA. We verified the previously reported binding specificity towards CpG- containing sequences (Koyama- Nasu et al., 2007; Farcas et al., 2012) by comparing two different DNA sequences that contained two CG dinucleotides each at different positions and we provide evidence of possible sequence-specific DNA recognition. Taking into consideration that DNA binding by KDM2B acts as a sampling mechanism for PRC1 docking and PRC2 recruitment that in turn leads to locus repression (Blackledge et al., 2014) and DNA hypomethylation maintenance (Boulard et al. 2015), this finding suggests that there is a rather more complicated level of molecular interactions underlying the DNA binding event, and further research is required. Furthermore, we investigated the effect of possible CxxC finger co-factors, like Zn^{2+} and Mg^{2+}, on DNA recognition. Based on the crystallographic structure of mKDM2B CxxC finger, we examined the importance of the two Zn^{2+} ions, which interact with the 8 cysteine residues of the domain (Long et al., 2013) and show that DNA binding capacity was abolished upon Zn^{2+} chelation, confirming that these ions play a major role in structural stability. Moreover, the addition of Mg^{2+} in the CxxC-DNA reaction illustrated no significant changes in the binding affinity, verifying previous data that showed this interaction being magnesium independent.

Subsequently we focused on elucidating the residues that participate in the DNA recognition event. We identified three conserved residues, R585, K608 and K616 (that correspond to R612, K635 and K643 in human KDM2B) as candidates for participation in this molecular interaction (*Figure 4.1).* Our results showed that R585, K608 & K616 participate in the DNA recognition as the single mutants and the double mutant manifested diminished binding to the substrate. Substitution of K616 revealed that this residue plays the most prominent role of the three tested, consistent with previous findings that report the direct interaction of the analogous residue in

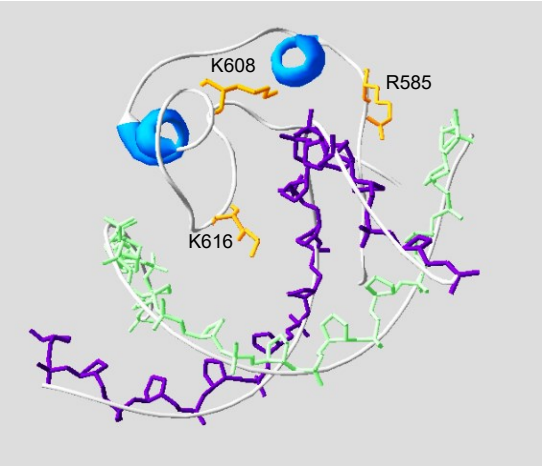

Figure 4.1. Close-up view of the interaction between the CxxC domain of KDM2B and DNA. This model was constructed by superposition of KDM2B CxxC onto MLL CxxC revealing the relative position of the residues that participate in DNA recognition. The residues R585, K608 and K616, shown in a yellow stick representation, interact with the major groove of a non-methylated CpG-containing DNA sequence shown in green and purple helices.

the MLL1 CxxC-finger with the major groove of the DNA (Cierpicki et al, 2010).

The significance of these residues was established by conducting *in vivo* assays, where the DNA binding capacity of KDM2B was correlated with its role in bypassing replicative senescence. The same point mutations that abrogated the DNA binding affinity of the recombinant CxxC finger were introduced into full-length mouse KDM2B and were overexpressed singly- and doubly-mutated forms in MEFs. All mutants failed to support replicative senescence bypass confirming the functional role of the CxxC finger in this process (S.C. Kampranis, personal communication). Notably, cells that overexpressed the two double mutant forms of KDM2B containing the K616A mutation (R585A/K616 and K608/K616) entered the replicative senescent state faster than empty vector-containing cells *(Figure 4.2)* (S.C. Kampranis, personal communication). Evaluating the ability of progressive truncations of KDM2B to support replicative senescence bypass upon ectopic expression in MEFs showed that deletion of the C-terminal half of the protein that includes the PHD domain did not abolish this activity (S.C. Kampranis, personal communication), which suggests that the combined action the JmjC and CxxC domains is by itself sufficient to inhibit cell cycle events that contribute to the bypass of replicative senescence, including the repression of the locus and also that the DNA binding capacity of KDM2B is not compromised upon deletion of the PHD domain. Numerous studies have implicated KDM2B in cancer (Kampranis and Tsichlis, 2009), therefore, confirming the key role of the CxxC finger in this process, in combination with the available structural information for this domain, has prompted further studies into the potential of development of CxxC-targeting inhibitors as cancer therapeutics.

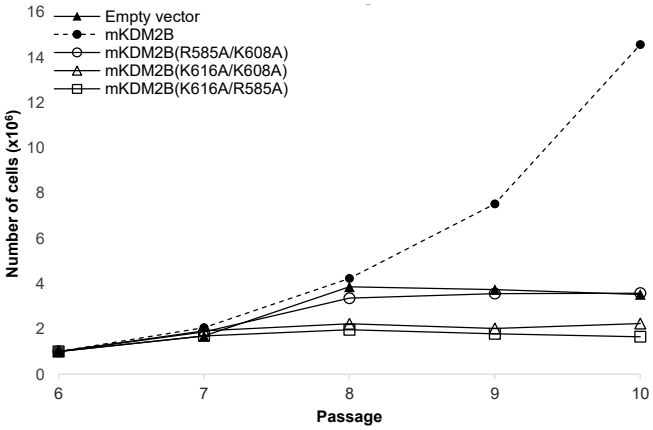

Figure 4.2. DNA binding is essential for KDM2B to support cell proliferation. Evaluation of the ability of mKDM2B double mutant variants to support replicative senescence bypass in MEFs.

In order to develop a CxxC-targeting inhibitor screening, efforts were put in setting up a fluorescence-based assay, which would provide a fast and easy way to assess the binding of DNA onto the mKDM2B CxxC finger. To this end, recombinant mKDM2B$_{577-707}$ was physically absorbed on the microplate well surface and the fluorescence of CxxC-bound FAM-CpG2 was measured. Our results showed fluorescence signal derived from FAM-CpG2 before and after addition of EDTA (which had been shown to abolish the interaction), indicating possible non-specific interactions of the DNA with the well surfaces, which lead us abandon this setup.

To overcome the limitations of the previously attempted assay, a FRET- based assay was designed. In our experiments we selected EGFP as donor and two possible acceptor candidates, each one meeting a required spectroscopic property (Pollok and Heim, 1999). Monitoring FRET signaling showed that mKDM2B$_{577-707}$–EGFP, but not mutant mKDM2B$_{577-707}$(K616A)–EGFP, was able to bind the CpG- containing sequences that carried the Cy3 fluorophore. This suggests that only upon CxxC-DNA binding, EGFP and Cy3 came relatively close in order to achieve energy transfer. Furthermore, in our attempt to increase the signal by bringing closer EGFP and Cy3, we tested a secondary shorter version of CpG2, but no signal was observed, supporting the idea that a certain spatial complex conformation may be essential for FRET. Moreover, the EGFP- TET pair illustrated very low signal-to-noise ratio, making it unsuitable for our purposes. These data altogether, proposed the two partners, mKDM2B$_{577-707}$–EGFP and Cy3- CpG2, as highly promising candidates for establishing FRET-based high throughput screening assay for identification KDM2B inhibitors.

However, when we proceeded to transfer this assay to a microplate format, using the available Perkin-Elmer Victor X5® plate reader, our attempts were unfruitful. This was due to the fact that the filters were unsuitable for fluorescence detection at the required wavelengths. As a result, EGFP-Cy3 complex in the plate reader showed an even lower signal-to-noise ratio (~0.2), at 535 nm where emission filter was set, compared to 1.6 measured in the spectrophotometer, suggesting significant background fluorescence being measured. In addition, by using another feature of Victor X5® that measured Time –Related Fluorescence, a setup of a fluorescence attenuation assay was designed, in which the quenching time of EGFP (and not Cy3) would be measured at 535 nm. This assay was based on the principle that DNA bound to CxxC, leads to fast photobleaching of EGFP fluorescence, due to FRET. As negative control mKDM2B$_{577-707}$(K616A)–EGFP was used, due to its reduced binding capacity but no difference between mKDM2B$_{577-707}$–EGFP and mKDM2B$_{577-707}$(K616A)–EGFP in quenching time was observed, suggesting that binding of Cy3-CpG could not promote a faster quenching of EGFP or at least a detectable signal. As a conclusion, our data suggest that a different fluorescence measuring setup with emission filter around 600 nm, or a monochromator, would be essential in order to improve the signal-to-noise ratio.

4.2. Biochemical characterization of mKDM2B PHD finger

The KDM2B PHD finger was initially suspected to be responsible for the interaction with other proteins such as HDACs (Barrett et al., 2007) or for the binding of KDM2B to methylated histone tail residues (Iwase et al., 2007; Shi et al., 2006; Taverna et al., 2007; Vermeulen et al., 2007; Wysocka et al., 2006, Janzer et al., 2012), however, its precise function had not been elucidated.

Using a commercially available modified histone array we screened 379 possible KDM2B PHD interactors and our initial results showed that PHD finger illustrates an unpreceded recognition capacity towards parts of histone H4 (either carrying or not posttranslational modifications) and more specifically, this analysis revealed a selective interaction with residues $H4_{11-30}$, and not $H4_{1-19}$, indicating that the recognition depends on residues that are present in the region 20-30 of histone H4. Furthermore, mKDM2B PHD finger interacted with oligopeptides corresponding to the N-terminal tail of histone H3 that carried trimethylation on lysine at position 4 (H3K4me3) but on interaction was observed with oligopeptides containing H3K36me2 modification, thus verifying previously reported data (Janzer et al., 2012). Moreover, significant interaction with $H2B_{1-19}$ was also observed, suggesting a broad spectrum of sequence-specific histone substrates.

Our first goal was to evaluate further, the interaction of KDM2B PHD finger with histone H4, thus we examined the binding events qualitatively via FRET- based experiments and quantitatively via Isothermal Titration Calorimetry. The first technique failed to provide sustainable data on the mH4 binding capacity of PHD finger, probably due to steric hindrance in the active site derived from the fluorophore fusion at the C- terminus of the recombinant proteins, or due to large distance between EGFP and mRFP. On the other hand, ITC experiments illustrated a weak but notable binding of $mKDM2B_{577-707}$-EGFP to $mH4_{49-69}$-mRFP but no interaction with $mH4_{1-18}$-mRFP, $mH4_{17-34}$-mRFP and $mH4_{33-50}$-mRFP. These data possibly suggest that a posttranslational modification is required to as well as multiple recognition events may take place during PHD-histone H4 binding.

In order to investigate whether a posttranslational modification on H4 is required, we examined synthetic oligopeptides $H4_{15-25}$ with mono-, di- and tri- methylated lysine 20 and as positive control we used $H3_{1-11}$ trimethylated at lysine 4. In addition, to further expand our research on other KDM2B histone interactors, $mKDM2B_{577-707}$ was tested also with synthetic oligopeptides, that simulated N-terminus tails of histone H2B and histone H3, but no significant interaction was observed. Our results show that PHD domain is able to recognize specifically the trimethylation on lysine 20 of histone H4 (K_d= 3 mM). The relatively high K_D measured in these experiments suggests that is possible that the overall interaction is facilitated by additional contacts between KDM2B and the nucleosome that could not be identified with the approach used here, but is supported by ITC results that showed a weak interaction of mKDM2B with $mH4_{49-69}$. Moreover, the previously reported interaction of the KDM2B PHD domain with H3K4me3 was confirmed, however it was 100-times weaker (K_D= 370 mM) compared to H4K20me3, indicating that this domain is able to recognize the trimethyl group on lysine residues but indicates strong preference towards histone H4 sequence. In agreement with recent ChIP-seq and CARIP-seq analyses in ESCs have shown that H3K4me3 and H4K20me3 can be found

co-localized at the same genomic regions and in the main bodies of actively transcribed genes (Xu & Kidder, 2018) and several non-coding RNAs associated with these two modifications are able to affect chromatin regulation (Kurup and Kidder, 2018).

While H3K4me3 mark is frequently found in the promoter and main bodies of highly transcribed genes (Barski et al., 2007), H4K20me3 mark is mostly part of condensed heterochromatin around centromeres (Schotta et al., 2004). Thus, the identification of H4K20me3 as the main chromatin modification targeted by KDM2B reveals potentially additional biological roles for this protein. Until now, the function of KDM2B has been correlated with Polycomb-regulated chromatin and the coordinated action of the Polycomb repressive complexes. By contrast, H4K20me3 is found in the condensed heterochromatin around centromeres and its levels are significantly increased in aging mammalian tissues (Sarg et al., 2002) and senescent cells (Nelson et al., 2016). Thus, it has been proposed that H4K20me3 plays a role in the heterochromatization and stabilization of the genome of pre-malignant cells, which contributes to long-term senescence-mediated tumor suppression (Nelson et al., 2016). Furthermore, in embryonic stem cells, depletion of the H4K20me3 levels lead to the de-repression of endogenous retroelements and the dysregulated expression of OCT4 targets, resulting to compromised self-renewal and perturbed differentiation (Kidder et al., 2017). Our findings suggest a tumor suppressive role for KDM2B that is mediated by its interaction with H4K20me3. In this context, depletion of KDM2B would lead to H4K20me3 deprotection and potential derepression of pluripotency genes or endogenous retroelements. This function is consistent with earlier observations that implicated KDM2B in tumor suppression. Specifically, in retroviral insertion mutagenesis studies in Blm-deficient mice, disruption of KDM2B (or Fbxl10) induced genome instability (Suzuki et al., 2006). In *C. elegans,* the homologue of KDM2B was essential for protection against genome-wide RNAi mutagenesis (Pothof et al., 2003). In HeLa cells, KDM2B was found to associate and repress the transcription of ribosomal DNA and downregulation of KDM2B promoted cell proliferation (Frescas et al, 2007). Furthermore, KDM2B was found to be essential for restraining RAS-driven myeloid transformation (Andricovich et al., 2016). This bivalent action of KDM2B is supported by its ability to participate in additional protein complexes, beyond PRC1, together with key regulatory factors like c-Jun and c-Myc (Koyama-Nasu et al., 2007; Tzatsos et al., 2013). Overall, our findings suggest that KDM2B may have pleiotropic functions that depend on the temporal and spatial intracellular context and are supported by a combination of versatile structural domains.

4.3. Comparing the PHD fingers of KDM2B and KDM2A.

In addition to KDM2B, mammalian cells also contain a closely related homolog, KDM2A, which has been shown to participate in chromatin silencing and heterochromatin formation and maintenance (Maison and Almouzni, 2004; Frescas et al., 2008). ChIP-seq studies in HeLa cells have shown that KDM2A associates with H3K9me3 repressive mark and also interacts with Heterochromatin Protein 1 (HP1), indicating a direct biological role in gene repression (Borgel et al., 2017). Since KDM2A has been shown to be involved in recognition of inactive chromatin, we questioned whether it has binding affinity for other repressive marks, such as H4K20me3. The recombinant mKDM2A$_{560-690}$ was analyzed via ITC using mKDM2B PHD finger substrates and our results showed that KDM2A did not specifically recognize H4K20me3, H3K4me3 or H2BK15ac. To elaborate further on these results we conducted a screening of KDM2A binders with the use of MODified histone peptide array. Our results showed the PHD finger of KDM2A interacting mostly with the unmodified sequence of histone H3 that spanned from residue 26 to 45 and with histone H4 sequence that spanned from residues 1 to 19 and more strongly when it carried markers such as H4S1P and H4R3me2s. The phosphorylation of serine 1 on histone H4 has been associated with the chromatin condensation during mitosis in fruit fly and *xenopus* (Barber et al., 2004) while the symmetric demethylation of R3 on has also been considered as mark of heterochromatin (Xu et al., 2010) suggesting that the PHD finger of KDM2A, similarly to KDM2B, also recognizes mostly repressive markers. However, PHD fingers that bind methylated arginine residues significantly differ in structure from those that recognize methylation on lysine residues, which bind their ligands through aromatic cages (Taverna et al., 2007; Kampranis and Tsichlis, 2009, Sanchez and Zhou, 2011). To examine whether this substrate specificity is derived from structural differences between KDM2A and KDM2B, we analyzed *in silico* the structure of the two PHD fingers. Using the online available RCSB PDB files we analyzed the structures on Swiss- PdbViewer v4.1.0 (Swiss Institute of Bioinformatics) and created a surface model of the two fingers. The structures were fitted using magic fit feature and the surface schemes revealed several structural differences *(Figure 4.3)* that could suggest a different binding specificity. This analysis laid in agreement with our ITC and MHPA results that failed to show any correlation between mKDM2A and mKDM2B binders, and supplemented the current belief that these two members of the KDM2 family are probably involved in distinct molecular mechanisms.

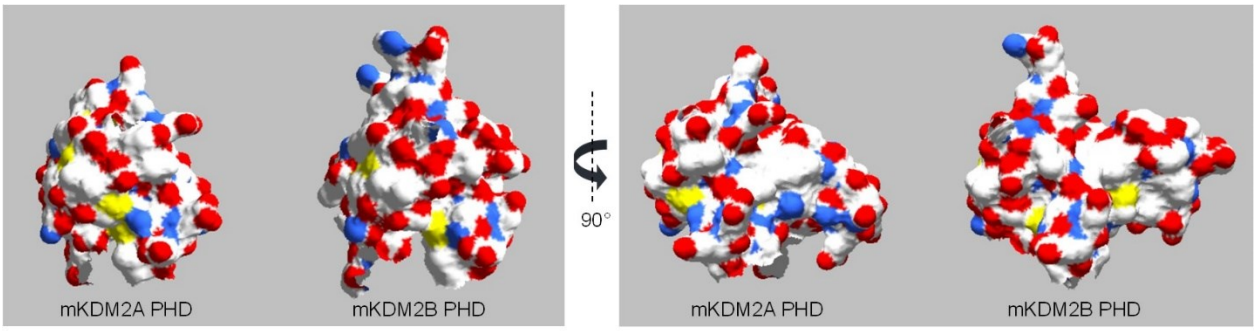

Figure 4.3. Surface models of mKDM2A and mKDM2B PHD fingers. The model of the crystal structures of mKDM2A (RCSB PDB entry P59997) and mKDM2B (RCSB PDB entry Q6P1G2) illustrate structural differences on the surface of the PHD finger. Over 408 carbon alpha atoms, the mKDM2B model had an overall – RMSE of 1.26 compared to mKDM2A.

4.4. Biological role of mKDM2B CxxC finger

The identification of the structural elements in the CxxC finger of KDM2B that participate in the DNA binding mechanism enabled us to correlate its function with its biological role. Since Koyama-nasu *et al.* in 2007 showed that the KDM2B CxxC finger is important for tethering transcription repression complexes to c-Jun promoter, numerous studies (Farcas *et al.*, 2012; Wu *et al.*, 2013; He *et al.*, 2013) have followed pinpointing the contribution of the KDM2B CxxC finger to an abundance of intracellular activities in both physiological and pathogenic status. Kottakis *et al*. (2011) had showed that the CxxC finger of NDY1/KDM2B is essential during EZH2/MiR101- mediated angiogenesis and cellular proliferation in bladder cancer while more recently Zacharopoulou *et al.* (2018) illustrated the vital role of KDM2B in actin cytoskeleton organization and cellular migration via regulation of Rho GTPases in prostate tumor cells. Focusing on elucidating a possible participation of KDM2B CxxC finger in this process, we employed *in vitro* wound healing assays with DU145 cells that overexpressed the wild type mouse KDM2B and the CxxC mutant mKDM2B(K616A). Our results showed the cancer cells that overexpressed the mutant protein failed to exhibit the same enhanced migration potential of those cells overexpressing of the wild type KDM2B, indicating an active role of the domain in regulating genes that are responsible for cellular motility. These findings further endorse the notion that most of the functions of KDM2B that include gene regulation, acting either on its own or as a component of the PRC1.1, preserve a high level of dependency on its ability to bind DNA, thus further research is required to fully understand the underlying mechanisms and pathways that KDM2B takes part in.

4.5. Significance and future prospects

In retrospect, the current work has succeeded in elucidating several aspects concerning the molecular interactions of two domains that are present in an essential chromatin- associated factor that is highly

conserved among eukaryotes from *C. elegans* to *H. sapiens*. Previous studies have addressed the role of KDM2B in cancer, tumorigenesis and leukemia, aiming to reveal the way of function for this novel oncogene. Hence, the identification of three key residues that participate in the DNA binding of the CxxC finger of the mouse KDM2B and the connection of this capacity to processes such as cell proliferation and migration, accompanied with other available structural information about this domain, could promote further studies into the potential of development CxxC-targeting inhibitors as cancer therapeutics. Here, our initial efforts in that research field fortunately resulted in the introduction of two highly promising candidates, mKDM2B$_{577-707}$–EGFP and Cy3- CpG2, for setting up a FRET-based high-throughput screening assay for identification of KDM2B CxxC inhibitors. Taking a step further from a technical point of view, the plasmid construct that fused the KDM2B domains with EGFP, could be used to clone any protein or domain of interest, creating a vast library of recombinant fluorescent proteins, to be biochemically examined and characterized. As far as the PHD finger is concerned, we reported for the first time a PHD finger that preferentially recognizes a methylation on histone H4, and specifically H4K20me3. The observed interaction is specific for the trimethyl mark and the overall recognition may be facilitated by additional contacts between KDM2B and the nucleosome. These findings suggest a tumor suppressive role for KDM2B since H4K20me3 has been proposed as a hallmark of cancer that also plays a critical role in the selection of active DNA replication initiation sites in heterochromatic regions during late S phase. In order to confirm this interaction, future research would include immunoprecipitation assays of KDM2B PHD finger with H4K20me3-containing nucleosomes, and ChIP- seq analysis to identify the chromosomal loci that are targets of this domain. In addition, site-directed mutagenesis on the PHD finger of KDM2B would shed light into the structure of the domain that could possibly provide new insights for its unique substrate specificity.

Chapter 5

References

Abidi, F. E., Holloway, L., Moore, C. A., Weaver, D. D., Simensen, R. J., Stevenson, R. E., Rogers, R. C., & Schwartz, C. E. Mutations in JARID1C are associated with X-linked mental retardation, short stature and hyperreflexia. *J Med Genet,* **45**(12), 787-793 (2008)

Abidi, F., Miano, M., Murray, J., & Schwartz, C. A novel mutation in the PHF8 gene is associated with X-linked mental retardation with cleft lip/cleft palate. *Clin. Genet.* **72**, 19–22 (2007)

Adamo, A., Barrero, M.J., Izpisua-Belmonte, J.C.. LSD1 and pluripotency: a new player in the network. *Cell Cycle* **10**(19):3215-6 (2011)

Addison Wesley Longman Publishing Pearson Education (1999)

Adegbola, A., Gao, H., Sommer, S., Browning, M. A novel mutation in JARID1C/SMCX in a patient with autism spectrum disorder (ASD) *Am J Med Genet A.* **146A**(4):505-11 (2008)

Agger, K., Cloos, P. A., Rudkjaer, L., Williams, K., Andersen, G., Christensen, J., & Helin, K. The H3K27me3 demethylase JMJD3 contributes to the activation of the INK4A-ARF locus in response to oncogene- and stress-induced senescence." *Genes Dev* **23**(10): 1171-1176 (2009).

Alvarez-Saavedra, M., Antoun, G., Yanagiya, A., Oliva-Hernandez, R., Cornejo-Palma, D., Perez-Iratxeta, C., Sonenberg, N., & Cheng, H. Y. miRNA-132 orchestrates chromatin remodeling and translational control of the circadian clock. *Human molecular genetics*, **20**(4), 731–751 (2011).

Anand, R. & Marmorstein, R. Structure and mechanism of lysine-specific demethylase enzymes. *J Biol Chem* **282**(49): 35425-35429. (2007).

Anderton, J. A., Bose, S., Vockerodt, M., Vrzalikova, K., Wei, W., Kuo, M., Helin, K., Christensen, J., Rowe, M., Murray, P. G., & Woodman, C. B. The H3K27me3 demethylase, KDM6B, is induced by Epstein-Barr virus and over-expressed in Hodgkin's Lymphoma. *Oncogene*, **30**(17), 2037-2043 (2011)

Andricovich, J., Kai, Y., Peng, W., Foudi, A. & Tzatsos, A. Histone demethylase KDM2B regulates lineage commitment in normal and malignant hematopoiesis. *JCI* **126**, 905-920 (2016).

Banito, A., Li, X., Laporte, A. N., Roe, J. S., Sanchez-Vega, F., Huang, C. H., Dancsok, A. R., Hatzi, K., Chen, C. C., Tschaharganeh, D. F., Chandwani, R., Tasdemir, N., Jones, K. B., Capecchi, M. R., Vakoc, C. R., Schultz, N., Ladanyi, M., Nielsen, T. O., & Lowe, S. W. The SS18-SSX Oncoprotein Hijacks KDM2B-PRC1.1 to Drive Synovial Sarcoma. *Cancer Cell* **33**, 527-541 (2018).

Barradas, M., Anderton, E., Acosta, J. C., Li, S., Banito, A., Rodriguez-Niedenführ, M., Maertens, G., Banck, M., Zhou, M. M., Walsh, M. J., Peters, G., & Gil, J. Histone demethylase JMJD3 contributes to epigenetic control of INK4a/ARF by oncogenic RAS. *Genes Dev* **23**(10): 1177-1182 (2009).

Barrett, A., Santangelo, S., Tan, K., Catchpole, S., Roberts, K., Spencer-Dene, B., Hall, D., Scibetta, A., Burchell, J., Verdin, E., Freemont, P., & Taylor-Papadimitriou, J. Breast cancer associated transcriptional repressor PLU-1/JARID1B interacts directly with histone deacetylases. *Int J Cancer*, **121**(2), 265-275 (2007)

Barski, A., Cuddapah, S., Cui, K., Roh, T.Y., Schones, D.E., Wang, Z., Wei, G., Chepelev, I., Zhao, K. High-Resolution Profiling of Histone Methylations in the Human Genome. *Cell.* **129**: 823–837 (2007).

Bennani-Baiti, I.M., Machado, I., Llombart-Bosch, A., Kovar, H. Lysine-specific demethylase 1 (LSD1/KDM1A/AOF2/BHC110) is expressed and is an epigenetic drug target in chondrosarcoma, Ewing's sarcoma, osteosarcoma, and rhabdomyosarcoma. *Hum Pathol.* **43**(8):1300-7 (2012).

Berger, S.L. The complex language of chromatin regulation during transcription. *Nature.* **447** (7143): 407-412 (2007)

Bhaumik, S.R., Smith, E., Shilatifard, A. Covalent modifications of histones during development and disease pathogenesis. *Nat Struct Mol Biol.* **14**: 1008–16 (2007)

Blackledge, N. P., Farcas, A. M., Kondo, T., King, H. W., McGouran, J. F., Hanssen, L. L., Ito, S., Cooper, S., Kondo, K., Koseki, Y., Ishikura, T., Long, H. K., Sheahan, T. W., Brockdorff, N., Kessler, B. M., Koseki, H., & Klose, R. J. Variant PRC1 complex-dependent H2A ubiquitylation drives PRC2 recruitment and polycomb domain formation. *Cell* **157**, 1445-1459 (2014).

Blackledge, N. P., Zhou, J. C., Tolstorukov, M. Y., Farcas, A. M., Park, P. J., & Klose, R. J. CpG islands recruit a histone H3 lysine 36 demethylase. *Mol Cell.* **38** (2): 179-90 (2010).

Boichenko, I., Deiss, S., Bär, K., Hartmann, M.D., Hernandez, A.B. FRET-Based Assay for the Identification and Characterization of Cereblon Ligands. *JMC* **59** (2), 770-774 (2016).

Borgel, J., Tyl, M., Schiller, K., Pusztai, Z., Dooley, C. M., Deng, W., Wooding, C., White, R. J., Warnecke, T., Leonhardt, H., Busch-Nentwich, E. M., & Bartke, T. KDM2A integrates DNA and histone modification signals through a CXXC/PHD module and direct interaction with HP1. *Nucleic acids research,* **45**(3), 1114–1129 (2017).

Bortoluzzi, A., Amato, A., Lucas, X., Blank, M., & Ciulli, A. Structural basis of molecular recognition of helical histone H3 tail by PHD finger domains. *The Biochemical journal*, **474**(10), 1633–1651 (2017).

Boulard, M., Edwards, J. R., Bestor, T. H. FBXL10 protects Polycomb-bound genes from hypermethylation. *Nat Genet.* **47** (5): 479-485 (2015)

Brink, M.C., van der Velden, Y., de Leeuw W., Mateos-Langerak, J., Belmont, A.S., Roel van Driel, Verschure, P.J. Truncated HP1 lacking a functional chromodomain induces heterochromatinization upon in vivo targeting. *Histochemistry and Cell Biology*, **125**(1-2): 53-61 (2006)

Brustel, J., Kirstein, N., Izard, F., Grimaud, C., Prorok, P., Cayrou, C., Schotta, G., Abdelsamie, A. F., Déjardin, J., Méchali, M., Baldacci, G., Sardet, C., Cadoret, J. C., Schepers, A., & Julien, E. Histone H4K20 tri-methylation at late-firing origins ensures timely heterochromatin replication. *EMBO J.* **36** (18): 2726-2741 (2017).

Caselle, M., Di Cunto, F. and Provero, P. Correlating overrepresented upstream motifs to gene expression: a computational approach to regulatory element discovery in eukaryotes. *BMC Bioinformatics.* **3** (7) (2002)

Chen, J. Y., Li, C. F., Chu, P. Y., Lai, Y. S., Chen, C. H., Jiang, S. S., Hou, M. F., & Hung, W. C. Lysine demethylase 2A promotes stemness and angiogenesis of breast cancer by upregulating Jagged1. *Oncotarget,* **7**(19), 27689–27710 (2016).

Chen, K., Chen, Z., Wu, D., Zhang, L., Lin, X., Su, J., Rodriguez, B., Xi, Y., Xia, Z., Chen, X., Shi, X., Wang, Q., & Li, W. Broad H3K4me3 is associated with increased transcription elongation and enhancer activity at tumor suppressor genes. *Nature Genetics*, **47**(10), 1149–1157 (2015).

Chen, Z., Wang, L., Wang, Q., Li, W. Histone modifications and chromatin organization in prostate cancer. *Epigenomics* **2**(4):551-60. (2010)

Chen, Z., Zang, J., Whetstine, J., Hong, X., Davrazou, F., Kutateladze, T.G., Simpson, M., Mao, Q., Pan, C.H., Dai, S., Hagman, J., Hansen, K., Shi, Y., Zhang, G. Structural insights into histone demethylation by JMJD2 family members. *Cell*, **125**(4):691-702 (2006)

Chicas, A., Kapoor, A., Wang, X., Aksoy, O., Evertts, A. G., Zhang, M. Q., Garcia, B. A., Bernstein, E., & Lowe, S. W. H3K4 demethylation by Jarid1a and Jarid1b contributes to retinoblastoma-mediated gene silencing during cellular senescence. *Natl Acad Sci U S A,* **109**(23), 8971–8976. (2012).

Choi, J., Jang, H., Kim, H., Kim, S.T., Cho, E.J., Youn, H.D. Histone demethylase LSD1 is required to induce skeletal muscle differentiation by regulating myogenic factors. *Biochem. Biophys. Res. Commun.* **401**:327–332 (2010)

Christensen, J., Agger, K., Cloos, P.A., Pasini, D., Rose, S., Sennels, L., Rappsilber, J., Hansen, K.H., Salcini, A.E., Helin, K. RBP2 belongs to a family of demethylases, specific for tri-and dimethylated lysine 4 on histone 3. *Cell.* **128**(6):1063-762007.

Ciccone, D.N., Su, H., Hevi, S., Gay, F., Lei, H., Bajko, J., Xu, G., Li, E., Chen, T. KDM1B is a histone H3K4 demethylase required to establish maternal genomic imprints. *Nature.* **461**:415–418 (2009)

Cierpicki, T., Risner, L. E., Grembecka, J., Lukasik, S. M., Popovic, R., Omonkowska, M., Shultis, D. D., Zeleznik-Le, N. J., & Bushweller, J. H. Structure of the MLL CXXC domain-DNA complex and its functional role in MLL-AF9 leukemia. *Nat Struc Mol Biol* **17**, 62-68 (2010).

Cloos, P. A., Christensen, J., Agger, K., Maiolica, A., Rappsilber, J., Antal, T., Hansen, K. H., & Helin, K. The putative oncogene GASC1 demethylates tri- and dimethylated lysine 9 on histone H3. *Nature*, **442**(7100), 307-311 (2006).

Dahle, Ø., Kumar, A., & Kuehn, M. R. Nodal signaling recruits the histone demethylase Jmjd3 to counteract polycomb-mediated repression at target genes. *Science signaling*, **3**(127): 8 (2010)

Dalgliesh, G. L., Furge, K., Greenman, C., Chen, L., Bignell, G., Butler, A., Davies, H., Edkins, S., Hardy, C., Latimer, C., Teague, J., Andrews, J., Barthorpe, S., Beare, D., Buck, G., Campbell, P. J., Forbes, S., Jia, M., Jones, D., Knott, H., Kok, C. Y., Lau, K. W., Leroy, C., Lin, M. L., McBride, D. J., Maddison, M., Maguire, S., McLay, K., Menzies, A., Mironenko, T., Mulderrig, L., Mudie, L., O'Meara, S., Pleasance, E., Rajasingham, A., Shepherd, R., Smith, R., Stebbings, L., Stephens, P., Tang, G., Tarpey, P. S., Turrell, K., Dykema, K. J., Khoo, S. K., Petillo, D., Wondergem, B., Anema, J., Kahnoski, R. J., Teh, B. T., Stratton, M. R., & Futreal, P. A. Systematic sequencing of renal carcinoma reveals inactivation of histone modifying genes. *Nature*, **463**(7279), 360-363 (2010).

Dey, B. K., Stalker, L., Schnerch, A., Bhatia, M., Taylor-Papidimitriou, J., & Wynder, C. The histone demethylase KDM5b/JARID1b plays a role in cell fate decisions by blocking terminal differentiation. *Mol Cell Biol,* **28**(17), 5312-5327. (2008).

Dhar, S.S., Alam, H., Li, N., Wagner, K.W., Chung, J., Ahn, Y.W., Lee, M.G. Transcriptional Repression of Histone Deacetylase 3 by the Histone Demethylase KDM2A is coupled to tumorigenicity of lung cancer cells. *J Biol Chem* **289**(11):7483-96 (2014)

Dimitrova, E., Turberfield, A. H., & Klose, R. J. Histone demethylases in chromatin biology and beyond. *EMBO reports*, **16**(12), 1620–1639 (2015).

DiTacchio, L., Le, H. D., Vollmers, C., Hatori, M., Witcher, M., Secombe, J., & Panda, S. Histone lysine demethylase JARID1a activates CLOCK-BMAL1 and influences the circadian clock. *Science (New York)*, **333**(6051), 1881–1885. (2011).

dos Remedios, C.G., M. Miki, and J.A. Barden. Fluorescence resonance energy transfer measurements of distances in actin and myosin: A critical evaluation. *J. Muscle Res. Cell Motil.* **8**:97–117 (1987).

Ehrbrecht, A., Müller, U., Wolter, M., Hoischen, A., Koch, A., Radlwimmer, B., Actor, B., Mincheva, A., Pietsch, T., Lichter, P., Reifenberger, G., Weber, R.G. Comprehensive genomic analysis of desmoplastic medulloblastomas: identification of novel amplified genes and separate evaluation of the different histological components. *J. Pathol.* **208**, 554–563 (2006)

Eid, A., Rodriguez-Terrones, D., Burton, A., Torres-Padilla M.E. SUV4-20 activity in the preimplantation mouse embryo controls timely replication. *Genes Dev.* **30** (22):2513-2526 (2016).

Fang, R., Barbera, A. J., Xu, Y., Rutenberg, M., Leonor, T., Bi, Q., Lan, F., Mei, P., Yuan, G. C., Lian, C., Peng, J., Cheng, D., Sui, G., Kaiser, U. B., Shi, Y., & Shi, Y. G. Human LSD2/KDM1b/AOF1 regulates gene transcription by modulating intragenic H3K4me2 methylation. *Molecular cell,* **39**(2), 222–233. (2010).

Farcas, A. M., Blackledge, N. P., Sudbery, I., Long, H. K., McGouran, J. F., Rose, N. R., Lee, S., Sims, D., Cerase, A., Sheahan, T. W., Koseki, H., Brockdorff, N., Ponting, C. P., Kessler, B. M., & Klose, R. J. KDM2B links the Polycomb Repressive Complex 1 (PRC1) to recognition of CpG islands. *eLife* **1**, e00205, doi:10.7554/eLife.00205 (2012).

Felsenfeld, G., and Groudine. M. Controlling the double helix. *Nature.* 421:448–453 (2003)

Fiedler, M., Sánchez-Barrena, M. J., Nekrasov, M., Mieszczanek, J., Rybin, V., Müller, J., Evans, P., & Bienz, M. Decoding of methylated histone H3 tail by the Pygo-BCL9 Wnt signaling complex. *Mol. Cell.* **30**: 507–518 (2008).

Fischle, W., Wang, Y., Allis, C. D. Histone and chromatin cross-talk. *Curr Opin Cell Biol.* **15** (2): 172–183 (2003)

Fraga, M.F., Ballestar, E., Villar-Garea, A., Boix-Chornet, M., Espada, J., Schotta, G., Bonaldi, T., Haydon, C., Ropero, S., Petrie, K., Iyer, N.G., Pérez-Rosado, A., Calvo, E., Lopez, J.A., Cano, A., Calasanz, M.J., Colomer, D., Piris, M.A., Ahn, N., Imhof, A., Caldas, C., Jenuwein, T., Esteller, M. Loss of acetylation at Lys16 and trimethylation at Lys20 of histone H4 is a common hallmark of human cancer. *Nat Genet.* **37** (4): 391-400 (2005)

Frescas, D., Guardavaccaro, D., Bassermann, F., Koyama-Nasu, R. & Pagano, M. JHDM1B/FBXL10 is a nucleolar protein that represses transcription of ribosomal RNA genes. *Nature* **450**, 309-313 (2007).

Frescas, D., Guardavaccaro, D., Kuchay, S. M., Kato, H., Poleshko, A., Basrur, V., Elenitoba-Johnson, K. S., Katz, R. A., & Pagano, M. KDM2A represses transcription of centromeric satellite repeats and maintains the heterochromatic state. *Cell Cycle.* **7** (22): 3539-47 (2008)

Gao, R., Dong, R., Du, J., Ma, P., Wang, S., Fan, Z. Depletion of histone demethylase KDM2A inhibited cell proliferation of stem cells from apical papilla by de-repression of p15INK4B and p27Kip1. *Mol Cell Biochem* **379**(1-2): 115-122 (2013).

Ge, R., Wang, Z., Zeng, Q., Xu, X, Olumi, A. F. F-box protein 10, an NF-κB-dependent anti-apoptotic protein, regulates TRAIL-induced apoptosis through modulating c-Fos/c-FLIP pathway. *Cell Death Differ.* **18** (7): 1184-95 (2011)

Ghosh, A., Ghosh, S., Maiti, G.P., Mukherjee, S., Mukherjee, N., Chakraborty, J., Roy, A., Roychoudhury, S., Panda, C.K. Association of FANCC and PTCH1 with the development of early dysplastic lesions of the head and neck.. *Ann Surg Oncol.* **3**:528-38. (2012)

Gilbert, T. M., McDaniel, S. L., Byrum, S. D., Cades, J. A., Dancy, B. C., Wade, H., Tackett, A. J., Strahl, B. D., & Taverna, S. D. A PWWP domain-containing protein targets the NuA3 acetyltransferase complex via histone H3 lysine 36 trimethylation to coordinate transcriptional elongation at coding regions. *Molecular & cellular proteomics* **13**(11), 2883–2895 (2014).

Grant, P. A. A tale of histone modifications. *Genome Biol.* **2** (4) (2001)

Gray, S. G., Iglesias, A. H., Lizcano, F., Villanueva, R., Camelo, S., Jingu, H., Teh, B. T., Koibuchi, N., Chin, W. W., Kokkotou, E., & Dangond, F. Functional characterization of JMJD2A, a histone deacetylase- and retinoblastoma-binding protein. *J Biol Chem*, **280**(31), 28507-28518 (2005).

Gui, Y., Guo, G., Huang, Y., Hu, X., Tang, A., Gao, S., Wu, R., Chen, C., Li, X., Zhou, L., He, M., Li, Z., Sun, X., Jia, W., Chen, J., Yang, S., Zhou, F., Zhao, X., Wan, S., Ye, R., Liang, C., Liu, Z., Huang, P., Liu, C., Jiang, H., Wang, Y., Zheng, H., Sun, L., Liu, X., Jiang, Z., Feng, D., Chen, J., Wu, S., Zou, J., Zhang, Z., Yang, R., Zhao, J., Xu, C., Yin, W., Guan, Z., Ye, J., Zhang, H., Li, J., Kristiansen, K., Nickerson, M. L., Theodorescu, D., Li, Y., Zhang, X., Li, S., Wang, J., Yang, H., Wang, J., & Cai, Z. Frequent mutations of chromatin remodeling genes in transitional cell carcinoma of the bladder. *Nat Genet*, **43**(9), 875-878 (2011).

Haque, A., Banik, N. L., & Ray, S. K. Molecular alterations in glioblastoma: potential targets for immunotherapy. *Prog Mol Biol Transl Sci,* **98**: 187-234 (2011)

Hata, K., Takashima, R., Amano, K., Ono, K., Nakanishi, M., Yoshida, M., Wakabayashi, M., Matsuda, A., Maeda, Y., Suzuki, Y., Sugano, S., Whitson, R. H., Nishimura, R., & Yoneda, T. Arid5b facilitates chondrogenesis by recruiting the histone demethylase Phf2 to Sox9-regulated genes. *Nat Commun*, **4**, 2850 (2013)

He, J., Kallin, E. M., Tsukada, Y. & Zhang, Y. The H3K36 demethylase Jhdm1b/Kdm2b regulates cell proliferation and senescence through p15 (Ink4b). *Nat Struc Mol Biol* **15**, 1169-1175 (2008).

He, J., Nguyen, A. T. & Zhang, Y. KDM2b/JHDM1b, an H3K36me2-specific demethylase, is required for initiation and maintenance of acute myeloid leukemia. *Blood* **117**, 3869-3880 (2011).

He, J., Shen, L., Wan, M., Taranova, O., Wu, H., & Zhang, Y. Kdm2b maintains murine embryonic stem cell status by recruiting PRC1 complex to CpG islands of developmental genes. *Nature cell biology* **15**, 373-384 (2013).

Helin, K., & Dhanak, D. Chromatin proteins and modifications as drug targets. *Nature,* **502** (7472), 480–488 (2013).

Hellman, L. M., & Fried, M. G. Electrophoretic mobility shift assay (EMSA) for detecting protein-nucleic acid interactions. *Nature protocols*, **2**(8), 1849–1861 (2007).

Hong, S., Cho, Y. W., Yu, L. R., Yu, H., Veenstra, T. D., & Ge, K. Identification of JmjC domain-containing UTX and JMJD3 as histone H3 lysine 27 demethylases. *Proc Natl Acad Sci U S A*, **104**(47), 18439-18444 (2007)

Horton, J. R., Upadhyay, A. K., Qi, H. H., Zhang, X., Shi, Y., & Cheng, X. Enzymatic and structural insights for substrate specificity of a family of jumonji histone lysine demethylases. *Nat Struct Mol Biol,* **17**(1), 38-43 (2010).

Horvath, J.E., Bailey, J.A., Locke, D.P., Eichler, E.E. Lessons from the human genome: transitions between euchromatin and heterochromatin. *Hum Mol Genet*. **10**(20): 2215-23 (2001)

Huang, C., Xiang, Y., Wang, Y., Li, X., Xu, L., Zhu, Z., Zhang, T., Zhu, Q., Zhang, K., Jing, N., & Chen, C. D. Dual-specificity histone demethylase KIAA1718 (KDM7A) regulates neural differentiation through FGF4. *Cell Res,* **20**(2), 154-165 (2010)

Ignea, C., Pontini, M., Maffei, M. E., Makris, A. M., Kampranis, S. C. Engineering monoterpene production in yeast using a synthetic dominant negative geranyl diphosphate synthase. *ACS synthetic biology.* **3**: 298–306 (2014)

Inagaki, T., Tachibana, M., Magoori, K., Kudo, H., Tanaka, T., Okamura, M., Naito, M., Kodama, T., Shinkai, Y., Sakai, J. Obesity and metabolic syndrome in histone demethylase JHDM2a-deficient mice. *Genes Cells* **14**, 991–1001 (2009)

Italiano, A., Attias, R., Aurias, A., Perot, G., Burel-Vandenbos, F., Otto, J., Venissac, N., & Pedeutour, F. Molecular cytogenetic characterization of a metastatic lung sarcomatoid carcinoma: 9p23 neocentromere and 9p23-p24 amplification including JAK2 and JMJD2C. *Cancer Genet Cytogenet*, **167**(2), 122-130 (2006)

Iuchi, S., Paulo, J.A. Lysine-specific demethylase 2A enhances binding of various nuclear factors to CpG-rich genomic DNAs by action of its CXXC-PHD domain. *Sci Rep.* **9**(1):5496 (2019)

Iwase, S., Lan, F., Bayliss, P., de la Torre-Ubieta, L., Huarte, M., Qi, H.H., Whetstine, J.R., Bonni, A., Roberts, T.M., Shi, Y. The X-linked mental retardation gene SMCX/JARID1C defines a family of histone H3 lysine 4 demethylases. *Cell* **128**, 1077-1088 (2007).

Iwase, S., Xiang, B., Ghosh, S., Ren, T., Lewis, P.W., Cochrane, J.C. ATRX ADD domain links an atypical histone methylation recognition mechanism to human mental-retardation syndrome. *Nat. Struct. Mol. Biol.* **18**, 769–776 (2011)

Jambhekar, A., Anastas, J. N., & Shi, Y. Histone Lysine Demethylase Inhibitors. Cold Spring *Harbor perspectives in medicine*, **7**(1), a026484. (2017).

Janardhan, A., Kathera, C., Darsi, A., Ali, W., He, L., Yang, Y., Luo, L., & Guo, Z. Prominent role of histone lysine demethylases in cancer epigenetics and therapy. *Oncotarget*, **9**(76), 34429–34448 (2018).

Janzer, A., Stamm, K., Becker, A., Zimmer, A., Buettner, R., & Kirfel, J. The H3K4me3 histone demethylase Fbxl10 is a regulator of chemokine expression, cellular morphology, and the metabolome of fibroblasts. *J Biol Chem* **287**, 30984-30992 (2012).

Jensen, L. R., Amende, M., Gurok, U., Moser, B., Gimmel, V., Tzschach, A., Janecke, A. R., Tariverdian, G., Chelly, J., Fryns, J. P., Van Esch, H., Kleefstra, T., Hamel, B., Moraine, C., Gecz, J., Turner, G., Reinhardt, R., Kalscheuer, V. M., Ropers, H. H., & Lenzner, S. Mutations in the JARID1C gene, which is involved in transcriptional regulation and chromatin remodeling, cause X-linked mental retardation. *American journal of human genetics*, **76**(2), 227–236 (2005)

Jensen, L. R., Bartenschlager, H., Rujirabanjerd, S., Tzschach, A., Nümann, A., Janecke, A. R., Spörle, R., Stricker, S., Raynaud, M., Nelson, J., Hackett, A., Fryns, J. P., Chelly, J., de Brouwer, A. P., Hamel, B., Gecz, J., Ropers, H. H., & Kuss, A. W. A distinctive gene expression fingerprint in mentally retarded male patients reflects disease-causing defects in the histone demethylase KDM5C. *PathoGenetics*, **3**(1), 2 (2010).

Jonkman, J. E., Cathcart, J. A., Xu, F., Bartolini, M. E., Amon, J. E., Stevens, K. M., & Colarusso, P. An introduction to the wound healing assay using live-cell microscopy. *Cell adhesion & migration*, **8**(5), 440–451 (2014)

Kahl, P., Gullotti, L., Heukamp, L.C., Wolf, S., Friedrichs, N., Vorreuther, R., Solleder, G., Bastian, P.J., Ellinger, J., Metzger, E., Schüle, R., Buettner, R. Androgen receptor coactivators lysine-specific histone demethylase 1 and four and a half LIM domain protein 2 predict risk of prostate cancer recurrence. *Cancer Res.* **66**(23):11341-7 (2006).

Kampranis, S. C. & Tsichlis, P. N. Histone Demethylases and Cancer. *Adv Cancer Res* **102**, 103-169 (2009).

Kang, J.Y., Kim, J.Y., Kim, K.B., Park, J.W., Cho, H., Hahm, J.Y., Chae, Y.C., Kim, D., Kook, H., Rhee, S., Ha, N.C., Seo, S.B. KDM2B is a histone H3K79 demethylase and induces transcriptional repression via SIRT1-mediated chromatin silencing. *FASEB J*: fj201800242R (2018).

Karytinos, A., Forneris, F., Profumo, A., Ciossani, G., Battaglioli, E., Binda, C., & Mattevi, A. A novel mammalian flavin-dependent histone demethylase. *The Journal of biological chemistry*, **284**(26), 17775–17782 (2009)

Kauffman, E. C., Robinson, B. D., Downes, M. J., Powell, L. G., Lee, M. M., Scherr, D. S., Gudas, L. J., & Mongan, N. P. Role of androgen receptor and associated lysine-demethylase coregulators,

LSD1 and JMJD2A, in localized and advanced human bladder cancer. *Molecular carcinogenesis*, **50**(12), 931–944 (2011).

Kidder, B. L., Hu, G., Cui, K. & Zhao, K. SMYD5 regulates H4K20me3-marked heterochromatin to safeguard ES cell self-renewal and prevent spurious differentiation. *Epigenetics Chromatin* **10**:8 (2017).

Kim, J., Shin, S., Subramaniam, M., Bruinsma, E., Kim, T. D., Hawse, J. R., Spelsberg, T. C., & Janknecht, R. Histone demethylase JARID1B/KDM5B is a corepressor of TIEG1/KLF10. *Biochem Biophys Res Commun,* **401**(3), 412-416. (2010).

Kim, T. D., Shin, S., Berry, W. L., Oh, S., & Janknecht, R. The JMJD2A demethylase regulates apoptosis and proliferation in colon cancer cells. *J Cell Biochem*, **113**(4), 1368-1376 (2012)

Kipreos, E. T., & Pagano, M. The F-box protein family. *Genome biology*, **1**(5) (2000).

Klose, R. J., Kallin, E.M., Zhang, Y. JmjC-domain-containing proteins and histone demethylation. *Nat Rev Genet* **7**(9): 715-727 (2006a).

Klose, R. J., Yamane, K., Bae, Y., Zhang, D., Erdjument-Bromage, H., Tempst, P., Wong, J., & Zhang, Y. The transcriptional repressor JHDM3A demethylates trimethyl histone H3 lysine 9 and lysine 36. *Nature*, **442**(7100), 312-316 (2006b)

Kottakis, F., Polytarchou, C., Foltopoulou, P., Sanidas, I., Kampranis, S. C., & Tsichlis, P. N. FGF-2 regulates cell proliferation, migration, and angiogenesis through an NDY1/KDM2B-miR-101-EZH2 pathway. *Mol. cell* **43**, 285-298 (2011).

Kottakis, F., Foltopoulou, P., Sanidas, I., Keller, P., Wronski, A., Dake, B. T., Ezell, S. A., Shen, Z., Naber, S. P., Hinds, P. W., McNiel, E., Kuperwasser, C., & Tsichlis, P. N. NDY1/KDM2B functions as a master regulator of polycomb complexes and controls self-renewal of breast cancer stem cells. *Can research* **74**, 3935-3946 (2014).

Kouzarides, T. Chromatin modifications and their function. *Cell* **128**, 693-705 (2007).

Koyama-Nasu, R., David, G. & Tanese, N. The F-box protein Fbl10 is a novel transcriptional repressor of c-Jun. *Nat Cell Biol* **9**, 1074-1080 (2007).

Krieg, A. J., Rankin, E. B., Chan, D., Razorenova, O., Fernandez, S., & Giaccia, A. J. Regulation of the histone demethylase JMJD1A by hypoxia-inducible factor 1 alpha enhances hypoxic gene expression and tumor growth. *Mol. Cell Biol.* **30**, 344–353 (2010)

Kurup, J.T. and Kidder B.L. Identification of H4K20me3- and H3K4me3-associated RNAs using CARIP-Seq expands the transcriptional and epigenetic networks of embryonic stem cells. *J Biol Chem.* **293** (39):15120-15135 (2018).

Kwon, H., Imbalzano, A.N., Khavari, P.A., Kingston, R.E., Green, M.R. Nucleosome disruption and enhancement of activator binding by a human SW1/SNF complex. *Nature*, **370** (6489): 477-81 (1994)

Lachner, M., O'Sullivan, R. J., Jenuwein, T. An epigenetic road map for histone lysine methylation. *J Cell Sci* **116**: 2117-2124 (2003)

Lađinović, D., Novotná, J., Jakšová, S., Raška, I., & Vacík, T. A demethylation deficient isoform of the lysine demethylase KDM2A interacts with pericentromeric heterochromatin in an HP1a-dependent manner. *Nucleus* **8**(5), 563–572 (2017)

Laity, J. H., Lee, B. M., Wright, P. E. Zinc finger proteins: new insights into structural and functional diversity. *Curr Opin Struc Biol*. **11** (1): 39–46 (2001)

Lan, F., Collins, R. E., De Cegli, R., Alpatov, R., Horton, J. R., Shi, X., Gozani, O., Cheng, X., & Shi, Y. Recognition of unmethylated histone H3 lysine 4 links BHC80 to LSD1-mediated gene repression. *Nature* **448**, 718-722 (2007).

Lan, F., Nottke, A. C., & Shi, Y. Mechanisms involved in the regulation of histone lysine demethylases. *Current opinion in cell biology*, **20**(3), 316–325 (2008).

Laumonnier, F., Holbert, S., Ronce, N., Faravelli, F., Lenzner, S., Schwartz, C. E., Lespinasse, J., Van Esch, H., Lacombe, D., Goizet, C., Phan-Dinh Tuy, F., van Bokhoven, H., Fryns, J. P., Chelly, J., Ropers, H. H., Moraine, C., Hamel, B. C., & Briault, S. Mutations in PHF8 are associated with X linked mental retardation and cleft lip/cleft palate. *J. Med. Genet.* **42**, 780–786. (2005)

Lee, C., Kim, B., Song, B., & Moon, K. C. Implication of PHF2 Expression in Clear Cell Renal Cell Carcinoma. *J Pathol Transl Med*, **51**(4), 359-364 (2017)

Lee, K. H., Ju, U. I., Song, J. Y., & Chun, Y. S. The histone demethylase PHF2 promotes fat cell differentiation as an epigenetic activator of both C/EBPalpha and C/EBPdelta. *Mol Cells*, **37**(10), 734-741 (2014)

Lee, K. H., Park, J. W., Sung, H. S., Choi, Y. J., Kim, W. H., Lee, H. S., Chung, H. J., Shin, H. W., Cho, C. H., Kim, T. Y., Li, S. H., Youn, H. D., Kim, S. J., & Chun, Y. S. PHF2 histone demethylase acts as a tumor suppressor in association with p53 in cancer. *Oncogene*, **34**(22), 2897-2909. (2015).

Lee, M. G., Villa, R., Trojer, P., Norman, J., Yan, K. P., Reinberg, D., Di Croce, L., & Shiekhattar, R. Demethylation of H3K27 regulates polycomb recruitment and H2A ubiquitination. *Science*, **318**(5849), 447-450 (2007a).

Lee, M.G., Norman, J., Shilatifard, A., Shiekhattar, R. Physical and functional association of a trimethyl H3K4 demethylase and Ring6a/MBLR, a polycomb-like protein. *Cell* **128**, 877–887 (2007b)

Lee, S., Lee, J. W., & Lee, S. K. UTX, a histone H3-lysine 27 demethylase, acts as a critical switch to activate the cardiac developmental program. *Dev Cell*, **22**(1), 25-37 (2012).

Li, B. X., Zhang, M. C., Luo, C. L., Yang, P., Li, H., Xu, H. M., Xu, H. F., Shen, Y. W., Xue, A. M., & Zhao, Z. Q. Effects of RNA interference-mediated gene silencing of JMJD2A on human breast cancer cell line MDA-MB-231 in vitro. *J Exp Clin Cancer Res*, **30**: 90 (2011).

Li, H., Ilin, S., Wang, W., Duncan, E. M., Wysocka, J., Allis, C. D., & Patel, D. J. Molecular basis for site-specific read-out of histone H3K4me3 by the BPTF PHD finger of NURF. *Nature.* **442**, 91–95 (2006)

Li, H., Lai, P., Jia, J., Song, Y., Xia, Q., Huang, K., He, N., Ping, W., Chen, J., Yang, Z., Li, J., Yao, M., Dong, X., Zhao, J., Hou, C., Esteban, M.A., Gao, S., Pei, D., Hutchins, A.P., Yao, H. RNA Helicase DDX5 Inhibits Reprogramming to Pluripotency by miRNA-Based Repression of RYBP and its PRC1-Dependent and -Independent Functions. *Cell stem cell* **20**, 462-477 (2017).

Li, K. K., Luo, C., Wang, D., Jiang, H., & Zheng, Y. G. Chemical and biochemical approaches in the study of histone methylation and demethylation. *Medicinal research reviews*, **32**(4), 815-67 (2012).

Li, Y. & Li, H. Many keys to push: diversifying the 'readership' of plant homeodomain fingers. *Acta Biochim. Biophys. Sin.* **44**, 28–39 (2012)

Liang, G., He, J. & Zhang, Y. Kdm2b promotes induced pluripotent stem cell generation by facilitating gene activation early in reprogramming. *Nat Cell Biol* **14**, 457-466 (2012).

Liefke, R., Oswald, F., Alvarado, C., Ferres-Marco, D., Mittler, G., Rodriguez, P., Dominguez, M., & Borggrefe, T. Histone demethylase KDM5A is an integral part of the core Notch-RBP-J repressor complex. *Genes & development,* **24**(6), 590–601 (2010)

Liggins, A. P., Lim, S. H., Soilleux, E. J., Pulford, K., & Banham, A. H. A panel of cancer-testis genes exhibiting broad-spectrum expression in haematological malignancies. *Cancer immunity*, **10**:8. (2010).

Lim, S., Janzer, A., Becker, A., Zimmer, A., Schüle, R., Buettner, R., Kirfel, J. Lysine-specific demethylase 1 (LSD1) is highly expressed in ER-negative breast cancers and a biomarker predicting aggressive biology. *Carcinogenesis* **31**(3):512-20 (2010).

Lin, S.L. Concise review: Deciphering the mechanism behind induced pluripotent stem cell generation. *Stem Cells*. **29**:1645–1649 (2011)

Liu, G., Bollig-Fischer, A., Kreike, B., van de Vijver, M. J., Abrams, J., Ethier, S. P., & Yang, Z. Q. Genomic amplification and oncogenic properties of the GASC1 histone demethylase gene in breast cancer. *Oncogene*, **28**(50), 4491-4500 (2009)

Liu, G., Xia, T., Chen, X. The activation domains, the proline-rich domain, and the C-terminal basic domain in p53 are necessary for acetylation of histones on the proximal p21 promoter and interaction with p300/CREB-binding protein. *J Biol Chem.* **278**(19): 17557-65 (2003)

Liu, L., Zhen, X.T., Denton, E., Marsden, B.D. and Schapira, M. ChromoHub: a data hub for navigators of chromatin-mediated signaling. *Bioinformatics* **28**, 2205–2206 (2012)

Liu, Z., Zhou, S., Liao, L., Chen, X., Meistrich, M., & Xu, J. Jmjd1a demethylase-regulated histone modification is essential for cAMP-response element modulator regulated gene expression and spermatogenesis. *J. Biol. Chem.* **285**, 2758–2770 (2010)

Lizcano, F. & Garcia, J. Epigenetic control and cancer: the potential of histone demethylases as therapeutic targets. *Pharmaceuticals (Basel, Switzerland*), **5**(9), 963–990 (2012).

Lizcano, F., Romero, C., & Vargas, D. Regulation of adipogenesis by nuclear receptor PPARγ is modulated by the histone demethylase JMJD2C. *Genetics and molecular biology*, **34**(1), 19–24 (2011)

Loh, Y. H., Zhang, W., Chen, X., George, J., & Ng, H. H. Jmjd1a and Jmjd2c histone H3 Lys 9 demethylases regulate self-renewal in embryonic stem cells. *Genes Dev.* **21**, 2545–2557 (2007)

Long, H. K., Blackledge, N. P. & Klose, R. J. ZF-CxxC domain-containing proteins, CpG islands and the chromatin connection. *Biochem Soc Trans* **41**, 727-740 (2013).

Lu, L., Gao, Y., Zhang, Z., Cao, Q., Zhang, X., Zou, J., Cao, Y. Kdm2a/b Lysine Demethylases Regulate Canonical Wnt Signaling by Modulating the Stability of Nuclear beta-Catenin. *Dev Cell* **33**, 660-674 (2015).

Lu, P.J., Sundquist, K., Baeckstrom, D., Poulsom, R., Hanby, A., Meier-Ewert, S., Jones, T., Mitchell, M., Pitha-Rowe, P., Freemont, P., Taylor-Papadimitriou, J. A novel gene (PLU-1) containing highly conserved putative DNA/chromatin binding motifs is specifically up-regulated in breast cancer. *J Biol Chem.* **274**(22):15633-45 (1999)

Lu, T., *et al.* Regulation of NF-kappaB by NSD1/FBXL11-dependent reversible lysine methylation of p65. *Proc Natl Acad Sci U S A* **107**(1): 46-51. (2010).

Lv, T., Yuan, D., Miao, X., Lv, Y., Zhan, P., Shen, X., & Song, Y. Over-expression of LSD1 promotes proliferation, migration and invasion in non-small cell lung cancer. *PloS one*, **7**(4), e35065 (2012).

Maison, C. & Almouzni, G. HP1 and the dynamics of heterochromatin maintenance. *Nat Rev Mol Cell Biol*. **5**(4): 296-304 (2004)

Mallette, F. A., Mattiroli, F., Cui, G., Young, L. C., Hendzel, M. J., Mer, G., Sixma, T. K., & Richard, S. RNF8- and RNF168-dependent degradation of KDM4A/JMJD2A triggers 53BP1 recruitment to DNA damage sites. *The EMBO journal,* **31**(8), 1865–1878 (2012).

Mar, B. G., Bullinger, L., Basu, E., Schlis, K., Silverman, L. B., Dohner, K., & Armstrong, S. A. Sequencing histone-modifying enzymes identifies UTX mutations in acute lymphoblastic leukemia. *Leukemia*, **26**(8), 1881-1883 (2012).

Margueron, R., Trojer, P., Reinberg, D. The key to development: interpreting the histone code? *Curr Opin Gen Dev* **15** (2): 163–176 (2005)

Martinelli, P., Bonetti, P., Sironi, C., Pruneri, G., Fumagalli, C., Raviele, P. R., Volorio, S., Pileri, S., Chiarle, R., McDuff, F. K., Tusi, B. K., Turner, S. D., Inghirami, G., Pelicci, P. G., & Colombo, E. The lymphoma-associated NPM-ALK oncogene elicits a p16INK4a/pRb-dependent tumor-suppressive pathway. *Blood*, **117**(24), 6617-6626 (2011).

McDevitt, M. A. Clinical applications of epigenetic markers and epigenetic profiling in myeloid malignancies. *Semin Oncol*, **39**(1), 109-122 (2012).

Moll, J. R., Acharya, A., Gal, J., Mir, A. A., & Vinson, C. Magnesium is required for specific DNA binding of the CREB B-ZIP domain. *Nucleic acids research*, **30**(5), 1240–1246 (2002).

Muramatsu, H., Makishima, H., & Maciejewski, J. P. Chronic myelomonocytic leukemia and atypical chronic myeloid leukemia: novel pathogenetic lesions. *Semin Oncol*, **39**(1), 67-73(2012).

Murr, R. Interplay between different epigenetic modifications and mechanisms. *Adv Genet*, **70**, 101-141 (2010)

Musselman, C. A., Kutateladze, T. G. Handpicking epigenetic marks with PHD fingers. *Nucleic Acids Res.* **39** (21): 9061–9071 (2011)

Nelson, D. M., Jaber-Hijazi, F., Cole, J. J., Robertson, N. A., Pawlikowski, J. S., Norris, K. T., Criscione, S. W., Pchelintsev, N. A., Piscitello, D., Stong, N., Rai, T. S., McBryan, T., Otte, G. L., Nixon, C., Clark, W., Riethman, H., Wu, H., Schotta, G., Garcia, B. A., Neretti, N., Adams, P. D. Mapping H4K20me3 onto the chromatin landscape of senescent cells indicates a function in control of cell senescence and tumor suppression through preservation of genetic and epigenetic stability. *Genome Biol* **17**, 158 (2016).

Niu, X., Zhang, T., Liao, L., Zhou, L., Lindner, D. J., Zhou, M., Rini, B., Yan, Q., & Yang, H. The von Hippel-Lindau tumor suppressor protein regulates gene expression and tumor growth through histone demethylase JARID1C. *Oncogene*, **31**(6), 776-786 (2012)

Noma K., Allis C.D., Grewal S.I. Transitions in distinct histone H3 methylation patterns at the heterochromatin domain boundaries. *Science*. **293** (5532), 1150-1155 (2001)

Oey, N. E., Leung, H. W., Ezhilarasan, R., Zhou, L., Beuerman, R. W., VanDongen, H. M., & VanDongen, A. M. A Neuronal Activity-Dependent Dual Function Chromatin-Modifying Complex Regulates Arc Expression. *eNeuro*, **2**(1) (2015).

Ohtani, K., Vlachojannis, G.J., Koyanagi, M., Boeckel, J.N., Urbich, C., Farcas, R., Bonig, H., Marquez, V.E., Zeiher, A.M., Dimmeler, S. Epigenetic regulation of endothelial lineage committed genes in pro-angiogenic hematopoietic and endothelial progenitor cells. *Circ Res*. **109**(11):1219-29 (2011)

Okada, Y., Scott, G., Ray, M.K., Mishina, Y., Zhang, Y. Histone demethylase JHDM2A is critical for Tnp1 and Prm1 transcription and spermatogenesis. *Nature* **450**, 119–123 (2007)

Okamoto, K., Tanaka, Y., Ogasawara, S., Obuse, C., Nakayama, J. I., Yano, H., & Tsuneoka, M. KDM2A-dependent reduction of rRNA transcription on glucose starvation requires HP1 in cells, including triple-negative breast cancer cells. *Oncotarget,* **10**(46), 4743–4760 (2019).

Okamoto, K., Tanaka, Y., Tsuneoka, M. SF-KDM2A binds to ribosomal RNA gene promoter, reduces H4K20me3 level, and elevates ribosomal RNA transcription in breast cancer cells. *Int J Oncol.* (2017)

Okuno, Y., Ohtake, F., Igarashi, K., Kanno, J., Matsumoto, T., Takada, I., Kato, S., & Imai, Y. Epigenetic regulation of adipogenesis by PHF2 histone demethylase. *Diabetes*, **62**(5), 1426–1434 (2013).

Osawa, T., Muramatsu, M., Wang, F., Tsuchida, R., Kodama, T., Minami, T., & Shibuya, M. Increased expression of histone demethylase JHDM1D under nutrient starvation suppresses tumor growth via down-regulating angiogenesis. *Proc Natl Acad Sci U S A*, **108**(51), 20725-20729. (2011)

Park, J. H., Jung, M., & Moon, K. C. The prognostic significance of nuclear expression of PHF2 and C/EBPα in clear cell renal cell carcinoma with consideration of adipogenic metabolic evolution. *Oncotarget*, **9**(1), 142–151 (2017).

Pedersen, M.T. & Helin, K. Histone demethylases in development and disease. *Trends Cell Biol.* **20**(11):662-71 (2010)

Peña, P. V., Davrazou, F., Shi, X., Walter, K. L., Verkhusha, V. V., Gozani, O., Zhao, R., & Kutateladze, T. G. Molecular mechanism of histone H3K4me3 recognition by plant homeodomain of ING2. *Nature*, **442**(7098), 100–103 (2006).

Pereira, F., Barbachano, A., Silva, J., Bonilla, F., Campbell, M. J., Munoz, A., & Larriba, M. J. KDM6B/JMJD3 histone demethylase is induced by vitamin D and modulates its effects in colon cancer cells. *Hum Mol Genet*, **20**(23), 4655-4665 (2011).

Pfau, R., Tzatsos, A., Kampranis, S. C., Serebrennikova, O. B., Bear, S. E., & Tsichlis, P. N. Members of a family of JmjC domain-containing oncoproteins immortalize embryonic fibroblasts via a JmjC domain-dependent process. *PNAS* **105**, 1907-1912 (2008)

Pollard, P. J., Loenarz, C., Mole, D. R., McDonough, M. A., Gleadle, J. M., Schofield, C. J., & Ratcliffe, P. J. Regulation of Jumonji-domain-containing histone demethylases by hypoxia-inducible factor (HIF)-1alpha. *Biochem J*, **416**(3), 387-394 (2008)

Pollok, B.A., and R. Heim. Using GFP in FRET-based applications. *Trends Cell Biol.* 9:57–60 (1999).

Polytarchou, C., Pfau, R., Hatziapostolou, M. & Tsichlis, P. N. The JmjC domain histone demethylase Ndy1 regulates redox homeostasis and protects cells from oxidative stress. *Mol Cell Biol* **28**, 7451-7464 (2008).

Pothof, J., van Haaften, G., Thijssen, K., Kamath, R. S., Fraser, A. G., Ahringer, J., Plasterk, R. H., & Tijsterman, M. Identification of genes that protect the C. elegans genome against mutations by genome-wide RNAi. *Genes Dev* **17**, 443-448 (2003).

Qian, Y., Chen, C., Jiang, L., Zhang, J., & Ren, Q. Genome-wide identification, classification and expression analysis of the JmjC domain-containing histone demethylase gene family in maize. *BMC genomics,* **20**(1), p. 256 (2019)

Reyes, J.C., Hennig, L., Gruissem, W. Chromatin-remodeling and memory factors. New regulators of plant development. *Plant Physiol.* **130**(3): 1090-1101 (2002)

Ribet, D. & Cossart, P. Post-translational modifications in host cells during bacterial infection. *FEBS Letters.* **584** (13): 2748-2758 (2010)

Rothbart, S. B. & Strahl, B. D. Interpreting the language of histone and DNA modifications. *Biochim Biophys Acta*, **1839**(8), 627-643 (2014).

Sánchez, C., Sánchez, I., Demmers, J.A., Rodriguez, P., Strouboulis, J., Vidal, M. Proteomics analysis of Ring1B/Rnf2 interactors identifies a novel complex with the Fbxl10/Jhdm1B histone demethylase and the Bcl6 interacting corepressor. *Mol Cell Proteomics.* (6) 820–834. (2007)

Sanchez, R., & Zhou, M.-M. The PHD Finger: A Versatile Epigenome Reader. *Trends Biochem Sci* **36** (7), 364–372 (2011).

Sarg, B., Koutzamani, E., Helliger, W., Rundquist, I., Lindner, H. H. Postsynthetic trimethylation of histone H4 at lysine 20 in mammalian tissues is associated with aging. *J Biol Chem.* **277**: 39195–201 (2002)

Satoh, T., Takeuchi, O., Vandenbon, A., Yasuda, K., Tanaka, Y., Kumagai, Y., Miyake, T., Matsushita, K., Okazaki, T., Saitoh, T., Honma, K., Matsuyama, T., Yui, K., Tsujimura, T., Standley, D. M., Nakanishi, K., Nakai, K., & Akira, S. The Jmjd3-Irf4 axis regulates M2 macrophage polarization and host responses against helminth infection. *Nat Immunol*, **11**(10), 936-944 (2010)

Schmitz, S. U., Albert, M., Malatesta, M., Morey, L., Johansen, J. V., Bak, M., Tommerup, N., Abarrategui, I., & Helin, K. Jarid1b targets genes regulating development and is involved in neural differentiation. *EMBO J,* **30**(22), 4586-4600 (2011)

Schotta, G., Lachner, M., Sarma, K., Ebert, A., Sengupta, R., Reuter, G., Reinberg, D., & Jenuwein, T. A silencing pathway to induce H3-K9 and H4-K20 trimethylation at constitutive heterochromatin. *Genes & Dev.* **18**:1251–1262 (2004)

Schulte, J.H., Lim, S., Schramm, A., Friedrichs, N., Koster, J., Versteeg, R., Ora, I., Pajtler, K., Klein-Hitpass, L., Kuhfittig-Kulle, S., Metzger, E., Schüle, R., Eggert, A., Buettner, R., Kirfel, J. Lysine-specific demethylase 1 is strongly expressed in poorly differentiated neuroblastoma: implications for therapy. *Cancer Res* 1;**69**(5):2065-71 (2009)

Seenundun, S., Rampalli, S., Liu, Q. C., Aziz, A., Palii, C., Hong, S., Blais, A., Brand, M., Ge, K., & Dilworth, F. J. UTX mediates demethylation of H3K27me3 at muscle-specific genes during myogenesis. *The EMBO journal*, **29**(8), 1401–1411 (2010).

Sekar, R. B., & Periasamy, A.. Fluorescence resonance energy transfer (FRET) microscopy imaging of live cell protein localizations. *JCB*, **160** (5), 629–633 (2003)

Sengoku, T., & Yokoyama, S. Structural basis for histone H3 Lys 27 demethylation by UTX/KDM6A. *Genes Dev*, **25**(21), 2266-2277 (2011).

Shi, G., Wu, M., Fang, L., Yu, F., Cheng, S., Li, J., Du, J. X., & Wong, J. PHD finger protein 2 (PHF2) represses ribosomal RNA gene transcription by antagonizing PHF finger protein 8 (PHF8) and recruiting methyltransferase SUV39H1. *J Biol Chem*, **289**(43), 29691-29700 (2014)

Shi, X., Hong, T., Walter, K. L., Ewalt, M., Michishita, E., Hung, T., Carney, D., Pena, P., Lan, F., Kaadige, M. R., Lacoste, N., Cayrou, C., Davrazou, F., Saha, A., Cairns, B. R., Ayer, D. E., Kutateladze, T. G., Shi, Y., Cote, J., Chua, K. F., & Gozani, O. ING2 PHD domain links histone H3 lysine 4 methylation to active gene repression. *Nature,* **442**(7098), 96-99. (2006).

Shi, Y. & Whetstine J. R. Dynamic regulation of histone lysine methylation by demethylases." *Mol Cell* **25**(1): 1-14. (2007).

Shi, Y.J., Matson, C., Lan, F., Iwase, S., Baba, T., Shi, Y. Regulation of LSD1 histone demethylase activity by its associated factors. *Mol. Cell.* **19**:857–864 (2005).

Smith, J. A., White, E. A., Sowa, M. E., Powell, M. L., Ottinger, M., Harper, J. W., & Howley, P. M. Genome-wide siRNA screen identifies SMCX, EP400, and Brd4 as E2-dependent regulators of human papillomavirus oncogene expression. *Proc Natl Acad Sci U S A*, **107**(8), 3752-3757 (2010)

Strahl, B. D. & Allis, C. D. The language of covalent histone modifications. *Nature.* **403**: 41-45 (2000)

Sun, G., Ye, P., Murai, K., Lang, M. F., Li, S., Zhang, H., Li, W., Fu, C., Yin, J., Wang, A., Ma, X., & Shi, Y. miR-137 Forms a regulatory loop with nuclear receptor TLX and LSD1 in neural stem cells. *Nat. Commun.* **2**:529 (2011)

Suzuki, T, Minehata, K., Akagi, K., Jenkins, N. A., Copeland, N. G. Tumor suppressor gene identification using retroviral insertional mutagenesis in Blm-deficient mice. *The EMBO Journal* **25**, 3422–3431 (2006)

Tahiliani, M., Mei, P., Fang, R., Leonor, T., Rutenberg, M., Shimizu, F., Li, J., Rao, A., & Shi, Y. The histone H3K4 demethylase SMCX links REST target genes to X-linked mental retardation. *Nature*, **447**(7144), 601-605 (2007)

Tanaka, Y., Umata, T., Okamoto, K., Obuse, C., Tsuneoka, M. CxxC-ZF domain is needed for KDM2A to demethylate histone in rDNA promoter in response to starvation. *Cell Struct Funct.* **39** (1):79-92. (2014)

Tarantino, C., Paolella, G., Cozzuto, L., Minopoli, G., Pastore, L., Parisi, S., & Russo, T. miRNA 34a, 100, and 137 modulate differentiation of mouse embryonic stem cells. *FASEB J,* **24**(9), 3255-3263 (2010)

Tateishi, K., Okada, Y., Kallin, E. M., & Zhang, Y. Role of Jhdm2a in regulating metabolic gene expression and obesity resistance. *Nature* **458**, 757–761 (2009)

Taverna, S. D., Li, H., Ruthenburg, A. J., Allis, C. D., Patel, D. J. How chromatin-binding modules interpret histone modifications: lessons from professional pocket pickers. *Nat Struct Mol Biol.* **14** (11): 1025-40 (2007).

Thieme, S., Gyárfás, T., Richter, C., Özhan, G., Fu, J., Alexopoulou, D., Muders, M.H., Michalk, I., Jakob, C., Dahl, A., Klink, B., Bandola, J., Bachmann, M., Schröck, E., Buchholz, F., Stewart, A.F., Weidinger, G., Anastassiadis, K., Brenner, S. The histone demethylase UTX regulates stem cell migration and hematopoiesis. *Blood*, **121**(13):2462-73 (2013)

Trojer, P., Zhang, J., Yonezawa, M., Schmidt, A., Zheng, H., Jenuwein, T., & Reinberg, D. Dynamic Histone H1 Isotype 4 Methylation and Demethylation by Histone Lysine Methyltransferase G9a/KMT1C and the Jumonji Domain-containing JMJD2/KDM4 Proteins. *The Journal of biological chemistry*, **284**(13), 8395–8405 (2009).

Tsukada, Y. & Zhang, Y. Purification of histone demethylases from HeLa cells. *Methods* **40**(4): 318-326 (2006).

Tsukada, Y., Ishitani, T., & Nakayama, K. I. KDM7 is a dual demethylase for histone H3 Lys 9 and Lys 27 and functions in brain development. *Genes Dev,* **24**(5), 432-437. (2010)

Tzatsos, A., Paskaleva, P., Ferrari, F., Deshpande, V., Stoykova, S., Contino, G., Wong, K. K., Lan, F., Trojer, P., Park, P. J., & Bardeesy, N. KDM2B promotes pancreatic cancer via Polycomb-dependent and -independent transcriptional programs. *JCI* **123**, 727-739 (2013).

Tzatsos, A., Paskaleva, P., Lymperi, S., Contino, G., Stoykova, S., Chen, Z., Wong, K. K., & Bardeesy, N. Lysine-specific demethylase 2B (KDM2B)-let-7-enhancer of zester homolog 2 (EZH2) pathway regulates cell cycle progression and senescence in primary cells. *J Biol Chem* **286**, 33061-33069, doi:10.1074/jbc.M111.257667 (2011).

Tzatsos, A., Pfau, R., Kampranis, S. C. & Tsichlis, P. N. Ndy1/KDM2B immortalizes mouse embryonic fibroblasts by repressing the Ink4a/Arf locus. *PNAS* **106**, 2641-2646 (2009).

Ueda, T., Nagamachi, A., Takubo, K., Yamasaki, N., Matsui, H., Kanai, A., Nakata, Y., Ikeda, K., Konuma, T., Oda, H., Wolff, L., Honda, Z., Wu, X., Helin, K., Iwama, A., Suda, T., Inaba, T., & Honda, H. Fbxl10 overexpression in murine hematopoietic stem cells induces leukemia involving metabolic activation and upregulation of Nsg2. *Blood* **125**, 3437-3446 (2015).

Vacík T, Lađinović D, Raška I KDM2A/B lysine demethylases and their alternative isoforms in development and disease. *Nucleus* **9**(1): 431-441 (2018).

van den Boom, V., Maat, H., Geugien, M., Rodríguez López, A., Sotoca, A.M., Jaques, J., Brouwers-Vos, A.Z., Fusetti, F., Groen, R.W., Yuan, H., Martens, A.C., Stunnenberg, H.G., Vellenga, E., Martens, J.H., Schuringa, J.J. Non-canonical PRC1.1 targets active genes independent of H3K27me3 and is essential for leukemogenesis. *Cell Rep.* **14** (2): 332-46 (2016).

Van Essen, D., Zhu, Y., Saccani, S. A feed-forward circuit controlling inducible NF-kappaB target gene activation by promoter histone demethylation. *Mol. Cell.* **39**:750–760 (2010)

van Haaften, G., Dalgliesh, G. L., Davies, H., Chen, L., Bignell, G., Greenman, C., Edkins, S., Hardy, C., O'Meara, S., Teague, J., Butler, A., Hinton, J., Latimer, C., Andrews, J., Barthorpe, S., Beare, D., Buck, G., Campbell, P. J., Cole, J., Forbes, S., Jia, M., Jones, D., Kok, C. Y., Leroy, C., Lin, M. L., McBride, D. J., Maddison, M., Maquire, S., McLay, K., Menzies, A., Mironenko, T., Mulderrig, L., Mudie, L., Pleasance, E., Shepherd, R., Smith, R., Stebbings, L., Stephens, P., Tang, G., Tarpey, P. S., Turner, R., Turrell, K., Varian, J., West, S., Widaa, S., Wray, P., Collins, V. P., Ichimura, K., Law, S., Wong, J., Yuen, S. T., Leung, S. Y., Tonon, G., DePinho, R. A., Tai, Y. T., Anderson, K. C., Kahnoski, R. J., Massie, A., Khoo, S. K., Teh, B. T., Stratton, M. R., & Futreal, P. A. Somatic mutations of the histone H3K27 demethylase gene UTX in human cancer. *Nat Genet*, **41**(5), 521-523 (2009).

van Zutven, L.J., Onen, E., Velthuizen, S.C., van Drunen, E., von Bergh, A.R., van den Heuvel-Eibrink, M.M., Veronese, A., Mecucci, C., Negrini, M., de Greef, G.E., Beverloo, H.B. Identification of NUP98 abnormalities in acute leukemia: JARID1A (12p13) as a new partner gene. *Genes Chromosomes Cancer.* 45(5):437-46 (2006)

Verrier, L., Escaffit, F., Chailleux, C., Trouche, D., & Vandromme, M. A new isoform of the histone demethylase JMJD2A/KDM4A is required for skeletal muscle differentiation. *PLoS Genet*, **7**(6), e1001390. (2011)

Vinatzer, U., Gollinger, M., Mullauer, L., Raderer, M., Chott, A., & Streubel, B. Mucosa-associated lymphoid tissue lymphoma: novel translocations including rearrangements of ODZ2, JMJD2C, and CNN3. *Clin Cancer Res*, **14**(20), 6426-6431 (2008)

Wang Y., Zhang H, Chen Y, Sun Y, Yang F, Yu W, Liang J, Sun L, Yang X, Shi L, Li R, Li Y, Zhang Y, Li Q, Yi X, Shang Y. LSD1 is a subunit of the NuRD complex and targets the metastasis programs in breast cancer. *Cell* **138**(4):660-72 (2009).

Wang, J. J., Dong, R., Wang, L. P., Wang, J. S., Du, J., Wang, S. L., Shan, Z. C., & Fan, Z. P. Histone demethylase KDM2B inhibits the chondrogenic differentiation potentials of stem cells from apical papilla. *Int J Clin Exp Med.* **8** (2): 2165-73 (2015).

Wang, Q., Ma, S., Song, N., Li, X., Liu, L., Yang, S., Ding, X., Shan, L., Zhou, X., Su, D., Wang, Y., Zhang, Q., Liu, X., Yu, N., Zhang, K., Shang, Y., Yao, Z., & Shi, L. Stabilization of histone demethylase PHF8 by USP7 promotes breast carcinogenesis. *J Clin Invest*, **126**(6), 2205-2220 (2016).

Wang, T., Chen, K., Zeng, X., Yang, J., Wu, Y., Shi, X., Qin, B., Zeng, L., Esteban, M.A., Pan, G., Pei, D. The histone demethylases Jhdm1a/1b enhance somatic cell reprogramming in a vitamin-C-dependent manner. *Cell stem cell* **9**, 575-587 (2011).

Wang, Z., Song, J., Milne, T. A., Wang, G. G., Li, H., Allis, C. D., & Patel, D. J. Pro isomerization in MLL1 PHD3-bromo cassette connects H3K4me readout to CyP33 and HDAC-mediated repression. *Cell.* **141**:1183–1194 (2010)

Wang, Z., Zang, C., Rosenfeld, J. A., Schones, D. E., Barski, A., Cuddapah, S., Cui, K., Roh, T. Y., Peng, W., Zhang, M. Q., & Zhao, K.. Combinatorial patterns of histone acetylations and methylations in the human genome. *Nature genetics*, **40**(7), 897–903 (2008).

Wen, H., Li, J., Song, T., Lu, M., Kan, P. Y., Lee, M. G., Sha, B., & Shi, X. Recognition of histone H3K4 trimethylation by the plant homeodomain of PHF2 modulates histone demethylation. *J Biol Chem*, **285**(13), 9322-9326 (2010)

Wong, P. P., Miranda, F., Chan, K. V., Berlato, C., Hurst, H. C., & Scibetta, A. G. Histone demethylase KDM5B collaborates with TFAP2C and Myc to repress the cell cycle inhibitor p21(cip) (CDKN1A). *Molecular and cellular biology*, **32**(9), 1633–1644 (2012).

Wong, S. J., Gearhart, M. D., Taylor, A. B., Nanyes, D. R., Ha, D. J., Robinson, A. K., Artigas, J. A., Lee, O. J., Demeler, B., Hart, P. J., Bardwell, V. J., & Kim, C. A. KDM2B recruitment of the Polycomb group complex, PRC1.1, requires cooperation between PCGF1 and BCORL1. *Structure.* **24** (10): 1795–1801 (2016).

Wu, J., Liu, S., Liu, G., Dombkowski, A., Abrams, J., Martin-Trevino, R., Wicha, M. S., Ethier, S. P., & Yang, Z. Q. Identification and functional analysis of 9p24 amplified genes in human breast cancer. *Oncogene*, **31**(3), 333-341(2012)

Wu, R., Wang, Z., Zhang, H., Gan, H., & Zhang, Z.. H3K9me3 demethylase Kdm4d facilitates the formation of pre-initiative complex and regulates DNA replication. *Nucleic Acids Res*, **45**(1), 169-180 (2017)

Wu, X., Johansen, J. V. & Helin, K. Fbxl10/Kdm2b recruits polycomb repressive complex 1 to CpG islands and regulates H2A ubiquitylation. *Mol. cell* **49**, 1134-1146 (2013).

Wysocka, J., Swigut, T., Xiao, H., Milne, T.A., Kwon, S.Y., Landry, J., Kauer, M., Tackett, A.J., Chait, B.T., Badenhorst, P., Wu, C., Allis, C.D. A PHD finger of NURF couples histone H3 lysine 4 trimethylation with chromatin remodelling. *Nature* **442,** 86–90 (2006).

Xiang, Y., Zhu, Z., Han, G., Lin, H., Xu, L., & Chen, C. D. JMJD3 is a histone H3K27 demethylase. *Cell Res*, **17**(10), 850-857 (2007a)

Xiang, Y., Zhu, Z., Han, G., Ye, X., Xu, B., Peng, Z., Ma, Y., Yu, Y., Lin, H., Chen, A. P., & Chen, C. D. JARID1B is a histone H3 lysine 4 demethylase up-regulated in prostate cancer. Proc *Natl Acad Sci U S A*, **104**(49), 19226-19231 (2007b)

Xu, C., Liu, K., Lei, M., Yang, A., Li, Y., Hughes, T.R., Min, J. DNA Sequence Recognition of Human CXXC Domains and Their Structural Determinants. *Structure* **26**, 85-95 e83 (2018a).

Xu, J., & Andreassi, M. Reversible histone methylation regulates brain gene expression and behavior. *Horm Behav*, **59**(3), 383-392 (2011).

Xu, J., & Kidder, B. L. H4K20me3 co-localizes with activating histone modifications at transcriptionally dynamic regions in embryonic stem cells. *BMC Genomics*, **19**, 514 (2018b).

Xu, X., Hoang, S., Mayo, M.W., Bekiranov, S. Application of machine learning methods to histone methylation ChIP-Seq data reveals H4R3me2 globally represses gene expression. *BMC Bioinformatics.* 11:396 (2010)

Yamane, K., Tateishi, K., Klose, R. J., Fang, J., Fabrizio, L. A., Erdjument-Bromage, H., Taylor-Papadimitriou, J., Tempst, P., & Zhang, Y. PLU-1 is an H3K4 demethylase involved in transcriptional repression and breast cancer cell proliferation. *Mol Cell*, **25**(6), 801-812 (2007)

Yamane, K., Toumazou, C., Tsukada, Y., Erdjument-Bromage, H., Tempst, P., Wong, J., Zhang, Y. JHDM2A, a JmjC-containing H3K9 demethylase, facilitates transcription activation by androgen receptor. *Cell* **125**, 483–495(2006)

Yang, M., Gocke, C.B., Luo, X., Borek, D., Tomchick, D.R., Machius, M., Otwinowski, Z., Yu, H. Structural basis for CoREST-dependent demethylation of nucleosomes by the human LSD1 histone demethylase. *Mol. Cell.* **23**:377–387 (2006)

Yap, D. B., Walker, D. C., Prentice, L. M., McKinney, S., Turashvili, G., Mooslehner-Allen, K., de Algara, T. R., Fee, J., de Tassigny, X., Colledge, W. H., & Aparicio, S. Mll5 is required for normal spermatogenesis. *PLoS One*, **6**(11), e27127 (2011).

Yasui, T., Hirose, J., Tsutsumi, S., Nakamura, K., Aburatani, H., & Tanaka, S. Epigenetic regulation of osteoclast differentiation: possible involvement of Jmjd3 in the histone demethylation of Nfatc1. *J Bone Miner Res*, **26**(11), 2665-2671 (2011)

Yu, X., Wang, J., Wu, J., Shi, Y. A systematic study of the cellular metabolic regulation of Jhdm1b in tumor cells. *Mol Biosyst.* **11** (7): 1867-75 (2015).

Zacharopoulou, N., Tsapara, A., Kallergi, G., Schmid, E., Alkahtani, S., Alarifi, S., Tsichlis, P.N., Kampranis, S.C., Stournaras, C. The Epigenetic Factor KDM2B Regulates EMT and Small Gtpases in Colon Tumor Cells. *Cell Physiol Biochem.* **47** (1):368-377 (2018a)

Zacharopoulou, N., Tsapara, A., Kallergi, G., Schmid, E., Tsichlis, P.N., Kampranis, S.C., Stournaras, C. The epigenetic factor KDM2B regulates cell adhesion, small rho GTPases, actin cytoskeleton and migration in prostate cancer cells. *Biochem Biophys Acta.* **1865** (4):587-597 (2018b)

Zeng, J., Ge, Z., Wang, L., Li, Q., Wang, N., Björkholm, M., Jia, J., Xu, D. The histone demethylase RBP2 Is overexpressed in gastric cancer and its inhibition triggers senescence of cancer cells. *Gastroenterology* **138**(3):981-92 (2010)

Zeng, L., Zhang, Q., Li, S., Plotnikov, A.N., Walsh, M.J. and Zhou, M.M. Mechanism and regulation of acetylated histone binding by the tandem PHD finger of DPF3b. *Nature* **466**, 258–262 (2010)

Zhang, Y., Lv, J., Liu, H., Zhu, J., Su, J., Wu, Q., Qi, Y., Wang, F., & Li, X. HHMD: the human histone modification database. *Nucleic acids research*, **38**: D149–D154 (2010)

Zhao, Y., & Garcia, B. A. Comprehensive Catalog of Currently Documented Histone Modifications. *Cold Spring Harb Perspect Biol,* **7**(9), a025064. (2015)

Zhou, J.C., Blackledge, N. P., Farcas, A. M., Klose, R. J. Recognition of CpG island chromatin by KDM2A requires direct and specific interaction with linker DNA. *Mol Cell Biol.* **32** (2): 479-89 (2012)

Zhou, Z., Yang, X., He, J., Liu, J., Wu, F., Yu, S., Liu, Y., Lin, R., Liu, H., Cui, Y., Zhou, C., Wang, X., Wu, J., Cao, S., Guo, L., Lin, L., Wang, T., Peng, X., Qiang, B., Hutchins, A.P., Pei, D., Chen, J. Kdm2b Regulates Somatic Reprogramming through Variant PRC1 Complex-Dependent Function. *Cell Rep.* **21** (8): 2160-2170 (2017)

Zoabi, M., Nadar-Ponniah, P. T., Khoury-Haddad, H., Usaj, M., Budowski-Tal, I., Haran, T., Henn, A., Mandel-Gutfreund, Y., & Ayoub, N. RNA-dependent chromatin localization of KDM4D lysine demethylase promotes H3K9me3 demethylation. *Nucleic Acids Res*, **42**(21), 13026-13038 (2014)

Chapter 6

Appendices

Appendix 1

Table 1: Chemicals

Name	Manufacturer	Cat. No
Acetone	Merck	320110-1L
Acrylamide:Bisacrylamide 37.5:1	AppliChem	A0857-0500
Agar	Scharlau	07-004-500
Agarose	Invitrogen	15510-019
Ammonium persulfate	AppliChem	A1142.0250
Ampicillin	Merck	A1593-25G
β-Mercaptoethanol	Merck	M6250-10ML
Bovine Serum Albumin	Roche	3117332001
Bromophenol Blue	Merck	B0176
BugBuster 10x	Novagen	70921
Calcium Chloride	Merck	C-3881
Chloramphenicol	Merck	C-0378
DC Protein Assay Kit	Bio-Rad	500-0113-5
DL-Dithiothreitol	Merck	D9779
DMEM medium	Fisher Scientific	11965092
DNA ladder	Jena Bioscience	M103L
ECL Western Blotting Kit	Fisher Scientific	32106
Ethanol Absolute	Fisher Scientific	E10650DF17
Ethylenediaminetetraacetic acid	Merck	E9884-1KG
Fetal Bovine Serum	Merck	F0615
GelRed®	Biotium	41009 - 41010
Glacial Acetic Acid	Merck	1.00063-2511
Glycerol	Merck	G-5516
Glycine	AppliChem	A1067.1000
Guanidine Hydrochloride	AppliChem	A-1499.1000
Hypercassette 18x24cm	Ameshram	240195, RPN1642
Imidazole	Merck	I2399
IPTG	AppliChem	A1008.0025
Kanamycin Sulfate	AppliChem	A1493.0025
Lysozyme	Fluka	62971
Methanol	Merck	18316-4
Nickel (II) Chloride	Merck	339350-50G
Ni-NTA Agarose Resin	Qiagen	1018244
Penicillin-Streptomycin	Merck	P4333-100ML
Phenylmethyl Sulfonyl Floride	Merck	P7626-5G
Potassium Chloride	Merck	1.04936-1000
Potassium Phosphate Dibasic	Merck	P3786-1KG
Potassium Phosphate Monobasic	Merck	P0662-1KG
Protein marker	Fermentas	MWP03
Protein marker	MyBiosource	MBS355493

Puromycin	Merck	58-58-2
PVDF Transfer membrane	ThermoFischer	88520
RPMI 1640 medium	ThermoFischer	61870-036
Sodium Chloride	AppliChem	A1149.1000
Sodium Dodecyl Sulfate	CalbioChem	428015
Sodium Hydroxide	Merck	1.06498-1000
TEMED	AppliChem	A1148.0025
Terrific Broth	Invitrogen	22711-022
Tris Base	AppliChem	A1086.1000
Tryptone	AppliChem	A1553.500
Yeast Extract	AppliChem	A1552-1000

Table 2: Enzymes

Name	5'-Restriction Sequence-3'	Manufacturer	Cat. No
AgeI-HF	A/CCGGT	New England Labs	R3552
AsiSI	GCGAT/CGC	New England Labs	R0630
BamHI-HF	G/GATCC	New England Labs	R3136
BglII	A/GATCT	New England Labs	R0144
EcoRI-HF	G/AATTC	New England Labs	R3101
HindIII-HF	A/AGCCT	New England Labs	R3104
MfeI	C/AATTG	New England Labs	R0589
Nb. BsmI	NG/CATTC	New England Labs	R0706
NotI-HF	G/CGGCCGC	New England Labs	R3189
SalI	G/TCGAC	New England Labs	R0138
XhoI	C/TCGAG	New England Labs	R0146
USER enzyme	Uracil Excision	New England Labs	M5505
NEB Buffers	-	New England Labs	B7001-4
Deoxynucleotides (dNTPs)	-	New England Labs	N0447
MyTaq Polymerase	-	New England Labs	M0267
Phusion-HF Polymerase	-	New England Labs	M0530
T4 Ligase	-	New England Labs	M0202
T4 Polynucleotide Kinase	-	New England Labs	M0201
Kapa HF U+ PCR Kit	-	Kapa/Roche	KK2801
pCRII-TOPO Cloning Kit	-	Invitrogen	451641

Table 3: Synthetic Oligopeptides

Histone/ modification	Position	Sequence (N→C)	N- term. modification
H2B	1-19	PDPAKSAPAPKKGSKKAVT	None
H2BK5ac	1-19	PDPA-K(ac)-SAPAPKKGSKKAVT	None
H2BK12ac	1-19	PDPAKSAPAPK-K(ac)-GSKKAVT	None
H2BK15ac	1-19	PDPAKSAPAPKKGS-K(ac)-KAVT	None
H3 Unmodified	1-11	ARTKQTARKST	None
H3K4me3	1-11	ART-K(me3)-QTARKST	None
H3K27	22-32	TKAARKSAPST	Acetyl Group

H3K27me3	22-32	TKAAR-K(me3)-SAPST	Acetyl Group
H3K36me2	30-40	PSTGGVKKPHR	Acetyl Group
H3K36me2	30-40	PSTGGV-K(me2)-KPHR	Acetyl Group
H4 Unmodified	15-25	AKRHRKVLRDN	Acetyl Group
H4 Unmodified	1-11	SGRGKGGKGLG	None
H4K20me1	15-25	AKRHR-K(me1)-VLRDN	Acetyl Group
H4K20me2	15-25	AKRHR-K(me2)-VLRDN	Acetyl Group
H4K20me3	15-25	AKRHR-K(me3)-VLRDN	Acetyl Group

Table 4: Antibodies

Name	Quatity	Manufacturer	Cat. No
Anti-V5 HRP	-	Thermo Fischer	R961-25
Anti-rabbit IgG	2mL	Millipore	AP132P
Anti-mouse IgG	2mL	Millipore	AP124P
Anti-tubulin	200ug	Millipore	05-829
Anti-JHDM1B(KDM2B)	300ug	Millipore	09-864
Anti-6xHis tag	1mg	Thermo Fisher	MA1-21315

Table 5: Machinery

Equipment	Model	Manufacturer
Centrifuge	KUBOTA 5800	KUBOTA
Centrifuge	Microfuge- Lite	Beckman
Developing Film	Super RX-N	Fuji
Film Processor	Curix 60	Agfa
Freezer	Culus-991	Thermo
Gauger	Mini 900	Thermo
Heatblock	Multi-Blok Heater	Lab-Line
Incubator	Excella E24	Eppendorf
Microcalorimeter	VP-ITC	MicroCal, LLC
Microplate reader	Victor X5	Perkin- Elmer
PCR	PCR TC312	Techne
Power Unit	Power Pack™ Basic (SDS)	Bio-Rad
Power Unit	Power Supply 1061 (Agarose)	Life Technologies
Sonicator	Vibra-Cell	Sonics
Spectrometer	NanoDrop	Thermo
Spectrophotometer	Fluoromax 2	SPEX
Microscope	DM IRE 2	Leica
Stirrer	GFL 3005	GFL
Waterbath	Medingen B16 E11	Medingen

Table 6. List of primers & oligonucleotides

	Name	5'- Sequence- 3'	Tm (˚C)	PCR Product (bp)
1	mKDM2B(R585A)	aggcgccggacgGCatgccgcaagtgcga	48,2/ 49,1	540
2	mKDM2B(K608A)	cacttttgcaaggacatgaagGCgtttggaggtcctgggc	50,6/ 50,4	480
3	mKDM2B(K616A)	gtcctgggcgcatgGCgcagagctgcatcatg	46,3/ 43,3	460
4	mKDM2B(F654A)	gaagaggaagaaggcaagGCtaacctcatgctcatggaa	46,9/ 47,2	340
5	T7 Reverse	tagttattgctcagcggtg	48,3	
6	EGFP F	AAGCTTatggtgagcaagggcgaggag	59,5	
7	EGFP R	ACCGGTagctcgagatctgagtccggactt	59,3	750
8	mRFP F	AAGCTTatggcctcctccgaggacg	58,1	
9	mRFP R	ACCGGTggcgccggtggagtgg	56	687
10	mKDM2B(K616A) USER F	ATGGCGCAGAGCUgcatcatgcggcagtgca	59,7	
11	mKDM2B(K616A) USER R	AGCTCTGCGCCAUgcgcccaggacctccaaa	58,2	*9105
12	mKDM2A USER F	CGTGCGAUtcaggagccaggcggagaa	58	
13	mKDM2A USER R	CACGCGAUtttccgcttcttctgggctttg	57,6	360
14	mH4(1-18) D	GATCCtcgggtcgcggcaagggaggaaaaggcctgggcaaaggcggcgctaagcgccacA		
15	mH4(1-18) C	AGCTTgtggcgcttagcgccgcctttgcccaggccttttcctcccttgccgcgacccgaG	75,5	
16	mH4(17-34) D	GATCCcgccaccgtaaggttctccgcgataacatccagggcatcaccaagcccgccatcA		
17	mH4(17-34) C	AGCTTgatggcgggcttggtgatgccctggatgttatcgcggagaaccttacggtggcgG	72,5	
18	mH4(33-50) D	GATCCgccatccgccgcctggcccggcgcgggggagtgaagcgcatctccggcctcatcA		
19	mH4(33-50) C	AGCTTgatgaggccggagatgcgcttcactcccccgcgccgggccaggcggcggatggcG	78,5	
20	mH4(49-69) D	GATCCctcatctacgaggagacccgcggtgtgctgaaggtgttcctggagaacgtgatccgcgacA		
21	mH4(49-69) C	AGCTTgtcgcggatcacgttctccaggaacaccttcagcacaccgcgggtctcctcgtagatgagG	73,3	
22	CpG6 D	taccCGttggacCGgactaaCGctagtaccCGttggacCGgactaaCGctag		
23	CpG6 C	ctagCGttagtcCGgtccaaCGggtactagCGttagtcCGgtccaaCGggta	70,6	
24	GpC6 D	taGCccttggagGCcactaaGCctagtaGCccttggagGCcactaaGCctag		
25	GpC6 C	ctagGCttagtgGCctccaaggGCtactagGCttagtgGCctccaaggGCta	70,6	
26	CpG2 D	gggtactagCGttagtcCGgtccaac		
27	CpG2 C	gttggacCGgactaaCGctagtaccc	64,3	
28	CpG2short D	tagCGttagtcCGgtc		
29	CpG2short C	gacCGgactaaCGcta	44,4	
30	ORI2.5 D	ctttCGCGttgcatttctg		
31	ORI2.5 R	cagaaatgcaaCGCGaaag	52,6	

Abbreviations:
F: Forward primer,
R: Reverse primer,
D: Direct strand,
C: Complementary strand.

***USER mutagenesis regenerates the whole construct**

Initial nucleotides in upper case indicate the point mutation being made (1-4), the restriction enzyme used for cloning (5-21), or the CxxC substrate CpG sequence (22-31).

Appendix 2

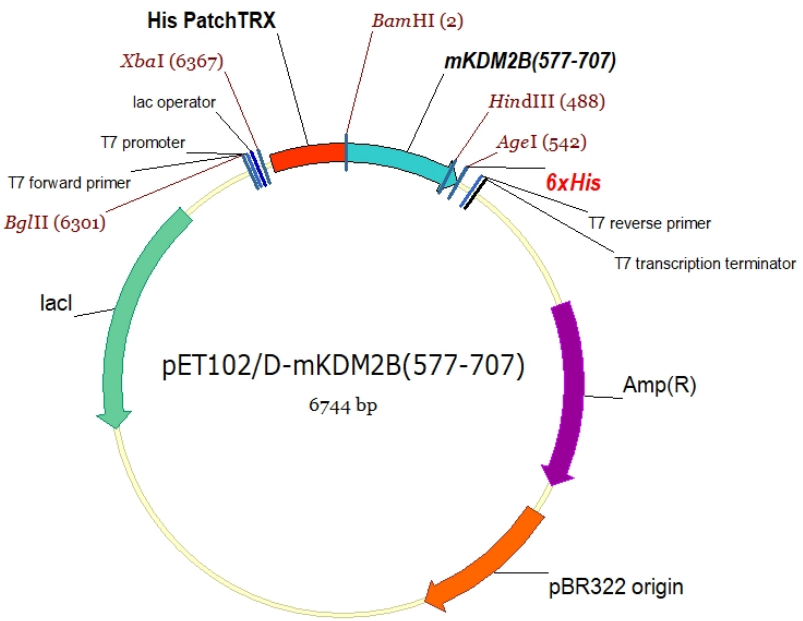
His PatchTRX
BamHI (2)
XbaI (6367)
mKDM2B(577-707)
lac operator
HindIII (488)
T7 promoter
AgeI (542)
T7 forward primer
6xHis
BglII (6301)
T7 reverse primer
T7 transcription terminator
lacI
pET102/D-mKDM2B(577-707)
6744 bp
Amp(R)
pBR322 origin

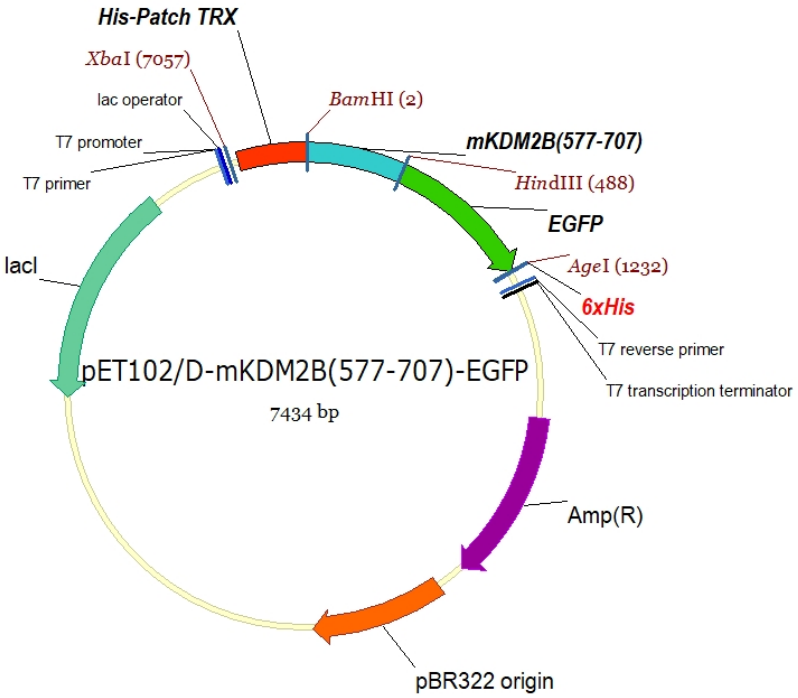
His-Patch TRX
XbaI (7057)
lac operator
BamHI (2)
T7 promoter
mKDM2B(577-707)
T7 primer
HindIII (488)
EGFP
lacI
AgeI (1232)
6xHis
T7 reverse primer
pET102/D-mKDM2B(577-707)-EGFP
T7 transcription terminator
7434 bp
Amp(R)
pBR322 origin

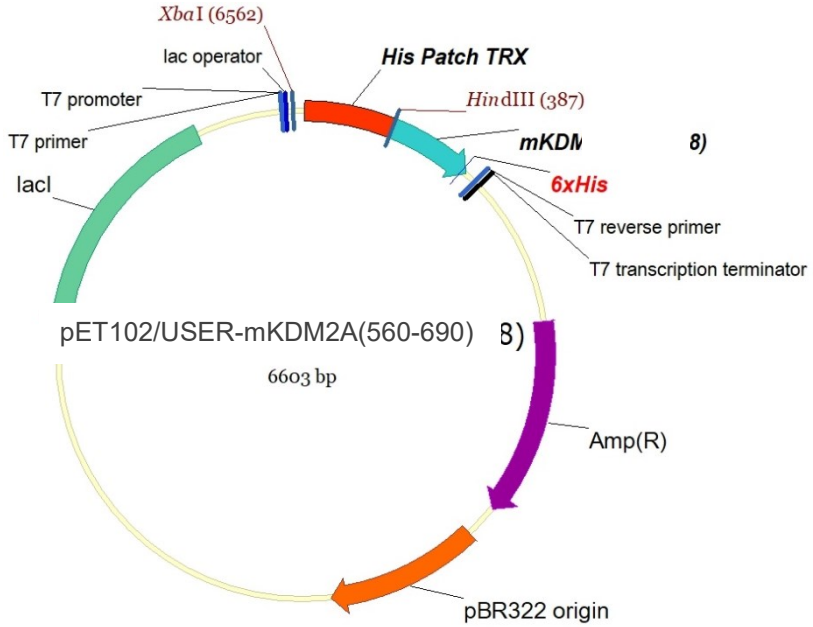
XbaI (6562)
lac operator
His Patch TRX
T7 promoter
HindIII (387)
T7 primer
mKDM 8)
6xHis
lacI
T7 reverse primer
T7 transcription terminator
pET102/USER-mKDM2A(560-690) 8)
6603 bp
Amp(R)
pBR322 origin

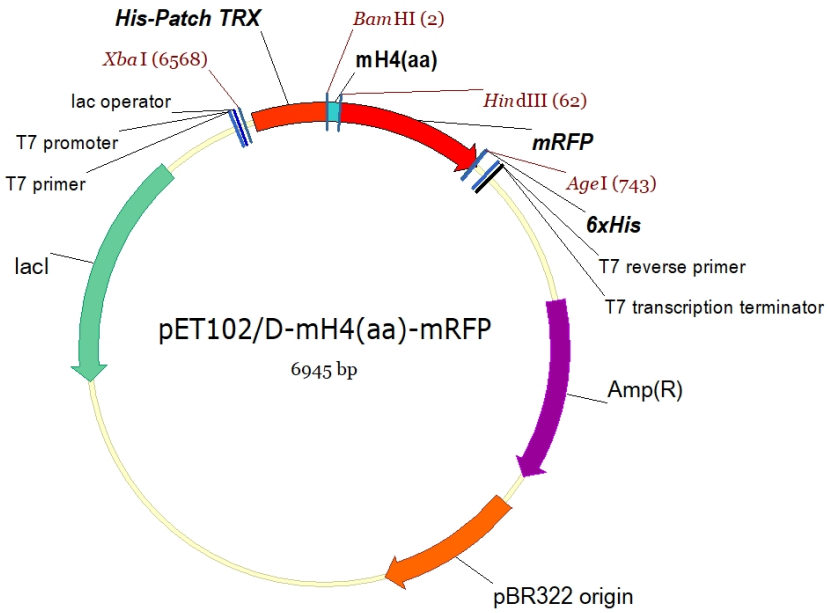
His-Patch TRX
BamHI (2)
XbaI (6568)
mH4(aa)
lac operator
HindIII (62)
T7 promoter
mRFP
T7 primer
AgeI (743)
6xHis
lacI
T7 reverse primer
T7 transcription terminator
pET102/D-mH4(aa)-mRFP
6945 bp
Amp(R)
pBR322 origin

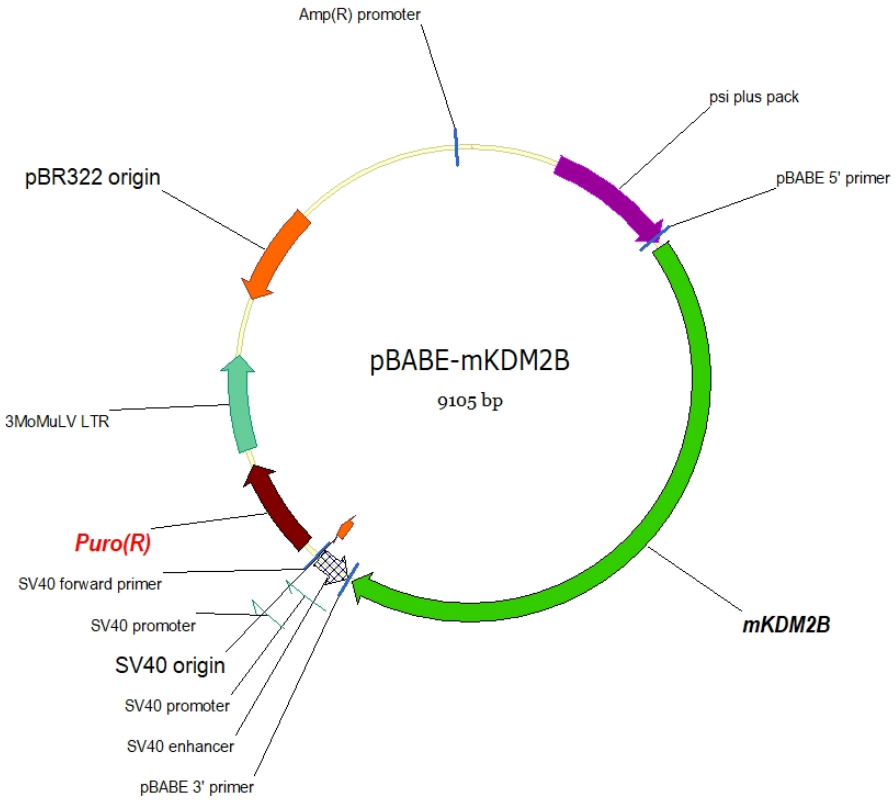
Amp(R) promoter
psi plus pack
pBABE 5' primer
pBR322 origin
pBABE-mKDM2B
9105 bp
3MoMuLV LTR
Puro(R)
SV40 forward primer
SV40 promoter
SV40 origin
SV40 promoter
SV40 enhancer
pBABE 3' primer
mKDM2B

Appendix 3

Amino acid sequence of TRX-mKDM2B$_{577-707}$

1 MGSDKIIHLTDDSFDTDVLKADGAILVDFWAHWCGPCKMIAPILDEIADE
51 YQGKLTVAKLNIDHNPGTAPKYGIRGIPTLLLFKNGEVAATKVGALSKGQ
101 LKEFLDANLAGSGSGDDDDKLGIDPFTMEAEKDSGRRLRAGARRRRTRCR
151 KCEACLRTECGECHFCKDMKKFGGPGRMKQSCIMRQCIAPVLPHTAVCLV
201 CGEAGKEDTVEEEEGKFNLMLMECSICNEIIHPGCLKIKESEGVVNDELP
251 NCWECPKCNHAGKTGKQKRGKGELKLEGKPIPNPLLGLDSTRTGHHHHHH

Amino acid sequence of TRX-mKDM2B$_{577-707}$(R585A)

1 MGSDKIIHLTDDSFDTDVLKADGAILVDFWAHWCGPCKMIAPILDEIADE
51 YQGKLTVAKLNIDHNPGTAPKYGIRGIPTLLLFKNGEVAATKVGALSKGQ
101 LKEFLDANLAGSGSGDDDDKLGIDPFTMEAEKDSGRRLRAGARRRRTACR
151 KCEACLRTECGECHFCKDMKKFGGPGRMKQSCIMRQCIAPVLPHTAVCLV
201 CGEAGKEDTVEEEEGKFNLMLMECSICNEIIHPGCLKIKESEGVVNDELP
251 NCWECPKCNHAGKTGKQKRGKGELKLEGKPIPNPLLGLDSTRTGHHHHHH

Amino acid sequence of TRX-mKDM2B$_{577-707}$(K608A)

1 MGSDKIIHLTDDSFDTDVLKADGAILVDFWAHWCGPCKMIAPILDEIADE
51 YQGKLTVAKLNIDHNPGTAPKYGIRGIPTLLLFKNGEVAATKVGALSKGQ
101 LKEFLDANLAGSGSGDDDDKLGIDPFTMEAEKDSGRRLRAGARRRRTRCR
151 KCEACLRTECGECHFCKDMKAFGGPGRMKQSCIMRQCIAPVLPHTAVCLV
201 CGEAGKEDTVEEEEGKFNLMLMECSICNEIIHPGCLKIKESEGVVNDELP
251 NCWECPKCNHAGKTGKQKRGKGELKLEGKPIPNPLLGLDSTRTGHHHHHH

Amino acid sequence of TRX-mKDM2B$_{577-707}$(K616A)

1 MGSDKIIHLTDDSFDTDVLKADGAILVDFWAHWCGPCKMIAPILDEIADE
51 YQGKLTVAKLNIDHNPGTAPKYGIRGIPTLLLFKNGEVAATKVGALSKGQ
101 LKEFLDANLAGSGSGDDDDKLGIDPFTMEAEKDSGRRLRAGARRRRTACR
151 KCEACLRTECGECHFCKDMKAFGGPGRMAQSCIMRQCIAPVLPHTAVCLV
201 CGEAGKEDTVEEEEGKANLMLMECSICNEIIHPGCLKIKESEGVVNDELP
251 NCWECPKCNHAGKTGKQKRGKGELKLEGKPIPNPLLGLDSTRTGHHHHHH

Amino acid sequence of TRX-mKDM2B$_{577-707}$(F654A)

1 MGSDKIIHLTDDSFDTDVLKADGAILVDFWAHWCGPCKMIAPILDEIADE
51 YQGKLTVAKLNIDHNPGTAPKYGIRGIPTLLLFKNGEVAATKVGALSKGQ
101 LKEFLDANLAGSGSGDDDDKLGIDPFTMEAEKDSGRRLRAGARRRRTRCR
151 KCEACLRTECGECHFCKDMKKFGGPGRMKQSCIMRQCIAPVLPHTAVCLV
201 CGEAGKEDTVEEEEGKANLMLMECSICNEIIHPGCLKIKESEGVVNDELP
251 NCWECPKCNHAGKTGKQKRGKGELKLEGKPIPNPLLGLDSTRTGHHHHHH

Amino acid sequence of TRX-mKDM2B$_{577-707}$ (R585A/K616A)

1 MGSDKIIHLTDDSFDTDVLKADGAILVDFWAHWCGPCKMIAPILDEIADE
51 YQGKLTVAKLNIDHNPGTAPKYGIRGIPTLLLFKNGEVAATKVGALSKGQ
101 LKEFLDANLAGSGSGDDDDKLGIDPFTMEAEKDSGRRLRAGARRRRTACR
151 KCEACLRTECGECHFCKDMKKFGGPGRMAQSCIMRQCIAPVLPHTAVCLV
201 CGEAGKEDTVEEEEGKFNLMLMECSICNEIIHPGCLKIKESEGVVNDELP
251 NCWECPKCNHAGKTGKQKRGKGELKLEGKPIPNPLLGLDSTRTGHHHHHH

Amino acid sequence of TRX-mKDM2B$_{577-707}$-EGFP

1 MGSDKIIHLTDDSFDTDVLKADGAILVDFWAHWCGPCKMIAPILDEIADE
51 YQGKLTVAKLNIDHNPGTAPKYGIRGIPTLLLFKNGEVAATKVGALSKGQ
101 LKEFLDANLAGSGSGDDDDKLGIDPFTMEAEKDSGRRLRAGARRRRTRCR
151 KCEACLRTECGECHFCKDMKKFGGPGRMKQSCIMRQCIAPVLPHTAVCLV
201 CGEAGKEDTVEEEEGKFNLMLMECSICNEIIHPGCLKIKESEGVVNDELP
251 NCWECPKCNHAGKTGKQKRGKGELKLMVSKGEELFTGVVPILVELDGDVN
301 GHKFSVSGEGEGDATYGKLTLKFICTTGKLPVPWPTLVTTLTYGVQCFSR
351 YPDHMKQHDFFKSAMPEGYVQERTIFFKDDGNYKTRAEVKFEGDTLVNRI
401 ELKGIDFKEDGNILGHKLEYNYNSHNVYIMADKQKNGIKVNFKIRHNIED
451 GSVQLADHYQQNTPIGDGPVLLPDNHYLSTQSALSKDPNEKRDHMVLLEF
501 VTAAGITLGMDELYKSGLRSRATGHHHHHH

Amino acid sequence of TRX-mKDM2B$_{577-707}$(K616A)-EGFP

1 MGSDKIIHLTDDSFDTDVLKADGAILVDFWAHWCGPCKMIAPILDEIADE
51 YQGKLTVAKLNIDHNPGTAPKYGIRGIPTLLLFKNGEVAATKVGALSKGQ
101 LKEFLDANLAGSGSGDDDDKLGIDPFTMEAEKDSGRRLRAGARRRRTRCR
151 KCEACLRTECGECHFCKDMKKFGGPGRMAQSCIMRQCIAPVLPHTAVCLV
201 CGEAGKEDTVEEEEGKFNLMLMECSICNEIIHPGCLKIKESEGVVNDELP
251 NCWECPKCNHAGKTGKQKRGKGELKLMVSKGEELFTGVVPILVELDGDVN
301 GHKFSVSGEGEGDATYGKLTLKFICTTGKLPVPWPTLVTTLTYGVQCFSR
351 YPDHMKQHDFFKSAMPEGYVQERTIFFKDDGNYKTRAEVKFEGDTLVNRI
401 ELKGIDFKEDGNILGHKLEYNYNSHNVYIMADKQKNGIKVNFKIRHNIED
451 GSVQLADHYQQNTPIGDGPVLLPDNHYLSTQSALSKDPNEKRDHMVLLEF
501 VTAAGITLGMDELYKSGLRSRATGHHHHHH

Amino acid sequence of TRX-mH4(aa)-mRFP

1 MGSDKIIHLTDDSFDTDVLKADGAILVDFWAHWCGPCKMIAPILDEIADE
51 YQGKLTVAKLNIDHNPGTAPKYGIRGIPTLLLFKNGEVAATKVGALSKGQ
101 LKEFLDANLAGSGS-----#-----KLMASSEDVIKEFMRFKV
151* RMEGSVNGHEFEIEGEGEGRPYEGTQTAKLKVTKGGPLPFAWDILSPQFQ
201* YGSKAYVKHPADIPDYLKLSFPEGFKWERVMNFEDGGVVTVTQDSSLQDG
251* EFIYKVKLRGTNFPSDGPVMQKKTMGWEASTERMYPEDGALKGEIKMRLK
301* LKDGGHYDAEVKTTYMAKKPVQLPGAYKTDIKLDITSHNEDYTIVEQYER
351* AEGRHSTGATGHHHHHH

\# mH4(1-18): SGRGKGGKGLGKGGAKRH
mH4(17-34): RHRKVLRDNIQGITKPAI
mH4(33-50): AIRRLARRGGVKRISGLI
mH4(49-69): LIYEETRGVLKVFLENVIRD

* (+2) for mH4(49-69)- mRFP

Amino acid sequence of TRX-mKDM2A$_{560-690}$

1 MGSDKIIHLTDDSFDTDVLKADGAILVDFWAHWCGPCKMIAPILDEIADE
51 YQGKLTVAKLNIDHNPGTAPKYGIRGIPTLLLFKNGEVAATKVGALSKGQ
101 LKEFLDANLAANACDSGARRRRVRCRKCKACVQGECGVCHYCRDMKKFGG
151 PGRMKQSCVLRQCLAPRLPHSVTCSLCGEVDQNEETQDFEKKLMECCICN
201 EIVHPGCLQMDGEGLLNEELPNCWECPKCYQEDSSDKAQKRKIACILHHHHHH

Amino acid sequence of mKDM2B(K616A)

1 MEAEKDSGRRLRAIDRQRYDENEDLSDVEEIVSVRGFSLEEKLRSQLYQG
51 DFVHAMEGKDFNYEYVQREALRVPLVFRDKDGLGIKMPDPDFTVRDVKLL
101 VGSRRLVDVMDVNTQKGTEMSMSQFVRYYETPEAQRDKLYNVISLEFSHT
151 KLEHLVKRPTVVDLVDWVDNMWPQHLKEKQTEATNALAEMKYPKVKKYCL
201 MSVKGCFTDFHIDFGGTSVWYHVFRGGKIFWLIPPTLHNLALYEEWVLSG
251 KQSDIFLGDRVERCQRIELKQGYTFFIPSGWIHAVYTPVDSLVFGGNILH
301 SFNVPMQLRIYEIEDRTRVQPKFRYPFYYEMCWYVLERYVYCVTQRSYLT
351 QEYQRELMLIDAPRKTSVDGFSSDSWLDMEEESCEQQPQEEEEEEEDKEE
401 EGDGADKTPKPPTDDPTSPTSTPPEDQDSTGKKPKAPAIRFLKRTLSNES
451 EESVKSTSMPMDDPKTPTGSPATEVSTKWTHLTEFELKGLKALVEKLESL
501 PENKKCVPEGIEDPQALLEGVKNVLKEHVDDDPTLAITGVPVVSWPKKTA
551 KNRVVGRPKGKLGPASAVKLAANRTTAGARRRRTRCRKCEACLRTECGEC
601 HFCKDMKKFGGPGRMAQSCIMRQCIAPVLPHTAVCLVCGEAGKEDTVEEE
651 EGKFNLMLMECSICNEIIHPGCLKIKESEGVVNDELPNCWECPKCNHAGK
701 TGKQKRGPGFKYASNLPGSLLKEQKMNRDNKEGQEPAKRRSECEEAPRRR
751 SDEHPKKVPADGILRRKSDDVHLRRKRKYEKPQELSGRKRASSLQTSPGS
801 SSHLSPRPPLGSSLSPWWRSSLTYFQQQLKPGKEDKLFRKKRRSWKNAED
851 RLSLANKPLRRFKQEPEDDLPEAPPKTRESDQSRSSSPTAGPSTEGAEGP
901 EEKKKVKMRRKRRLVNKELSKELSKELNHEIQKTESTLAHESQQPIKSEP
951 ESENDEPKRPLSHCERPHRFSKGLNGTPRELRHSLGPGLRSPPRVMSRPP
1001 PSASPPKCIQMERHVIRPPPISPPPDSLPLDDGAAHVMHREVWMAVFSYL
1051 SHRDLCVCMRVCRTWNRWCCDKRLWTRIDLNRCKSITPLMLSGIIRRQPV
1101 SLDLSWTNISKKQLSWLINRLPGLRDLVLSGCSWIAVSALCSSSCPLLRT
1151 LDVQWVEGLKDAQMRDLLSPPTDNRPGQMDNRSKLRNIVELRLAGLDITD
1201 VSLRLIIRHMPLLSKLQLSYCNHINDQSINLLTAVGTTTRDSLTEVNLSD
1251 CNKVTDLCLSFFKRCGNICHIDLRYCKQVTKEGCEQFIAEMSVSVQFGQV
1301 EEKLLQKLS

Appendix 4

List and position of peptides in MODified™ Histone Peptide Array slide (Active Motif) Catalog Nos. 13001 & 13005. Peptides with position written in **bold** are acetylated at the N-terminus. The peptide array is spotted in duplicate on the left and right hand side of the slide.

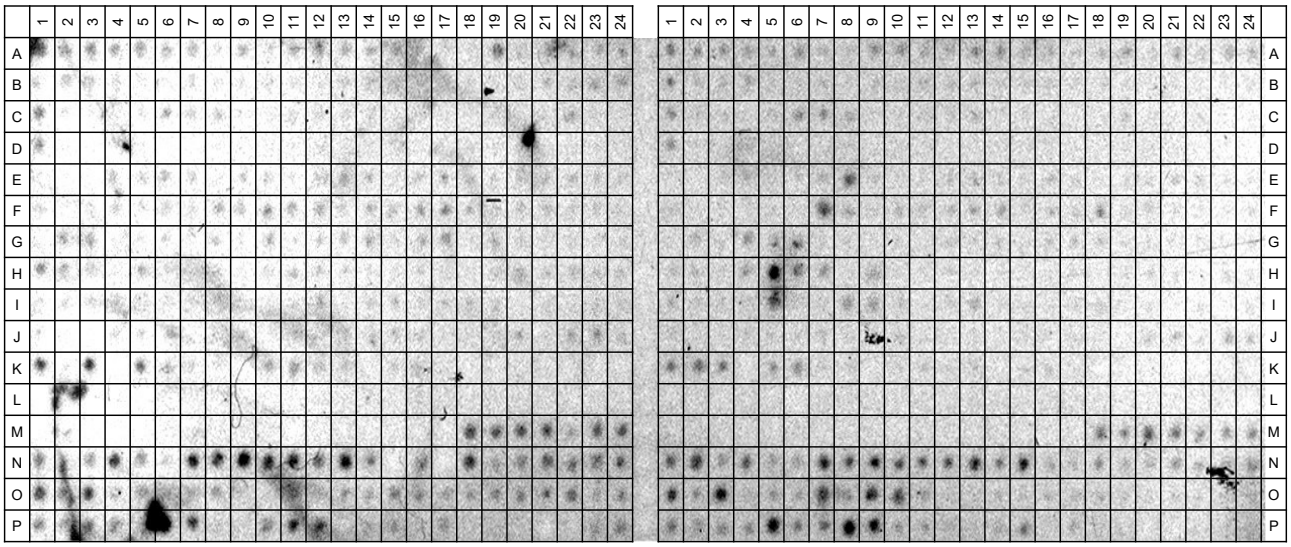

peptide location	*Peptide sequence*
A 1	A R T K Q T A R K S T G G K A P R K Q
A 2	A Rme2s T K Q T A R K S T G G K A P R K Q
A 3	A Rme2a T K Q T A R K S T G G K A P R K Q
A 4	A Cit T K Q T A R K S T G G K A P R K Q
A 5	A R pT K Q T A R K S T G G K A P R K Q
A 6	A R T Kme1 Q T A R K S T G G K A P R K Q
A 7	A R T Kme2 Q T A R K S T G G K A P R K Q
A 8	A R T Kme3 Q T A R K S T G G K A P R K Q
A 9	A R T Kac Q T A R K S T G G K A P R K Q
A10	A R T K Q T A Rme2s K S T G G K A P R K Q
A11	A R T K Q T A Rme2a K S T G G K A P R K Q
A12	A R T K Q T A Cit K S T G G K A P R K Q
A13	A R T K Q T A R Kme1 S T G G K A P R K Q
A14	A R T K Q T A R Kme2 S T G G K A P R K Q
A15	A R T K Q T A R Kme3 S T G G K A P R K Q
A16	A R T K Q T A R Kac S T G G K A P R K Q
A17	A R T K Q T A R K pS T G G K A P R K Q
A18	A R T K Q T A R K S pT G G K A P R K Q
A19	A R T K Q T A R K S T G G Kac A P R K Q
A20	A Rme2s pT K Q T A R K S T G G K A P R K Q
A21	A Rme2s T Kme1 Q T A R K S T G G K A P R K Q
A22	A Rme2s T Kme2 Q T A R K S T G G K A P R K Q
A23	A Rme2s T Kme3 Q T A R K S T G G K A P R K Q
A24	A Rme2s T Kac Q T A R K S T G G K A P R K Q
B 1	A Rme2a pT K Q T A R K S T G G K A P R K Q
B 2	A Rme2a T Kme1 Q T A R K S T G G K A P R K Q
B 3	A Rme2a T Kme2 Q T A R K S T G G K A P R K Q
B 4	A Rme2a T Kme3 Q T A R K S T G G K A P R K Q
B 5	A Rme2a T Kac Q T A R K S T G G K A P R K Q
B 6	A Cit pT K Q T A R K S T G G K A P R K Q
B 7	A Cit T Kme1 Q T A R K S T G G K A P R K Q
B 8	A Cit T Kme2 Q T A R K S T G G K A P R K Q
B 9	A Cit T Kme3 Q T A R K S T G G K A P R K Q
B10	A Cit T Kac Q T A R K S T G G K A P R K Q
B11	A R pT Kme1 Q T A R K S T G G K A P R K Q
B12	A R pT Kme2 Q T A R K S T G G K A P R K Q
B13	A R pT Kme3 Q T A R K S T G G K A P R K Q
B14	A R pT Kac Q T A R K S T G G K A P R K Q
B15	A Rme2s pT Kme1 Q T A R K S T G G K A P R K Q
B16	A Rme2s pT Kme2 Q T A R K S T G G K A P R K Q
B17	A Rme2s pT Kme3 Q T A R K S T G G K A P R K Q
B18	A Rme2s pT Kac Q T A R K S T G G K A P R K Q
B19	A Rme2a pT Kme1 Q T A R K S T G G K A P R K Q
B20	A Rme2a pT Kme2 Q T A R K S T G G K A P R K Q
B21	A Rme2a pT Kme3 Q T A R K S T G G K A P R K Q
B22	A Rme2a pT Kac Q T A R K S T G G K A P R K Q
B23	A R T K Q T A Rme2a Kme1 S T G G K A P R K Q
B24	A R T K Q T A Rme2a Kme2 S T G G K A P R K Q
C 1	A R T K Q T A Rme2a Kme3 S T G G K A P R K Q
C 2	A R T K Q T A Rme2a Kac S T G G K A P R K Q

Peptide location	*Peptide sequence*
I 1	A Rme2a T Kme2 Q T A Rme2a Kme1 S T G G K A P R K Q
I 2	A Rme2a T Kme3 Q T A Rme2a Kme1 S T G G K A P R K Q
I 3	A Rme2a T Kac Q T A Rme2a Kme1 S T G G K A P R K Q
I 4	A Rme2s T Kme1 Q T A Rme2a Kme2 S T G G K A P R K Q
I 5	A Rme2s T Kme2 Q T A Rme2a Kme2 S T G G K A P R K Q
I 6	A Rme2s T Kme3 Q T A Rme2a Kme2 S T G G K A P R K Q
I 7	A Rme2s T Kac Q T A Rme2a Kme2 S T G G K A P R K Q
I 8	A Rme2a T Kme1 Q T A Rme2a Kme2 S T G G K A P R K Q
I 9	A Rme2a T Kme2 Q T A Rme2a Kme2 S T G G K A P R K Q
I10	A Rme2a T Kme3 Q T A Rme2a Kme2 S T G G K A P R K Q
I11	A Rme2a T Kac Q T A Rme2a Kme2 S T G G K A P R K Q
I12	A Rme2s T Kme1 Q T A Rme2a Kme3 S T G G K A P R K Q
I13	A Rme2s T Kme2 Q T A Rme2a Kme3 S T G G K A P R K Q
I14	A Rme2s T Kme3 Q T A Rme2a Kme3 S T G G K A P R K Q
I15	A Rme2s T Kac Q T A Rme2a Kme3 S T G G K A P R K Q
I16	A Rme2a T Kme1 Q T A Rme2a Kme3 S T G G K A P R K Q
I17	A Rme2a T Kme2 Q T A Rme2a Kme3 S T G G K A P R K Q
I18	A Rme2a T Kme3 Q T A Rme2a Kme3 S T G G K A P R K Q
I19	A Rme2a T Kac Q T A Rme2a Kme3 S T G G K A P R K Q
I20	A Rme2s T Kme1 Q T A Rme2a Kac S T G G K A P R K Q
I21	A Rme2s T Kme2 Q T A Rme2a Kac S T G G K A P R K Q
I22	A Rme2s T Kme3 Q T A Rme2a Kac S T G G K A P R K Q
I23	A Rme2s T Kac Q T A Rme2a Kac S T G G K A P R K Q
I24	A Rme2a T Kme1 Q T A Rme2a Kac S T G G K A P R K Q
J 1	A Rme2a T Kme2 Q T A Rme2a Kac S T G G K A P R K Q
J 2	A Rme2a T Kme3 Q T A Rme2a Kac S T G G K A P R K Q
J 3	A Rme2a T Kac Q T A Rme2a Kac S T G G K A P R K Q
J 4	A R K S T G G K A P R K Q L A T K A A R
J 5	A R K S T G G Kac A P R K Q L A T K A A R
J 6	A R K pS T G G Kac A P R K Q L A T K A A R
J 7	A R K S pT G G Kac A P R K Q L A T K A A R
J 8	A R K S T G G K A P Rme2s K Q L A T K A A R
J 9	A R K S T G G K A P Rme2a K Q L A T K A A R
J10	A R K S T G G K A P Cit K Q L A T K A A R
J11	A R K S T G G K A P R Kac Q L A T K A A R
J12	A R K S T G G Kac A P Rme2s K Q L A T K A A R
J13	A R K S T G G Kac A P Rme2a K Q L A T K A A R
J14	A R K S T G G Kac A P R Kac Q L A T K A A R
J15	A R K S T G G K A P Rme2s Kac Q L A T K A A R
J16	A R K S T G G K A P Rme2a Kac Q L A T K A A R
J17	A R K S T G G K A P Cit Kac Q L A T K A A R
J18	A R K S T G G Kac A P Rme2s Kac Q L A T K A A R
J19	A R K S T G G Kac A P Rme2a Kac Q L A T K A A R
J20	P R K Q L A T K A A R K S A P A T G G
J21	P R K Q L A T K A A Rme2s K S A P A T G G
J22	P R K Q L A T K A A Rme2a K S A P A T G G
J23	P R K Q L A T K A A Cit K S A P A T G G
J24	P R K Q L A T K A A R Kme1 S A P A T G G
K 1	P R K Q L A T K A A R Kme2 S A P A T G G
K 2	P R K Q L A T K A A R Kme3 S A P A T G G

C 3 A R T K Q T A Rme2a K pS T G G K A P R K Q
C 4 A R T K Q T A Rme2a K S pT G G K A P R K Q
C 5 A R T K Q T A Rme2a Kme1 S T G G K A P R K Q
C 6 A R T K Q T A Rme2a Kme2 S T G G K A P R K Q
C 7 A R T K Q T A Rme2a Kme3 S T G G K A P R K Q
C 8 A R T K Q T A Rme2a Kac S T G G K A P R K Q
C 9 A R T K Q T A Rme2a K pS T G G K A P R K Q
C10 A R T K Q T A Rme2a K S pT G G K A P R K Q
C11 A R T K Q T A Cit Kme1 S T G G K A P R K Q
C12 A R T K Q T A Cit Kme2 S T G G K A P R K Q
C13 A R T K Q T A Cit Kme3 S T G G K A P R K Q
C14 A R T K Q T A Cit Kac S T G G K A P R K Q
C15 A R T K Q T A Cit K pS T G G K A P R K Q
C16 A R T K Q T A Cit K S pT G G K A P R K Q
C17 A R T K Q T A R Kme1 pS T G G K A P R K Q
C18 A R T K Q T A R Kme1 S pT G G K A P R K Q
C19 A R T K Q T A R Kme1 S T G G Kac A P R K Q
C20 A R T K Q T A R Kme2 pS T G G K A P R K Q
C21 A R T K Q T A R Kme2 S pT G G K A P R K Q
C22 A R T K Q T A R Kme2 S T G G Kac A P R K Q
C23 A R T K Q T A R Kme3 pS T G G K A P R K Q
C24 A R T K Q T A R Kme3 S pT G G K A P R K Q
D 1 A R T K Q T A R Kme3 S T G G Kac A P R K Q
D 2 A R T K Q T A R Kac pS T G G K A P R K Q
D 3 A R T K Q T A R Kac S pT G G K A P R K Q
D 4 A R T K Q T A R Kac S T G G Kac A P R K Q
D 5 A R T K Q T A R K pS pT G G K A P R K Q
D 6 A R T K Q T A R K pS T G G Kac A P R K Q
D 7 A R T K Q T A R K S pT G G Kac A P R K Q
D 8 A R T K Q T A Rme2s Kme1 pS T G G K A P R K Q
D 9 A R T K Q T A Rme2s Kme2 pS T G G K A P R K Q
D10 A R T K Q T A Rme2s Kme3 pS T G G K A P R K Q
D11 A R T K Q T A Rme2s Kac pS T G G K A P R K Q
D12 A R T K Q T A Rme2s Kme1 S pT G G K A P R K Q
D13 A R T K Q T A Rme2s Kme2 S pT G G K A P R K Q
D14 A R T K Q T A Rme2s Kme3 S pT G G K A P R K Q
D15 A R T K Q T A Rme2s Kac S pT G G K A P R K Q
D16 A R T K Q T A Rme2a Kme1 pS T G G K A P R K Q
D17 A R T K Q T A Rme2a Kme2 pS T G G K A P R K Q
D18 A R T K Q T A Rme2a Kme3 pS T G G K A P R K Q
D19 A R T K Q T A Rme2a Kac pS T G G K A P R K Q
D20 A R T K Q T A Rme2a Kme1 S pT G G K A P R K Q
D21 A R T K Q T A Rme2a Kme2 S pT G G K A P R K Q
D22 A R T K Q T A Rme2a Kme3 S pT G G K A P R K Q
D23 A R T K Q T A Rme2a Kac S pT G G K A P R K Q
D24 A R T K Q T A Rme2a Kme1 pS pT G G K A P R K Q
E 1 A R T K Q T A Rme2a Kme2 pS pT G G K A P R K Q
E 2 A R T K Q T A Rme2a Kme3 pS pT G G K A P R K Q
E 3 A R T K Q T A Rme2a Kac pS pT G G K A P R K Q
E 4 A Rme2s T Kme1 Q T A Rme2s K S T G G K A P R K Q
E 5 A Rme2s T Kme2 Q T A Rme2s K S T G G K A P R K Q
E 6 A Rme2s T Kme3 Q T A Rme2s K S T G G K A P R K Q
E 7 A Rme2s T Kac Q T A Rme2s K S T G G K A P R K Q
E 8 A Rme2a T Kme1 Q T A Rme2a K S T G G K A P R K Q
E 9 A Rme2a T Kme2 Q T A Rme2a K S T G G K A P R K Q
E10 A Rme2a T Kme3 Q T A Rme2a K S T G G K A P R K Q
E11 A Rme2a T Kac Q T A Rme2a K S T G G K A P R K Q
E12 A Rme2s T Kme1 Q T A R Kme1 S T G G K A P R K Q
E13 A Rme2s T Kme2 Q T A R Kme1 S T G G K A P R K Q
E14 A Rme2s T Kme3 Q T A R Kme1 S T G G K A P R K Q
E15 A Rme2s T Kac Q T A R Kme1 S T G G K A P R K Q
E16 A Rme2a T Kme1 Q T A R Kme2 S T G G K A P R K Q
E17 A Rme2a T Kme2 Q T A R Kme2 S T G G K A P R K Q
E18 A Rme2a T Kme3 Q T A R Kme2 S T G G K A P R K Q
E19 A Rme2a T Kac Q T A R Kme2 S T G G K A P R K Q
E20 A Rme2s T Kme1 Q T A R Kme3 S T G G K A P R K Q
E21 A Rme2s T Kme2 Q T A R Kme3 S T G G K A P R K Q
E22 A Rme2s T Kme3 Q T A R Kme3 S T G G K A P R K Q
E23 A Rme2s T Kac Q T A R Kme3 S T G G K A P R K Q
E24 A Rme2a T Kme1 Q T A R Kac S T G G K A P R K Q
F 1 A Rme2a T Kme2 Q T A R Kac S T G G K A P R K Q
F 2 A Rme2a T Kme3 Q T A R Kac S T G G K A P R K Q
F 3 A Rme2a T Kac Q T A R Kac S T G G K A P R K Q
F 4 A R T Kme1 Q T A Rme2s Kme1 S T G G K A P R K Q
F 5 A R T Kme2 Q T A Rme2s Kme1 S T G G K A P R K Q
F 6 A R T Kme3 Q T A Rme2s Kme1 S T G G K A P R K Q
F 7 A R T Kac Q T A Rme2s Kme1 S T G G K A P R K Q
F 8 A R T Kme1 Q T A Rme2a Kme1 S T G G K A P R K Q
F 9 A R T Kme2 Q T A Rme2a Kme1 S T G G K A P R K Q
F10 A R T Kme3 Q T A Rme2a Kme1 S T G G K A P R K Q
F11 A R T Kac Q T A Rme2a Kme1 S T G G K A P R K Q
F12 A R T Kme1 Q T A Rme2s Kme2 S T G G K A P R K Q
F13 A R T Kme2 Q T A Rme2s Kme2 S T G G K A P R K Q
F14 A R T Kme3 Q T A Rme2s Kme2 S T G G K A P R K Q
F15 A R T Kac Q T A Rme2s Kme2 S T G G K A P R K Q
F16 A R T Kme1 Q T A Rme2a Kme2 S T G G K A P R K Q
F17 A R T Kme2 Q T A Rme2a Kme2 S T G G K A P R K Q
F18 A R T Kme3 Q T A Rme2a Kme2 S T G G K A P R K Q
F19 A R T Kac Q T A Rme2a Kme2 S T G G K A P R K Q
F20 A R T Kme1 Q T A Rme2s Kme3 S T G G K A P R K Q
F21 A R T Kme2 Q T A Rme2s Kme3 S T G G K A P R K Q
F22 A R T Kme3 Q T A Rme2s Kme3 S T G G K A P R K Q
F23 A R T Kac Q T A Rme2s Kme3 S T G G K A P R K Q
F24 A R T Kme1 Q T A Rme2a Kme3 S T G G K A P R K Q
G 1 A R T Kme2 Q T A Rme2a Kme3 S T G G K A P R K Q
G 2 A R T Kme3 Q T A Rme2a Kme3 S T G G K A P R K Q
G 3 A R T Kac Q T A Rme2a Kme3 S T G G K A P R K Q

K 3 P R K Q L A T K A A R Kac S A P A T G G
K 4 P R K Q L A T K A A R K pS A P A T G G
K 5 P R K Q L A T K A A Rme2s Kme1 S A P A T G G
K 6 P R K Q L A T K A A Rme2s Kme2 S A P A T G G
K 7 P R K Q L A T K A A Rme2s Kme3 S A P A T G G
K 8 P R K Q L A T K A A Rme2s Kac S A P A T G G
K 9 P R K Q L A T K A A Rme2s K pS A P A T G G
K10 P R K Q L A T K A A Rme2a Kme1 S A P A T G G
K11 P R K Q L A T K A A Rme2a Kme2 S A P A T G G
K12 P R K Q L A T K A A Rme2a Kme3 S A P A T G G
K13 P R K Q L A T K A A Rme2a Kac S A P A T G G
K14 P R K Q L A T K A A Rme2a K pS A P A T G G
K15 P R K Q L A T K A A Cit Kme1 S A P A T G G
K16 P R K Q L A T K A A Cit Kme2 S A P A T G G
K17 P R K Q L A T K A A Cit Kme3 S A P A T G G
K18 P R K Q L A T K A A Cit K pS A P A T G G
K19 P R K Q L A T K A A R Kme1 pS A P A T G G
K20 P R K Q L A T K A A R Kme2 pS A P A T G G
K21 P R K Q L A T K A A R Kme3 pS A P A T G G
K22 P R K Q L A T K A A R Kac pS A P A T G G
K23 P R K Q L A T K A A Rme2s Kme1 pS A P A T G G
K24 P R K Q L A T K A A Rme2s Kme2 pS A P A T G G
L 1 P R K Q L A T K A A Rme2s Kme3 pS A P A T G G
L 2 P R K Q L A T K A A Rme2s Kac pS A P A T G G
L 3 P R K Q L A T K A A Rme2a Kme1 pS A P A T G G
L 4 P R K Q L A T K A A Rme2a Kme2 pS A P A T G G
L 5 P R K Q L A T K A A Rme2a Kme3 pS A P A T G G
L 6 P R K Q L A T K A A Rme2a Kac pS A P A T G G
L 7 R K S A P A T G G V K K P H R Y R P G
L 8 R K S A P A T G G V Kme1 K P H R Y R P G
L 9 R K S A P A T G G V Kme2 K P H R Y R P G
L10 R K S A P A T G G V Kme3 K P H R Y R P G
L11 R K S A P A T G G V Kac K P H R Y R P G
L12 S G R G K G G K G L G K G G A K R H R
L13 pS G R G K G G K G L G K G G A K R H R
L14 S G Rme2s G K G G K G L G K G G A K R H R
L15 S G Rme2a G K G G K G L G K G G A K R H R
L16 S G R G Kac G G K G L G K G G A K R H R
L17 S G R G K G G Kac G L G K G G A K R H R
L18 S G R G K G G K G L G Kac G G A K R H R
L19 S G R G K G G K G L G K G G A Kac R H R
L20 pS G Rme2s G K G G K G L G K G G A K R H R
L21 pS G Rme2a G K G G K G L G K G G A K R H R
L22 pS G R G Kac G G K G L G K G G A K R H R
L23 S G Rme2s G Kac G G K G L G K G G A K R H R
L24 S G Rme2s G K G G Kac G L G K G G A K R H R
M 1 S G Rme2a G Kac G G K G L G K G G A K R H R
M 2 S G Rme2a G K G G Kac G L G K G G A K R H R
M 3 S G R G Kac G G Kac G L G K G G A K R H R
M 4 S G R G K G G Kac G L G Kac G G A K R H R
M 5 S G R G K G G Kac G L G K G G A Kac R H R
M 6 S G R G K G G K G L G Kac G G A Kac R H R
M 7 pS G Rme2s G Kac G G K G L G K G G A K R H R
M 8 pS G Rme2a G Kac G G K G L G K G G A K R H R
M 9 S G Rme2s G Kac G G Kac G L G K G G A K R H R
M10 S G Rme2a G Kac G G Kac G L G K G G A K R H R
M11 S G R G Kac G G Kac G L G Kac G G A K R H R
M12 S G R G K G G Kac G L G Kac G G A Kac R H R
M13 pS G Rme2s G Kac G G Kac G L G K G G A K R H R
M14 pS G Rme2a G Kac G G Kac G L G K G G A K R H R
M15 S G Rme2s G Kac G G Kac G L G Kac G G A K R H R
M16 S G Rme2a G Kac G G Kac G L G Kac G G A K R H R
M17 S G R G Kac G G Kac G L G Kac G G A Kac R H R
M18 G K G G A K R H R K V L R D N I Q G I T
M19 G Kac G G A K R H R K V L R D N I Q G I T
M20 G K G G A Kac R H R K V L R D N I Q G I T
M21 G K G G A K Rme2s H R K V L R D N I Q G I T
M22 G K G G A K Rme2a H R K V L R D N I Q G I T
M23 G K G G A K R H Rme2s K V L R D N I Q G I T
M24 G K G G A K R H Rme2a K V L R D N I Q G I T
N 1 G K G G A K R H R Kme1 V L R D N I Q G I T
N 2 G K G G A K R H R Kme2 V L R D N I Q G I T
N 3 G K G G A K R H R Kme3 V L R D N I Q G I T
N 4 G K G G A K R H R Kac V L R D N I Q G I T
N 5 G K G G A K R H R K V L Rme2a D N I Q G I T
N 6 G K G G A K R H R K V L Rme2s D N I Q G I T
N 7 G Kac G G A Kac R H R K V L R D N I Q G I T
N 8 G K G G A Kac Rme2s H R K V L R D N I Q G I T
N 9 G K G G A Kac Rme2a H R K V L R D N I Q G I T
N10 G K G G A Kac R H Rme2s K V L R D N I Q G I T
N11 G K G G A Kac R H Rme2a K V L R D N I Q G I T
N12 G K G G A Kac R H R Kme1 V L R D N I Q G I T
N13 G K G G A Kac R H R Kme2 V L R D N I Q G I T
N14 G K G G A Kac R H R Kme3 V L R D N I Q G I T
N15 G K G G A Kac R H R Kac V L R D N I Q G I T
N16 G Kac G G A Kac R H R Kme1 V L R D N I Q G I T
N17 G Kac G G A Kac R H R Kme2 V L R D N I Q G I T
N18 G Kac G G A Kac R H R Kme3 V L R D N I Q G I T
N19 G Kac G G A Kac R H R Kac V L R D N I Q G I T
N20 G K G G A K R H Rme2a Kme1 V L R D N I Q G I T
N21 G K G G A K R H Rme2a Kme2 V L R D N I Q G I T
N22 G K G G A K R H Rme2a Kme3 V L R D N I Q G I T
N23 G K G G A K R H Rme2a Kac V L R D N I Q G I T
N24 G K G G A K R H Rme2s Kme1 V L R D N I Q G I T
O 1 G K G G A K R H Rme2s Kme2 V L R D N I Q G I T
O 2 G K G G A K R H Rme2s Kme3 V L R D N I Q G I T
O 3 G K G G A K R H Rme2s Kac V L R D N I Q G I T

G 4	A R T Kme1 Q T A Rme2s Kac S T G G K A P R K Q
G 5	A R T Kme2 Q T A Rme2s Kac S T G G K A P R K Q
G 6	A R T Kme3 Q T A Rme2s Kac S T G G K A P R K Q
G 7	A R T Kac Q T A Rme2s Kac S T G G K A P R K Q
G 8	A R T Kme1 Q T A Rme2a Kac S T G G K A P R K Q
G 9	A R T Kme2 Q T A Rme2a Kac S T G G K A P R K Q
G10	A R T Kme3 Q T A Rme2a Kac S T G G K A P R K Q
G11	A R T Kac Q T A Rme2a Kac S T G G K A P R K Q
G12	A Rme2s T Kme1 Q T A Rme2s Kme1 S T G G K A P R K Q
G13	A Rme2s T Kme2 Q T A Rme2s Kme1 S T G G K A P R K Q
G14	A Rme2s T Kme3 Q T A Rme2s Kme1 S T G G K A P R K Q
G15	A Rme2s T Kac Q T A Rme2s Kme1 S T G G K A P R K Q
G16	A Rme2a T Kme1 Q T A Rme2s Kme1 S T G G K A P R K Q
G17	A Rme2a T Kme2 Q T A Rme2s Kme1 S T G G K A P R K Q
G18	A Rme2a T Kme3 Q T A Rme2s Kme1 S T G G K A P R K Q
G19	A Rme2a T Kac Q T A Rme2s Kme1 S T G G K A P R K Q
G20	A Rme2s T Kme1 Q T A Rme2s Kme2 S T G G K A P R K Q
G21	A Rme2s T Kme2 Q T A Rme2s Kme2 S T G G K A P R K Q
G22	A Rme2s T Kme3 Q T A Rme2s Kme2 S T G G K A P R K Q
G23	A Rme2s T Kac Q T A Rme2s Kme2 S T G G K A P R K Q
G24	A Rme2a T Kme1 Q T A Rme2s Kme2 S T G G K A P R K Q
H 1	A Rme2a T Kme2 Q T A Rme2s Kme2 S T G G K A P R K Q
H 2	A Rme2a T Kme3 Q T A Rme2s Kme2 S T G G K A P R K Q
H 3	A Rme2a T Kac Q T A Rme2s Kme2 S T G G K A P R K Q
H 4	A Rme2s T Kme1 Q T A Rme2s Kme3 S T G G K A P R K Q
H 5	A Rme2s T Kme2 Q T A Rme2s Kme3 S T G G K A P R K Q
H 6	A Rme2s T Kme3 Q T A Rme2s Kme3 S T G G K A P R K Q
H 7	A Rme2s T Kac Q T A Rme2s Kme3 S T G G K A P R K Q
H 8	A Rme2a T Kme1 Q T A Rme2s Kme3 S T G G K A P R K Q
H 9	A Rme2a T Kme2 Q T A Rme2s Kme3 S T G G K A P R K Q
H10	A Rme2a T Kme3 Q T A Rme2s Kme3 S T G G K A P R K Q
H11	A Rme2a T Kac Q T A Rme2s Kme3 S T G G K A P R K Q
H12	A Rme2s T Kme1 Q T A Rme2s Kac S T G G K A P R K Q
H13	A Rme2s T Kme2 Q T A Rme2s Kac S T G G K A P R K Q
H14	A Rme2s T Kme3 Q T A Rme2s Kac S T G G K A P R K Q
H15	A Rme2s T Kac Q T A Rme2s Kac S T G G K A P R K Q
H16	A Rme2a T Kme1 Q T A Rme2s Kac S T G G K A P R K Q
H17	A Rme2a T Kme2 Q T A Rme2s Kac S T G G K A P R K Q
H18	A Rme2a T Kme3 Q T A Rme2s Kac S T G G K A P R K Q
H19	A Rme2a T Kac Q T A Rme2s Kac S T G G K A P R K Q
H20	A Rme2s T Kme1 Q T A Rme2a Kme1 S T G G K A P R K Q
H21	A Rme2s T Kme2 Q T A Rme2a Kme1 S T G G K A P R K Q
H22	A Rme2s T Kme3 Q T A Rme2a Kme1 S T G G K A P R K Q
H23	A Rme2s T Kac Q T A Rme2a Kme1 S T G G K A P R K Q
H24	A Rme2a T Kme1 Q T A Rme2a Kme1 S T G G K A P R K Q

O 4	G K G G A K R H R Kme1 V L Rme2a D N I Q G I T
O 5	G K G G A K R H R Kme2 V L Rme2a D N I Q G I T
O 6	G K G G A K R H R Kme3 V L Rme2a D N I Q G I T
O 7	G K G G A K R H R Kac V L Rme2a D N I Q G I T
O 8	G K G G A K R H R Kme1 V L Rme2s D N I Q G I T
O 9	G K G G A K R H R Kme2 V L Rme2s D N I Q G I T
O10	G K G G A K R H R Kme3 V L Rme2s D N I Q G I T
O11	G K G G A K R H R Kac V L Rme2s D N I Q G I T
O12	S G R G K Q G G K A R A K A K S R S S
O13	pS G R G K Q G G K A R A K A K S R S S
O14	S G R G Kac Q G G K A R A K A K S R S S
O15	S G R G K Q G G Kac A R A K A K S R S S
O16	S G R G K Q G G K A R A Kac A K S R S S
O17	pS G R G Kac Q G G K A R A K A K S R S S
O18	pS G R G K Q G G Kac A R A K A K S R S S
O19	pS G R G K Q G G K A R A Kac A K S R S S
O20	S G R G Kac Q G G Kac A R A K A K S R S S
O21	S G R G Kac Q G G K A R A Kac A K S R S S
O22	S G R G K Q G G Kac A R A Kac A K S R S S
O23	pS G R G Kac Q G G Kac A R A K A K S R S S
O24	pS G R G Kac Q G G K A R A Kac A K S R S S
P 1	pS G R G K Q G G Kac A R A Kac A K S R S S
P 2	S G R G Kac Q G G Kac A R A Kac A K S R S S
P 3	pS G R G Kac Q G G Kac A R A Kac A K S R S S
P 4	P D P A K S A P A P K K G S K K A V T
P 5	P D P A Kac S A P A P K K G S K K A V T
P 6	P D P A K S A P A P K Kac G S K K A V T
P 7	P D P A K S A P A P K K G pS K K A V T
P 8	P D P A K S A P A P K K G S Kac K A V T
P 9	P D P A Kac S A P A P K Kac G S K K A V T
P10	P D P A Kac S A P A P K K G pS K K A V T
P11	P D P A Kac S A P A P K K G S Kac K A V T
P12	P D P A K S A P A P K Kac G pS K K A V T
P13	P D P A K S A P A P K Kac G S Kac K A V T
P14	P D P A K S A P A P K K G pS Kac K A V T
P15	P D P A Kac S A P A P K Kac G pS K K A V T
P16	P D P A Kac S A P A P K Kac G S Kac K A V T
P17	P D P A Kac S A P A P K K G pS Kac K A V T
P18	P D P A K S A P A P K Kac G pS Kac K A V T
P19	P D P A Kac S A P A P K Kac G pS Kac K A V T
P20	Bio A A N W S H P Q F E K A A
P21	E Q K L I S E E D L A
P22	HAc
P23	K Kme1 Kme2 Kme3 Kac R Rme2s R Rme2a R Cit K Kme1 Kac Kme3 RK
P24	R Rme2s K Kme1 Kac R Rme2a Kme2 K Kme3 R Kme1 Rme2s K Kac RK

Appendix 5

List of Figures

List of Tables

Appendix 6

The Protein Journal
https://doi.org/10.1007/s10930-020-09895-z

Identification of Structural Elements of the Lysine Specific Demethylase 2B CxxC Domain Associated with Replicative Senescence Bypass in Primary Mouse Cells

Eleftherios E. Deiktakis[1] · Matthew Abrams[2,4] · Anna Tsapara[1] · Christos Stournaras[1] · Christos Tsatsanis[1] · Philip N. Tsichlis[2] · Sotirios C. Kampranis[1,2,3]

Abstract

Background Lysine specific demethylase 2B, KDM2B, regulates genes that participate in cellular development, morphogenesis, differentiation and metabolism as a component of the polycomb repressive complex 1 (PRC1). The CxxC finger of KDM2B is responsible for the DNA binding capacity of this epigenetic regulator, acting as a sampling mechanism across chromatin for gene repression

Objectives The molecular determinants of the CxxC—DNA interaction remain largely unknown, revealing a significant knowledge gap to be explored. Our goal was to elucidate the key residues of the CxxC domain that contribute to its function as well as to further elaborate on the significance of this domain in the KDM2B role

Methods By using electrophoresis mobility swift assay, we identified structural elements of CxxC domain that participate in the DNA recognition. We created mouse embryonic fibroblasts overexpressing different truncated and point-mutated mouse KDM2B variants to examine the contribution of the KDM2B domains in replicative senescence bypass

Results In this study, we show that only the CxxC finger is essential for the ability of mKDM2B to bypass replicative senescence in primary cells by *ink4A-Arf-ink4B* locus repression, and that this is mediated by specific interactions of residues R585, K608 and K616 with non-methylated CpG containing DNA

Conclusions These results provide new structural insights into the molecular interactions of CxxC and could serve as a stepping-stone for developing domain-specific inhibitors for KDM2B.

Keywords Lysine demethylase · Polycomb repressive complex · Oncogene · Zn-finger · Non-methylated CpG · Replicative senescence

Electronic supplementary material The online version of this article (https://doi.org/10.1007/s10930-020-09895-z) contains supplementary material, which is available to authorized users.

✉ Eleftherios E. Deiktakis
medp2011689@med.uoc.gr

[1] Medical School, University of Crete, PO. Box. 2208, 71003 Heraklion, Crete, Greece

[2] Molecular Oncology Research Institute, Tufts Medical Center, Boston, MA 02111, USA

[3] Present Address: Department of Plant and Environmental Sciences, University of Copenhagen, Thorvaldsensvej 40, 1871 Frederiksberg C, Denmark

[4] Present Address: Department of Radiation Oncology, Beth Israel Deaconess Medical Center, Boston, MA 02215, USA

Published online: 09 April 2020

Abbreviations

PRC1 Polycomb repressive complex 1
KDM2B Lysine specific demethylase 2B
MEFs Mouse embryonic fibroblasts

1 Introduction

The fine line between physiological and pathological cell fate does not only depend on DNA sequence but also on a multifaceted matrix of regulatory elements derived from chemical modifications on the histone proteins or the DNA itself [1–9]. The plethora of histone readers has been under intense investigation in recent years, but essential information for key cellular factors is still missing. One such case is the lysine-specific demethylase 2B (KDM2B), a major PRC1-associated factor and a *bona fide* oncogene [10–14].

Elucidating the detailed biochemical properties of KDM2B will help understanding its role in cellular biology and cancer pathology.

KDM2B (also known as Fblx10, Ndy1, and Jhdm1b) is a lysine-specific histone demethylase that targets H3K36me2 [11, 12], H3K4me3 [12, 14] and H3K79me2/3 [15]. Upon PRC2 recruitment, KDM2B participates in the repression of the senescence-associated expression of the $p15^{Ink4b}$ [11], $p16^{Ink4a}$ and $p19^{Arf}$ proteins [12] and act as promoter of mouse embryo fibroblasts (MEFs) immortalization by allowing them to bypass replicative senescence [10]. KDM2B functions by coupling several chromatin modifi- cations, including histone H3K36me2 demethylation, with histone H3K27 trimethylation and histone H2AK119 mon-oubiquitination. This is mediated by the KDM2B-dependent upregulation of EZH2, along with the KDM2B-dependent binding of EZH2 to the promoters of a subset of target genes [12, 16].

Numerous studies revealed that KDM2B has a central role in epigenetic regulation [17–19] as well as in occur- rences of colon [20], prostate [21], pancreatic [22] cancer and leukemogenesis [13, 16, 23]. In addition, KDM2B functions as a master regulator of a set of microRNAs that target several members of the Polycomb complexes PRC1 and PRC2 and its deregulation has important effects on PRC gene expression in both normal and cancer cells [24, 25]. KDM2B has also been associated with inhibition of NF-κB/p65-dependent cellular apoptosis, by a mechanism where NF-κB upregulates KDM2B expression, resulting in the repression of c-FOS and the interception of apoptosis in human cancer cells [26]. Moreover, KDM2B has been suggested to regulate genes of the glycolytic pathway [27] and proteoglycan synthesis [28], as well as several other metabolic [14], antioxidant [29] and pluripotency genes [30–33] during morphogenesis and development.

The KDM2B protein contains several functional domains. The N-terminal JmjC domain is responsible for the histone demethylation reaction [12]. At the C-terminal part of the protein, a leucine-rich region (LRR) and an F-box domain participate in protein–protein interactions and are involved in ubiquitination. This region is essential for the ability of KDM2B to tether a ubiquitin chain to H2AK119 leading to gene repression [12, 34–38]. In addition, KDM2B con- tains two zinc-finger motifs, CxxC and PHD (Plant homeo-domain), located at the center of the amino acid sequence. There is strong structural interdependence between these domains that prevents either of the two from being produced independently in a stable form [39]. The KDM2B CxxC domain has similar structure to that of the CxxC fingers of MLL and CFP1 proteins, consisting of two cysteine- rich clusters that chelate two Zn^{2+} ions and stabilize the domain [40]. This domain has been implicated in DNA binding and the recognition of non-methylated CpG DNA sequences [37, 41]. It has been shown to be essential for the recruitment of KDM2B and the tethering of PRC1 to the c-jun promoter [40] and for protecting CG- islands from hypermethylation [42]. KDM2B regulates the transcription of mir-101, which controls the expression of EZH2, in a CxxC and JmjC-dependent manner [10, 12, 16]. Moreover, both the JmjC and CxxC domains of KDM2B are required for the activation of early responsive genes in reprogram- ming of induced pluripotency stem cells (iPSCs) [33, 43]. Furthermore, studies in the closely related lysine specific demethylase, KDM2A, showed that the PHD does not play a direct or indirect role in the interaction with DNA since destabilization of the PHD domain by replacing one of the structural cysteine residues did not reduce the efficiency of DNA binding [44]. These results highlight the importance of a functional CxxC domain, but do not correlate these phenotypes with the DNA-binding function of the protein as they were performed with CxxC deletion or structure-destabilizing mutants. Considering that the loss of 60–80 amino acids from the central part of the protein or the destabilization of Zn coordination could have a strong impact on the proper structure of the enzyme, these experiments do not discern the involvement of the CxxC domain from that of other structural components of the protein.

Elucidating the function of the zinc-finger CxxC domain of KDM2B will improve our understanding in a molecular level of the involvement of this epigenetic key regulator in cell physiology and disease. In the present study, we set out identify the key structural determinants of the DNA recognition and analyze the contribution of this interaction in the ability of KDM2B to mediate replicative senescence bypass in primary mouse cells.

2 Materials and Methods

2.1 Cloning CxxC and PHD Domains of mKDM2B in Bacterial Expression Vector

The coding sequences of CxxC and PHD domains of the mouse Lysine- specific demethylase 2B, mKDM2B, were cloned in a pET102 vector with a V5 epitope, using the TOPO® TA Cloning® Protocol. The recombinant protein, $mKDM2B_{577-707}$, was Thioredoxin- fused at the N-terminus and carried a 6 × His-tag at the C-terminus. Transformed Mach1 $T1^R$ *E. coli* cells with the pET102/D-$mKDM2B_{577-707}$ construct (6.7 kbp) were grown on Luria- Bertani (LB) agar plates supplemented with 100 µg/mL of ampicillin overnight at 37 °C. Single colonies were picked to inoculate 6 mL of LB medium with ampicillin and incubated overnight at 37 °C. The plasmid DNA was isolated with QIAprep Spin Miniprep Kit. The $mKDM2B_{577-707}$ cloning was confirmed via enzymatic digestion and agarose gel electrophoresis.

2.2 Site-Directed Mutagenesis of CxxC and PHD

In order to generate the mKDM2B and mKDM2B$_{577-707}$ mutants, we followed the protocol described in [45]. The mutations were introduced into pET102/D–mKDM2B$_{577-707}$ by polymerase chain reaction (PCR) amplification of the original construct using Phusion® HF DNA Polymer- ase with a specific forward primer for each mutation (Table S1). The PCR primers are shown in Table S2. The single point mutations (R585A, K608A and K616A) and the double point mutation (R585A/K616A) of the pET102/ D-mKDM2B$_{577-707}$ construct were confirmed via Sanger sequencing (CEMIA, Greece). Replication and isolation of the mutant mKDM2B$_{577-707}$ constructs was performed as described above.

2.3 Heterologous Expression and Purification of the Recombinant Proteins

BL21 CodonPlus *E. coli* cells were transformed for the heterologous expression of the proteins. The successfully transformed cells were cultivated in Luria- Bertani (LB) medium in the presence of ampicillin, kanamycin and chloramphenicol in concertation of 50, 50 and 12 μg/mL, respectively. The cells were incubated for 3 h at 37 °C before adding 0.5 mM of IPTG, followed by incubation for another 24 h at 17 °C before cell harvest. Osmotic disruption of cells in Lysis buffer (Tris-HCl (0.06 M) pH 8.0, 0.3 M NaCl, 0.01 M Imi- dazole, 0.1 mM PMSF, 0.5% w/v Lysozyme) was followed by 10 min sonication at max power, to obtain soluble recom- binant proteins from the lysate. SDS-PAGE was used to quantify the efficiency of the protein expression before fur- ther purification. The recombinant proteins were isolated via His-tag Affinity Chromatography protocol using Ni–NTA agarose resin. Wild type and mutant mKDM2B$_{577-707}$ proteins were dialyzed through SnakeSkin® Dialysis tubing and stored in Reaction Buffer (Tris–HCl (0.06 M) pH 8.0, 0.3 M NaCl, 1 mM β- mercaptoethanol, 10% Glycerol) without prior cleavage of the tag sequences. The final concentrations of the protein solutions, measured in Nanodrop™ Spectrophotometer (ThermoFisher) ranged from 25 to 30 μM and showed more than 90% purity with Coomassie staining of the SDS Polyacrylamide Gel (Figure S2B).

2.4 [γ- ^{32}P] ATP Labelling of DNA Substrate

The 26-mer fully complementary strands of DNA (CpG2F: 5′-GGG TACTAGCGTTAGTCCGGTCCAAC-3′ and CpG2R: 5′-GTTGGACCGGACTAACGCTAGTACCC-3′) were chemically synthesized and purified by Invitrogen, UK. The 5′ radio phosphorylation of 50 pmol single strand CpG2F was based on the T4 PNK protocol (New England Biolabs). The radioactive ssDNA strands were separated in a denaturing 15% polyacrylamide gel electrophoresis and extracted overnight with gel extraction buffer (0.4 M CH_3COONa, 0.001 M EDTA pH 8.0, Phenol 20%). Phenol/ $CHCl_3$ DNA purification protocol obtained 20–25 pmol of radiolabeled CpG2F strands.

2.5 Electrophoresis Mobility Shift Assay (EMSA)

The radioactive synthetic double-stranded CpG2 was produced by annealing of the single-stranded ssDNA strands (^{32}P-CpG2F and CpG2R). In these EMSA experiments, wild type mKDM2B$_{577-707}$ and its mutants (2–360 pmol) were incubated with 0.5 pmol ^{32}P-end-labelled dsDNA CpG2 in Reaction Buffer supplemented with 0.006 M $MgCl_2$ and 10 μg/mL BSA, in total volume of 10 μL for 30 min at 37 °C. The samples were analyzed in a native 8% polyacrylamide gel in 0.5 × TBE. Bands were visualized by autoradiography.

2.6 Construction of Truncated KDM2B Vectors

Construct pBABE-puro-NDY1 [12] was used as template in Quickchange deletion mutagenesis (Agilent Inc.) using the primers described in Table S2.

2.7 MEF Culture

Cell culture procedures and evaluation of replicative senescence bypass were performed as described previously [10, 12].

All restriction enzymes, Phusion® HF DNA Polymer- ase and T4 PNK were purchased by New England Biolabs. Bacterial expression vector pET102, *E. coli* competent cells, TOPO® TA Cloning® Kit and SnakeSkin® Dialysis tub- ing were purchased by ThermoFisher Scientific. PCR prim- ers were purchased by Invitrogen. QIAprep Spin Miniprep Kit and Ni–NTA agarose resin were purchased by Qiagen. Ampicillin, Kanamycin, Chloramphenicol, PMSF, EDTA, Imidazole, Glycerol and β-mercaptoethanol were purchased by Sigma Aldrich. All other chemicals were purchased by AppliChem GmbH.

3 Results

3.1 Biochemical Analysis of DNA Recognition by the mKDM2B CxxC Finger

The CxxC domain of KDM2B binds non-methylated CpG DNA sequences [36, 39, 41, 46]. As DNA recognition can act as a sampling mechanism of KDM2B target genes [39], elucidating the structural determinants of this interac- tion will enable targeted studies to understand its role in

KDM2B-associated gene regulation. When these studies were initiated, the structure of the mKDM2B CxxC and PHD domains (RCSB PDB entry No 4O64; Figure S1a) was not yet available. Therefore, we constructed a model of the CxxC-DNA interaction based on the structure of the MLL1-CxxC-DNA complex [47]. Based on this analysis, we identified candidate residues for DNA interaction, including R585, K608 and K616 (Figure S1b). To confirm whether these amino acids interact with DNA, we constructed and expressed a fragment of mouse KDM2B that spans residues 577–707 and contains the CxxC and PHD domains along with three single variants mKDM2B$_{577-707}$ (R585A), mKDM2B$_{577-707}$ (K608A), mKDM2B$_{577-707}$ (K616A) and one double mKDM2B$_{577-707}$ (R585A/K616A) (Figure S2). We studied the binding of the wild-type and mutant recom- binant proteins on a 26-mer DNA molecule containing two CpG sequences using electrophoresis mobility shift assay. All three mKDM2B$_{577-707}$ mutants indicated significantly reduced binding affinity compared to the wild-type protein (Fig. 1). Increasing protein concentration in the reaction resulted in a rough quantification of the mutants' affinity showing up to 24-fold reduced DNA binding capacity (Fig- ure S3). Overall, these results confirm that residues R585, K608 and K616 are responsible for the DNA binding capac- ity of mKDM2B CxxC domain.

3.2 The PHD Domain is not Required for KDM2B-Supported Bypass of Replicative Senescence

Previous studies have shown that overexpression of KDM2B enables Mouse Embryonic Fibroblasts (MEFs) to bypass replicative senescence through repression of the *Ink4a-Arf-Ink4b* locus [10–12]. To elucidate the contribution of the different KDM2B domains in this process, we examined the function of a set of progressively truncated forms of mouse KDM2B (Fig. 2a). A series of pBABE-based retrovi- ral insertion constructs were produced and used to establish MEFs stably expressing different C-terminally truncated KDM2B proteins. Our data showed that cells expressing the full-length mKDM2B or the variants ending upstream of the LRR domain or immediately after the PHD domain (mKDM2B$_{1-1045}$ and mKDM2B$_{1-707}$, respectively) were able to bypass replicative senescence and undergo cellu- lar immortalization (Fig. 2b). Based on previous data [37] showing that the LRR domain of KDM2B is crucial for recruiting the rest of PRC1.1 components on the PcG tar- get genes and leading to H2AK119 monoubiqitination, we conclude that histone H2A ubiquitination is not required for KDM2B-mediated *Ink4a-Arf-Ink4b* repression. Notably, the variant ending right before the PHD domain, mKDM2B$_{1-630}$, was also able to sustain replicative senescence bypass, suggesting that the histone binding function supported by the PHD domain is not essential for efficient repression of the *Ink4a-Arf-Ink4b* locus in the context of PRC1 (Fig. 2b).

3.3 The DNA Binding Capacity of mKDM2B is Essential for Replicative Senescence Bypass in MEFs

To understand the contribution of the CxxC finger-mediated DNA binding to the biological function of mKDM2B, retroviral vectors for three variants of the full-length mKDM2B

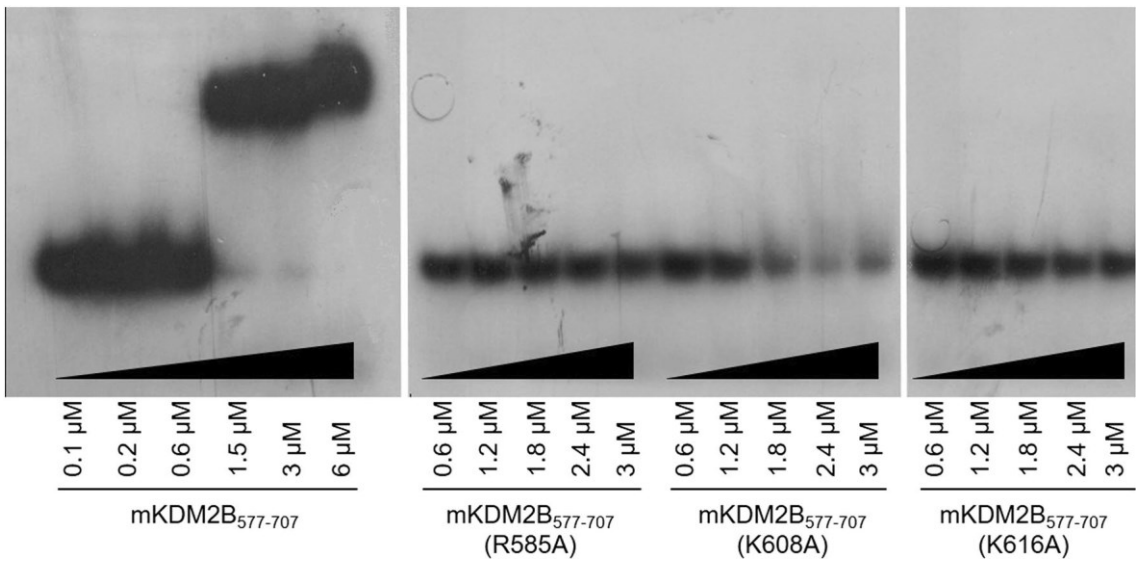

Fig. 1 mKDM2B$_{577-707}$ mutants exhibit reduced DNA binding affin- ity. 10 nM radiolabeled dsDNA were incubated with mKDM2B$_{577-707}$ and mKDM2B$_{577-707}$ mutants for 30 min at 37 °C. Formation of the protein-DNA complex results in a band shift during 8% native PAGE. No band shift of the mKDM2B$_{577-707}$ mutant samples confirms the involvement of the specific residues in the interaction with DNA

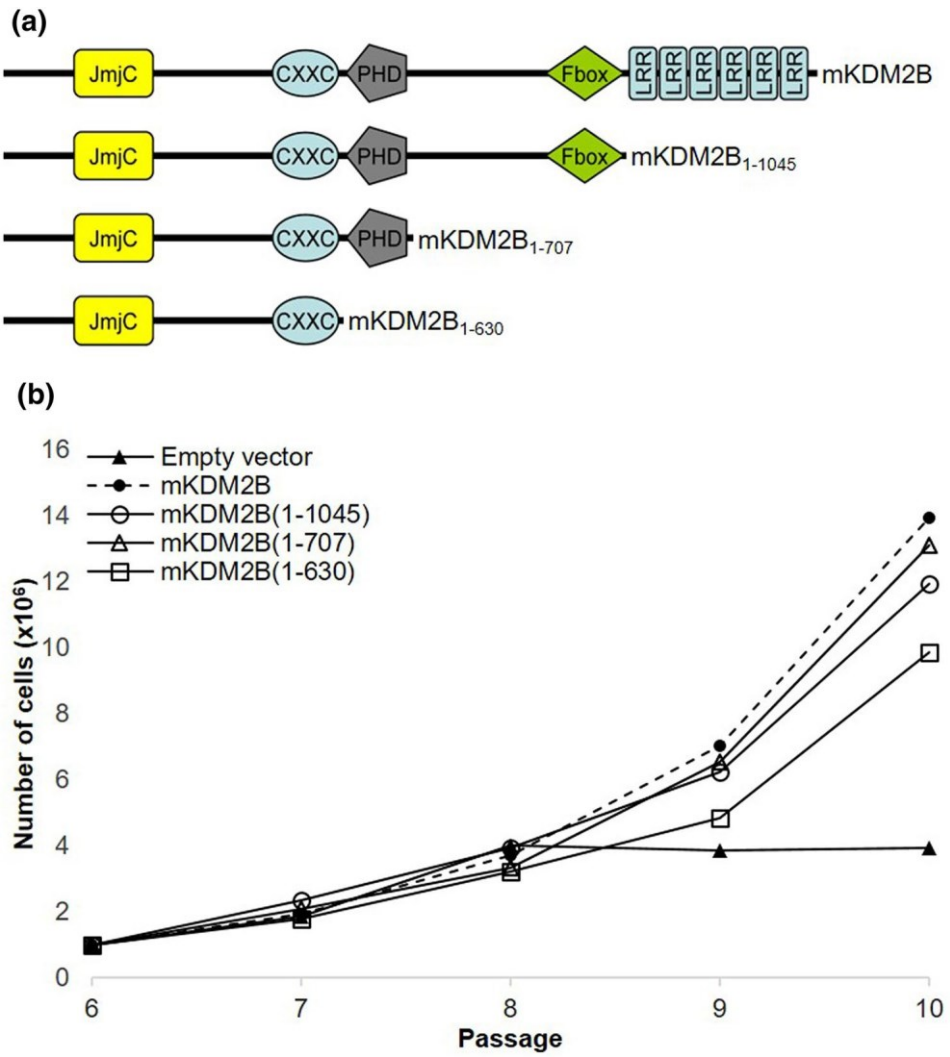

Fig. 2 Evaluation of the ability of different forms of mKDM2B to support replicative senescence bypass in MEFs. **a** Schematic representation of the truncated mKDM2B proteins. **b** MEFs transduced with full-length and truncated forms of mKDM2B were passaged and the total number of cells were counted. Empty pBABE-puro vector was used as control

containing the single residue CxxC mutations shown to abolish DNA binding in the in vitro assays (R585A, K608A and K616A) and three additional variants containing their pair wise combinations (R585A/K608A, R585A/K616A and K608A/K616A) were constructed. Following transduction of MEFs, the ability of the different variants to sustain replicative senescence bypass was evaluated. Our results confirmed that DNA binding was essential for mKDM2B to support cell proliferation (Fig. 3a). Notably, the K616A variant and any of the double mutants containing the K616A substitution (R585A/K616A and K608A/K616A) showed the strongest effect in abolishing the KDM2B phenotype (Fig. 3b). These results confirm that the DNA binding capacity of CxxC is essential for its role in replicative senescence.

4 Discussion

In order to understand the interplay between KDM2B and chromatin, we investigated the DNA interactions of the zinc-finger CxxC of mouse KDM2B. We confirmed the DNA binding function of the CxxC finger and identified key residues involved in this interaction. Using electrophoresis mobility shift assays, we showed that residues R585, K608 and K616 on the mKDM2B play a key role in the binding of non-methylated CpG-containing DNA. The K616A substitution revealed that this residue plays the most prominent role of the three tested, consistent with previous findings that reported the direct interaction

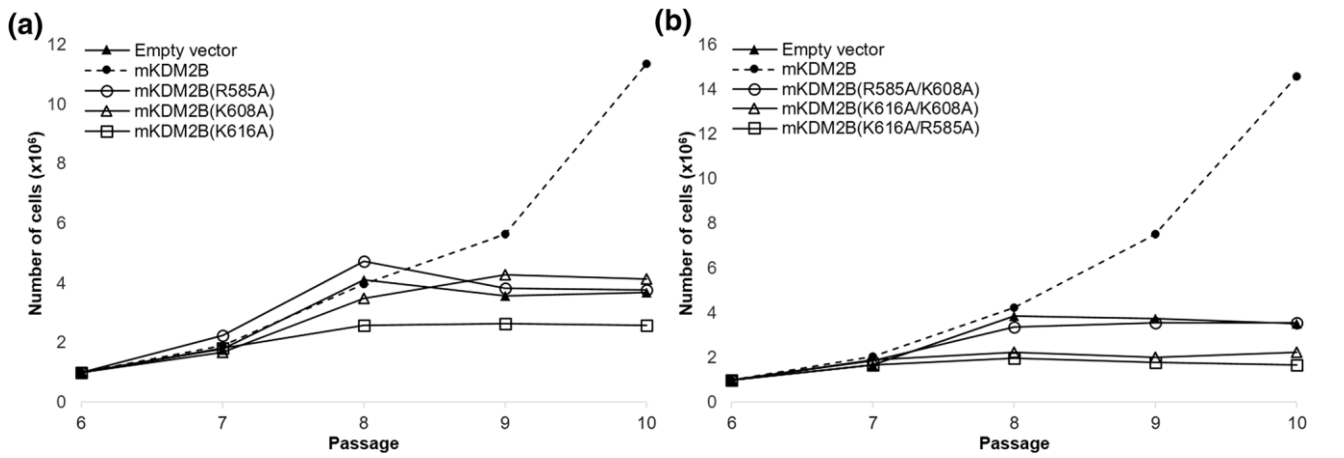

Fig. 3 DNA recognition is required for KDM2B- mediated replica- tive senescence bypass in MEFs. **a** Mutation of R585, K608 or K616 compromises the ability of full-length mKDM2B to support repli-cative senescence bypass. **b** Evaluation of the ability of the double mutants mKDM2B(R585A/K608A), mKDM2B(R585A/K616A) and mKDM2B(K608A/K616A) to bypass replicative senescence

of the analogous residue in the MLL1 CxxC-finger with the major groove of the DNA [47]. Further experiments in which these residues are substituted by amino acids with larger or differently charged side-chains will further improve our understanding of the molecular details of this interaction. Taking a step further, we correlated the DNA binding capacity of the mouse KDM2B with its functional role. To this end, we introduced the same point mutations that abrogated the DNA binding affinity of the recombinant CxxC finger into full-length mouse KDM2B and we over- expressed singly- and doubly-mutated forms in MEFs. All mutants failed to support replicative senescence bypass confirming the functional role of the CxxC finger in this process. Notably, cells that overexpressed the two double mutant forms of mKDM2B containing the K616A muta- tion (R585A/K616A and K608A/K616A) entered the rep- licative senescent state faster than empty vector-containing cells. Furthermore deletion of the C-terminal half of the protein that includes the PHD domain did not abolish this activity. This suggested that the combined action of the JmjC and CxxC domains is by itself sufficient to inhibit cell cycle events that contribute to the bypass of repli- cative senescence, including the repression of the locus. These results also showed that the DNA binding capacity of mKDM2B is not compromised upon deletion of the PHD domain, similar to previous findings with the closely related histone demethylase KDM2A, which supported that the CxxC and PHD fingers are functionally independ- ent in DNA binding [44].

Numerous studies have implicated KDM2B in cancer [48, 49]. Therefore, confirming the key role of the CxxC finger in this process, in combination with the available structural information for this domain, prompts further studies into the potential of development of CxxC-targeting inhibitors as cancer therapeutics.

Acknowledgements We thank Prof. Kriton Kalantidis (IMBB-FORTH) and Dr. Ioannis Vlatakis (Department of Biology, University of Crete) for their help with the EMSA experiments.

Author Contributions EED, MA and SCK carried out experiments; SCK, PNT and CT designed experiments; EED, MA, and SCK analyzed data; EED, PNT and SCK wrote and revised the manuscript.

Funding This research was funded by a State Scholarship Founda- tion (IKY) Partnership Agreement Program (ΕΣΠΑ 2014-20) that was co-financed by the European Social Fund (ESF), grant no. 2017- 050-0504-10806. Work in PNT's laboratory was supported by grant R01 CA109747 from the National Cancer Institute. These two funding sources did not overlap.

Compliance with Ethical Standards

Conflict of interest The authors declare no conflict of interest.

References

1. Strahl BD, Allis CD (2000) The language of covalent histone modifications. Nature 403:41–45
2. Grant PA (2001) A tale of histone modifications. Genome Biol. https://doi.org/10.1186/gb-2001-2-4-reviews0003
3. Berger SL (2007) The complex language of chromatin regulation during transcription. Nature 447:407–412
4. Lachner M, O'Sullivan RJ, Jenuwein T (2003) An epigenetic road map for histone lysine methylation. J Cell Sci 116:2117–2124
5. Caselle M, Di Cunto F, Provero P (2002) Correlating overrep- resented upstream motifs to gene expression: a computational approach to regulatory element discovery in eukaryotes. BMC Bioinform 3:7
6. Fischle W, Wang Y, Allis CD (2003) Histone and chromatin cross-talk. Curr Opin Cell Biol 15(2):172–183

7. Margueron R, Trojer P, Reinberg D (2005) The key to development: interpreting the histone code? Curr Opin Gen Dev 15(2):163–176
8. Kouzarides T (2007) Chromatin modifications and their function. Cell 28:693–705
9. Taverna SD, Li H, Ruthenburg AJ, Allis CD, Patel DJ (2007) How chromatin-binding modules interpret histone modifications: lessons from professional pocket pickers. Nat Struct Mol Biol 14(11):1025–1040
10. Pfau R, Tzatsos A, Kampranis SC, Serebrennikova OB, Bear SE, Tsichlis PN (2008) Members of a family of JmjC domain-containing oncoproteins immortalize embryonic fibroblasts via a JmjC domain-dependent process. Proc Natl Acad Sci USA 105(6):1907–1912
11. He J, Kallin EM, Tsukada Y, Zhang Y (2008) The H3K36 demethylase Jhdm1b/Kdm2b regulates cell proliferation and senescence through p15 (Ink4b). Nat Struct Mol Biol 15:1169–1175
12. Tzatsos A, Pfau R, Kampranis SC, Tsichlis PN (2009) Ndy1/KDM2B immortalizes mouse embryonic fibroblasts by repressing the Ink4a/Arf locus. PNAS 106:2641–2646
13. He J, Nguyen AT, Zhang Y (2011) KDM2b/JHDM1b, an H3K36me2-specific demethylase, is required for initiation and maintenance of acute myeloid leukemia. Blood 117:3869–3880
14. Janzer A, Stamm K, Becker A, Zimmer A, Buettner R, Kirfel J (2012) The H3K4me3 histone demethylase Fbxl10 is a regulator of chemokine expression, cellular morphology, and the metabolome of fibroblasts. J Biol Chem 287(37):30984–30992
15. Kang JY, Kim JY, Kim KB, Park JW, Cho H, Hahm JY, Chae YC, Kim D, Kook H, Rhee S, Ha NC, Seo SB (2018) KDM2B is a histone H3K79 demethylase and induces transcriptional repression via SIRT1-mediated chromatin silencing. FASEB J. https://doi.org/10.1096/fj.201800242R
16. Kottakis F, Polytarchou C, Foltopoulou P, Sanidas I, Kampranis SC, Tsichlis PN (2011) FGF-2 regulates cell proliferation, migration, and angiogenesis through an NDY1/KDM2B-miR-101-EZH2 pathway. Mol Cell 43(2):285–298
17. Vacík T, Lađinović D, Raška I (2018) KDM2A/B lysine demethylases and their alternative isoforms in development and disease. Nucleus 9(1):431–441
18. Frescas D, Guardavaccaro D, Bassermann F, Koyama-Nasu R, Pagano M (2007) JHDM1B/FBXL10 is a nucleolar protein that represses transcription of ribosomal RNA genes. Nature 450:309–313
19. Blackledge NP, Farcas AM, Kondo T, King HW, McGouran JF, Hanssen LL, Ito S, Cooper S, Kondo K, Koseki Y, Ishikura T, Long HK, Sheahan TW, Brockdorff N, Kessler BM, Koseki H, Klose RJ (2014) Variant PRC1 complex-dependent H2A ubiquitylation drives PRC2 recruitment and polycomb domain formation. Cell 157(6):1445–1459
20. Zacharopoulou N, Tsapara A, Kallergi G, Schmid E, Alkahtani S, Alarifi S, Tsichlis PN, Kampranis S, Stournaras C (2018) The epigenetic factor KDM2B regulates EMT and small GTPases in colon tumor cells. Cell Physiol Biochem 47:368–377
21. Zacharopoulou N, Tsapara A, Kallergi G, Schmid E, Tsichlis PN, Kampranis SC, Stournaras C (2018) The epigenetic fac- tor KDM2B regulates cell adhesion, small rho GTPases, actin cytoskeleton and migration in prostate cancer cells. Biochem Biophys Acta 1865(4):587–597
22. Tzatsos A, Paskaleva P, Ferrari F, Deshpande V, Stoykova S, Contino G, Wong KK, Lan F, Trojer P, Park PJ, Bardeesy N (2013) KDM2B promotes pancreatic cancer via Polycomb-depend- ent and -independent transcriptional programs. J Clin Invest 123(2):727–739
23. Ueda T, Nagamachi A, Takubo K, Yamasaki N, Matsui H, Kanai A, Nakata Y, Ikeda K, Konuma T, Oda H, Wolff L, Honda Z, Wu X, Helin K, Iwama A, Suda T, Inaba T, Honda H (2015) Fbxl10 overexpression in murine hematopoietic stem cells induces leukemia involving metabolic activation and upregulation of Nsg2. Blood 125:3437–3446
24. Tzatsos A, Paskaleva P, Lymperi S, Contino G, Stoykova S, Chen Z, Wong KK, Bardeesy N (2011) Lysine-specific demethylase 2B (KDM2B)-let-7-enhancer of zester homolog 2 (EZH2) pathway regulates cell cycle progression and senescence in primary cells. J Biol Chem 286(38):33061–33069
25. Kottakis F, Foltopoulou P, Sanidas I, Keller P, Wronski A, Dake BT, Ezell SA, Shen Z, Naber SP, Hinds PW, McNiel E, Kuperwasser C, Tsichlis PN (2014) NDY1/KDM2B functions as a master regulator of polycomb complexes and controls self-renewal of breast cancer stem cells. Cancer Res 74(14):3935–3946
26. Ge R, Wang Z, Zeng Q, Xu X, Olumi AF (2011) F-box protein 10, an NF-κB-dependent anti-apoptotic protein, regulates TRAIL-induced apoptosis through modulating c-Fos/c-FLIP pathway. Cell Death Differ 18(7):1184–1195
27. Yu X, Wang J, Wu J, Shi Y (2015) A systematic study of the cellular metabolic regulation of Jhdm1b in tumor cells. Mol Biosyst 11(7):1867–1875
28. Wang JJ, Dong R, Wang LP, Wang JS, Du J, Wang SL, Shan ZC, Fan ZP (2015) Histone demethylase KDM2B inhibits the chondrogenic differentiation potentials of stem cells from apical papilla. Int J Clin Exp Med 8(2):2165–2173
29. Polytarchou C, Pfau R, Hatziapostolou M, Tsichlis PN (2008) The JmjC domain histone demethylase Ndy1 regulates redox homeostasis and protects cells from oxidative stress. Mol Cell Biol 28:7451–7464
30. Lu L, Gao Y, Zhang Z, Cao Q, Zhang X, Zou J, Cao Y (2015) Kdm2a/b lysine demethylases regulate canonical wnt signaling by modulating the stability of nuclear beta-catenin. Dev Cell 33:660–674
31. Zhou Z, Yang X, He J, Liu J, Wu F, Yu S, Liu Y, Lin R, Liu H, Cui Y, Zhou C, Wang X, Wu J, Cao S, Guo L, Lin L, Wang T, Peng X, Qiang B, Hutchins AP, Pei D, Chen J (2017) Kdm2b regulates somatic reprogramming through variant PRC1 complex-dependent function. Cell Rep 21(8):2160–2170
32. Li H, Lai P, Jia J, Song Y, Xia Q, Huang K, He N, Ping W, Chen J, Yang Z, Li J, Yao M, Dong X, Zhao J, Hou C, Esteban MA, Gao S, Pei D, Hutchins AP, Yao H (2017) RNA helicase DDX5 inhibits reprogramming to pluripotency by miRNA-based repression of RYBP and its PRC1-dependent and -independent functions. Cell Stem Cell 20:462–477
33. Wang T, Chen K, Zeng X, Yang J, Wu Y, Shi X, Qin B, Zeng L, Esteban MA, Pan G, Pei D (2011) The histone demethylases Jhdm1a/1b enhance somatic cell reprogramming in a vitamin-C-dependent manner. Cell Stem Cell 9:575–587
34. He J, Shen L, Wan M, Taranova O, Wu H, Zhang Y (2013) Kdm2b maintains murine embryonic stem cell status by recruiting PRC1 complex to CpG islands of developmental genes. Nat Cell Biol 15:373–384
35. Sánchez C, Sánchez I, Demmers JA, Rodriguez P, Strouboulis J, Vidal M (2007) Proteomics analysis of Ring1B/Rnf2 interactors identifies a novel complex with the Fbxl10/Jhdm1B histone demethylase and the Bcl6 interacting corepressor. Mol Cell Proteom 6:820–834
36. Farcas AM, Blackledge NP, Sudbery I, Long HK, McGouran JF, Rose NR, Lee S, Sims D, Cerase A, Sheahan TW, Koseki H, Brockdorff N, Ponting CP, Kessler BM, Klose RJ (2012) KDM2B links the Polycomb Repressive Complex 1 (PRC1) to recognition of CpG islands. eLife 1:e00205
37. Wu X, Johansen JV, Helin K (2013) Fbxl10/Kdm2b recruits polycomb repressive complex 1 to CpG islands and regulates H2A ubiquitylation. Mol Cell 49:1134–1146
38. Wong SJ, Gearhart MD, Taylor AB, Nanyes DR, Ha DJ, Robinson AK, Artigas JA, Lee OJ, Demeler B, Hart PJ, Bardwell VJ, Kim

CA (2016) KDM2B recruitment of the Polycomb group complex, PRC11, requires cooperation between PCGF1 and BCORL1. Structure 24(10):1795–1801
39. Xu C, Liu K, Lei M, Yang A, Li Y, Hughes TR, Min J (2018) DNA sequence recognition of human CXXC domains and their structural determinants. Structure 26:85–95
40. Long HK, Blackledge NP, Klose RJ (2013) ZF-CxxC domain-containing proteins, CpG islands and the chromatin connection. Biochem Soc Trans 41:727–740
41. Koyama-Nasu R, David G, Tanese N (2007) The F-box protein Fbl10 is a novel transcriptional repressor of c-Jun. Nat Cell Biol 9:1074–1080
42. Boulard M, Edwards JR, Bestor TH (2015) FBXL10 protects Polycomb-bound genes from hypermethylation. Nat Genet 47(5):479–485
43. Liang G, He J, Zhang Y (2012) Kdm2b promotes induced pluri- potent stem cell generation by facilitating gene activation early in reprogramming. Nat Cell Biol 14:457–466
44. Zhou JC, Blackledge NP, Farcas AM, Klose RJ (2012) Recognition of CpG island chromatin by KDM2A requires direct and specific interaction with linker DNA. Mol Cell Biol 32(2):479–489
45. Ignea C, Pontini M, Maffei ME, Makris AM, Kampranis SC (2014) Engineering monoterpene production in yeast using a synthetic dominant negative geranyl diphosphate synthase. ACS Synth Biol 3:298–306
46. Blackledge NP, Zhou JC, Tolstorukov MY, Farcas AM, Park PJ, Klose RJ (2010) CpG islands recruit a histone H3 lysine 36 demethylase. Mol Cell 38(2):179–190
47. Cierpicki T, Risner LE, Grembecka J, Lukasik SM, Popovic R, Omonkowska M, Shultis DD, Zeleznik-Le NJ, Bushweller JH (2010) Structure of the MLL CXXC domain-DNA complex and its functional role in MLL-AF9 leukemia. Nat Struct Mol Biol 17:62–68
48. Kampranis SC, Tsichlis PN (2009) Histone demethylases and cancer. Adv Cancer Res 102:103–169
49. Yan M, Yang X, Wang H, Shao Q (2018) The critical role of histone lysine demethylase KDM2B in cancer. Am J Transl Res 10(8):2222–2233